

Advanced Calibration for Process Simulation User Guide

Version T-2022.03, March 2022

SYNOPSYS®

Copyright and Proprietary Information Notice

© 2022 Synopsys, Inc. This Synopsys software and all associated documentation are proprietary to Synopsys, Inc. and may only be used pursuant to the terms and conditions of a written license agreement with Synopsys, Inc. All other use, reproduction, modification, or distribution of the Synopsys software or the associated documentation is strictly prohibited.

Destination Control Statement

All technical data contained in this publication is subject to the export control laws of the United States of America. Disclosure to nationals of other countries contrary to United States law is prohibited. It is the reader's responsibility to determine the applicable regulations and to comply with them.

Disclaimer

SYNOPSYS, INC., AND ITS LICENSORS MAKE NO WARRANTY OF ANY KIND, EXPRESS OR IMPLIED, WITH REGARD TO THIS MATERIAL, INCLUDING, BUT NOT LIMITED TO, THE IMPLIED WARRANTIES OF MERCHANTABILITY AND FITNESS FOR A PARTICULAR PURPOSE.

Trademarks

Synopsys and certain Synopsys product names are trademarks of Synopsys, as set forth at <https://www.synopsys.com/company/legal/trademarks-brands.html>.

All other product or company names may be trademarks of their respective owners.

Free and Open-Source Licensing Notices

If applicable, Free and Open-Source Software (FOSS) licensing notices are available in the product installation.

Third-Party Links

Any links to third-party websites included in this document are for your convenience only. Synopsys does not endorse and is not responsible for such websites and their practices, including privacy practices, availability, and content.

www.synopsys.com

Contents

Conventions	13
Customer Support	13

Part I: Advanced Calibration in Sentaurus Process

1. Using Advanced Calibration File of Sentaurus Process	16
Location of Advanced Calibration File	16
Using Advanced Calibration	17
Optional Modules	17
Additional Calibration by Users	19
Earlier Versions of Advanced Calibration	19
Combining Advanced Calibration S-2021.06 and T-2022.03	21
Changes in Advanced Calibration From S-2021.06 to T-2022.03	21
Using Selected Improvements of Advanced Calibration T-2022.03	22
Improved Calibration for MeV Implantation With Sentaurus MC	22
Improved Calibration for Oxidation in N ₂ O Ambient	23
Advanced Calibration File for Kinetic Monte Carlo Simulations	24
Sentaurus Workbench Splits: Saving in TDR Format	24
 2. Advanced Calibration for Silicon, SiGe, and Germanium	26
Part 1: Basic Model Switches	27
Diffusion Models in Silicon and Germanium	27
Dopant Cluster Models in Silicon and Germanium	28
Defect Cluster Models in Silicon and Germanium	30
Poisson Equation	31
Channeling Dose in Analytic Implantations	32
Boundary Conditions	32
Numeric Solver	33
Summary of Model Switches	33

Contents

Part 2: Constant Parameters	35
Basic Point-Defect Parameters	36
Bulk Parameters for Free Interstitials	37
Bulk Parameters for Free Vacancies	37
Bulk Recombination of Point Defects	38
Boundary Conditions for Point Defects	38
Oxidation-Enhanced Diffusion	38
Transient-Enhanced Diffusion	39
Boron Diffusion and Activation	40
Boron Diffusion Coefficient	40
Effect of Fluorine	41
Boron Clustering	41
Boron Dose Loss	44
Fluorine	45
Nitrogen	45
Arsenic Diffusion and Activation	46
Arsenic Diffusivity	46
Arsenic Clusters	47
Arsenic Dose Loss	48
Phosphorus Diffusion and Activation	48
Phosphorus Diffusivity	48
Phosphorus Clusters	49
Phosphorus Dose Loss	51
Arsenic–Phosphorus Co-Diffusion	52
Indium Parameters	54
Antimony Parameters	54
Carbon Diffusion	55
Carbon Diffusivity in Silicon	55
Carbon Clustering in Silicon	55
Carbon in Germanium	56
Intrinsic Carrier Concentration	56
Oxidation	57
Massoud Model Parameters for Wet Oxidation of Silicon	57
Parameters for Wet and Dry Oxidation of SiGe	57
Oxidation of Silicon in N ₂ O Ambient	58
Smoothing of Amorphous–Crystalline Interface	59
Selecting Implantation Tables	59
Effect of Germanium and Stress	60
Arguments of SiGe_and_Stress_Effect	61
Ge Chemical Effect (Ge_Chem_Eff)	61
Stress Effect (Stress_Eff)	61
Segregation at Si–SiGe Interface (Segreg_Model)	62

Contents

Effect of Strained Overlayers (Strained_Overlayer)	62
Implementation of SiGe_and_Stress_Effect	63
Chemical SiGe Alloy Effects	63
Stress Effects	69
Segregation at Si–SiGe Interface (Segreg_Model)	75
Effect of Strained Overlayers (Strained_Overlays)	77
Part 3: Ion Implantation and Initial Conditions	78
User-Defined Defect Initialization	78
impPostProcess_AdvCal	79
Scaling Factors for Point Defects and Damage	79
Values for Initial Dopant Activation	82
Sum of As-Implanted Point Defects and Crystal Damage	82
Subroutines for Setting ifactor and dfactor	83
ifactor	83
vfactor	84
dfactor	85
Thermal Implantations	85
Scope of Calibration	87
Debye Temperature, Electronic Stopping, and Damage	87
Initial Conditions	88
Implantation Preprocessing and Postprocessing	88
Analytic Implantation	88
Monte Carlo Implantation (General)	89
Carborane	93
Part 4: Comprehensive and Slow Models	94
Interstitial Clusters	95
Boron–Interstitial Clusters	97
Arsenic Parameters in AdvancedModels	98
Phosphorus Parameters in AdvancedModels	98
ChargedCluster Model for Indium	99
Fluorine Diffusion and Clustering	99
Carbon Diffusion and Clustering	100
Nitrogen Diffusion and Clustering	100
Solid Phase Epitaxial Regrowth	101
Recrystallization Speed	102
Doping Redistribution	104
Melting Laser Anneal	107
Using AdvancedMLAModel for MLA Simulation	107
Seed Term	108
Settings in AdvancedMLAModel	109
Meshing	111

Contents

Thermodynamics of Silicon, Germanium, and SiGe	111
Silicon Absorptivity	113
MLA Calibration	113
MLA Calibration for SiGe	116
Limitations of MLA Model	117
Part 5: Accelerating Simulations for Power Technologies	117
Using AdvancedPowerDeviceMode	119
Variant 1: Explicitly Reverting to Standard Models	119
Variant 2: Automatically Reverting to Standard Models	119
Contents of AdvancedPowerDeviceMode	120
Increased Time Steps, Deposition Steps, and Temperature Steps ..	120
Simplified Physics	121
Speedup Methods Not Included in AdvancedPowerDeviceMode ..	121
References	122
<hr/>	
3. Guidelines for Additional Calibration	136
Accuracy and Limitations of Advanced Calibration of Sentaurus Process	136
Error Control	137
Point Defects	138
Bulk Parameters	138
Surface Boundary Conditions	138
Oxidation-Enhanced Diffusion	139
Clusters of Interstitials	139
Vacancy Clusters	141
Boron Diffusion and Clustering	141
Diffusion and Pairing in Silicon	141
Migration Distance (for ChargedReact Model)	143
Effect of Fluorine	144
Boron Clustering and Activation	145
Boron Dose Loss	149
Arsenic Diffusion and Activation	150
Arsenic-Doped Epitaxy	151
Phosphorus Diffusion and Activation	153
Phosphorus Diffusion in Silicon	153
Phosphorus Activation in Silicon	153
Phosphorus Dose Loss at Oxide–Silicon Interfaces	154
Phosphorus-Doped Epitaxial Silicon	154
Co-diffusion of Arsenic and Phosphorus	158
Indium Diffusion and Activation	163
Nonamorphizing Condition	163
Amorphizing Ion Implantation	163

Contents

SPER Model Usage	163
Antimony Diffusion and Activation	166
Carbon	167
Carbon–Interstitial Clusters	167
Carbon–Boron Clusters	168
Impact of Carbon on Hole Mobility	168
Molecular Implantation	169
Analytic Implantation	170
Sentaurus MC	170
Fluorine Diffusion and Clustering	171
Nitrogen Diffusion and Clustering	172
Diffusion in Strained Silicon and Silicon Germanium	173
As-Implanted Dopant Profiles	174
Coimplantation Model	175
Preamorphization Implantation Model	175
Cold and Hot Implantation	175
Dose Loss at Silicon–Oxide Interfaces	176
Calibration of ThreePhaseSegregation Model	177
Oxidation	178
Bird’s Beak in CMOS Devices	179
Diffusion in Polysilicon and Out-Diffusion From Polysilicon	179
Dopant Penetration Through Gate Oxide	180
Diffusion and Activation in Germanium	180
Performing Additional Calibration	180
Calibration Procedure	181
Fine-Tuning Parameters Defined in Callback Procedures	182
Loading a User Calibration File	183
Recommendations	183
Miscellaneous	183
Lateral Diffusion Along Interface	184
Example of a User Calibration File	184
Recommended Numeric Settings for Monte Carlo Implantation	186
Monte Carlo Pocket Implantation	186
Monte Carlo Source/Drain Implantation	188
Additional Calibration for Power Technologies	189
Calibration	189
Oxide Thickness and Oxide Shape	189
Ion Implantation	189
Initial Conditions After Implantation	190
Thermal Annealing	190

Contents

Meshing	190
Recommendations for Bulk Refinement With Adaptive Meshing . .	191
Refinement at Material Interfaces	193
Calibration of Wet Etching Rate Modification by Ion Implantation	193
Calibration	194
Application	195
References	196
4. Advanced Calibration for 4H-SiC Process Simulation	200
Content of Advanced Calibration File for 4H-SiC Simulation	200
Part 1: Basic Model Switches	200
Poisson Equation	201
Dopant Cluster Models in 4H-SiC	202
Dopant Transport at the Oxide–SiC Interface	203
Boron Evaporation From the SiC Surface	203
Part 2: Settings for Monte Carlo Implantation	204
Parameters Used in the Calibration	205
LSS.pre, nucl.cor	206
DebyeTemperature, d.sim	206
nloc.pre, nloc.exp, scr.par	207
surv.rat, sat.par	207
Interp.Min.Energy, Interp.Max.Energy	207
Recommendations for Fine-Tuning of Amorphization	208
Illustration of Calibration Results	208
Part 3: Ion Implantation and Initial Conditions	209
References	209
Part II: Advanced Calibration in Sentaurus Process Kinetic Monte Carlo	
5. Using Advanced Calibration File of Sentaurus Process KMC	213
Location of Advanced Calibration File	213
Using Advanced Calibration	214
Additional Calibration by Users	215

Contents

6. Contents of Advanced Calibration of Sentaurus Process KMC	216
Overview	216
Supported Materials	217
Part 1: Model Parameters for Implantation Damage and Point Defects	218
Amorphization and Recrystallization	218
Amorphous Silicon and Germanium	219
Diffusion, Generation, and Recombination	220
Charge States	223
Extended Defects	223
SiGe	225
Linear Germanium Correction Factors	225
Silicon and Germanium Parameter Interpolation	227
Stress Effects	229
Amorphization and Recrystallization	229
Band Gap	229
Diffusion, Generation, and Recombination	230
Extended Defects	231
Part 2: Model Parameters for Impurities	231
Implantation	231
Diffusion	232
Boron	233
Arsenic	235
Phosphorus	236
Indium	238
Carbon	238
Fluorine	239
Nitrogen	240
Clusters	240
Boron	241
Arsenic	242
Phosphorus	242
Arsenic and Phosphorus	243
Indium	244
Carbon	244
Boron and Carbon	245
Fluorine	245
Nitrogen	245
Boron and Nitrogen	246
Carbon and Nitrogen	246
Segregation	246
Boron	246

Contents

Arsenic	247
Phosphorus	247
Indium.	247
Carbon	247
Fluorine	248
Nitrogen	248
Recrystallization.	248
Boron	248
Arsenic	249
Phosphorus	249
Indium.	249
Carbon	250
Fluorine	250
Nitrogen	250
Epitaxy	250
Boron	250
Arsenic	251
Phosphorus	251
Carbon	251
SiGe	251
Linear Germanium Correction Factors	251
Silicon and Germanium Parameter Interpolation	252
Stress Effects	254
Boron	254
Arsenic	255
Phosphorus	255
Indium.	256
Section 4: Model Parameters for Epitaxial Growth	256
Coordinations.Planes Model	256
Coordinations Model	257
Coordinations.Reactions Model	258
Epitaxial Growth	258
Etching	260
References.	261
<hr/>	
7. Guidelines for Additional Calibration	272
Accuracy and Limitations of Advanced Calibration of Sentaurus Process KMC	272
Damage and Point Defects	273
Amorphization	273
Recrystallization	274
Diffusion, Generation, and Recombination.	275

Contents

Extended Defects	275
Impurities	276
Diffusion	276
Activation	278
Dose Loss	280
Recrystallization	280
Stress and SiGe Effects	281
References	282

Part III: Advanced Calibration for Mechanics Simulations

8. Using Advanced Calibration File for Mechanics Simulations	286
Location of Advanced Calibration File	286
Using Advanced Calibration	287
Earlier Versions of Advanced Calibration	287
9. Contents of Advanced Calibration for Mechanics Simulations	289
Overview	289
Switches for Interpolation in Mole Fraction–Dependent Mechanical Models	289
Parameters for Mechanics	291
Suppression of Dilatational Viscosity	291
Mole Fraction–Dependent Mechanics Parameters for SiGe	291
Cubic Crystal Anisotropy for Silicon and Germanium	292
Temperature Dependency of Stiffness Coefficients for Silicon and Germanium	292
Isotropic Elastic Moduli for Germanium	293
Polysilicon	293
Viscosity of Oxide and Nitride	293
Isotropic Moduli for Titanium and Titanium Silicide	294
Amorphous Germanium Oxide	294
Titanium Nitride	294
Hafnium Oxide	295
Silicon Carbide	295
References	296

About This Guide

Synopsys® is working continually on improving the simulation models and optimizing the model parameters for the latest technology nodes. This effort is based on long-standing experience of model calibration for customers and a comprehensive, growing database of state-of-the-art secondary ion mass spectroscopy (SIMS) profiles. The variety of partners and data ensures that systematic and random errors in experimental work are minimized in this model representation. Advanced Calibration provides users with a set of parameters that have been calibrated to many technologies, ranging from power technologies to deep-submicron CMOS, including ultrashallow junction formation, surface dose loss, oxidation, and channel and halo dopant implantation, co-doping, and diffusion, for Si, SiGe, Ge, and other materials.

Sentaurus™ Process offers the Tcl-based scripting language Aligator for the implementation of diffusion and reaction models. This allows users to implement models or to model extensions. This possibility is also used in the Advanced Calibration of Sentaurus Process: The Advanced Calibration file of Sentaurus Process contains model selections, parameter specifications, and some model extensions. This file can be sourced at the beginning of a Sentaurus Process simulation. In analogy, the Advanced Calibration file of Sentaurus Process Kinetic Monte Carlo contains model selections and parameter specifications. This file can be sourced at the beginning of a Sentaurus Process simulation in atomistic mode as well.

The Advanced Calibration of Sentaurus Interconnect is based on the Advanced Calibration of Sentaurus Process, in particular, the part for mechanics simulations. This file can be sourced at the beginning of a Sentaurus Interconnect simulation.

Current and future efforts of Synopsys are focused on the integration of the Advanced Calibration in the process simulators Sentaurus Process, Sentaurus Process Kinetic Monte Carlo, and Sentaurus Interconnect, and on further improvements of its accuracy.

This user guide explains the Advanced Calibration files for the process simulators Sentaurus Process, Sentaurus Process Kinetic Monte Carlo, and Sentaurus Interconnect. It is intended for users who are familiar with Sentaurus Process and want to obtain a higher accuracy in process simulation. For detailed information about these process simulators, see the *Sentaurus™ Process User Guide* and *Sentaurus™ Interconnect User Guide*.

The user guide is divided into the following parts:

- Part I: Advanced Calibration in Sentaurus Process – These chapters describe the contents and the use of the Advanced Calibration file of Sentaurus Process. They describe the use of Advanced Calibration for silicon, silicon germanium, germanium, and silicon carbide. In addition, they explain the accuracy and limitations of the Advanced Calibration of Sentaurus Process and provides guidelines for additional calibration.

About This Guide

Conventions

- Part II: Advanced Calibration in Sentaurus Process Kinetic Monte Carlo – These chapters describe the contents and the use of the Advanced Calibration file of Sentaurus Process Kinetic Monte Carlo. They explain the accuracy and limitations of the Advanced Calibration of Sentaurus Process Kinetic Monte Carlo and provides guidelines for additional calibration.
- Part III: Advanced Calibration for Mechanics Simulations – These chapters describe the contents and the use of the Advanced Calibration file for mechanics simulations for Sentaurus Process and Sentaurus Interconnect.

For additional information, see:

- The TCAD Sentaurus release notes, available on the Synopsys SolvNetPlus support site (see [Accessing SolvNetPlus on page 14](#))
- Documentation available on the SolvNetPlus support site

Conventions

The following conventions are used in Synopsys documentation.

Convention	Description
Bold text	Identifies a selectable icon, button, menu, or tab. It also indicates the name of a field or an option.
Courier font	Identifies text that is displayed on the screen or that the user must type. It identifies the names of files, directories, paths, parameters, keywords, and variables.
<i>Italicized text</i>	Used for emphasis, the titles of books and journals, and non-English words. It also identifies components of an equation or a formula, a placeholder, or an identifier.
Key+Key	Indicates keyboard actions, for example, Ctrl+I (press the I key while pressing the Control key).
Menu > Command	Indicates a menu command, for example, File > New (from the File menu, choose New).

Customer Support

Customer support is available through the Synopsys SolvNetPlus support site and by contacting the Synopsys support center.

Accessing SolvNetPlus

The SolvNetPlus support site includes an electronic knowledge base of technical articles and answers to frequently asked questions about Synopsys tools. The site also gives you access to a wide range of Synopsys online services, which include downloading software, viewing documentation, and entering a call to the Support Center.

To access the SolvNetPlus site:

1. Go to <https://solvnetplus.synopsys.com>.
 2. Enter your user name and password. (If you do not have a Synopsys user name and password, follow the instructions to register.)
-

Contacting Synopsys Support

If you have problems, questions, or suggestions, you can contact Synopsys support in the following ways:

- Go to the Synopsys [Global Support Centers](#) site on www.synopsys.com. There you can find email addresses and telephone numbers for Synopsys support centers throughout the world.
 - Go to either the Synopsys SolvNetPlus site or the Synopsys Global Support Centers site and open a case (Synopsys user name and password required).
-

Contacting Your Local TCAD Support Team Directly

Send an email message to:

- support-tcad-us@synopsys.com from within North America and South America
- support-tcad-eu@synopsys.com from within Europe
- support-tcad-ap@synopsys.com from within Asia Pacific (China, Taiwan, Singapore, Malaysia, India, Australia)
- support-tcad-kr@synopsys.com from Korea
- support-tcad-jp@synopsys.com from Japan

Part I: Advanced Calibration in Sentaurus Process

This part of the *Advanced Calibration for Process Simulation User Guide* contains the following chapters:

- [Chapter 1, Using Advanced Calibration File of Sentaurus Process](#)
- [Chapter 2, Advanced Calibration for Silicon, SiGe, and Germanium](#)
- [Chapter 3, Guidelines for Additional Calibration](#)
- [Chapter 4, Advanced Calibration for 4H-SiC Process Simulation](#)

1

Using Advanced Calibration File of Sentaurus Process

This chapter gives a brief introduction to the use of Advanced Calibration in a process simulation with Sentaurus Process.

Advanced Calibration is a selection of models and parameters, which is recommended by Synopsys to be used for accurate process simulation. In Sentaurus Process, this selection of models and parameters is contained in a text file, which can be opened with any standard text editor.

By sourcing the Advanced Calibration file at the beginning of a process simulation, the standard calibration of Synopsys is selected. If needed, you can change or extend the Advanced Calibration. This can be performed by sourcing an additional calibration file, which contains the required parameter changes, or by editing the Advanced Calibration file with a text editor.

Location of Advanced Calibration File

The Advanced Calibration file is the ultimate product of Synopsys' calibration efforts. For each release of Sentaurus Process, there is a new Advanced Calibration file that includes the best and latest set of models and parameters. To ensure backward compatibility, previous Advanced Calibration files are still available.

The files for the Advanced Calibration of Sentaurus Process in this release are located at:

```
$STROOT/tcad/$STRELEASE/lib/sprocess/TclLib/AdvCal
```

The default file is named `AdvCal_2022.03.fps`. It represents the first version of Advanced Calibration T-2022.03. Older versions of the Advanced Calibration file can be found in the same directory. For example, the file `AdvCal_2021.06.fps` contains the Advanced Calibration file for Version S-2021.06 and is available for backward compatibility.

The default Advanced Calibration parameter file contains parameters for Si, SiGe and Ge-based processes. An additional parameter file `AdvCal_SiC_2022.03.fps` targets process simulation of semiconductor devices based on 4H-SiC.

Using Advanced Calibration

To use the Advanced Calibration of Sentaurus Process, at the beginning of the input file, insert the line:

```
AdvancedCalibration
```

or, better:

```
AdvancedCalibration 2022.03
```

Alternatively, this file can be sourced by using:

```
source $AdvCalDir/AdvCal_2022.03.fps
```

The procedure `AdvancedCalibration` has two optional parameters `<version>` and `<material>`. The order of arguments is not important. The allowed values for `<material>` are Si, SiGe, Ge, 4H-SiC, and SiC:

- Si, SiGe, and Ge as well as no material value call the default Advanced Calibration parameter file for Si, SiGe, and Ge materials.
- 4H-SiC and SiC call the Advanced Calibration file for 4H-SiC.

For example, the following command calls the Advanced Calibration file for 4H-SiC (`AdvCal_SiC_2022.03.fps`):

```
AdvancedCalibration 2022.03 4H-SiC
```

Optional Modules

`AdvCal_2022.03.fps` includes a base set of models and parameters, and several optional modules, which are not switched on automatically. Each module can be selected by a single command after loading Advanced Calibration.

`AdvancedThermalImplantModel` switches on the impact of temperature on ion implantation. This module is recommended for the simulation of processes, which include implantations at temperatures that differ from room temperature. See [Thermal Implantations on page 85](#).

Three modules are useful for selected technologies, and their corresponding commands are as follows:

- `SiGe_and_Stress_Effect` switches on the impact of Ge and stress on dopant diffusion and activation. It is recommended for PMOS devices with SiGe pockets and also can be used for HBT devices with SiGe layers. See [Effect of Germanium and Stress on page 60](#).
- `AdvancedPowerDeviceMode` is used to speed up the process simulation for many types of power device. For simulation of power devices, see [Part 5: Accelerating Simulations](#)

Chapter 1: Using Advanced Calibration File of Sentaurus Process

Optional Modules

for Power Technologies on page 117 and Additional Calibration for Power Technologies on page 189.

- AdvancedMLAModel is recommended for modeling melting laser anneal. See Melting Laser Anneal on page 107.

Other modules switch on physical models that are more complex and more time-consuming alternatives to the Advanced Calibration default models:

- AdvancedFluorineModel models the impact of fluorine on transient-enhanced diffusion and on boron dose loss. It is recommended for processes that include atomic F implantations. It is also beneficial for the accurate modeling of processes including high-dose BF₂ implantations. See Fluorine Diffusion and Clustering on page 99.
- AdvancedNitrogenModel switches on equations for the diffusion and clustering of nitrogen in silicon. It can be considered for use in processes that include nitrogen implantations. See Nitrogen Diffusion and Clustering on page 100.
- AdvancedModels switches on complex physical models for various clustering phenomena in silicon, such as interstitial clusters, boron–interstitial clusters, and fluorine clusters. In total, many equations and model parameters are used to describe these phenomena. Process simulations become slower but are not always more accurate. Therefore, AdvancedModels is considered mainly for the purpose of fundamental research. See Part 4: Comprehensive and Slow Models on page 94.
- AdvancedSPERModel switches on the solid phase epitaxial regrowth (SPER) model and sets the calibrated parameters for it. AdvancedSPERModel adds complexity to the simulation of anneals after amorphizing implantations. See Solid Phase Epitaxial Regrowth on page 101.

Note:

After amorphizing implantations, the amorphized regions recrystallize by SPER in subsequent thermal anneals. By default, Sentaurus Process assumes that SPER is completed instantaneously at the beginning of thermal annealing. Amorphization is only taken into account by setting special initial conditions for dopants and point defects in amorphized semiconductor regions at the beginning of diffusion. The SPER model simulates the movement of the amorphous–crystalline transition region during SPER and the dopant redistribution during such a process. In particular, the SPER model simulates diffusion in amorphous silicon and the snow plow effect during SPER. The snow plow effect is the redistribution of certain impurity species (for example, indium), which prefer to stay at the amorphous side of the amorphous–crystalline interface, toward the surface.

Additional Calibration by Users

Advanced Calibration is based on the assumption that all parameters that are not changed in the parameter files are the default parameters of Sentaurus Process. To use the Advanced Calibration file `AdvCal_2022.03.fps`, it must be sourced before the real process description.

After sourcing `AdvCal_2022.03.fps`, you can change the model switches or parameter values of the physical models. This should ideally be performed by experienced users with a good understanding of the diffusion models of Sentaurus Process.

For the process simulation of silicon technology, Advanced Calibration is usually the best starting point. You can further increase the accuracy for a certain technology by additional fine-tuning of a few physical parameters.

The best way to perform this is to put all additional calibration in a user calibration file, for example, `my_calibration.fps`. This file includes the commands to select optional modules of Advanced Calibration such as `AdvancedFluorineModel` or `AdvancedPowerDeviceMode`, and it includes all project-specific changes to the physical models or parameters with respect to Advanced Calibration.

In the process simulation file, at the beginning of the process simulation, insert the lines:

```
AdvancedCalibration 2022.03  
source ./my_calibration.fps
```

This approach allows you to:

- Separate completely the calibration and the process description.
- Use the Advanced Calibration file as a starting point.
- Summarize all project-specific calibration in a short and clear text file.

For detailed information about how to perform additional calibration, see [Chapter 3 on page 136](#).

Earlier Versions of Advanced Calibration

You can source earlier versions of the Advanced Calibration file by inserting, for example, the line:

```
AdvancedCalibration 2021.06
```

This is converted internally to:

```
source $AdvCalDir/AdvCal_2021.06.fps
```

Chapter 1: Using Advanced Calibration File of Sentaurus Process

Earlier Versions of Advanced Calibration

Table 1 lists earlier versions of the Advanced Calibration file that can be loaded with Sentaurus Process Version T-2022.03.

This possibility is available to provide backward compatibility. You can run simulations with the latest version of Sentaurus Process, but the simulations can still be based on an old calibration. For new TCAD projects, it is recommended to load the latest version of Advanced Calibration.

The original versions of the earlier Advanced Calibration files cannot be used in the latest version of Sentaurus Process, due to changes in the source code and the model library of Sentaurus Process, which affect the functionality of the old files. Therefore, Synopsys has adapted the earlier Advanced Calibration files to cope with those changes. Modifications have been undertaken in such a way that the choice of physical models and parameters is still the one from the corresponding release. The `AdvancedCalibration` command always loads the modified versions.

Table 1 Earlier versions of Advanced Calibration file and their corresponding commands

Advanced Calibration file	Corresponding command
AdvCal_2021.06.fps	<code>AdvancedCalibration 2021.06</code>
AdvCal_2020.09.fps	<code>AdvancedCalibration 2020.09</code>
AdvCal_2019.12.fps	<code>AdvancedCalibration 2019.12</code>
AdvCal_2019.03.fps	<code>AdvancedCalibration 2019.03</code>
AdvCal_2018.06.fps	<code>AdvancedCalibration 2018.06</code>
AdvCal_2017.09.fps	<code>AdvancedCalibration 2017.09</code>
AdvCal_2016.12.fps	<code>AdvancedCalibration 2016.12</code>
AdvCal_2016.03.fps	<code>AdvancedCalibration 2016.03</code>
AdvCal_2015.06.fps	<code>AdvancedCalibration 2015.06</code>
AdvCal_2014.09.fps	<code>AdvancedCalibration 2014.09</code>
AdvCal_2013.12.fps	<code>AdvancedCalibration 2013.12</code>
AdvCal_2013.03.fps	<code>AdvancedCalibration 2013.03</code>
AdvCal_2012.06.fps	<code>AdvancedCalibration 2012.06</code>
AdvCal_2011.09.fps	<code>AdvancedCalibration 2011.09</code>

Chapter 1: Using Advanced Calibration File of Sentaurus Process

Combining Advanced Calibration S-2021.06 and T-2022.03

Table 1 Earlier versions of Advanced Calibration file and their corresponding commands

Advanced Calibration file	Corresponding command
AdvCal_2010.12.fps	AdvancedCalibration 2010.12
AdvCal_2010.03.fps	AdvancedCalibration 2010.03
AdvCal_2009.06.fps	AdvancedCalibration 2009.06
AdvCal_2008.09.fps	AdvancedCalibration 2008.09
AdvCal_2007.12.fps	AdvancedCalibration 2007.12
AdvCal_2007.03.fps	AdvancedCalibration 2007.03
AdvCal_2006.06.fps	AdvancedCalibration 2006.06
AdvCal_2005.10.fps	AdvancedCalibration 2005.10

Most earlier versions of Advanced Calibration contain the `Compatibility` command. For example, `AdvCal_2021.06.fps` contains the command `Compatibility 2021.06`, which applies the default parameters and model settings of Sentaurus Process Version S-2021.06 before setting the Advanced Calibration models and parameters.

Combining Advanced Calibration S-2021.06 and T-2022.03

Changes in the Advanced Calibration parameter files offer improved accuracy or usability. For backward compatibility, older versions of the Advanced Calibration set of models and parameters can still be loaded in Sentaurus Process Version T-2022.03.

Sometimes, you might want to take advantage of only selected parameter updates. This section explains how you can do this.

Changes in Advanced Calibration From S-2021.06 to T-2022.03

Two changes have been made in `AdvCal_2022.03.fps` with respect to the previous Advanced Calibration file:

1. The calibration of Sentaurus MC for ion implantation has been updated for high-energy B and P implantation, for the following energies:
 - B implantation at room temperature for energies higher than 400 keV

Chapter 1: Using Advanced Calibration File of Sentaurus Process

Combining Advanced Calibration S-2021.06 and T-2022.03

- B implantation at other temperatures for energies higher than 130 keV
- P implantation for energies higher than 343 keV

The corresponding parameter changes are all implemented in the callback procedures `_AdvCal::ImpPreProcess` and `_AdvCal::MCPostProcess` (section 3.6 of `AdvCal_2022.03.fps`) as well as `AdvancedThermalImpPreProcess` (section 3.2.4.1 of `AdvCal_2022.03.fps`).

The new calibration benefits from Sentaurus Process Version T-2022.03, which offers an expanded energy range of scattering tables used to calculate binary collisions. Using these new tables is switched on by a new parameter, which has the default value 1 in Sentaurus Process. For example:

```
pdbSet MCImplant HighE.Scatter.Table 1
```

In `AdvCal_2022.03.fps`, the new scattering tables are selected for all species except for H and He.

2. Oxidation rates for N₂O ambient have been calibrated against hardware data. The corresponding parameters are included in section 2.11.4 and (as part of `AdvancedNitrogenModel`) section 4.9.3 of `AdvCal_2022.03.fps`.

Also related to N₂O oxidation, the Sentaurus Process parameters `c0.1` and `c0.h`, which scale the oxidation rate enhancement for very thin oxides, have changed from Version S-2021.06 to Version T-2022.03, for N₂O ambient and surfaces with <111> crystal orientation.

Using Selected Improvements of Advanced Calibration T-2022.03

This section discusses the changes previously mentioned.

Improved Calibration for MeV Implantation With Sentaurus MC

To use only the improved calibration for MeV Monte Carlo (MC) implantation, while keeping the Advanced Calibration S-2021.06 parameters for N₂O oxidation, the following approach is the simplest:

1. Load Advanced Calibration T-2022.03.
2. Revert parameters for N₂O oxidation to the values used in S-2021.06.

This can be achieved by the following code lines:

```
AdvancedCalibration 2022.03  
N2O_Oxidation_Defaults  
solution name = Nitrogen nosolve store
```

Chapter 1: Using Advanced Calibration File of Sentaurus Process

Combining Advanced Calibration S-2021.06 and T-2022.03

```
pdbSet Oxide_Silicon      N2O 111 C0.1 3.98e-2
pdbSet Oxide_Silicon      N2O 111 C0.h 3.98e-2
pdbSet GeOxide_Germanium N2O 111 C0.1 3.98e-2
pdbSet GeOxide_Germanium N2O 111 C0.h 3.98e-2
pdbSet Germanium_Oxide   N2O 111 C0.1 3.98e-2
pdbSet Germanium_Oxide   N2O 111 C0.h 3.98e-2
```

The procedure `N2O_Oxidation_Defaults` is implemented in `AdvCal_2022.03.fps`. It reverts parameters to the default values of Sentaurus Process, T-2022.03, and sets the solution Nitrogen to solve. For consistency with Advanced Calibration S-2021.06, Nitrogen must be set to nosolve.

The last six lines set the parameters `C0.1` and `C0.h` to (very high) values, which were the default in Sentaurus Process S-2021.06. (In T-2022.03, these values were reduced by a factor of 100.)

In process simulations where `AdvancedNitrogenModel` is used, in addition to the previous code lines, insert the following lines after the command `AdvancedNitrogenModel`, to revert to the behavior of S-2021.06:

```
pdbSetDouble Ox_Si N2O 100 N.Thin.Max 1.55e14
pdbSetDouble Ox_Si N2O 110 N.Thin.Max 1.55e14
pdbSetDouble Ox_Si N2O 111 N.Thin.Max 1.55e14
pdbSetDouble Ge_Ox N2O 100 N.Thin.Max 1.55e14
pdbSetDouble Ge_Ox N2O 110 N.Thin.Max 1.55e14
pdbSetDouble Ge_Ox N2O 111 N.Thin.Max 1.55e14
```

Improved Calibration for Oxidation in N₂O Ambient

To use only the improved calibration for N₂O oxidation, while keeping the choice of models and parameters for high-energy implantation from Advanced Calibration S-2021.06, do the following:

1. Load Advanced Calibration S-2021.06.
2. Set the parameters for N₂O oxidation, as calibrated for Advanced Calibration T-2022.03.

This can be achieved by the following code lines:

```
AdvancedCalibration 2021.06

pdbSet Ox_Si N2O 100 L0.1 1.72e-6
pdbSet Ox_Si N2O 100 L0.h 1.72e-6
pdbSet Ox_Si N2O 100 LW.1 0.3
pdbSet Ox_Si N2O 100 LW.h 0.3
pdbSet Ox_Si N2O 100 C0.1 3.522
pdbSet Ox_Si N2O 100 C0.h 3.522
pdbSet Ox_Si N2O 100 CW.1 2.062
pdbSet Ox_Si N2O 100 CW.h 2.062

pdbSet Ox_Si N2O 110 L0.1 1.72e-6
```

Chapter 1: Using Advanced Calibration File of Sentaurus Process

Advanced Calibration File for Kinetic Monte Carlo Simulations

```
pdbSet Ox_Si N2O 110 L0.h 1.72e-6
pdbSet Ox_Si N2O 110 LW.l 0.3
pdbSet Ox_Si N2O 110 LW.h 0.3
pdbSet Ox_Si N2O 110 C0.l 3.522
pdbSet Ox_Si N2O 110 C0.h 3.522
pdbSet Ox_Si N2O 110 CW.l 2.062
pdbSet Ox_Si N2O 110 CW.h 2.062

pdbSet Ox_Si N2O 111 L0.l 8.6e-8
pdbSet Ox_Si N2O 111 L0.h 8.6e-8
pdbSet Ox_Si N2O 111 LW.l 0.0
pdbSet Ox_Si N2O 111 LW.h 0.0
pdbSet Ox_Si N2O 111 C0.l 42.269
pdbSet Ox_Si N2O 111 C0.h 42.269
pdbSet Ox_Si N2O 111 CW.l 2.229
pdbSet Ox_Si N2O 111 CW.h 2.229

pdbSet GeOxide_Germanium N2O 111 C0.l 3.98e-4      ;# T-2022.03
pdbSet GeOxide_Germanium N2O 111 C0.h 3.98e-4      ;# default values.
pdbSet Germanium_Oxide   N2O 111 C0.l 3.98e-4
pdbSet Germanium_Oxide   N2O 111 C0.h 3.98e-4

pdbSetDouble Ox_Si N2O 100 N.Thin.Max 1.0e30
pdbSetDouble Ox_Si N2O 110 N.Thin.Max 1.0e30
pdbSetDouble Ox_Si N2O 111 N.Thin.Max 1.0e30
pdbSetDouble Ge_Ox N2O 100 N.Thin.Max 1.0e30
pdbSetDouble Ge_Ox N2O 110 N.Thin.Max 1.0e30
pdbSetDouble Ge_Ox N2O 111 N.Thin.Max 1.0e30
```

Advanced Calibration File for Kinetic Monte Carlo Simulations

An Advanced Calibration file is available for simulations with the kinetic Monte Carlo mode of Sentaurus Process. The use and contents of this file are described in [Chapter 5 on page 213](#) and [Chapter 6 on page 216](#).

Sentaurus Workbench Splits: Saving in TDR Format

Note:

This section is intended for users of Advanced Calibration Version D-2010.03 or earlier.

Sentaurus Process can be used within Sentaurus Workbench projects. If split commands of Sentaurus Workbench are used inside the input file of Sentaurus Process, at each split command, the structure with all the data fields is saved in a TDR format file. In a subsequent tool instance, the process simulation starts by loading the previously saved structure.

Chapter 1: Using Advanced Calibration File of Sentaurus Process

Sentaurus Workbench Splits: Saving in TDR Format

Sentaurus Process does not always save and load the *complete* status of the process simulation. In particular, the definitions of Aligator terms and solution commands are only saved in TDR format if the keyword `store` is used in the term definition command lines, and Tcl procedures are only saved if they have been defined by the command `fproc` (rather than `proc`). Furthermore, entries in the parameter database are only saved if the TDR format is used for saving and loading.

The Advanced Calibration file contains the definitions of terms and procedures. In the latest file, the definitions of terms, solutions, and procedures are performed in such a way that they are saved to the TDR format and are reloaded. No additional attention is needed.

In an earlier version of the file (`AdvCal_2010.03.fps`), a series of terms inside the procedure `SiGe_and_Stress_Effect` was modified with the command `MultiplyTerm`. Since `AddToTerm`, `SubFromTerm`, and `MultiplyTerm` modify terms without the keyword `store`, the corresponding term modifications were not stored in the TDR format. Therefore, the command `MultiplyTerm` is no longer used in newer versions of Advanced Calibration.

In early versions of the Advanced Calibration files (`AdvCal_2007.12.fps` and before), the definitions of terms and procedures are not saved. Therefore, when using these versions of Advanced Calibration files, you must ensure that the files are loaded at the beginning of each part of a split process simulation.

2

Advanced Calibration for Silicon, SiGe, and Germanium

This chapter explains how to use Advanced Calibration of Sentaurus Process for silicon, silicon germanium (SiGe), and germanium and documents the origin of the parameter values.

The focus of Advanced Calibration is monocrystalline silicon, germanium, and SiGe for all Ge mole fractions. The calibration for silicon and SiGe with low Ge mole fraction (≤ 0.5) is the most mature and reliable. On the other hand, the one for pure Ge is less mature and reliable, and the one for SiGe with high Ge mole fraction (> 0.5) is the least mature and reliable. Many model equations and model parameters are taken from reliable publications. In addition, a rigorous calibration has been performed by Synopsys, based on a SIMS database.

The book *Intrinsic Point Defects, Impurities, and Their Diffusion in Silicon* by Pichler [1] is a good reference source for parameter values. It refers to more than 3000 scientific papers and gives a comprehensive overview of the experimental data available for the calibration of fundamental parameters for diffusion in silicon. For many relevant parameters, Pichler compares the results from many authors, which can be used to estimate the error bars of the parameter values.

The Advanced Calibration file `AdvCal_2022.03.fps` is divided into the following parts, which contain numbered sections and are executed in sequence:

- Part 1: Basic model switches
- Part 2: Constant parameters
- Part 3: Ion implantation and initial conditions
- Part 4: Comprehensive and slow models
- Part 5: Accelerating simulations for power technologies

Part 1: Basic Model Switches

In Sentaurus Process, Advanced Calibration covers several alternatives for diffusion and activation models. Some models are relatively simple, such as the `ChargedPair` model for dopant diffusion or the `Transient` activation of dopants. Other models are more sophisticated (for example, the `ChargedReact` model for dopant diffusion and the `ChargedCluster` model for dopant activation) but require more equations to be solved in the diffusion solver and, therefore, require more CPU time. These different models coexist in Advanced Calibration so that, in simple limiting situations (for example, in thermal equilibrium for low dopant concentration), different models give the same results. In more complex situations, for example, during transient-enhanced diffusion (TED), the more complex models will often give better results.

The best choice of fundamental models depends on the problem to be solved. Part 1 of the Advanced Calibration represents a choice that is recommended by Synopsys for most applications. For most devices, the modeling of TED and dopant activation is important, and it is necessary to use some models that describe the underlying physics accurately.

It is often useful to reduce the number of equations to be solved in order to save CPU time. On the other hand, it might be sometimes necessary to select models that are more sophisticated than the default choice, even at the cost of increasing the CPU time. In this chapter, the possible changes with respect to the default model switches are explained.

The most elegant way to change a basic model switch is adding a corresponding line at the beginning of a project-specific or user-specific calibration file, which is sourced after loading the Advanced Calibration file. In this way, you can track the differences to the default suggestions of Synopsys.

CPU time is an important issue for the process simulation of power device fabrication, which often includes a large number of thermal anneals. A summary of the methods to speed up the simulation of power device processes is given in [Additional Calibration for Power Technologies on page 189](#).

Part 4 of the Advanced Calibration file contains the procedure `AdvancedModels`, which offers an option to switch to a consistently calibrated set of complex models for dopant and defect clustering with a single command line. This option is recommended for fundamental research and also can be considered to be used in very advanced CMOS technology. It is described in [Part 4: Comprehensive and Slow Models on page 94](#).

Diffusion Models in Silicon and Germanium

See section 1.1 of `AdvCal_2022.03.fps`.

The default choice is the pair diffusion model `ChargedPair`. The dopants diffuse only through dopant-defect pairs, where defects can be either interstitials or vacancies. All

Chapter 2: Advanced Calibration for Silicon, SiGe, and Germanium

Part 1: Basic Model Switches

charge states of defects and dopant-defect pairs are taken into account, and the concentration of pairs is assumed to be in local equilibrium with unpaired dopants and defects.

A more sophisticated alternative is the `ChargedReact` model, a so-called five-stream model. It is widely used for process simulation of deep-submicron devices and is selected by:

```
pdbSet Si Dopant DiffModel ChargedReact
```

Here, the diffusion of dopants is simulated through dopant-defect pairs. In contrast to the `ChargedPair` model, the simplifying assumption of local equilibrium between pairs and unpaired dopants is omitted. Instead, the kinetics of pair formation and dissolution is taken into account. This model needs more CPU time than the `ChargedPair` model, because additional equations need to be solved for each dopant. It is possible to select the `ChargedReact` model individually for some dopants. For example, it might be reasonable to select it only for boron but not for other dopants. This can be performed by adding the line:

```
pdbSet Si Boron DiffModel ChargedReact
```

It is possible to use the `ChargedReact` model for some dopants and the `ChargedPair` model for all other dopants. In contrast, it is not recommended to mix the `ChargedFermi` model with either of the `ChargedReact` or `ChargedPair` model, because the treatment of point defects would become inconsistent.

Dopant Cluster Models in Silicon and Germanium

See section 1.2 of `AdvCal_2022.03.fps`.

These models govern the dopant activation during thermal annealing. The simplest and fastest model is `None`, which means that there are no dopant clusters. This model is recommended for dopants for which clustering has no influence. This is typically the case when the maximum concentration of a dopant is far below the solid solubility. For example, in an NMOS simulation with a very low indium dose for the channel implantation (for example, 10^{12} cm^{-2}), it is reasonable to set the indium activation model to `None`, to speed up the simulation.

For the dopant impurities boron, indium, arsenic, phosphorus, and antimony in silicon as well as for the dopant impurities boron, arsenic, phosphorus, antimony, and carbon in germanium, the activation model `Transient` is used as the default. In this model, dopants can be bound in clusters, which consist only of dopants of one species. The equilibrium distribution of dopants into clusters and substitutional impurities is governed by the solid `Solubility`; the rate at which the equilibrium is reached is governed by the parameter `CluRate`. Both `Solubility` and `CluRate` are Arrhenius-type constants with individual parameters for each dopant.

For boron, the equations of the `Transient` cluster model are modified to take into account the role of interstitials in the cluster formation (see [Boron Clustering on page 41](#)).

Chapter 2: Advanced Calibration for Silicon, SiGe, and Germanium

Part 1: Basic Model Switches

Special models exist for boron, arsenic, phosphorus, indium, carbon, and fluorine clustering in silicon.

Boron can form so-called boron–interstitial clusters (BICs) together with silicon interstitials. BICs exist in various sizes, as $B_m I_n$ ‘molecules’ inside silicon, which grow or evaporate by the incorporation or emission of silicon interstitials or boron-interstitial pairs.

The BIC model can be selected by using:

```
pdbSet Si Boron ActiveModel ChargedCluster
```

The BIC model is not used by default because the solution of individual equations for all BICs is numerically expensive and, on average, the simpler

Boron ActiveModel Transient model provides slightly better overall accuracy.

Furthermore, the BIC model should only be used in combination with the Full model for interstitial clusters, which uses more equations than the 1Moment model for interstitial clusters, which is the Advanced Calibration default. The recommended way to use the BIC model is to execute the procedure AdvancedModels defined in part 4 of the Advanced Calibration file (see [Part 4: Comprehensive and Slow Models on page 94](#)).

To model very high phosphorus concentrations, which are present after highly strained SiP (HSSiP) epitaxy or after ultralow-energy P implantation, you can use a second type of P cluster, P_7I , which forms and dissolves in addition to the P_3 clusters present in the Transient model. P_7I clusters describe that large and very stable P clusters (or P precipitates) can form at extremely high concentrations of P. For HSSiP processes, the formation of large P_7I clusters is responsible for the relaxation of tensile strain associated with substitutional P and small P clusters. You can switch on P_7I clusters in addition to the Transient model for P by using:

```
Use_P7I
```

The equations for cluster formation and dissolution are implemented inside the Advanced Calibration file (see [Phosphorus Clusters on page 49](#)).

Arsenic and phosphorus can form clusters together with point defects, which are so-called arsenic–vacancy (As–V), phosphorus–vacancy (P–V), and phosphorus–interstitial (P–I) clusters. To take these into account, you can switch on the ChargedCluster model for silicon using:

```
pdbSet Si Arsenic ActiveModel ChargedCluster  
pdbSet Si Phosphorus ActiveModel ChargedCluster
```

In the case of arsenic, a family of four different As–V clusters and pure As clusters will form. In the case of phosphorus, two different P–V clusters, one pure P cluster, and one P–I cluster are modeled. The models can be used with both the 1Moment and Full models for interstitial clusters. The formation and dissolution of As–V, P–V, and P–I clusters change the local concentration of silicon point defects (interstitials and vacancies).

Chapter 2: Advanced Calibration for Silicon, SiGe, and Germanium

Part 1: Basic Model Switches

The older `Cluster` model, in which As_4V is the only type of As cluster, is not recommended to be used, as it sometimes overestimates the impact of As-cluster formation and dissolution on the point-defect concentration in silicon. Instead, the default choice for As clustering is the `Transient` model, in which As_3 is the only As cluster and which is easy to understand and calibrate.

The activation model `ChargedCluster` can also be applied to simulate formation of indium clusters. This model is invoked in the procedure `AdvancedModels` (see [Part 4: Comprehensive and Slow Models on page 94](#)).

Carbon can form carbon–interstitial clusters in silicon, with a similar reaction chain as for BICs. The formation of carbon–interstitial clusters is activated by:

```
pdbSet Si Carbon ActiveModel NeutralCluster
```

Solving a transient equation for the formation and dissolution of Ge–B pairs in silicon is not considered necessary. Instead, in cases where the chemical effect of Ge on B diffusion must be taken into account, you can select a calibrated modification of B diffusivity in the presence of germanium by using the following line immediately after sourcing the Advanced Calibration file:

```
SiGe_and_Stress_Effect 1 1 1 0
```

This is explained in [Effect of Germanium and Stress on page 60](#).

Defect Cluster Models in Silicon and Germanium

See section 1.3 of `AdvCal_2022.03.fps`.

For silicon and germanium, interstitial clustering is described by the `1Moment` cluster model. In this model, the capturing and release of interstitials from $\{311\}$ defects is described according to a publication by Rafferty *et al.* [2]. This model uses only a single equation to describe the time evolution of interstitial clusters and is considered a good compromise between accuracy and computation speed.

A complex silicon interstitial-clustering model, including small interstitial clusters, $\{311\}$ defects, and dislocation loops, is used in the `AdvancedModels` set and described in [Interstitial Clusters on page 95](#).

Vacancy clusters are not simulated by default in Advanced Calibration because their modeling is not needed for regular processes. If vacancy clusters are relevant, for example, in processes that include vacancy engineering, that is, the creation of a vacancy-rich region by high-energy implantation, you have the option of three different models for vacancy clusters in silicon.

The simplest model is switched on by:

```
pdbSet Si Vac ClusterModel 1Moment
```

Chapter 2: Advanced Calibration for Silicon, SiGe, and Germanium

Part 1: Basic Model Switches

In this case, the nucleation, growth, and dissolution of vacancy clustering are modeled with arbitrary calibrated parameters, which is analogous to the standard model for interstitial clusters.

A more comprehensive model as proposed in the ATOMICS research project [3] is activated by:

```
pdbSet Si Vac ClusterModel Full
```

By default, if the `Full` model is selected for vacancy clusters, Sentaurus Process will solve seven equations for small vacancy clusters (V_2 – V_8), with calibrated parameters including binding energies based on *ab initio* simulations [3].

For numeric efficiency, an alternative calibration of the `Full` model using fewer equations can be selected by using:

```
pdbSet Si Vac ClusterModel      Full
pdbSet Si Vac MultiClusterModel Full {2Moment}

pdbSetDouble      Si Vac CL.Size 3
pdbSetDoubleArray Si V3 kfV { 0 {[expr 4*3.1415*2.97e-8*[pdbGet \
    Si Vac D 0]]} }
pdbSetDoubleArray Si V3 krV { 0 0 }
pdbSetDoubleArray Si V3 kfI { 0 0 }
pdbSetDoubleArray Si V3 krI { 0 0 }
```

In this case, one equation for the small vacancy clusters V_2 and two equations for the voids (`DVoid` for the concentration of V-clusters, and `CVoid` for the total concentrations of vacancies in these clusters) are solved with arbitrary calibrated parameters.

Poisson Equation

See section 1.4 of `AdvCal_2022.03.fps`.

In Advanced Calibration, the Poisson equation for the electrical potential is solved for both silicon and germanium. Alternatively, you can switch off the Poisson equation with the command:

```
pdbSetBoolean Si Potential Poisson 0
```

In this case, local charge neutrality is assumed and the number of partial differential equations is reduced by one. In most situations, local charge neutrality gives approximately the same results as the Poisson equation. At p-n junctions, the assumption of charge neutrality gives a sharper peak of the electric field than the Poisson equation, which results in slightly sharper kinks of dopant profiles at p-n junctions.

Modern submicron CMOS devices have very thin dielectrics. Therefore, the electrostatic interaction between the gate and the channel region in such devices is strong. This interaction results in the presence of an additional potential at semiconductor surfaces

Chapter 2: Advanced Calibration for Silicon, SiGe, and Germanium

Part 1: Basic Model Switches

(under the gate) and strong electric fields in the semiconductor near semiconductor–oxide interfaces. To take this electrostatic interaction into account, the Poisson equation with proper boundary conditions can be solved in all materials, including dielectrics, especially under the gate [4]. Ideally, also quantum corrections to the distribution of electrons and holes can be taken into account in the simulation [4]. These effects, with a small but noticeable impact on CMOS device characteristics [4], are not included in Advanced Calibration for Sentaurus Process.

Channeling Dose in Analytic Implantations

See section 1.5 of `AdvCal_2022.03.fps`.

For analytic implantations, the switch `ChanDoseInterpolation` 1 selects the correct method of interpolation of the ion-channeling dose between the tabulated values of the `Default` tables.

The coimplantation model [5] for damage accumulation is switched on. This model provides a description of ion channeling for successive ion implantations.

Boundary Conditions

See section 1.6 of `AdvCal_2022.03.fps`.

In the pair diffusion model, the segregation of dopants at silicon and germanium surfaces involves the capture or creation of dopant–defect pairs at the silicon side of the interface.

In the pair segregation model used in Advanced Calibration, when a dopant–defect pair diffuses to an interface between semiconductor and another material, the dopant can enter the other material (or, for three-phase segregation, the interface layer), whereas the point defect remains on the semiconductor side of the interface.

The following selection means that the point defect released can have any charge state (and not only a neutral charge state):

```
pdbSet Ox_Si Boundary UseUnpairedTotalInt 1  
pdbSet Gas_Si Boundary UseUnpairedTotalInt 1  
pdbSet Nit_Si Boundary UseUnpairedTotalInt 1
```

Similarly, for the opposite segregation reaction, when a dopant–defect pair is formed at the silicon side of the interface, a point defect with any charge state can be consumed at the silicon side of the interface.

As a consequence of this selection, the time at which segregation equilibrium is reached in highly doped regions, where most point defects are charged, is decreased. The segregation equilibrium itself is not affected. Although the name of the Boolean parameter is `UseUnpairedTotalInt`, the selection is applied to both interstitials and vacancies.

Chapter 2: Advanced Calibration for Silicon, SiGe, and Germanium

Part 1: Basic Model Switches

The selection:

```
pdbSetSwitch Ox_Si I Surf.Recomb.Vel Normalized
```

and the corresponding lines for vacancies and other interfaces allow the generation and recombination of point defects at silicon surfaces in all charge states.

For B, As, and P at Si–SiO₂, Si–Si₃N₄, Ge–SiO₂, and Ge–GeO₂ interfaces, the three-phase segregation model is the default in Advanced Calibration. For In and Sb, the simpler segregation model is the default.

Numeric Solver

See section 1.7 of `AdvCal_2022.03.fps`.

By default, the direct solver PARDISO is used for 1D and 2D simulations, and the iterative solver ILS is used for 3D simulations. For better performance, Advanced Calibration selects ILS to solve the linear systems also in 2D. Specific parameters can be set for ILS in 2D. While `nd` is selected by default for `ILS.symmOrdering` as the optimum for multithreaded calculations, you should consider switching to `mmd` for single-thread calculations.

Summary of Model Switches

[Table 2](#) and [Table 3 on page 34](#) summarize the default model switches and all the alternatives supported by Advanced Calibration. For all supported model switches, the corresponding calibrated parameters are included in the Advanced Calibration file (`AdvCal_2022.03.fps`) and are ready to be applied automatically when alternative models are selected. The procedure `AdvancedModels`, which switches on several more complex models at the same time, is explained in [Part 4: Comprehensive and Slow Models on page 94](#).

Table 2 Model switches for silicon in Advanced Calibration

Model	Default	Supported alternatives
<code>pdbSet Si Dopant DiffModel</code>	<code>ChargedPair</code>	<code>ChargedReact</code> ¹
<code>pdbSet Si Boron ActiveModel</code>	<code>Transient</code>	<code>None</code>
<code>pdbSet Si Indium ActiveModel</code>	<code>Transient</code>	<code>None</code>
<code>pdbSet Si Arsenic ActiveModel</code>	<code>Transient</code>	<code>None, ChargedCluster</code>
<code>pdbSet Si Phosphorus ActiveModel</code>	<code>Transient</code>	<code>None, ChargedCluster</code>

Chapter 2: Advanced Calibration for Silicon, SiGe, and Germanium

Part 1: Basic Model Switches

Table 2 Model switches for silicon in Advanced Calibration (Continued)

Model	Default	Supported alternatives
pdbSet Si Antimony ActiveModel	Transient	None
pdbSet Si Germanium ActiveModel	None	
pdbSet Si Carbon ActiveModel	NeutralCluster	None
pdbSet Si Int ClusterModel	1Moment	
pdbSet Si Vac ClusterModel	None	1Moment, Full
pdbSet Si Potential Poisson	1	0
pdbSet ImplantData UseCoImplant	1	0
pdbSet Ox_Si Boundary Use UnpairedTotalInt 1		

1. If the basic choice is ChargedPair, it is possible to select ChargedReact for individual dopants.

Table 3 Model switches for germanium in Advanced Calibration

Model	Default	Supported alternatives
pdbSet Ge Dopant DiffModel	ChargedPair	ChargedReact ¹
pdbSet Ge Boron ActiveModel	Transient	None
pdbSet Ge Arsenic ActiveModel	Transient	None
pdbSet Ge Phosphorus ActiveModel	Transient	None
pdbSet Ge Antimony ActiveModel	Transient	None
pdbSet Ge Carbon ActiveModel	Transient	None
pdbSet Ge Int ClusterModel	1Moment	None
pdbSet Ge Vac ClusterModel	None	
pdbSet Ge Potential Poisson	1	0

Chapter 2: Advanced Calibration for Silicon, SiGe, and Germanium

Part 2: Constant Parameters

Table 3 Model switches for germanium in Advanced Calibration (Continued)

Model	Default	Supported alternatives
pdbSet ImplantData UseCoImplant	1	0
pdbSet GeOx_Ge Boundary UseUnpairedTotalInt 1		

1. If the basic choice is ChargedPair, it is possible to select ChargedReact for individual dopants.

Part 2: Constant Parameters

This part of the Advanced Calibration file contains the parameters for the diffusion and reaction equations, which are set at the beginning of the process simulation and remain valid for all process steps until the end of the simulation. The parameters are set for all alternatives listed in [Table 2 on page 33](#). This allows you to select any of the alternatives models with all corresponding parameters by using a single command line, which can be ideally placed in a user calibration file, which is sourced immediately after sourcing `AdvCal_2022.03.fps`.

Many parameters are taken from either the literature or carefully designed experiments or the publication by Pichler [1], which gives an outstanding, comprehensive overview on the publications of impurity diffusion and activation in silicon. Other parameters have been calibrated or numerically optimized based on the SIMS database of Synopsys.

In brief, parameters for pure Si and pure Ge are set in sections 2.1–2.12. Section 2.13 deals with the choice of implant tables, and section 2.14 contains parameters for SiGe and strained Si. Section 2.15 contains parameters for mechanics.

In the Advanced Calibration models for SiGe, it is assumed that germanium is treated as an impurity in the material Silicon. The material `SiGe` should not be used in process simulations with Advanced Calibration. To take into account the impact of Ge and strain in Si, use the `SiGe_and_Stress_Effect` procedure (see [Effect of Germanium and Stress on page 60](#)).

In some processes, Ge is deposited or grown directly on Si. This results in a Ge–Si material interface. The difference in lattice constants induces very high strain. For the process modeling with Advanced Calibration, the following should be noted:

- You should not use Ge material adjacent to Si material. Ge–Si interfaces should be avoided in process simulations because the transport of dopants and defects across the Ge–Si interface is described incorrectly. In addition, for the material Ge, some of the strain effects on dopants and the band gap are not switched on in the procedure `SiGe_and_Stress_Effect`, because the calibration for pure Ge is based on hardware data measured on unstrained Ge wafers.

Chapter 2: Advanced Calibration for Silicon, SiGe, and Germanium

Part 2: Constant Parameters

- The best way to handle such structures with Advanced Calibration is to introduce the material Germanium as Silicon with 100% Ge mole fraction. In that case, Si and Ge are considered a single material without a material interface. The models contained in SiGe_and_Stress_Effect can be used, and point-defect transport as well as dopant segregation due to gradients of Ge mole fraction or pressure can be described correctly by the equations in the bulk.
- There might still be challenges:
 - Strains are very high (up to 4 GPa). It is not clear if the calibration holds for such high values.
 - Strain relaxation is likely to occur. In reality, this occurs by the formation of dislocations, which might have side effects, for example, on point defects. However, strain relaxation and the impact of the corresponding dislocations are not captured by the models of Advanced Calibration.

Model parameters, which depend on particular ion implantation steps, are included in the third part of the Advanced Calibration file and are described in [Part 3: Ion Implantation and Initial Conditions on page 78](#). Examples of these are the number of point defects generated by ion implantation, which can depend on the implantation conditions.

Basic Point-Defect Parameters

See section 2.1 of `AdvCal_2022.03.fps`.

The bulk parameters for interstitials and vacancies (sections 2.1.1–2.1.3 of `AdvCal_2022.03.fps`) are the most fundamental parameters in the pair diffusion model. They have been carefully selected from the literature. Any change affects not only the diffusion of point defects, but also the diffusion of all dopant species that diffuse in dopant-defect pairs. Changing the point-defect parameters with every new technology calibration would make it difficult to compare the results of different calibration projects. Therefore, it is strongly recommended that these parameters are *not* changed in any way.

To some extent, this is also true for the surface boundary conditions (BCs) for point defects (section 2.1.4 of `AdvCal_2022.03.fps`). Changing them will affect the calibration of all models for TED and the diffusion of all dopants. However, the BCs depend on the capping material and the local concentration of impurities. For polysilicon and oxynitride, the BCs can depend on the details of the process flow. Therefore, in practice, the surface recombination lengths of point defects can be considered to be calibration parameters for the fine-tuning of process simulation. See [Boundary Conditions for Point Defects on page 38](#).

Oxidation and nitridation cause the injection of interstitials and vacancies, respectively, at the exposed surface. A calibration of interstitial injection has been performed for dry oxidation. For nitridation and wet oxidation, the surface boundary conditions for point

Chapter 2: Advanced Calibration for Silicon, SiGe, and Germanium

Part 2: Constant Parameters

defects are less reliable than for inert atmosphere and can be considered to be calibration parameters for the fine-tuning of diffusion processes.

Bulk Parameters for Free Interstitials

See section 2.1.1 of `AdvCal_2022.03.fps`.

For silicon, the diffusivity of interstitials D_i is taken from Bracht *et al.* [6]. The equilibrium concentration C_{star} is chosen such that the product $D_i * C_{\text{star}}$ has the value $1.59 \times 10^{-25} \times \exp(-4.702 \text{ eV}/kT) \text{ cm}^{-1} \text{ s}^{-1}$. This is a reasonable compromise between conflicting suggestions in the literature [1][7][8] and is in acceptable agreement with various ‘clean’ data on silicon isotope diffusion and dopant diffusion in silicon that has been published [6][8][9]. The same value for $D_i * C_{\text{star}}$ was also used in [10].

The charge distribution for free interstitials and vacancies was taken from `method.advanced` of the Synopsys Taurus™ TSUPREM-4™ process simulator and is based on various publications [11][12][13]. During calibration, a small change with respect to the TSUPREM-4 parameters has been introduced for the relative abundance of negatively charged vacancies.

For germanium, there is a lack of experimental data on self-interstitial properties. For the diffusivity D_i of interstitials in germanium, a migration energy of 1.6 eV is assumed, which is 0.4 eV higher than calculation results for uncharged interstitials published by Vanhellemont *et al.* [14]. The equilibrium concentration C_{star} is estimated based on the formation energy (2.78 eV), which is 0.4 eV less than the calculated value of Vanhellemont *et al.* [15]. This choice is partially motivated by the parameter choice for pure silicon, where the activation energy for high-temperature interstitial migration, derived from experiments by Bracht [6], is higher than the value calculated with *ab initio* methods. For simplicity, the prefactors for the diffusivity and the equilibrium concentration have the same values as in silicon.

Bulk Parameters for Free Vacancies

See section 2.1.2 of `AdvCal_2022.03.fps`.

For silicon, the diffusivity of vacancies D_v is taken from [6]. The equilibrium concentration C_{star} is chosen such that $D_v * C_{\text{star}}$ corresponds to the value from [6] at 1014.25°C. The activation energy for $D_v * C_{\text{star}}$ (4.14 eV) is taken from [7].

For germanium, the equilibrium concentration of vacancies C_{star} is based on [14], but with the formation energy reduced by 0.4 eV. The diffusion barrier of vacancies D_v is derived from the vacancy equilibrium concentration and the experimental vacancy-mediated self-diffusion coefficient of germanium ($13.6 \times \exp(-3.09 \text{ eV}/kT) \text{ cm}^{(-2)} \text{ s}^{-1}$) following [16]. The resulting migration barrier is 1.14 eV.

Bulk Recombination of Point Defects

See section 2.1.3 of `AdvCal_2022.03.fps`.

It is assumed that the bulk recombination is diffusion limited. Furthermore, the recombination of interstitials and vacancies, which are both positively or both negatively charged, is assumed to be suppressed by electrostatic repulsion. In regions of high phosphorus doping, the rate of I–V recombination increases as a function of substitutional phosphorus (`PActive`).

Boundary Conditions for Point Defects

See section 2.1.4 of `AdvCal_2022.03.fps`.

Natural boundaries for both vacancies and interstitials are assumed. The surface recombination length is 1 nm for Si–SiO₂, Ge–SiO₂, and Ge–GeO₂ boundaries. Therefore, point-defect recombination is very fast at interfaces to oxide. This has been found to work well for many experimental conditions.

At Si–SiN boundaries, the surface recombination length for interstitials and vacancies is set to 10 nm. This value has not been calibrated, because there is a lack of data. Therefore, the value can be considered for fine-tuning process simulation results in devices that include Si–SiN boundaries.

Gas–silicon and gas–germanium boundaries are used only during epitaxy. In all other thermal process steps, bare silicon and germanium surfaces should be covered by a thin native oxide, which is needed for modeling dose loss. At gas–Si and gas–Ge boundaries, a surface recombination length of 1 nm is assumed for interstitials and vacancies. For vacancies, it is not fully clear from experiments whether this is correct. The corresponding parameter `Ksurf` can be considered for fine-tuning dopant diffusion during epitaxy. For further discussion, see [Surface Boundary Conditions on page 138](#).

Oxidation-Enhanced Diffusion

See section 2.1.5 of `AdvCal_2022.03.fps`.

During oxidation, there is an additional flux of interstitials into silicon. The rate of interstitial injection by oxidation is proportional to the parameter `theta` and depends on the velocity `v` of the moving Si–SiO₂ interface and the electron concentration at the silicon side of the interface by the factor:

$$v^{(1 + Gpow)} \times \frac{mm + m + 1 + p + pp}{mm \times (n/n_i)^2 + m \times (n/n_i) + 1 + p \times (n/n_i)^{-1} + pp \times (n/n_i)^{-2}} \quad (1)$$

where `theta`, `Gpow`, `mm`, `m`, `p`, and `pp` are defined in `AdvCal_2022.03.fps`.

Chapter 2: Advanced Calibration for Silicon, SiGe, and Germanium

Part 2: Constant Parameters

For dry oxidation of silicon, the values of `theta` and `Gpow` at `Oxide_Silicon` were calibrated with experimental data from [17] and [18] for low-doped silicon. For wet atmosphere (partial pressure of $H_2O > 0$), a smaller value of `theta` has been calibrated from corresponding SIMS data. `theta` is frequently adjusted for fine-tuning OED. The values of `mm`, `m`, `p`, and `pp` have been calibrated with data from ultrashallow junction (USJ) formation in dry, oxidizing atmosphere. They can be modified for the purpose of fine-tuning OED for high surface doping.

Note:

The reference [17] includes data for oxidation-enhanced diffusion (OED) of P and B. A higher diffusion enhancement was reported for P than for B, which was ascribed to a 20% vacancy component of boron diffusion. Recent experiments indicate that the vacancy component for B diffusion should be much less than 20% (for an overview, see [1]). Therefore, instead of ascribing the lower OED of boron to diffusion of B–V pairs, the calibration of `theta` with data from [17] was performed under the assumption that the observed difference between the OED of P and B was mainly due to experimental inaccuracies. Giving equal weight to the P and B data, Synopsys obtained a 10% reduction of `theta` with respect to using only the P data for the extraction of `theta`.

Interstitial injection during dry oxidation appears to be suppressed in the case of high mole-fraction SiGe [19]. Therefore, the value of `theta` at `Oxide_Germanium`, the upper mole-fraction limit for SiGe– SiO_2 interfaces, is set to a five orders of magnitude lower value for oxidation in general compared to the value at `Oxide_Silicon` for dry oxidation. For the calibration of oxidation of SiGe for all mole fractions, see [SiGe Oxidation on page 68](#).

Note:

No calibration parameters for germanium OED are included in Advanced Calibration. By default, no interstitial injection at `GeOxide_Germanium` is assumed.

In addition to interstitial injection into silicon, the boundary condition for vacancies at the moving Si– SiO_2 interface during oxidation is altered. The equilibrium concentration of vacancies defined for the moving interface is lower compared to the bulk. This effect is implemented by the term `VacInterfaceCStarFactorOED` and is calibrated based on dopant SIMS and SiGe interdiffusion profiles of oxidation experiments.

Transient-Enhanced Diffusion

See section 2.2 of `AdvCal_2022.03.fps`.

The model of Rafferty *et al.* [2] is used to simulate the evaporation of silicon interstitials from {311} defects. The reaction rates for the capture and evaporation of interstitials have been calibrated with transmission electron microscope (TEM) data on the dissolution of {311} defects published by Stolk *et al.* [20] and Saleh *et al.* [21].

Chapter 2: Advanced Calibration for Silicon, SiGe, and Germanium

Part 2: Constant Parameters

As an initial condition, it is assumed that all interstitials generated by ion implantation are bound in {311} clusters (`InitPercent=1.0`).

The selected model gives accurate results for the dissolution of {311} defects, as illustrated in [Figure 20 on page 140](#). However, note that the model is too simple to describe the initial phase of ultrahigh interstitial supersaturation after ion implantation, which was reported by Cowern *et al.* [9] and is ascribed to the formation and dissolution of small interstitial clusters, and which is illustrated in [Figure 10 on page 96](#). In addition, the model underestimates the stability of interstitial clusters in situations where dislocation loops form and where most of the excess interstitials are bound to dislocation loops rather than {311} defects. This might happen, for example, after amorphizing implantations into silicon, as illustrated in [Figure 11 on page 96](#).

In situations where TED is not governed by {311} defects, but rather by small clusters or dislocation loops, the model is less accurate. A more comprehensive model for silicon interstitial clusters has been calibrated by Zographos *et al.* [22]. This is switched on if you execute the procedure `AdvancedModels`, defined in part 4 of the Advanced Calibration file.

The model of Rafferty *et al.* [2] also is used to simulate the evolution of extended interstitial defects in germanium. The reaction rates for the capture and evaporation of interstitials have been calibrated [23] with experimental data from Napolitani *et al.* [24], where B diffusion events are correlated quantitatively with the measured positive strain associated with the end of range (EOR) damage.

Boron Diffusion and Activation

See section 2.3 of `AdvCal_2022.03.fps`.

Boron Diffusion Coefficient

Macroscopic values for boron diffusivity in silicon are based on the literature [1] and on comparison to SIMS data. The diffusion of boron is assumed to be only interstitial mediated:

```
pdbSetDoubleArray Si B Int D { 0 {[Arr 0.123 3.566]}  
                                1 {[Arr 3.00 3.640]}  
                                2 {[Arr 1.01 3.98]} }
```

The pairing constants have been derived from Synopsys' in-house density field theory (DFT) analysis of B–I binding energies. They are very small, meaning that the concentration of B–I pairs is always very small.

The migration distance of B–I pairs is close to the values proposed by Giles *et al.* [25] and is based on B marker layer diffusion data in the temperature range of 500°C–800°C. It is only relevant if the `ChargedReact` model is switched on for boron. In this case, the migration distance has an influence on the length of the tail of the profile.

Chapter 2: Advanced Calibration for Silicon, SiGe, and Germanium

Part 2: Constant Parameters

The Boolean switch `Kick.Out.Rate.Based.On.Lambda` is set to 1. With this setting, relevant only when the `ChargedCluster` model is selected, the average migration distance between formation and dissolution of B–I pairs equals the parameter `lambda`, unless you scale the kick-out reaction rate by the user-defined term `React<dopant><defect>Factor`. (With `Kick.Out.Rate.Based.On.Lambda` 0, which was the only option in Sentaurus Process Version K-2015.06 and earlier, this is not strictly the case in strained Si and SiGe, and in the presence of diffusion enhancement factors.)

To preserve backward compatibility for unstrained Si, the term `ReactBoronIntFactor` is defined as "`1.0/BoronDiffFactor`". In this way, the migration distance of B–I pairs in unstrained Si regions of high F concentration is the same as in `AdvCal_2015.06.fps`.

The macroscopic values for boron diffusivity in germanium are based on the literature [26], and the diffusion of boron is assumed to be only interstitial mediated [23]. For consistency with the diffusivity in silicon, a negligible contribution of $B^{-1^{++}}$ pairs is included as well. Boron undergoes very little intrinsic or transient-enhanced diffusion in germanium.

Effect of Fluorine

It is known that boron diffusion in silicon can be reduced by the presence of fluorine. The main reason for this is that F–V clusters, which form after ion implantation, catch excess interstitials, which are also present in silicon after implantation [27]. A complete physics-based model for the interactions between B, I, and F must be very complex, because F atoms are redistributed during solid phase epitaxial regrowth of amorphized layers. Instead, in the Advanced Calibration, a simpler approach is used by default.

It is assumed that F atoms are immobile after ion implantation and that the presence of F atoms reduces directly the diffusivity of B atoms by a factor (`BoronDiffFactor`), which depends on the F concentration. This factor is close to 1 for F concentrations smaller than 1×10^{20} and becomes important only for very high F concentrations. It has been calibrated by comparisons of USJ boron SIMS profiles, which were made by boron implantation and annealing, and BF_2 implantation and annealing, respectively. This simple approach is not very predictive. Since it assumes a local B–F interaction, it is not suitable to study USJ formation after Ge+F+B cocktail implantations.

A sophisticated F–V clustering model is available. The model is invoked by the procedures `AdvancedFluorineModel` and `AdvancedModels` (see [Part 4: Comprehensive and Slow Models on page 94](#)). This model describes the fluorine effect on boron diffusion in silicon more accurately.

For germanium, no effect of fluorine on boron diffusion is assumed.

Boron Clustering

The Transient cluster model is used for silicon and germanium. Four boron atoms form a cluster. For the solid solubility, two Arrhenius functions are combined: one covers the range

Chapter 2: Advanced Calibration for Silicon, SiGe, and Germanium

Part 2: Constant Parameters

$T < 1000^{\circ}\text{C}$ and the other, $T > 1000^{\circ}\text{C}$. In the Transient model, solid solubility defines the balance between substitutional boron and boron in B_4 clusters as follows: The active boron reaches the solid solubility if the total B concentration reaches `TotSolubility`, which is defined in Advanced Calibration as three times the B solid solubility.

Note:

The definition of *solid solubility* as used in the Transient model refers to the balance between substitutional electrically active dopants and small dopant clusters. This differs from the meaning of solid solubility in the context of reading Si:B phase diagrams, where solid solubility usually describes the maximum total concentration of B, whether substitutional or in small clusters, in the silicon-rich phase that might coexist with a different phase such as SiB_3 .

The rate at which the equilibrium between active and clustered B is reached is given by the parameter `CluRate`. `CluRate` has been calibrated by Synopsys using experimental data from the Synopsys SIMS database.

Accelerated boron-cluster formation at the initial annealing stage after implantation is taken into account by introducing the dependency of the forward-clustering rate on the interstitial supersaturation:

```
pdbSetDouble Si B TClusterForwardFac.Exp 3.088
pdbSetDouble Ge B TClusterForwardFac.Exp 0.0
term Si name=BoronTClusterForwardFac store add \
    egn = {(Int/EqInt)^[pdbGet Si B TClusterForwardFac.Exp]}
term Ge name=BoronTClusterForwardFac store add \
    egn = {(Int/EqInt)^[pdbGet Ge B TClusterForwardFac.Exp]}
```

This basically means that interstitials serve as a catalyst for boron deactivation. In silicon, some (an average of 1.152) interstitials are also incorporated in each B cluster formed. This is achieved by the following statements:

```
pdbSetDouble Si Int Int.In.B4.Cluster 1.152
pdbSetDouble Ge Int Int.In.B4.Cluster 0.0

pdbUnSetString Si Int UserEquation
UserAddEqnTerm Si Int {ddt(B4*[pdbGet Si I Int.In.B4.Cluster])}
pdbUnSetString Ge Int UserEquation
UserAddEqnTerm Ge Int {ddt(B4*[pdbGet Ge I Int.In.B4.Cluster])}
```

With these statements, the formation or dissolution of boron clusters is accompanied by the capture or release of silicon interstitials. The first statement is needed to ensure that the term in the second statement is not added twice, in case you source the Advanced Calibration file a second time.

In process simulations for SiGe in which mole fraction effects are activated by calling `SiGe_and_Stress_Effect`, the terms `BoronTClusterForwardFac` and `UserAddEqnTerm` are defined by the `_AlloyCompound::redefineUserTerms` callback procedure, which is defined in section 2.14.5 of `AdvCal_2022.03.fps`. The existing definitions of these terms

Chapter 2: Advanced Calibration for Silicon, SiGe, and Germanium

Part 2: Constant Parameters

are thereby overwritten. The parameters `Int.In.B4.Cluster` and `TClusterForwardFac.Exp` are subject to mole fraction interpolation.

By default, `Int.In.B4.Cluster` depends linearly on the Ge mole fraction, while `TClusterForwardFac.Exp` has a parabolic dependence on Ge mole fraction, governed by:

```
pdbSetDouble SiGe B TClusterForwardFac.Exp.X2 -0.84
```

For the initial activation of boron after implantation, the basic assumption is that it is given by a small value in crystalline silicon (`AcInit=2.443e18`) and by a higher value (`AmInit=2.113e20`) in recrystallized areas. `AmInit` is in agreement with measurements by Pawlak *et al.* [28].

The parameters `Solubility`, `CluRate`, `AcInit`, and `AmInit`, as well as the parameters for the role of interstitials in B clusters have been calibrated by computer-aided optimization against a large collection of SIMS and sheet resistance data.

For germanium, the solid solubility, the clustering rate, and the initial activation levels after implantation (`AcInit` and `AmInit`) are calibrated against published data [26][29][30] and data provided by AMAT-VSE (Applied Materials - Varian Semiconductor Equipment). For long-time anneals (hours at 900°C), boron shows a very low solid solubility [26], which was used in earlier calibration work [23].

However, higher activation levels (similar to boron activation in silicon) have been observed after implantation and short-time anneals. To reproduce sheet resistance data for germanium, `AcInit` is defined in section 3.2.1 of `AdvCal_2022.03.fps`, as a function of the local implanted B concentration:

```
fproc acinit_Germanium_Boron { Energy Dose } {
    return "(Boron_Implant*0.2+5.0e17)"
}
```

The apparent discrepancy between long-time and short-time anneals might indicate that different mechanisms are responsible for B deactivation in Ge, that is:

- The formation of small B clusters as in silicon
- A different mechanism that requires a higher thermal budget

In the Transient model, only a single type of B clusters with a single deactivation reaction is assumed. In `AdvCal_2022.03.fps`, the solubility of boron in Ge has been calibrated to a high value typical for post-implantation anneal with small or medium thermal budgets (up to several minutes at 860°C). As for silicon, the term `BoronTClusterForwardFac` for the dependency of the forward-clustering rate on the interstitial supersaturation is defined for germanium.

For the initial activation in the case of *in situ* boron-doped epitaxial growth of silicon and germanium, an activation level of $4 \times 10^{20} \text{ cm}^{-3}$ is assumed and defined by the `EpiInit` parameter.

Chapter 2: Advanced Calibration for Silicon, SiGe, and Germanium

Part 2: Constant Parameters

Sometimes, for computational efficiency, the process simulation of epitaxial growth of a film is mimicked by a combination of a deposition step and a subsequent thermal anneal. With this simplification, results will be similar but not 100% identical to an exact simulation of epitaxy. In this case, the value of `EpiInit` is ignored and you must ensure there is the proper initialization of active and clustered dopants. For example, a 10 minutes epitaxial growth of 10 nm of boron-doped silicon at 700°C, with a chemical B concentration of 1.0e21 could be simplified by the following commands:

```
deposit Silicon fields.values= { Boron= 4.e20 B4= 1.5e20 } \
    thickness= 0.01 temperature=700

diffuse temp= 700 time= 10
```

Boron Dose Loss

For B, As, and P, the three-phase segregation model is used for dose loss modeling.

In Sentaurus Process, by default, these dopants do not share trap sites at the interface with other dopants. For the `ChargedPair` model and the `ChargedReact` diffusion model, the flux of dopants from silicon or germanium into the interface layer is proportional to the concentration of dopant–defect pairs on the silicon side of the interface, and the out-diffusion from the interface to silicon or germanium is proportional to the concentration of point defects on the silicon side of the interface.

The number `CMax` of trap sites at the interface and the trapping and emission rates of the three-phase segregation model have been calibrated by Synopsys, based on a collection of boron SIMS profiles.

The diffusivity of trapped B atoms along the Si–SiO₂, Ge–SiO₂, and Ge–GeO₂ interfaces is set to zero. It can be set to a value higher than zero for increasing the lateral diffusion in 2D or 3D simulations [31].

In oxide, the boron diffusivity is increased for very high B concentrations ($> 1 \times 10^{21} \text{ cm}^{-3}$) and for high F concentrations. This diffusion enhancement has been calibrated by Synopsys, based on SIMS profiles. For very high B concentration in oxide ($> 1 \times 10^{21} \text{ cm}^{-3}$), out-diffusion into the gas contributes to the dose loss. The out-diffusion rate has been calibrated by Synopsys, using SIMS data.

Spacer oxides that are formed by a TEOS process and capped by a SiN layer can contain a high concentration of hydrogen, which increases the boron diffusivity in oxide. This case is not taken into account in the Advanced Calibration file.

Out-diffusion from bare silicon surfaces (without an oxide layer between silicon and the gas ambient) has not been calibrated yet.

Dose loss parameters also are provided for nitride–silicon interfaces. These have the same values as for oxide–silicon interfaces and will be considered only as a starting point for a calibration to be performed by users.

Chapter 2: Advanced Calibration for Silicon, SiGe, and Germanium

Part 2: Constant Parameters

Based on the experimental data available, boron shows no significant dose loss at the Ge– GeO_2 interface. The trapping rate at the semiconductor side is set to a lower value than for Si– SiO_2 .

Fluorine

See section 2.4.1 of `AdvCal_2022.03.fps`.

As previously explained, Advanced Calibration offers two modeling approaches for the effects of fluorine in silicon: a very simple approach and a sophisticated approach.

In the very simple approach, it is assumed that fluorine is completely immobile after ion implantation. Three empirical effects of fluorine on B diffusion are implemented in section 2.3 of `AdvCal_2022.03.fps`:

- Fluorine reduces directly the B diffusivity in Si (using `BoronDiffFactor`).
- Fluorine increases the B diffusivity in oxide and, therefore, increases the dose loss.
- Fluorine increases the B out-diffusion from oxide to the gas and, therefore, increases the B dose loss.

The effect of fluorine on boron diffusion and dose loss has been calibrated with SIMS data from BF_2 implantation and annealing. For all data, B and F have approximately the same spatial distribution after ion implantation. The calibration is valid only for this particular situation. Experimental data where fluorine was implanted separately was not taken into account in the calibration. When F is implanted separately from B, the simple approach for the influence of F on B diffusion is not predictive.

The sophisticated physics-based fluorine model is explained in [Part 4: Comprehensive and Slow Models on page 94](#).

For germanium, the very simple approach, with the assumption that fluorine is completely immobile after ion implantation, is also chosen by default. No effect on boron diffusion is assumed.

Nitrogen

See section 2.4.2 of `AdvCal_2022.03.fps`.

By default, the solution `Nitrogen` is set to `nosolve`. This means that nitrogen is ignored for diffusion, activation, and oxidation modeling. Only nitrogen implantation is simulated.

In device fabrication, there are very different use cases of nitrogen in silicon:

- Coimplantation of nitrogen, to reduce the diffusion of dopants in subsequent thermal anneals. This can be simulated with a model for nitrogen diffusion and for the reactions

Chapter 2: Advanced Calibration for Silicon, SiGe, and Germanium

Part 2: Constant Parameters

between N atoms or N₂ dimers in silicon, with silicon self-interstitials and vacancies. Such a model is switched on by the procedure `AdvancedNitrogenModel` (see [Nitrogen Diffusion and Clustering on page 100](#)).

- Silicon oxidation in N₂O (or NO) ambient. During N₂O oxidation, N atoms can be released and then trapped at the oxide–silicon interface. These trapped N atoms were found to reduce the oxidation rate, especially for very thin oxides.

Sentaurus Process provides a model that describes the accumulation of nitrogen at the oxide–silicon interface during N₂O oxidation. In that model, the Massoud correction term for thin oxides is reduced by a factor that depends on the concentration of nitrogen trapped at the interface. However, this model is inconsistent with the `AdvancedNitrogenModel` procedure for nitrogen coimplantations, in some respects: equations for nitrogen in silicon, boundary conditions at the oxide–silicon interface, and parameter values. Therefore, the two models should not be used together.

This is for historical reasons. The two models were developed independently, and a combination of N implantation and N₂O oxidation rarely occurs in the same process flow. Nitrogen implantation is not widely used and N₂O oxidation is used even more rarely.

Because of its inconsistency with the `AdvancedNitrogenModel` procedure, the N₂O oxidation model is not used by default in Advanced Calibration. Instead, the parameters of the Massoud model have been calibrated against measured oxide thickness after N₂O oxidation without accounting for nitrogen trapping during N₂O oxidation. See [Oxidation of Silicon in N₂O Ambient on page 58](#).

Arsenic Diffusion and Activation

See section 2.5 of `AdvCal_2022.03.fps`.

Arsenic Diffusivity

The values for the diffusivity of arsenic in silicon have been calibrated by Synopsys based on SIMS data. For regions with high As concentration ($> 2.0 \times 10^{20} \text{ cm}^{-3}$), the diffusivity of As is increased sharply, following the measurements by Larsen *et al.* [32] and using a formula that is based on the percolation theory and lattice Monte Carlo simulations [33]. It is assumed that a high concentration of P increases the diffusivity of As–V pairs in a similar way as a high concentration of As using percolation. Both vacancy and interstitial components of the diffusion coefficients were calibrated to obtain better simulation results in the high As concentration region. Following TSUPREM-4, the pairing constants are chosen such that the diffusivity of arsenic-defect pairs has the same order of magnitude as the diffusivity of unpaired defects.

The macroscopic value for arsenic diffusivity in germanium is calibrated [23] based on different data [34][35][36][37][38], and the diffusion of arsenic is assumed to be dominated

by As⁺V⁻⁻ pairs. For consistency with the diffusivity in silicon, As–I and As–V pairs with different charge states are included as well. In pure germanium, As diffusion is dominated by diffusion of As⁺V⁻⁻ pairs. However, other arsenic-defect pair diffusivities are relevant as well, in particular, for mole fraction–interpolated diffusivities in SiGe. Under extrinsic doping, the diffusion of arsenic is strongly enhanced.

Arsenic Clusters

Arsenic forms clusters with vacancies in silicon [1][39] and germanium [40]. However, the activation model `Transient` is the default one for simplicity. It is assumed that three arsenic atoms form an As₃ cluster. The values of the solid solubility and the clustering rate have been calibrated by Synopsys.

For silicon, the calibration includes an Arrhenius break at 880°C for `CluRate` to allow for good accuracy of As deactivation at low-temperature processes:

```
pdbSet Si As CluRate {[ArrBreak 7.4974e-5 1.40 5.51647e3 3.2 880]}
```

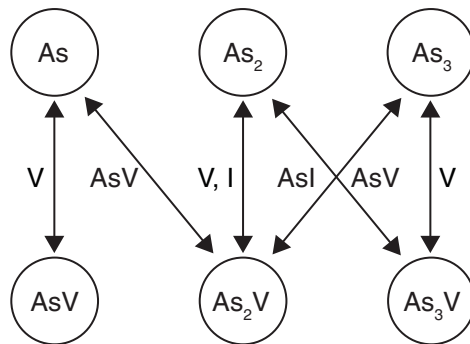
The parameter `KcEq.From.Default.Formula` is set to 1. This option is relevant for mole-fraction interpolation in SiGe. With the option switched on, the equilibrium active concentration corresponds to the solubility specified in SiGe exactly as intended.

The impact of phosphorus on arsenic activation in silicon is taken into account by an empirical expression for the cluster dissolution rate:

```
term Si name=ArsenicTClusterBackwardFac store add \
eqn= "1.0+PActive/1e20"
```

A more complex As–V clustering (`ChargedCluster`) model can be selected as well to simulate arsenic activation in silicon. The kinetics of As cluster formation is described with a family of four neutral clusters: As₂, As₂V, A₃, and As₃V. The model reaction pathway is shown in [Figure 1](#).

Figure 1 Reaction pathway for As–V clustering model



Chapter 2: Advanced Calibration for Silicon, SiGe, and Germanium

Part 2: Constant Parameters

In this model, as for the BIC model, the most important calibration parameters are the formation energies (`ClusterFormE`). The most stable cluster type at high arsenic concentration is As_3 .

For the initial activation of arsenic after implantation, the basic assumption is that it is given by a small value of $2 \times 10^{16} \text{ cm}^{-3}$ in nonamorphized crystalline silicon (`AcInit`) and by a higher value of $2 \times 10^{20} \text{ cm}^{-3}$ (`AmInit`) in recrystallized silicon.

For germanium, the solid solubility, the clustering rate, and the initial activation levels after implantation (`AcInit` and `AmInit`) are calibrated [23] based on a collection of data [35][36] [37].

For the initial activation in the case of *in situ* arsenic-doped epitaxial growth of silicon and germanium, an activation level of $2 \times 10^{20} \text{ cm}^{-3}$ is assumed and defined by the parameter `EpiInit`.

Arsenic Dose Loss

Arsenic dose loss is modeled by the three-phase segregation model, following the experimental work of Kasnavi *et al.* [41] and the model of Oh and Ward [31]. In the Advanced Calibration, arsenic atoms do not share interface trap sites with other dopants such as P. The parameters for As dose loss have been calibrated by Synopsys based on SIMS data. The parameter `CMax`, which gives the maximum concentration of As atoms that can be stored per cm^2 of the interface, is used to fine-tune the As dose loss. In the `ChargedPair` model and the `ChargedReact` model, the segregation rate is proportional to the concentration of As–I and As–V pairs.

Phosphorus Diffusion and Activation

See section 2.6 of `AdvCal_2022.03.fps`.

Phosphorus Diffusivity

In silicon, phosphorus diffuses predominantly through interstitials at high temperatures. The diffusivity of P–I pairs has a similar value as the fit to literature data in [1], but with an increased relative contribution of P^+I^0 pairs and a reduced contribution of P^+I^- pairs. The diffusivity of P through P–V pairs is smaller. It is relevant only at very high P concentration and is most relevant when C co-doping is used.

The macroscopic value for phosphorus diffusivity in germanium is calibrated based on different data [34][35][36][37][42][43][44][45][46], and the diffusion of phosphorus is assumed to be dominated by P^+V^{--} pairs. For consistency with the diffusivity in silicon and for the purpose of mole-fraction interpolation of diffusivities in SiGe, P–I and P–V pairs with different charge states are included as well. Under extrinsic doping, the diffusion of phosphorus is strongly enhanced due to the increased abundance of mobile P^+V^{--} pairs.

Chapter 2: Advanced Calibration for Silicon, SiGe, and Germanium

Part 2: Constant Parameters

The pairing constants are set to 1e-22. These are very small values, so the *dilute approximation* (the concentration of pairs is much smaller than the concentration of substitutional P) is always valid. Synopsys' in-house DFT calculations support the choice of very small pairing constants.

The migration distance of P–I pairs is reduced in the presence of C, so as to model extremely steep P profiles in the presence of C. This is achieved by scaling the rate of P–I pair formation and pair dissolution by the following factor:

```
term Si name=ReactPhosphorusIntFactor store add \
eqn = "1.0+(CTotal/2.6e19)"
```

Phosphorus Clusters

Phosphorus forms clusters with vacancies in silicon [1][39] and germanium [47], and in addition with interstitials in silicon [1][39]. However, the activation model Transient is the default one for simplicity. The model parameters for the formation and dissolution of P clusters have been calibrated by Synopsys, based on SIMS data at high concentrations. It is assumed that three P atoms can form a P_3 cluster.

Unlike all other clusters used, P_3 clusters are assumed to be mobile and can diffuse through negatively charged “pairs” between P_3 clusters and V^- . As a consequence, a peak of P_3 clusters will broaden during thermal annealing. The macroscopic diffusivity of P_3 clusters in intrinsic Si and Ge, at equilibrium concentration of V, is given by the parameters:

```
pdbSetDouble Si P P3_diff {[Arr 0.0662 2.8]}
pdbSetDouble Ge P P3_diff {[Arr 0.4 2.2]}
```

You can use `P3_diff` to fine-tune P diffusion in regions of high P_3 cluster concentration. It is also a recommended parameter for fine-tuning the diffusion of P during the growth of P-doped epitaxial films (see [Phosphorus-Doped Epitaxial Silicon on page 154](#)).

The clustering model with P_3 clusters only underestimates the stability of P complexes for extremely high P concentrations ($> 10^{22} \text{ cm}^{-3}$) in silicon near the surface, which can be obtained after high-dose implantation (for example, $5 \times 10^{15} \text{ cm}^{-2}$) with low energy (for example, 2 keV), or after epitaxial growth of highly strained P-doped Si (HSSiP). To cope with very high P concentrations, you can add a second type of P cluster by the following line:

```
Use_P7I
```

This line switches on equations for P_7I clusters, which can form and dissolve according to the reaction $2 P_3 + PI \leftrightarrow P_7I$. This equation and the necessary adjustments to the equations for P_3 clusters and P–I pairs are defined in the procedure `Use_P7I`, implemented in section 2.6.2.3 of `AdvCal_2022.03.fps`.

Chapter 2: Advanced Calibration for Silicon, SiGe, and Germanium

Part 2: Constant Parameters

The model offers the following parameters for fine-tuning:

- `rcap_4pi_P7I` scales the formation rate of P₇I clusters. The parameter name reflects its physical meaning: $4 \times \pi \times r_{cap}$, where `rcap` is the capture radius (in cm).
- `backward_P7I` scales the dissolution rate of P₇I clusters.
- `vol_P7I_reac` is the volume relaxation upon formation of a single P₇I cluster. Substitutional P and P₃ clusters create tensile stress, while P₇I clusters create compressive strain in the model (see below). Accordingly, the stability of P₇I clusters increases in regions with tensile strain. This is modeled by multiplying the cluster dissolution rate by the Boltzmann factor $\exp(P \times vol_P7I_react/kT)$, where P is the pressure in dyn/cm², and kT is the thermal energy in erg.

A high concentration of P and P₃ clusters causes tensile strain, which is modeled by:

```
pdbSetDoubleArray Si P Conc.Strain { 0.0 0.0 1.0 -0.096 }
pdbSetDoubleArray Si P3 Conc.Strain { 0.0 0.0 1.0 -0.292 }
```

P₇I clusters cause compressive strain in the model. In this way, their formation describes strain relaxation in highly P-doped regions:

```
pdbSetDoubleArray Si P7I Conc.Strain { 0.0 0.0 1.0 0.59 }
```

Strain relaxation of epitaxially grown HSSiP layers during post-epi thermal annealing has been calibrated against data from Li *et al.* [48] and additional data provided by AMAT-VSE. In that calibration, stress effects in the procedure `SiGe_and_Stress_Effect` have been activated.

A more complex P–V and P–I clustering (`ChargedCluster`) model can be selected as well to simulate phosphorus activation in silicon. The kinetics of P cluster formation is described with a family of four neutral clusters: P₂, P₂V, P₃V, and P₂I. In this model, as for the BIC model, the most important calibration parameters are the formation energies (`ClusterFormE`). Note that the complex model does not have a higher accuracy than the default one in general.

For the initial activation of phosphorus after implantation, the basic assumption is that it is given by a small value of 4×10^{18} cm⁻³ in nonamorphized crystalline silicon (`AcInit`) and by a higher value of 3.0×10^{20} cm⁻³ (`AmInit`) in recrystallized areas.

For germanium, the solid solubility, the clustering rate, and the initial activation levels after implantation (`AcInit` and `AmInit`) are calibrated based on a collection of data [35][36] [37][42][43][44][45][46].

For the initial activation in the case of *in situ* phosphorus-doped epitaxial growth of silicon and germanium, an activation level of 2×10^{20} cm⁻³ is assumed and defined by the `EpiInit` parameter.

As–P Clusters in Silicon

A simple model for As–P clusters in silicon is implemented in section 2.6.2.4 of `AdvCal_2022.03.fps` as an alternative approach to reduce P diffusion in the region with high As concentration. It is not switched on by default because the calibration is not reliable and because the direct modification of P diffusivity and As diffusivity in co-doped regions provides a superior overall accuracy.

After sourcing the Advanced Calibration file, you can switch on the As–P cluster model with the command:

```
Use_As3P_clusters
```

The command `Use_As3P_clusters` is a procedure defined in section 2.6.2.4 of `AdvCal_2022.03.fps`, which instructs Sentaurus Process to solve for the mixed cluster As3P. The parameters `As3P_k1` and `As3P_k2`, defined in section 2.6.2.4, govern the formation and dissolution rate of such clusters.

Note:

The As–P clustering model must only be used when using the `Transient` cluster model for As.

Phosphorus Dose Loss

Phosphorus dose loss is described by the three-phase segregation model. Phosphorus atoms can be incorporated into the silicon–SiO₂ interface.

In addition, it is assumed that two P atoms located at the silicon–SiO₂ interface can form P₂ pairs. The equilibrium concentration of pairs increases quadratically with the concentration of unpaired P atoms trapped at the interface. The maximum concentration of P₂ pairs can be reached theoretically when the concentration of unpaired P atoms equals its maximum value `CMax` and is governed by the parameter `P2trapMax`.

The calibration of P and P₂ trapping at the interface is performed in such a way that, for low P concentrations at the silicon side of the interface ($< 10^{17} \text{ cm}^{-3}$), unpaired P atoms govern the P dose loss. For high P concentrations ($> 10^{20} \text{ cm}^{-3}$) and inert anneals (Si–SiO₂ interface not moving), a considerable fraction of phosphorus trapped at the interface is bound in P₂ pairs. For oxidation (Si–SiO₂ interface moving), only a small concentration of P₂ pairs is formed even at high P concentration.

The following observation can be useful for fine-tuning. The high default value of `CMax` works well for thermal anneal after implantations. For thermal anneals after epitaxial growth of SiP layers, a much smaller value of `CMax` might be needed. Apparently, the dose loss corresponding to the trapping of single P atoms at the oxide–silicon interface is higher in the presence of implantation damage at such an interface. In contrast, the calibrated value for `P2trapMax`, governing the maximum concentration of P₂ pairs trapped at the interface, works for both implantation + anneal and epitaxy + anneal recipes.

Chapter 2: Advanced Calibration for Silicon, SiGe, and Germanium

Part 2: Constant Parameters

At oxide–silicon interfaces, the presence of arsenic reduces phosphorus dose loss. Likely, As atoms block interface traps for P. To take this into account, the parameters `CMax` and `P2trapMax` are modified by the following expressions, in which `Arsenic` represents the concentration of As trapped at the interface:

```
term Ox /Si name=PhosphorusCMaxFactor add \
    eqn="(1.8e13/(1.8e13+Arsenic))"
term Ox /Si name=P2trapMaxFactor add eqn="(2.5e13/(2.5e13+Arsenic))"
```

This dose loss model was developed due to the need to calibrate, with a consistent set of parameters, the P dose loss for low and high interface concentrations, using the Synopsys SIMS database. The model is supported by the results of first-principles calculations on the mechanism of P segregation at the Si–SiO₂ interface [49]. At the Ge–GeO₂ interface, P shows strong dose loss also at low concentrations [50].

The interface trap density, emission, and trapping rates, and the pair formation and dissolution rates have been calibrated by Synopsys based on phosphorus SIMS data ranging from ultrashallow junction formation to long-time oxidation.

The last lines of section 2.6.3 of `AdvCal_2022.03.fps` contain the Alagator implementation of the P₂ pair trap formation at Si–SiO₂ interfaces.

Note:

When using Segregation boundary conditions at Si–SiO₂, Si–Si₃N₄, or Ge–SiO₂ interfaces instead of ThreePhaseSegregation boundary conditions, switch off the solution `P2trap`:

```
pdbSet Ox_Si P BoundaryCondition Segregation
solution name=P2trap nosolve store
```

Arsenic–Phosphorus Co-Diffusion

The physics of P and As diffusion is very complex if P and As are implanted and annealed together, in particular, for high As implantation doses ($> 10^{14} \text{ cm}^{-2}$). The following empirical approaches are included in the Advanced Calibration file to achieve a good accuracy for As–P co-diffusion in silicon:

- The P diffusivity is modified as a function of arsenic concentration using the terms `PhosphorusIntDiffFactor` and `PhosphorusVacDiffFactor`. These terms, if defined, are multiplied by the diffusivity of P–I and P–V pairs, respectively. The diffusivity decreases as follows (section 2.6.1.4 of `AdvCal_2022.03.fps`):

```
term Si name=AsAs3 store add eqn= {(Arsenic + As3 * 0.6)}
term Si name=PhosphorusIntDiffFactorDopant store add \
    eqn= {[([Arr 2.2e25 1.5]+[Arr 4.2e31 3.0])/([Arr 2.2e25 1.5]+ \
        [Arr 4.2e31 3.0])+AsAs3)}}
term Si name=PhosphorusVacDiffFactorDopant store add \
    eqn= {[([Arr 2.7e22 0.5])/([Arr 2.7e22 0.5]+AsAs3))}
```

Chapter 2: Advanced Calibration for Silicon, SiGe, and Germanium

Part 2: Constant Parameters

- The diffusivity of P₃ clusters is also modified as a function of arsenic concentration. It is multiplied by the term `P3DiffFactor`, which is defined as (section 2.6.2.1 of `AdvCal_2022.03.fps`):

```
term Si name=P3DiffFactor store add eqn= {(1.2e20/(1.2e20+AsAs3))}
```

- The pressure effects are redefined inside the `SiGe_and_Stress_Effect` procedure (section 2.14.2 of `AdvCal_2022.03.fps`):

```
term Si name=PhosphorusIntDiffFactorPressure store add eqn= 1.0
term Si name=PhosphorusVacDiffFactorPressure store add eqn= 1.0
term Si name=PhosphorusIntDiffFactor store add \
    eqn= {PhosphorusIntDiffFactorDopant * \
        PhosphorusIntDiffFactorPressure}
term Si name=PhosphorusVacDiffFactor store add \
    eqn= {PhosphorusVacDiffFactorDopant * \
        PhosphorusVacDiffFactorPressure}
```

- In this implementation, `PhosphorusIntDiffFactor` is defined as a product of two terms. The factor `PhosphorusIntDiffFactorDopant` describes the modification of P–I diffusivity in the presence of As. The factor `PhosphorusIntDiffFactorPressure` can be used to describe the impact of pressure on P–I diffusivity. It is 1.0 by default and can be redefined to include the impact of pressure if you switch on stress effects in a process simulation with the `SiGe_and_Stress_Effect` procedure (see [Stress Effect \(Stress_Eff\) on page 61](#)). This implementation allows you to separately fine-tune the impact of dopants and the impact of stress on the diffusivity of P–I pairs.
- Similarly, the terms `PhosphorusVacDiffFactor`, `ArsenicVacDiffFactor`, and `ArsenicIntDiffFactor` also are defined as a product of two terms.
- The As diffusivity is modified as a function of arsenic and phosphorus concentration using the terms `ArsenicVacDiffFactor` and `ArsenicIntDiffFactor`. The diffusivity increases as follows (section 2.5.1.1 of `AdvCal_2022.03.fps`):

```
term Si name=ArsenicIntDiffFactorDopant store add \
    eqn= {(1.0+((PActive*0.6+AsActive)/[Arr 1.8e21 0.25])^3.5)}
term Si name=ArsenicVacDiffFactorDopant store add \
    eqn= {(1.0+[ArrBreak 1.0 0 5.1920595e-7 -1.65 1050] \
        *((PActive*0.3+AsActive)/2.1e20)^3.0)}
```

- The pressure effects are redefined inside `SiGe_and_Stress_Effect` (section 2.14.2 of `AdvCal_2022.03.fps`):

```
term Si name=ArsenicIntDiffFactorPressure store add eqn= 1.0
term Si name=ArsenicVacDiffFactorPressure store add eqn= 1.0
term Si name=ArsenicIntDiffFactor store add \
    eqn= {ArsenicIntDiffFactorDopant * ArsenicIntDiffFactorPressure}
term Si name=ArsenicVacDiffFactor store add \
    eqn= {ArsenicVacDiffFactorDopant * ArsenicVacDiffFactorPressure}
```

- The dissolution of As clusters is modified in the presence of substitutional P using the term `ArsenicTClusterBackwardFac` (section 2.5.2.1 of `AdvCal_2022.03.fps`):

```
term Si name=ArsenicTClusterBackwardFac store add \
eqn= "1.0+PActive/1e20"
```

Depending on the process window of interest (window of As dose, As energy, P dose, P energy, and annealing conditions), you might need some additional fine-tuning of the P or As parameters to achieve a good fit between simulation and experimental data.

For more information, see [Co-diffusion of Arsenic and Phosphorus on page 158](#).

Indium Parameters

See section 2.7 of `AdvCal_2022.03.fps`.

For silicon, the diffusivity values have been obtained by Synopsys from calibration of SIMS data. The pairing constants are chosen such that the diffusivity of In–In pairs is approximately equal to the diffusivity of free interstitials. The indium solid solubility and the clustering rate have been calibrated by Synopsys.

The dose loss of indium during annealing is diffusion limited. Almost all indium atoms, which diffuse to the Si–SiO₂ interface, are built into the oxide. This is reflected by a very low segregation coefficient. Furthermore, it is assumed that indium evaporates at the oxide–gas surface.

The indium diffusion and dose loss is well calibrated for typical indium channel or halo implantations below the amorphization dose. For high indium doses (typically $> 5 \times 10^{13} \text{ cm}^{-2}$) and for the annealing of preamorphized wafers, the modeling of indium is not accurate for the following reason: During solid phase epitaxial regrowth (SPER), indium atoms are pushed towards the surface, due to a segregation effect between the crystalline and amorphous phases of silicon [51][52]. This segregation increases the overall dose loss of indium dramatically. However, the SPER is not modeled by default in the Advanced Calibration of Sentaurus Process, but it can be activated by the procedure `AdvancedSPERModel` (see [Solid Phase Epitaxial Regrowth on page 101](#)).

Indium diffusion, clustering, and segregation in germanium has not yet been calibrated by Synopsys. Therefore, the same parameter values are assumed in germanium as in silicon.

Antimony Parameters

See section 2.8 of `AdvCal_2022.03.fps`.

The macroscopic values for antimony diffusivity in silicon are based on the literature [1]. Antimony diffuses through Sb–V pairs. In highly doped regions (antimony concentration $> 2.0 \times 10^{20}$), the diffusivity is enhanced as observed by Larsen *et al.* [32].

Chapter 2: Advanced Calibration for Silicon, SiGe, and Germanium

Part 2: Constant Parameters

The macroscopic values for antimony diffusivity in germanium are calibrated based on a single literature source [37], and the diffusion of antimony is assumed to be dominated by $\text{Sb}^+ \text{V}^-$ pairs. For consistency with the diffusivity in silicon, Sb–V pairs with different charge states are included as well. Their diffusivity is small in pure Ge, but is relevant for the mole-fraction interpolation of Sb–V diffusivities in SiGe.

The pairing constants are chosen such that the Sb–defect pair diffusivity has a similar value as the diffusivity of the unpaired defect.

The cluster parameters and the interface segregation have been calibrated by Synopsys based on SIMS data and sheet resistance data. No ultrashallow junction Sb profiles in silicon have been used for the calibration, therefore, the model parameters are not expected to be predictive for Sb ultrashallow junction formation. The diffusivity of Sb in SiO_2 is taken from Aoyama *et al.* [53], and the ones in Si_3N_4 and GeO_2 are assumed to be the same.

Carbon Diffusion

See section 2.9 of `AdvCal_2022.03.fps`.

Carbon Diffusivity in Silicon

The macroscopic diffusivity of carbon in silicon is taken from the literature [1]. The diffusivity of C–I pairs has been calibrated by Synopsys. The Frank–Turnbull mechanism is switched off. Carbon interstitials are only formed by the kick-out mechanism.

Carbon Clustering in Silicon

Four types of carbon–interstitial cluster are taken into account: C_2 , C_2I , C_3I_2 , and C_3I_3 .

The following reactions for the formation and dissolution of clusters are considered:

- $\text{C}-\text{I} + \text{C} \rightleftharpoons \text{C}_2\text{I}$
- $\text{C}_2 + \text{I} \rightleftharpoons \text{C}_2\text{I}$
- $\text{C}_2\text{I} + \text{C}-\text{I} \rightleftharpoons \text{C}_3\text{I}_2$
- $\text{C}_3\text{I}_2 \rightleftharpoons \text{C}_3\text{I}_3 + \text{V}$

The clustering rates, together with the diffusivity of C–I pairs, have been calibrated by Synopsys using SIMS data from marker layer experiments [54][55][56] and from data on ultrashallow junction formation following $\text{Ge}+\text{C}+\text{B}$ [57] and $\text{Ge}+\text{C}+\text{BF}_2$ ‘cocktail’ implantations. The migration distance of C–I pairs is calibrated in the Sentaurus Process defaults. It is assumed that, in regions that are amorphized by ion implantation and recrystallized by solid phase epitaxy, carbon is in the substitutional state up to concentrations of $3.0 \times 10^{20} \text{ cm}^{-3}$ and else in C_2 clusters immediately after the

Chapter 2: Advanced Calibration for Silicon, SiGe, and Germanium

Part 2: Constant Parameters

recrystallization. In contrast, in nonamorphized regions, carbon is assumed to be mostly in C_3I_2 clusters at the beginning of thermal annealing.

During the formation of C–I clusters, the concentration of free interstitials is reduced and vacancies are created. As a consequence, B diffusion is retarded and Sb diffusion is enhanced. The increase of the solid solubility of boron in regions of high carbon concentration [57] is not taken into account in the Advanced Calibration.

The C–I clustering model allows you to obtain accurate results also for the analysis of phosphorus ultrashallow junction formation by Si+C+P ‘cocktail’ implantations and subsequent spike annealing [58][59].

Carbon in Germanium

According to the literature [60], carbon diffuses very slowly through interstitials in germanium. Carbon diffusion is modeled by the `ChargedPair` model, but it is assumed to be uncharged.

Detailed information or experimental data on the solubility or substitutionality of carbon in germanium after implantation, SPER, or annealing is missing. Therefore, the current assumption is that carbon has a high solubility and initial activation after implantation (`AcInit` and `AmInit`). The `Transient` cluster model is used for carbon clustering, with two carbon atoms assumed to form a cluster without interstitials.

Based on atomistic simulation [61][62] and comparison with experiments [60], carbon forms mixed clusters with arsenic or phosphorus and vacancies, which reduce dopant diffusion. Mixed As–C–V and P–C–V clusters are modeled by the `ComplexCluster` model. The clustering and dissolution rates are calibrated [23] based on literature data [45][60].

Based on the experimental data available, carbon shows no significant dose loss at the Ge– GeO_2 interface. Therefore, the simple `Segregation` model is used with balanced segregation.

Intrinsic Carrier Concentration

See section 2.10 of `AdvCal_2022.03.fps`.

For silicon, the intrinsic carrier concentration n_i is taken from Morin and Maita [63]. As an alternative, a simplified formula (`ni_MM_simple`) has been prepared. This simplified formula is frequently used in other silicon process simulators.

The intrinsic carrier concentration is based on the one from silicon and corrections for band gap and effective density-of-states for SiGe with Ge mole fraction 1 (see [Impact of Stress on Electrostatic Potential on page 69](#)).

Oxidation

See section 2.11 of `AdvCal_2022.03.fps`.

By default, the parameters of the Deal–Grove model [64] for thick oxides and the parameters of the Massoud model for the initial regime of the oxidation are well calibrated for silicon. Only the Massoud model parameters for wet oxidation are redefined in Advanced Calibration, as described in [Massoud Model Parameters for Wet Oxidation of Silicon](#).

For germanium oxidation, only dry oxidation of Ge (100) and (111) surfaces [65] has been calibrated, and the calibration parameters are available as Sentaurus Process defaults.

SiGe oxidation has been calibrated and calibration parameters are included in Advanced Calibration, as described in [Parameters for Wet and Dry Oxidation of SiGe](#).

Massoud Model Parameters for Wet Oxidation of Silicon

Advanced Calibration contains parameters for the Massoud model for wet (H_2O) atmosphere. According to this model, for very thin oxides (thickness < 15 nm), the silicon oxidation rate is increased with respect to the Deal–Grove model for oxidation.

Without Advanced Calibration, the parameters c_0 and c_w default to zero for wet oxidation, which means that the Massoud model is effectively switched off and underestimates the oxide growth of thin oxides in wet atmosphere.

For silicon surfaces with a (100) crystal orientation, the calibration gives an immediate accuracy of $\pm 15\%$ for oxidation rates in wet or mixed atmosphere. For other crystal orientations, less data was available for calibration and the parameters are less reliable. If fine-tuning is required, you need to consider adjusting the parameters c_0 ($\pm 25\%$) and L_0 ($\pm 25\%$). If this is not sufficient, you can consider other parameters for calibration such as the initial oxide thickness, or doping and pressure dependency of the oxidation rate. For the pressure dependency of the Massoud correction term, the parameter value `MassoudPress=1.0` is proposed. If necessary, slightly smaller values (for example, 0.8 or 0.9) can be considered for fine-tuning.

Parameters for Wet and Dry Oxidation of SiGe

Advanced Calibration contains parameters for the Deal–Grove model and the Massoud model for wet and dry oxidation of SiGe. The parameters for `Oxide_Germanium`, the upper mole-fraction limit for SiGe– SiO_2 interfaces, are included in section 2.11.2 and section 2.11.3 of `AdvCal_2022.03.fps`, and are effective when SiGe parameter interpolation is activated (see [Effect of Germanium and Stress on page 60](#)).

For details on the calibration of oxidation rates, see [SiGe Oxidation on page 68](#).

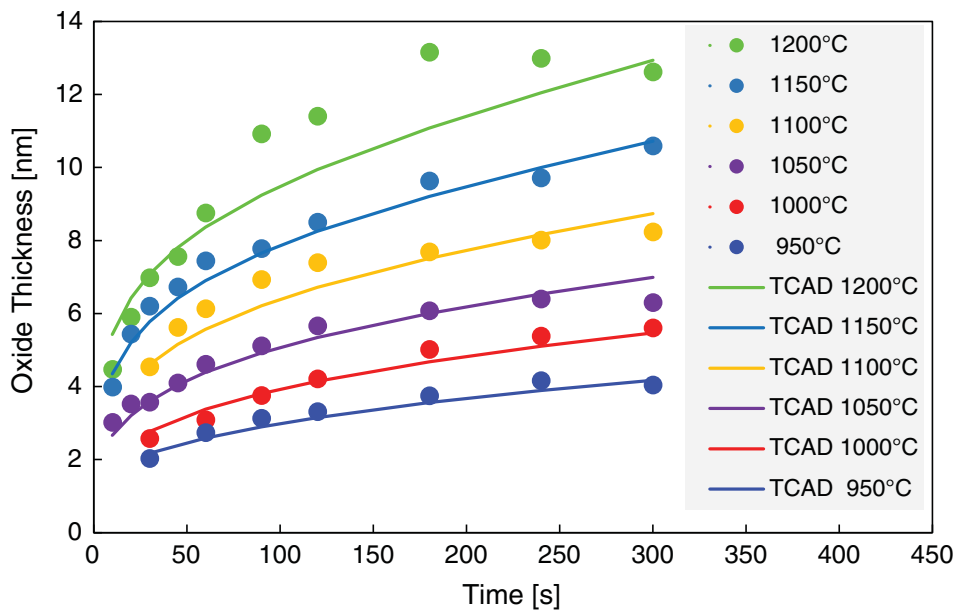
Oxidation of Silicon in N₂O Ambient

In Advanced Calibration, the solution Nitrogen is set to nosolve. The parameters of the Massoud model have been calibrated against measured oxide thickness after N₂O oxidation without accounting for nitrogen trapping during N₂O oxidation.

This calibration is contained in section 2.11.4.1 of AdvCal_2022.03.fps. It is based on hardware data for oxidation of <100> surfaces [66][67][68][69][70] in the temperature range 885–1200°C and on data for oxidation of <111> surfaces [66][71] in the temperature range 900–1100°C. For <110> surfaces, no calibration has been performed, but the parameter values have been copied from the calibrated values for <100> surfaces.

For simple oxidation recipes in N₂O ambient, the hardware data is well reproduced, as for example shown in Figure 2. However, this calibration, which does not explicitly model the accumulation of nitrogen at the interface, has limitations when applied to sequences of several oxidation steps in different atmospheres.

Figure 2 Oxide thickness after oxidation in N₂O atmosphere: comparison of measurements of Ting et al. [66] (symbols) to process simulation results with Sentaurus Process Advanced Calibration (lines)



In section 2.11.4.2 of AdvCal_2022.03.fps, the procedure N2O_Oxidation_Defaults is defined. It allows you to switch on the N₂O oxidation model of Sentaurus Process in one line. In that procedure, the parameters of the Massoud model for N₂O oxidation are reverted to the Sentaurus Process defaults.

This procedure is provided for the convenience of those who prefer the N₂O oxidation model of Sentaurus Process. It is usually not advised, because better accuracy for simple N₂O

Chapter 2: Advanced Calibration for Silicon, SiGe, and Germanium

Part 2: Constant Parameters

oxidation recipes is obtained with the Advanced Calibration defaults. In studies where several oxidation steps are combined (for example, N₂O oxidation after O₂ oxidation), the N₂O model with its additional parameters for the accumulation of nitrogen at the interface and for its impact on the oxidation rate might be a good choice.

In any case, you should not use `N2O_Oxidation_Defaults` together with `AdvancedNitrogenModel`. These two models are inconsistent.

Smoothing of Amorphous–Crystalline Interface

See section 2.12 of `AdvCal_2022.03.fps`.

After ion implantation some silicon regions can be amorphized. By default, the solid phase epitaxial regrowth is not simulated explicitly in Advanced Calibration, but the initial conditions for point defects and dopant activation are set differently in amorphized or crystalline regions.

At the amorphous–crystalline interface, there is a sharp step in the initial conditions for the diffusion solver. Unless the mesh is very fine at the amorphous–crystalline interface, this might lead to a numeric error in the result. To reduce this error, Sentaurus Process can smooth the initial point-defect concentration at the amorphous–crystalline interface with the parameter `AmorpGamma`. Synopsys has investigated typical situations and has found that the value `AmorpGamma=0.8` often gives the smallest numeric error.

In simulations with coarse meshes (mesh spacing of 2–4 nm across amorphous–crystalline interfaces), the smallest numeric error is obtained with even smaller values of `AmorpGamma`, for example, `AmorpGamma=0.6`.

Selecting Implantation Tables

See section 2.13 of `AdvCal_2022.03.fps`.

For analytic implantation, improved tables are switched on by the following statements:

```
pdbSet      ImplantData BF2 TableVersion 2008.09
pdbSet      ImplantData In  TableVersion 2008.09
pdbSetString ImplantData As  TableVersion 2010.12
pdbSetString ImplantData B   TableVersion 2010.12
pdbSetString ImplantData P   TableVersion 2010.12
pdbSetString ImplantData Sb  TableVersion 2010.12
```

For high-energy boron implantations, an improved table is available, but it is not switched on by default. To select it for energy > 200 keV, set the switch:

```
pdbSetBoolean ImplantData B UseHighEnergyBoronTable 1
```

For details, see the corresponding explanations in [Implantation Preprocessing and Postprocessing on page 88](#).

Effect of Germanium and Stress

See section 2.14 of `AdvCal_2022.03.fps`.

Strained and relaxed SiGe, strained-silicon layers, and process-induced stress are used widely in state-of-the-art silicon process technology. Section 2.14 of `AdvCal_2022.03.fps` is dedicated to the effects of Ge concentration and stress on the diffusion, clustering, and segregation of dopants and point defects. Some models and part of the calibration are summarized in [72].

Note:

In the Advanced Calibration models for the impact of Ge on dopant and defect diffusion, it is assumed that germanium is treated as an impurity in silicon (rather than being present in a separate ‘SiGe’ material).

The calibration focuses on the full Ge mole fraction range from 0% to 100%. However, it is less predictive for very high concentrations of Ge (> 55%). Most of the experimental data available for calibration covers only low Ge mole fractions (< 55%) or pure Ge (100%).

The calibration of stress and Ge effects is based on a relatively small set of measured data, many of them published marker layer experiments, which focus on equilibrium conditions. The models have not yet been tested rigorously against SIMS data for nonequilibrium annealing conditions and against electrical data from real-device fabrication processes.

Bandgap narrowing due to Ge content is always taken into account.

The diffusivity for Ge in silicon and oxide [73] are defined for constant diffusion models. However, the Ge diffusion is only assumed to be constant if no SiGe effects are activated as described in the following.

The calibration of additional physical effects related to Ge or stress is contained in the procedure `SiGe_and_Stress_Effect`. It has four Boolean arguments: `Ge_Chem_Eff`, `Stress_Eff`, `Segreg_Model`, and `Strained_Overlayer`. Each of these, if set to 1, will switch on additional physical effects. By default, none of these additional effects is switched on. This saves CPU time in situations where the effects can be neglected. After sourcing `AdvCal_2022.03.fps`, you can switch on the required effects by a single command.

For example, the following command switches on the first three effects (chemical effect of germanium, stress effects in bulk silicon, and segregation at Si–SiGe interfaces), but not the fourth effect (strained overlayer):

```
SiGe_and_Stress_Effect 1 1 1 0
```

Arguments of SiGe_and_Stress_Effect

Before describing in detail the impact of `SiGe_and_Stress_Effect`, the impact of each argument is summarized individually.

Ge Chemical Effect (Ge_Chem_Eff)

Switching on `Ge_Chem_Eff` activates SiGe parameter interpolation between the silicon and germanium parameters.

Note:

Interpolation is performed only in silicon regions where the maximum Ge concentration exceeds the threshold concentration `Min.Conv.Conc` defined by the parameter `pdbGet SiGe Ge Min.Conv.Conc`. By default, `Min.Conv.Conc` is equal to `5e20`.

Germanium content dependency of the following parameters is taken into account in `AdvCal_2022.03.fps`:

- Band gap, carrier effective density-of-states (DOS), intrinsic carrier concentration, and permittivity
- Point-defect diffusivities, equilibrium concentrations, and surface recombination rates
- Dissolution rate of {311} defects, and rate of {311} defect transformation to dislocation loops
- B, As, P, and Sb diffusivity, migration distance, solubility, clustering rate, dose loss, and initial conditions after implantation

The value of `Ge_Chem_Eff` controls the definition of the `xMoleFraction` field saved into the TDR file and controls whether the new or the old syntax is used for interpolation of mechanical parameters and the lattice mismatch stress simulation. For details, see [Overview on page 289](#).

In addition, an equation for Ge diffusion in SiGe is defined, which takes into account the dependency of Si or Ge interdiffusion on the point-defect concentration.

Stress Effect (Stress_Eff)

Switching on `Stress_Eff` causes additional physics to be taken into account. The stress effect is included for the following parameters:

- Band gap
- Point-defect equilibrium concentration and diffusivity

Chapter 2: Advanced Calibration for Silicon, SiGe, and Germanium

Part 2: Constant Parameters

- Dissolution rate of {311} defects, and rate of {311} defect transformation to dislocation loops
- B, As, P, Sb, In, and Ge diffusivity
- B, As, P, and Sb solid solubility
- Formation energy of BICs and As–V clusters

Except for the additional bandgap narrowing, which depends on individual strain-tensor components, only the hydrostatic pressure is used for the modification of the diffusion and activation models. Anisotropic effects, which would require the use of diffusivity tensors, are not included in Advanced Calibration. The unit of pressure in Sentaurus Process is dyn/cm² (10 dyn/cm² = 1 Pa).

Sentaurus Process takes into account various stress-causing mechanisms (see the *Sentaurus™ Process User Guide*). One of these is stress from lattice mismatch due to the presence of impurities. The lattice mismatch due to Ge and C is taken into account, with the parameters adjusted according to the literature (see [Mole Fraction–Dependent Mechanics Parameters for SiGe on page 291](#)). In typical cases, the impact of carbon-induced strain on dopant diffusion and activation is small, but not negligible. Tensile stress from lattice mismatch due to high concentrations of P, P₃ clusters, and – if P₇I clusters are switched on – compressive stress from P₇I clusters is taken into account, as well. Stress from other stress-causing impurities, such as B or extended defects, has not been taken into account in the calibration of Advanced Calibration.

This additional stress source can be switched on with the `strain_profile` command, as shown below, but – since all models are calibrated without this additional stress source – switching on stress from impurities other than Ge might require a recalibration of other process model parameters, such as B solid solubility:

```
strain_profile Si species=Boron strain= { 0 -0.30 } ratio= { 0 1 }
```

Segregation at Si–SiGe Interface ([Segreg_Model](#))

Boron and phosphorus have been found to segregate at Si–SiGe interfaces, in experiments using epitaxial layers of strained SiGe embedded in Si, or strained silicon embedded in relaxed SiGe. Boron segregates into SiGe; whereas, phosphorus is pushed out of the SiGe region. A theoretical analysis [74] indicates that the dominant driving force for this segregation is the pressure gradient in the case of boron, and the difference in band structure between Si and SiGe in the case of phosphorus. The same but weaker effect as for phosphorus is assumed for arsenic as well.

Effect of Strained Overlayers ([Strained_Overlayer](#))

The model developed by Cowern [75] predicts an influence of overlayer strain on the point-defect concentration in the silicon. That effect was confirmed by experiments showing a strong dopant diffusion change under high-level stressed nitride layers [76][77].

Chapter 2: Advanced Calibration for Silicon, SiGe, and Germanium

Part 2: Constant Parameters

The change of equilibrium concentration due to overlayer strain can be expressed by the factor $\exp(P_{ov}V_f/kT)$, in which P_{ov} is the hydrostatic pressure in the overlayer, and V_f is the volume of an atom in silicon. This effect is switched on by setting the argument `Strained_Overlayer` in the procedure `SiGe_and_Stress_Effect` to 1.

Since the impact of strained overlayers is not fully understood yet (especially in the situation where thin oxides are in between silicon and strained overlayers), the procedure `SiGe_and_Stress_Effect` is most widely applied with the arguments 1 1 1 0:

```
SiGe_and_Stress_Effect 1 1 1 0
```

Implementation of SiGe_and_Stress_Effect

This section discusses the implementation of `SiGe_and_Stress_Effect`.

Chemical SiGe Alloy Effects

If `Ge_Chem_Eff` is equal to 1, then the SiGe parameter interpolation between the silicon and germanium parameters is activated by:

```
pdbSet Si Skip.Parameter.Interpolation 0  
pdbSet Ge Skip.Parameter.Interpolation 0
```

This also switches on the following mapping of Ge concentration to the Ge mole fraction in Si:

$$xMoleFraction = \frac{C_{Ge}}{LD_{Si} + \sqrt{LD_{Si}^2 + 4C_{Ge}(LD_{Ge} - LD_{Si})}} \quad (2)$$

This complex formula (and a similar one for Ge material) replaces the simpler formula:

$$xMoleFraction = \frac{C_{Ge}}{LD_{Si}} \quad (3)$$

which is used for `Skip.Parameter.Interpolation 1`. `xMoleFraction` is used for parameter interpolation in SiGe in process and device simulation models. The complex formula gives slightly higher `xMoleFraction` for the same Ge concentration, due to the different lattice constants of Si and Ge.

Impact of Germanium on Electrostatic Potential

The energy bandgap change along with mole fraction shows a very nonlinear curve due to the transition between the X-valley ($x < 0.8$) and L-valley ($x > 0.8$) [78]. With activated SiGe parameter interpolation, the parameter `de1Eg.Function` for the generic interpolation method is used for SiGe to model such nonlinearity.

Chapter 2: Advanced Calibration for Silicon, SiGe, and Germanium

Part 2: Constant Parameters

The following default bandgap narrowing expression, fitting experimental data based on optical measurements from [78], is used:

$$\Delta Eg = (0.3758 \times (0.7795 - x)^2 - 0.22835) - 0.2406 \times \exp(-((1-x)/0.1176)^2) \quad (4)$$

Additional effects are taken into account as follows:

- The permittivity of Ge-doped silicon is calculated by the following formula, in which x_{Ge} is the Ge concentration in Si, $\epsilon_{\text{Si}} = 11.7$ and $\epsilon_{\text{Ge}} = 15.8$:

$$\epsilon = (1 - x_{\text{Ge}}) \times \epsilon_{\text{Si}} + x_{\text{Ge}} \times \epsilon_{\text{Ge}} \quad (5)$$

- The mole fraction dependency of the product of the DOS in the conduction and valence bands, $N_C \times N_V$, is assumed to be linear for computational efficiency $(1 - x_{\text{Ge}} \times 0.705)$, which is a good approximation of the following nonlinear factor taken from [79]:

$$(1 - x_{\text{Ge}} \times 0.47/0.81)^{3/4} \quad (6)$$

Note:

Since the Potential Use.DOS model is deactivated, the (small) change of electron affinity between Si and SiGe is not taken into account in a precise way. For simplicity, it is assumed that the midgap energy level does not depend on the Ge concentration.

Impact of Germanium on Point Defects

In contrast to III-V compound semiconductors, which have well-defined stoichiometry with distinct lattice sites for group III and group V atoms, SiGe allows arbitrary stoichiometry and random ordering of Si and Ge atoms. As a consequence, in SiGe, there is no need to differentiate between Si-like and Ge-like interstitials, or to define Si-type and Ge-type vacancies. Instead, it is fully sufficient to consider the density of ‘interstitials’ (extra (Si or Ge) atoms in the lattice) and ‘vacancies’ (vacant lattice sites) in the model.

In the literature, there is no agreement on the impact of Ge on point-defect parameters except for the vacancy transport capacity and equilibrium concentration. Computational studies of vacancies in SiGe have found an ~1.0 eV vacancy formation energy decrease in Ge [80][81] [82]. However, in Advanced Calibration, a decrease of the V formation energy of only 0.39 eV is assumed in germanium. The main difference of the transport capacities for silicon and germanium is modeled by different vacancy diffusivities. The interpolation between silicon and germanium is parabolic in logarithmic scale and was calibrated based on SiGe interdiffusion experiments [83].

Both the interstitial equilibrium concentration and the interstitial diffusivity in Ge are assumed to be larger than in silicon. In SiGe, a parabolic mole-fraction interpolation in logarithmic scale is applied for interstitial diffusivity, as well as for the equilibrium concentration.

Chapter 2: Advanced Calibration for Silicon, SiGe, and Germanium

Part 2: Constant Parameters

The I–V bulk recombination in SiGe is increased by a mole fraction–dependent factor `BulkRecFac`, which equals 1.0 for pure Si and pure Ge, and has its maximum value for $\text{Si}_{50}\text{Ge}_{50}$. This increased I–V recombination in SiGe has been found to be beneficial for the modeling of phosphorus transient-enhanced diffusion in SiGe after low-dose or high-dose P implantation. I–V recombination reduces the P diffusion tail from P–I diffusion most efficiently for high-dose P implantations.

To ensure the same surface recombination length of point defects for Si, SiGe, and Ge surfaces, the SiGe interpolation of the surface recombination rate follows the interpolation of the point-defect diffusivities.

Impact of Germanium on Extended Defect Parameters

The {311} interstitial clusters are less stable in the presence of Ge, and the transformation of {311} defects into dislocation loops is faster [3][84][85]. The effects have been calibrated by Synopsys based on experimental data generated from the ATOMICS research project [3].

For the `Moment` model for I-clusters, the parameters for growth (`Ikfi` and `Ikfc`) and dissolution (`Ikxr`) are interpolated between Si and Ge, parabolic, and in logarithmic scale.

Since the `Full` model for I-clusters is not defined for Ge, the parameter adjustment prefactors `C311DiffIntFactor` and `CLoopTransfer` are used instead of parameter interpolation between Si and Ge. The impact of Ge is taken into account only if `Ge_Chem_Effect=1`:

```
term Si name= C311DissIntFactor store add \
eqn= "(1.0+2.0*xMoleFraction+0.5*xMoleFraction*xMoleFraction)"

term Si name= CLoopTransfer store add \
eqn= "(1.0+25.*xMoleFraction+18.*xMoleFraction*xMoleFraction)"
```

Note that the terms for `C311DissIntFactor` and `CLoopTransfer` as listed above do not include the effect of stress, which is included in the Advanced Calibration file (see [Impact of Stress on Extended Defect Parameters on page 71](#)).

SiGe Interdiffusion

The interdiffusion model [86][87] is switched on to describe interdiffusion of Si and Ge. Its parameters were extracted and calibrated against data from [88][89][90][91][92]. While the (dominant) interdiffusivity from vacancies can be extracted reliably, the parameter error might be larger for the smaller component of interdiffusivity from the diffusion of interstitials. Data for interdiffusion during oxidation [93] was used to test assumptions on the parameters for SiGe interdiffusion using interstitials.

The biggest uncertainties in calibration exist for highly n-doped SiGe, where interdiffusion is believed to have a dominant contribution from P–V or As–V pairs, which is not yet included in the calibration, due to lack of experimental data suitable for calibration. To include

Chapter 2: Advanced Calibration for Silicon, SiGe, and Germanium

Part 2: Constant Parameters

contributions from dopant–vacancy pair diffusion in SiGe interdiffusion, you can define the term `InterVDiffFactor`, which is 1.0 by default, as a function of dopant concentration. This factor is then multiplied to the interdiffusion caused by V diffusion in SiGe.

By default, for simplicity, no drift component is assumed in SiGe interdiffusion. As Ge atoms are larger in size than Si atoms, you might expect that a gradient in pressure adds a drift term to SiGe interdiffusion. To switch on this drift term, insert the following lines after calling the procedure `SiGe_and_Stress_Effect`:

```
pdbSet      Si  Ge  Interdiffusion.Drift 1  
pdbSet      Ge  Si  Interdiffusion.Drift 1  
pdbSetDouble SiGe Vac D.Inter.X2 {[Arr 1.2e5 1.52]}
```

Here, the first two lines switch on the drift contribution to interdiffusion, which effectively increases Si and Ge interdiffusion because the pressure gradient is, in many cases (and precisely in all 1D cases), parallel to the gradient of Ge concentration. The third line sets the interdiffusivity in SiGe using vacancies to a value smaller than the one calibrated for `Interdiffusion.Drift 0`. With this reduced value, the published interdiffusivity data used for model calibration matches `Interdiffusion.Drift 1`.

Germanium Effect on Dopant Diffusivity

Arsenic, Sb, and Ge diffusion in relaxed SiGe is much faster than in Si [94][95][96]. A nonlinear dependency of the vacancy-mediated diffusivity activation energy on the Ge content was first measured for Sb by Larsen and Kringshoj [94]. In Advanced Calibration, it is assumed that the vacancy components of the As, P, and Sb diffusivities show a similar trend with Ge mole fraction and temperature, as the diffusivity of free vacancies. Therefore, the calibration of the corresponding parameters for parabolic mole-fraction interpolation started from the values for vacancies and has been fine-tuned with the help of SIMS data provided by AMAT-VSE [83].

There is a lack of published experimental work devoted to P diffusion in SiGe, especially for high Ge mole fractions. The marker layer experiments performed by Zangenberg [96] indicate an increase of diffusivity with small Ge contents up to ~25%, and saturation or even a little decrease of Ge content of 40%. However, P diffusivity in pure Ge [23] is much higher than the one in SiGe with Ge content $\leq 40\%$. The parameters for logarithmic mole-fraction interpolation of P–V and P–I diffusivities have been calibrated against dedicated data provided by AMAT-VSE [83] and with the help of numeric optimization.

According to most experimental work [97][98][99], interstitial-mediated B diffusion in relaxed SiGe is retarded with increasing Ge content up to ~50%. For higher Ge contents, the boron diffusion is again enhanced [100]. Therefore, a linear expression for the diffusivity activation energy as derived by Ahn [101] for small Ge mole fractions is not adequate, and a parabolic one is used for the full Ge mole fraction range instead. Finally, the retardation effect of F on B diffusion decreases linearly with increasing Ge mole fraction.

Chapter 2: Advanced Calibration for Silicon, SiGe, and Germanium

Part 2: Constant Parameters

Table 4 summarizes the SiGe interpolation for the diffusivity components for different dopants.

Table 4 Germanium chemical effect on dopant diffusivity components

Diffusivity component	Logarithmic parabolic interpolation factor	Comments on data used for calibration
Sb–V	$\ln([\text{Arr } 1.5e12 \ 3.22]) \times x_{\text{Ge}} \times (1 - x_{\text{Ge}})$	Marker layer experiments [94]. Dedicated experiments from AMAT-VSE.
As–I	0	Marker layer experiments [95]. USJ experiments [102][103][104].
As–V	$\ln([\text{Arr } 9e10 \ 3.22]) \times x_{\text{Ge}} \times (1 - x_{\text{Ge}})$	Marker layer experiments [95]. USJ experiments [102][103][104]. Dedicated experiments from AMAT-VSE.
B–I	$\ln(8.0 \times 10^{-3}) \times x_{\text{Ge}} \times (1 - x_{\text{Ge}})$	Dedicated experiments from AMAT-VSE. USJ experiments [3][100][105][106]. Marker layer experiments [97].
P–I	$\ln([\text{Arr } 8e13 \ 2.13]) \times x_{\text{Ge}} \times (1 - x_{\text{Ge}})$	Dedicated experiments from AMAT-VSE [83]. USJ experiments [102].
P–V	$\ln([\text{Arr } 3e13 \ 3.46]) \times x_{\text{Ge}} \times (1 - x_{\text{Ge}})$	Dedicated experiments from AMAT-VSE [83]. USJ experiments [102].

Germanium Effect on Dopant Activation

The solubility of boron is slightly higher in SiGe than in pure Si. For the solubility of boron in SiGe, parabolic mole-fraction interpolation is used in logarithmic scale. For the solubility of As, P, and Sb in SiGe, parabolic mole-fraction interpolation is used in linear scale.

The dopant clustering reaction rates `CluRate` are interpolated parabolically in logarithmic scale.

Germanium Effect on Interface Segregation

The interface segregation has been calibrated based on SIMS. For B, As, and P, the `ThreePhaseSegregation` parameters for trapping and emission rates as well as the interface trap number `CMax` are interpolated between Si and Ge in logarithmic scale. In addition, parabolic interpolation is used for `CMax` for As and P, as well as for the parameters `P2trapMax`, `k1`, and `k3`, which govern the formation and dissolution of P_2 pairs at the

interface. The interstitial fraction of dopant trapping in equilibrium is interpolated in linear scale.

Germanium Effect on Initial Conditions After Implantation

For the initial activation parameters `AmInit` and `AcInit`, linear interpolation is used for SiGe.

The `ifactor` for SiGe of both As and P is interpolated linearly between Si and Ge. The interpolation is defined in the `ifactor_arsenic` and `ifactor_phosphorus` procedures. Similarly, `mcdfactor` for B, As, and P is subject to linear mole-fraction interpolation.

SiGe Oxidation

During oxidation of SiGe, Ge enhances oxidation rates and is completely rejected from the oxide, so that it piles up at the SiO_2 –SiGe interface [107]. This effect is exploited by the Ge condensation technique to enrich the Ge mole fraction of SiGe layers on insulators by oxidation [108]. The selective Si consumption by oxidation at the SiO_2 –SiGe interface is compensated by the thermal diffusion of Si from the bulk SiGe layer. However, when the Ge composition of the SiGe layer exceeds approximately 80%, the Si flux by thermal diffusion from the bulk SiGe layer cannot compensate the Si consumption by oxidation, resulting in the simultaneous oxidation of Si and Ge [109].

The parameters for dry SiGe oxidation were extracted and calibrated against literature data for oxide growth rates [108][109][110][111][112][113][114][115] and Ge pileup profiles [109][111][114][115]. The oxidation rate depends on the Ge mole fraction on the SiGe side of the SiO_2 –SiGe interface, which itself strongly depends on SiGe interdiffusion, which was first calibrated mainly based on inert anneals (see [SiGe Interdiffusion on page 65](#)). For strong Ge pileup by oxidation leading to high Ge mole fractions and compressive strain, SiGe interdiffusion is enhanced, which again leads to a lower and wider Ge pileup. Unfortunately, this interdependency is difficult to calibrate because the experimental Ge profiles available have, in general, limited accuracy. In addition, some uncertainties in the calibration exist for the influence of oxidation on the strain by SiGe lattice mismatch and on SiGe interdiffusion. Moreover, the self-limiting oxidation effect due to melting of the Ge pileup layer at the oxide–SiGe interface [116], or other causes [117], has not been included in the calibration.

The selective Si oxidation in general and the combined Si and Ge oxidation only at high Ge mole fraction (Ge concentration $> 3.8\text{e}22 \text{ cm}^{-3}$) have been implemented by terms for the segregation ratio and the transfer rate for Ge at the SiO_2 –SiGe interface, which depend on the oxidation rate (`ReactionSpeed`) and Ge concentration in silicon (`Germanium_Silicon`):

```
term Ox /Si name=GermaniumSegregationFactor store add \
eqn= {(1.0+ReactionSpeed*[Arr 1.0e26 2.0] * \
(Germanium_Silicon>3.8e22 ? 0.0 : (1.0-Germanium_Silicon/ \
3.8e22)) * \
(Germanium_Silicon>1.0e18 ? 1.0 : (Germanium_Silicon/1.0e18)))}
```

Chapter 2: Advanced Calibration for Silicon, SiGe, and Germanium

Part 2: Constant Parameters

```
term Ox /Si name=GermaniumTransferFactor store add \
eqn= {(1.0+ReactionSpeed*[Arr 1.0e35 4.0] * \
(Germanium_Silicon>3.8e22 ? 0.0 : (1.0-Germanium_Silicon/ \
3.8e22)) * \
(Germanium_Silicon>1.0e18 ? 1.0 : (Germanium_Silicon/1.0e18)))}
```

In addition, the parameters for wet SiGe oxidation were extracted and calibrated against literature data for oxide growth rates [118][119]. The accuracy is limited in general.

OED is suppressed already for small Ge mole fractions [19]. This effect is achieved by logarithmic scale interpolation of the interstitial injection parameter theta between a high value for Oxide_Silicon and a low value for Oxide_Germanium (see [Oxidation-Enhanced Diffusion on page 38](#)).

Stress Effects

To keep the implementation short, the abbreviations `vt_i`, `kT_i`, `PR`, and `PR_Si` are defined. The pressure abbreviations `PR` and `PR_Si` are limited by a maximum-allowed value of 4 GPa, which is defined in section 2.14 by the following parameter:

```
pdbSetDouble SiGe Mechanics MaxPressure 4.0e10
```

In structures with very high pressure in some corners, including pressure effects in the process models might adversely affect convergence. If convergence is degraded, then consider reducing the value of `MaxPressure`.

The definition of `PR` is:

```
set maxP [pdbGet SiGe Mechanics MaxPressure]
if { $Stress_Eff } { set PR \
    ((Pressure>$maxP)?$maxP:((Pressure<(-$maxP))?(-$maxP):Pressure)) \
} else { set PR 0.0 }
```

See section 2.14.2 of `AdvCal_2022.03.fps`.

Impact of Stress on Electrostatic Potential

If `Stress_Eff` is equal to 1, bandgap narrowing due to stress is calculated according to the deformation potential theory as published by [120]. If `Ge_Chem_Eff` is switched on as well, the deformation potential constants are interpolated linearly between values for pure silicon and values for pure germanium. If `Ge_Chem_Eff` is switched off, the silicon parameters are used. The deformation potential constants for Si and Ge proposed by Van de Walle [121] were chosen for Advanced Calibration.

The model is switched on using the command:

```
pdbSet Si Potential niMod StrainDependent
```

Chapter 2: Advanced Calibration for Silicon, SiGe, and Germanium

Part 2: Constant Parameters

Impact of Stress on Point-Defect Parameters

The diffusivities and equilibrium concentrations of interstitials and vacancies are modified in the presence of hydrostatic pressure using the terms `IntDiffFactor`, `VacDiffFactor`, `IntCStarFactor`, and `VacCStarFactor`, which are defined for both silicon and germanium, and are interpolated for SiGe:

```
pdbSetDouble Si Int idf -0.142e-23
pdbSetDouble Si Int icf -1.211e-23
pdbSetDouble Si Vac vdf 1.195e-23
pdbSetDouble Si Vac vcf 1.324e-23

pdbSetDouble Ge Int idf -0.142e-23
pdbSetDouble Ge Int icf -2.800e-23
pdbSetDouble Ge Vac vdf 8.000e-24
pdbSetDouble Ge Vac vcf 1.324e-23

pdbSetDouble SiGe Vac vdf.x2 1.9e-23
pdbSetDouble SiGe Vac vcf.x2 2.0e-23

term Si name=IntDiffFactor store add \
    eqn= "exp($PR*[_MoleFraction::Param Si Int idf]*$kT_i)"
term Si name=VacDiffFactor store add \
    eqn= "exp($PR*[_MoleFraction::Param Si Vac vdf]*$kT_i)"
term Si name=IntCStarFactor store add \
    eqn= "exp($PR*[_MoleFraction::Param Si Int icf]*$kT_i)"
term Si name=VacCStarFactor store add \
    eqn= "exp($PR*[_MoleFraction::Param Si Vac vcf]*$kT_i)"
term Ge name=IntDiffFactor store add \
    eqn= "exp($PR*[_MoleFraction::Param Ge Int idf]*$kT_i)"
term Ge name=VacDiffFactor store add \
    eqn= "exp($PR*[_MoleFraction::Param Ge Vac vdf]*$kT_i)"
term Ge name=IntCStarFactor store add \
    eqn= "exp($PR*[_MoleFraction::Param Ge Int icf]*$kT_i)"
term Ge name=VacCStarFactor store add \
    eqn= "exp($PR*[_MoleFraction::Param Ge Vac vcf]*$kT_i)"
```

In SiGe, the actual definition of the mole fraction-dependent terms is performed inside the procedure `_AlloyCompound`, which is defined in section 2.14.5 of `AdvCal_2022.03.fps`. (Sentaurus Process calls the `_AlloyCompound` procedure during diffusion preprocessing if SiGe is to be modeled as an alloy. Terms including mole fraction-interpolated parameters are best defined in this procedure.)

Compressive hydrostatic pressure decreases the equilibrium concentration of interstitials and increases the equilibrium concentration of vacancies. If `Stress_Eff=1`, then the diffusivities of point defects are modified as a function of pressure. The activation volumes for the above prefactors were derived from the induced strain values calculated by Diebel [122].

Chapter 2: Advanced Calibration for Silicon, SiGe, and Germanium

Part 2: Constant Parameters

For the vacancy diffusivity, a parabolic decrease of the activation volume is assumed between pure Si and pure Ge. The value for pure Ge has been adjusted to match experimental data reported by Kawamura *et al.* [123].

The modified equilibrium concentrations are used automatically by Sentaurus Process in the definition of surface boundary conditions.

The point-defect interface and bulk recombinations are diffusion-limited processes, but the modified diffusivities are not taken into account automatically in surface boundary conditions and bulk recombination rates. Therefore, together with changing the diffusivity of interstitials and vacancies, the surface and bulk recombination rates are adjusted accordingly.

In the drift-diffusion equation for point defects, the pressure gradient is implicitly taken into account as an additional force, which pushes interstitials towards regions of tensile stress and vacancies towards regions of compressive stress.

Impact of Stress on Extended Defect Parameters

The {311} interstitial clusters are less stable in the presence of compressive hydrostatic pressure, and the transformation of {311} defects into dislocation loops is faster [3][84][85].

The corresponding parameter adjustment prefactors `IClusterDissIntFactor` (used in the `1Moment` model for I-clusters), as well as `C311DissIntFactor` and `CLoopTransfer` (used in the `Full` model for I-clusters), have been calibrated by Synopsys based on experimental data generated within the ATOMICS research project [3].

The impact of stress is taken into account only if `Stress_Eff=1`:

```
term Si name=IClusterDissIntFactor store add eqn=
  "exp($PR*2.6e-23*$kT_i)"

term Si name=C311DissIntFactor store add \
  eqn= "(1.0+2.0*xMoleFraction+0.5*xMoleFraction*xMoleFraction)* \
    exp($PR*1.6e-23*$kT_i)"

term Si name=CLoopTransfer store add \
  eqn= "(1.0+25.*xMoleFraction+18.*xMoleFraction*xMoleFraction)* \
    exp($PR*3.3e-23*$kT_i)"
```

Note that the terms for `C311DissIntFactor` and `CLoopTransfer` as listed above also include the effect of Ge as included in the Advanced Calibration file (see [Impact of Germanium on Extended Defect Parameters on page 65](#)).

Impact of Pressure on Dopant Diffusivity

The diffusivity of dopants changes as a function of hydrostatic pressure. With increasing compressive pressure, diffusion using dopant–interstitial pairs is reduced, and diffusion using dopant–vacancy pairs is increased.

Chapter 2: Advanced Calibration for Silicon, SiGe, and Germanium

Part 2: Constant Parameters

The following formula for the macroscopic diffusivity D_{AX} using AX dopant–defect pairs is used:

$$D_{AX}(P) = D_{AX}(P = 0) \exp(-P V_{AX}/kT) \quad (7)$$

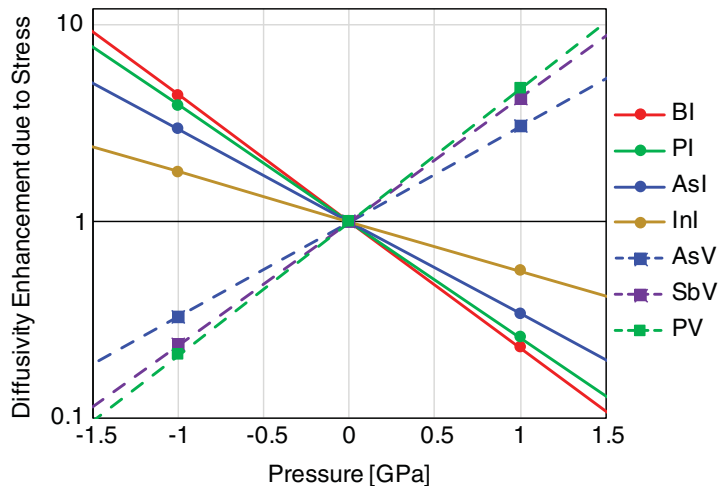
where P is the hydrostatic pressure (positive sign means compressive pressure), and V_{AX} is the activation volume. The activation volume values for different dopants are listed in [Table 5](#).

Table 5 Activation volumes for dopant diffusivity components in silicon

Diffusivity component prefactor	Activation volume [cm ³]	Comments on the data used
AntimonyVacDiffFactor	-2.334e-23	<i>Ab initio</i> calculations of the strain impact by Ahn [101]
ArsenicIntDiffFactorPressure	1.746e-23	<i>Ab initio</i> calculations of the strain impact by Ahn [101]
ArsenicVacDiffFactorPressure	-1.800e-23	<i>Ab initio</i> calculations of the strain impact by Ahn [101] , slightly reduced during calibration against experimental data
BoronIntDiffFactor	2.394e-23	Average value from <i>ab initio</i> calculations of the strain impact for different diffusion directions by Diebel [122]
GermaniumDiffFactor	-3.000e-23	Marker layer experiments by Zangenberg [96]
IndiumIntDiffFactor	0.936e-23	<i>Ab initio</i> calculations of the strain impact by Ahn [101]
PhosphorusIntDiffFactorPressure	2.200e-23	Average value from <i>ab initio</i> calculations of the strain impact for different diffusion directions by Ahn [101] , slightly reduced during calibration against experimental data
PhosphorusVacDiffFactorPressure	VacDiffFactor* VacCStarFactor	

The pressure dependency of diffusivities by different dopant–defect pairs is illustrated in [Figure 3](#). The stress effect on dopant diffusivity is superimposed on the chemical effect of Ge in a multiplicative way.

Figure 3 Enhancement of macroscopic diffusivity using selected dopant–defect pairs as a function of hydrostatic pressure, at T = 900°C in pure silicon



The stress effect is simulated by the activation energy correction using diffusivity prefactors. For example, in the case of boron, it is performed by the term `BoronIntDiffFactor`, which is defined in silicon:

```
term Si name=BoronIntDiffFactor store add \
eqn= "exp(-2.394e-23*$PR*$kT_i)"
```

During assembly of the diffusion equations, Sentaurus Process checks each dopant and material to assess whether such diffusion factors exist. The diffusivity through dopant–interstitial or dopant–vacancy pairs then is multiplied by the corresponding diffusion enhancement factors.

Impact of Pressure on Dopant Activation

If `Stress_Eff` is switched on, the solid solubility of dopants depends on the strain. In general, for compressive strain, the solubility of atoms smaller than Si increases; whereas, the solubility of larger atoms decreases. In the `Transient` model, the stress effect is taken into account by introducing pressure-dependent correction factors to `Solubility` and `TotalSolubility`:

$$S(P) = S(P = 0) \exp(-PV/kT) \quad (8)$$

where S is the dopant solid solubility, and V is the activation volume. The activation volume values for different dopants are presented in [Table 6](#). The same volumes were chosen for `Solubility` and `TotalSolubility`.

Chapter 2: Advanced Calibration for Silicon, SiGe, and Germanium

Part 2: Constant Parameters

Table 6 Activation volumes for dopant solid solubility

Dopant	Activation volume [cm ³]	Comments on the data used
Antimony	5.796e-24	Theoretical value from <i>ab initio</i> calculations of the induced strains by Ahn <i>et al.</i> [124] multiplied by a factor of 0.6 according to experimental data [3]
Arsenic	1.062e-24	<i>Ab initio</i> calculations of the induced strains by Ahn <i>et al.</i> [124]
Boron	-3.636e-24	Theoretical value from <i>ab initio</i> calculations of the induced strains by Ahn <i>et al.</i> [124] multiplied by a factor of 0.2 according to experimental data [3]
Phosphorus	-4.596e-24	<i>Ab initio</i> calculations of the induced strains by Ahn <i>et al.</i> [124]

The formulas for As and P are taken from *ab initio* calculations [124]. The impact of pressure on B solubility is chosen to be only 20% of the theoretical prediction in [124], as this better fits the experimental work performed in the ATOMICS research project [3] and experimental data from B ultrashallow junction formation with different variants of Ge preamorphization. The impact of pressure on Sb solubility is chosen to be 60% of the theoretical calculation in [124]. The relative change of solid solubility for different dopants as a function of pressure is shown in [Figure 4 on page 75](#).

An example of the definition of B pressure-dependent solid solubility is:

```
pdbSetString Si B SS.Factor      "exp(3.636e-24*$PR*$kT_i)"
pdbSetString Si B Total.SS.Factor "exp(3.636e-24*$PR*$kT_i)"
```

Since the emission rate for the silicon side in the three-phase segregation models is proportional to the solid solubility, corresponding modification should also be included in the boundary condition. For example, it was performed by the following line for B:

```
pdbSetString Si B Side.SS.Factor "exp(3.636e-24*$PR_Si*$kT_i)"
```

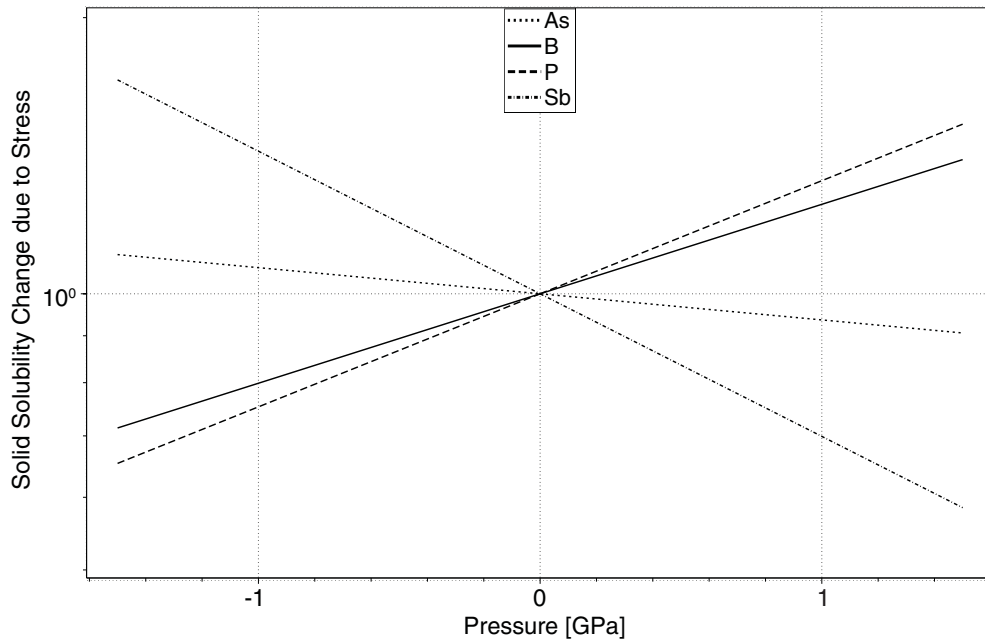
Note:

Arbitrary Alagator expressions for the dopant solid solubility prefactors can be defined by users in Sentaurus Process. The names of terms used for the solid solubility, the total solid solubility, and the emission rate correction are SS.Factor, Total.SS.Factor, and Side.SS.Factor, respectively.

In the ChargedCluster model, the solid solubility is not defined explicitly but results from the formation energies of the various clusters. Therefore, the formation energies of the clusters are modified as a function of pressure. This has been performed for boron and arsenic in such a way that the overall effect of pressure on dopant activation is similar as in

the Transient model. The calibration is arbitrary, because not enough experimental data is available to calibrate the effect of pressure on each BIC or AsV cluster individually.

Figure 4 Relative change of solid solubility of As, B, P, and Sb as a function of pressure, at T = 900°C



Segregation at Si–SiGe Interface (Segreg_Model)

Boron and P have been found to segregate at Si–SiGe interfaces, in experiments using epitaxial layers of strained SiGe embedded in Si, or strained Si embedded in relaxed SiGe. Boron segregates into SiGe; whereas, P is pushed out of the SiGe region. A theoretical analysis [74] indicates that the dominant driving force for this segregation is the pressure gradient in the case of B, and the difference in band structure between Si and SiGe in the case of P.

If Segreg_Model is switched on, an additional driving force for the drift-diffusion of B, As, and P is taken into account by using the PDependent model for both Si and Ge (not shown here):

```

if { $Segreg_Model } {
    pdbSetSwitch Si B StressModel PDependent
    term Si name=BoronIntSSFactor store add \
        eqn= "exp($Vt_i*(0.5*(Pressure/5.11e10)))"
    term Si name=BoronIntSPFactor store add \
        eqn= "exp($Vt_i*(0.5*(Pressure/5.11e10)))"

    pdbSetSwitch Si AsStressModel PDependent
    term Si name=ArsenicIntSSFactor store add \

```

Chapter 2: Advanced Calibration for Silicon, SiGe, and Germanium

Part 2: Constant Parameters

```

eqn= "exp($Vt_i*(-0.2*xMoleFraction))"
term Si name=ArsenicIntSPFactor store add \
eqn= "exp($Vt_i*(-0.2*xMoleFraction))"
term Si name=ArsenicVacSSFactor store add \
eqn= "exp($Vt_i*(-0.2*xMoleFraction))"
term Si name=ArsenicVacSPFactor store add \
eqn= "exp($Vt_i*(-0.2*xMoleFraction))"

pdbSetSwitch Si P StressModel PDependent
term Si name=PhosphorusIntSSFactor store add \
eqn= "exp($Vt_i*(-0.6*xMoleFraction))"
term Si name=PhosphorusIntSPFactor store add \
eqn= "exp($Vt_i*(-0.6*xMoleFraction))"
term Si name=PhosphorusVacSSFactor store add \
eqn= "exp($Vt_i*(-0.6*xMoleFraction))"
term Si name=PhosphorusVacSPFactor store add \
eqn= "exp($Vt_i*(-0.6*xMoleFraction))"
}

```

In this calibration, the potentials behind the additional driving forces can be expressed as:

$$E_{\text{mech,B}} = -0.5 \times \text{Pressure} / 5.11e10 \quad (9)$$

$$E_{\text{chem,As}} = 0.2 \times x_{\text{Ge}} \quad (10)$$

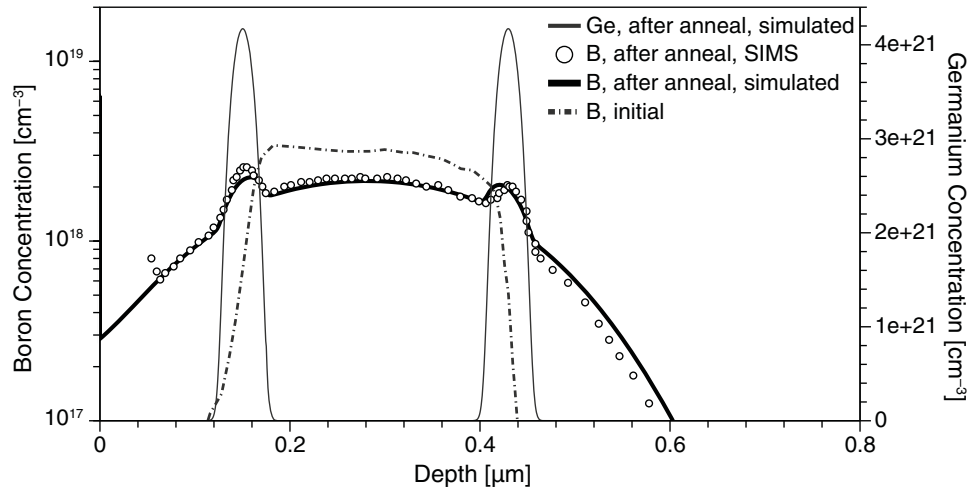
$$E_{\text{chem,P}} = 0.6 \times x_{\text{Ge}} \quad (11)$$

where:

- $E_{\text{mech,B}}$ is the mechanical potential of substitutional boron.
- $E_{\text{chem,As}}$ and $E_{\text{chem,P}}$ are the chemical potential of substitutional As and P, respectively, in eV.
- Pressure is the hydrostatic pressure in dyn/cm².
- x_{Ge} is the fractional Ge concentration.

These formulas have been calibrated to experimental data [125][126], as illustrated in [Figure 5](#). It should be noted that all measured data, which can be directly used for calibration, is extracted from plane wafer experiments with SiGe marker layers. In these wafers, the biaxial stress is approximately proportional to the Ge concentration. At present, a clear separation, whether the segregation is caused by a mechanical or an electrochemical potential, is not possible from available experimental data.

Figure 5 *B diffusion (56 hours at 850°C) in SiGe marker layers; SIMS data is extracted from [125] and simulations are performed with "SiGe_and_Stress_Effect 1 1 1 0"*



Effect of Strained Overlays (Strained_Overlays)

The model developed by Cowern [75] predicts an influence of overlayer strain on the point-defect concentration in the silicon. That effect was confirmed by experiments showing a strong dopant diffusion change under high-level stressed nitride layers [76][77].

The change of equilibrium concentration due to overlayer strain can be expressed by the factor $\exp(P_{ov}V_f/kT)$, in which P_{ov} is the hydrostatic pressure in the overlayer, and V_f is the volume of an atom in Si. This effect is switched on by setting the argument `Strained_Overlays` in the procedure `SiGe_and_Stress_Effect` to 1.

Unfortunately, it is not clear yet from experiments how intermediate layers such as an oxide layer between strained nitride and silicon influence the point-defect boundary conditions. With the current model implementation, a thin, unstrained, oxide layer would shield very effectively the impact of a strained SiN overlayer, in contrast to what has been observed in experiment [3]. Therefore, you need to be very careful in using this model in 2D or 3D process simulations, which usually include native oxide layer deposition steps.

In addition, as thermal expansion is another source of stress, the temperature at which native oxide layers are deposited in the process simulation can have a significant impact on point-defect concentrations at oxide–silicon boundaries, and inaccuracies in thermal expansion coefficients at elevated temperatures will translate into inaccurate calculations of point-defect concentrations.

Note:

It is recommended to define the same internal stress values in the native oxide as in the nitride to obtain the strained overlayer effect on the point-defect concentration in silicon.

Part 3: Ion Implantation and Initial Conditions

In this part of the Advanced Calibration file, the initial conditions for diffusion data fields after ion implantation are set immediately after implantation or immediately before the diffusion. In particular, the concentration of point defects or point-defect clusters present after ion implantation is specified dependent on the implantation species, energy, and dose. Furthermore, a framework is provided for a user-defined specification of initial electrical activation of as-implanted dopants.

In general, the initial conditions are important for annealing steps with small thermal budget. This is typically the case in deep-submicron technology.

Advanced Calibration for Sentaurus Process continuum can be used with analytic implantation or with Monte Carlo implantation (Sentaurus MC). In typical applications, it should not be used in combination with the options `cascades` and `frenkel.pair` of Sentaurus MC. These options calculate very high concentrations of self-interstitials and vacancies after ion implantation, which would require a dedicated calibration of clustering and recombination processes of point defects at very high concentrations. Such a calibration is not included in Advanced Calibration for Sentaurus Process continuum process simulation, which focuses on analytic implantation or the standard Monte Carlo implantation model (that is, without the options `cascades` and `frenkel.pair`).

The contents of part 3 of the Advanced Calibration file are described in the next sections.

User-Defined Defect Initialization

See sections 3.1, 3.4, and 3.5 of `AdvCal_2022.03.fps`.

The following command is selected:

```
pdbSet ImplantData defect.model user.defined
```

Using this command, Sentaurus Process expects the updating of data fields after ion implantation to be performed by the Aligator procedure `UserPointDefectModel`, which is defined in section 3.5.

The `UserPointDefectModel` procedure is called once after each ion implantation. (For Monte Carlo implantation of the molecular species BF_2 , the procedure `UserPointDefectModel` is actually called once for each element (boron and fluorine). This special case is taken into account in the implementation of `UserPointDefectModel`.)

The procedure is called once after each ion implantation to perform the following tasks:

- It calls the `impPostProcess_AdvCal` procedure, implemented in section 3.3 of `AdvCal_2022.03.fps`. This procedure updates the data fields and parameters for initialization of defect and dopant data fields for all materials after ion implantation and

Chapter 2: Advanced Calibration for Silicon, SiGe, and Germanium

Part 3: Ion Implantation and Initial Conditions

before diffusion, depending on implantation conditions. The same physical parameters are applied to analytic and Monte Carlo implantations.

- For Monte Carlo implantation, it calls additional procedures. First, it calls the procedure `ctrimDamageModels_AdvCal` in the case of Crystal-TRIM implantation, which is implemented in section 3.4 of `AdvCal_2022.03.fps`. This is needed for storing the Monte Carlo amorphization data field. Second, it calls the procedure `CoImpPostProcess` if the Coimplant model is switched on. (For analytic implantations, `CoImpPostProcess` is already in the regular implantation postprocessing procedures of Sentaurus Process and does not need to be called again in `UserPointDefectModel`.)
- For Monte Carlo implantation of molecules, `UserPointDefectModel` is called once for each atom species. In the special case of BF_2 implantation, care has been taken that `impPostProcess_AdvCal` is called only once (with the argument `Name=Boron`, but not with the argument `Name=Fluorine`). For all other molecular species with more than one atom species, such as $\text{B}_{18}\text{H}_{22}$ or $\text{C}_2\text{B}_{10}\text{H}_{12}$, the procedure `impPostProcess_AdvCal` is called once for each atom species. This might cause (a) the damage field to be added several times and (b) excess interstitials to be added for each implantation ion species:
 - (a) can be compensated by setting a small value of the corresponding `mcdfactor` procedure for molecular species, and (b) might be wrong for molecules that include H atoms, because H is likely to remain in interstitial positions (like F). This is performed automatically in the case of $\text{C}_2\text{B}_{10}\text{H}_{12}$ in the `_AdvCal::ImpPreProcess` and `_AdvCal::MCPostProcess` procedures, implemented in section 3.6 of `AdvCal_2022.03.fps`, as explained in [Implantation Preprocessing and Postprocessing on page 88](#). For implantations of molecules other than BF_2 and $\text{C}_2\text{B}_{10}\text{H}_{12}$, such as $\text{B}_{18}\text{H}_{22}$, it is recommended to subtract excess interstitials generated by H as shown in [Molecular Implantation on page 169](#).

All data-field processing for dopants and point defects is performed in the Alagator procedure named `impPostProcess_AdvCal`.

impPostProcess_AdvCal

See section 3.3 of `AdvCal_2022.03.fps`.

Scaling Factors for Point Defects and Damage

See section 3.3.1 of `AdvCal_2022.03.fps`.

Point Defects

The amount of point defects generated by ion implantation is calculated with the Advanced Calibration ‘+x’ model. The point defects are located at the same position as the as-implanted ions. The interstitial concentration originating from ion implantation is the

Chapter 2: Advanced Calibration for Silicon, SiGe, and Germanium

Part 3: Ion Implantation and Initial Conditions

as-implanted dopant profile multiplied by `ifactor`. The vacancy concentration is the as-implanted dopant profile multiplied by `vfactor`.

Unless specified directly in the `implant` command, `ifactor` and `vfactor` are calculated in the following way. If a procedure `ifactor_${mat}_${Species}` (`ifactor_Germanium_Arsenic`, for example) is defined for the current implantation species into a specific material, `ifactor` for this specific material is calculated in this procedure as a function of the implantation energy and dose. Otherwise, if a procedure `ifactor_${Species}` (for example, `ifactor_Arsenic`) is defined for the current implantation species (for any material), `ifactor` is calculated in this procedure as a function of the implantation energy and dose. Otherwise, `ifactor` has the value 1. Similarly, if a procedure `vfactor_${Species}` is defined for the current implantation species (for a specific material or any material), `vfactor` (for this specific material or any material) is calculated in this procedure as a function of energy and dose. Otherwise, `vfactor` has the value 0.

In section 3.2 of `AdvCal_2022.03.fps`, procedures are defined for the calculation of `ifactor` after implantation of As, B, BF_2 , C, $\text{C}_2\text{B}_{10}\text{H}_{12}$, Ge, In, P, or Si ions. `vfactor` equals 0 for all implantation species. In Advanced Calibration, `ifactor` is calibrated for pure Si but is not defined to be silicon specific. Therefore, in the case of other materials, the same `ifactor` as for Si is used, unless a material-specific `ifactor` is defined, for example, for `ifactor_Germanium_Germanium` and `ifactor_Germanium_Silicon`.

The concept behind this type of implementation is that it is very convenient for users to fine-tune `ifactor` or `vfactor` for any species as a function of implantation energy and dose, according to their needs.

For this purpose, it is sufficient to (re-)define a very short procedure `ifactor_${Species}` or `vfactor_${Species}`. This can be performed ideally after sourcing the Advanced Calibration file.

The return value of `ifactor_${Species}` and `ifactor_${mat}_${Species}` is usually a number, but it is also possible to define an expression as the return value.

For example, after sourcing `AdvCal_2022.03.fps`, you can define the following procedure to create one excess interstitial per B atom in pure Si, and a slightly reduced number of interstitials in regions that have a high concentration of Ge before the B implantation:

```
fproc ifactor_Boron {Energy Dose} {
    return "(1e22/(Germanium+1e22))"
}
```

You can specify `ifactor` directly in the `implant` command. In that case, the directly specified values are used instead of the return values of `ifactor_${Species}` or `ifactor_${mat}_${Species}`.

With Advanced Calibration loaded, you cannot define `ifactor` or `vfactor` with `pdbSet` commands such as:

```
pdbSet <material> <dopant> IFactor <value>
```

Chapter 2: Advanced Calibration for Silicon, SiGe, and Germanium

Part 3: Ion Implantation and Initial Conditions

The value of the `pdb` parameter `IFactor` is ignored, and `ifactor` is calculated as described in the text.

Similarly, the parameter database entries for `VFactor`, `MCIFactor`, `MCVFactor`, and `DFactor` are ignored when Advanced Calibration is used.

Damage

The crystal damage is proportional to the concentration of displaced atoms in silicon, including Frenkel pairs. It is scaled by `dfactor`. The damage field is used by Sentaurus Process to determine whether a region is amorphous or crystalline at the beginning of the annealing.

By default, the damage model (`AmModel1`) is `Damage`. In this case, the damage field is calculated during ion implantation, using the damage accumulation model of Sentaurus MC or Crystal-TRIM for Monte Carlo ion implantation or analytic damage profiles suggested by Hobler and Selberherr [127] for analytic ion implantation. The damage field is scaled by `dfactor`. For analytic implantation, `dfactor` can depend on implantation energy and dose if a procedure `dfactor_$Species` or `dfactor_${mat}$_{Species}` is defined for the implantation species.

Similarly, for Monte Carlo implantation, `dfactor` can depend on implantation energy and dose if a procedure `mcdfactor_$Species` or `mcdfactor_${mat}$_{Species}` is defined. These procedures are defined in section 3.2.2 of `AdvCal_2022.03.fps`. For most species, the procedure `mcdfactor_$Species` returns a constant value. The calibration of damage scaling for Monte Carlo implantation has been performed for Sentaurus MC.

To change the damage scaling for Monte Carlo implantation, you have the following options:

- Redefine the `mcdfactor_$Species` or `mcdfactor_${mat}$_{Species}` procedure. This is the best method.
- Define the parameter `MCDFactor` for a material and species. By default, `MCDFactor` is undefined for all materials and all species. If you define it, `MCDFactor` will be used instead of the return value of the `mcdfactor` procedures defined in the Advanced Calibration file.
- Specify the `mc.dfactor` argument directly in the `implant` command. In that case, for this particular implantation, the specified value will be used.

You can use a ‘+x’ damage model by defining a procedure `AmModel1$_Species` or `AmModel1$_{mat}$_{Species}`, which gives the return value ‘+1’. In this case, the crystal damage is the product of the as-implanted dopant profile and `dfactor`. The ‘+x’ damage model can be helpful to describe situations where buried amorphous layers are formed after medium-dose implantation of heavy ions (for example, indium implantation with 100 keV, $6 \times 10^{13} \text{ cm}^{-2}$). With the ‘+x’ damage model, it is necessary to define very high values for `dfactor` to adjust the measured and simulated amorphization.

Values for Initial Dopant Activation

See section 3.3.2 of `AdvCal_2022.03.fps`.

`AcInit` and `AmInit` determine the initial activation of dopants after implantation. For regions with an as-implanted dopant concentration higher than `AcInit` (`AmInit`), the surplus dopants are assumed to be in clusters at the beginning of a diffusion process. Both `AcInit` and `AmInit` are applied in subroutines of the callback procedure `diffPreProcess`, which is called before each diffusion simulation. `AcInit` is used for regions that are not amorphized by ion implantation, and `AmInit` is used for regions that are amorphized by ion implantation and recrystallize at the beginning of the diffusion process.

For most dopants, `AcInit` and `AmInit` are defined in part 2 of the calibration file as constant parameters. Only `AcInit` for B and BF_2 is defined in a similar way to `ifactor`.

You can define `AcInit` and `AmInit` in a similar way to `ifactor`. If a procedure `acinit_${mat}_${Species}` (for example, `acinit_Germanium_Arsenic`) is defined for a specific material, `AcInit` for this specific material is calculated in this procedure as a function of the implantation energy and dose. Otherwise, if a procedure `acinit_${Species}` (for example, `acinit_Arsenic`) is defined (for any material), `AcInit` is calculated in this procedure as a function of the implantation energy and dose. The same applies to `AmInit`.

By using expressions as the return value of the function `acinit_${Species}`, `aminit_${Species}`, it is possible to define `AcInit`, `AmInit` as terms.

Sum of As-Implanted Point Defects and Crystal Damage

See sections 3.3.3 of `AdvCal_2022.03.fps`.

The data fields `Int_LastImp` and `Vac_LastImp`, which are generated during implantation, are added to the fields `Int_Implant` and `Vac_Implant`, respectively, which are used in the callback procedure `diffPreProcess` for generating the initial conditions for diffusion. This activates a correct treatment of several subsequent implantations of the same dopant.

Similarly, the crystal damage from individual implantation steps is added to the field `Damage`, which is used during diffusion preprocessing to determine amorphous regions. In Advanced Calibration, `AmModel` is `Damage` for all species by default.

Therefore, the damage field `Damage_LastImp` is added to `Damage`. `Damage_LastImp` has been calculated during ion implantation using either the damage accumulation model of the Monte Carlo ion implantation or analytic damage formulas suggested by Hobler and Selberherr [127] for analytic ion implantation.

Subroutines for Setting ifactor and dfactor

See section 3.2 of `AdvCal_2022.03.fps`.

In the Advanced Calibration, `ifactor`, `vfactor`, `dfactor`, `AcInit`, and `AmInit` can depend on the material, species, energy, and dose of the ion implantation. All values and formulas in section 3.2 have been calibrated by Synopsys, using mainly SIMS data. The guidelines used for the calibration are explained here.

ifactor

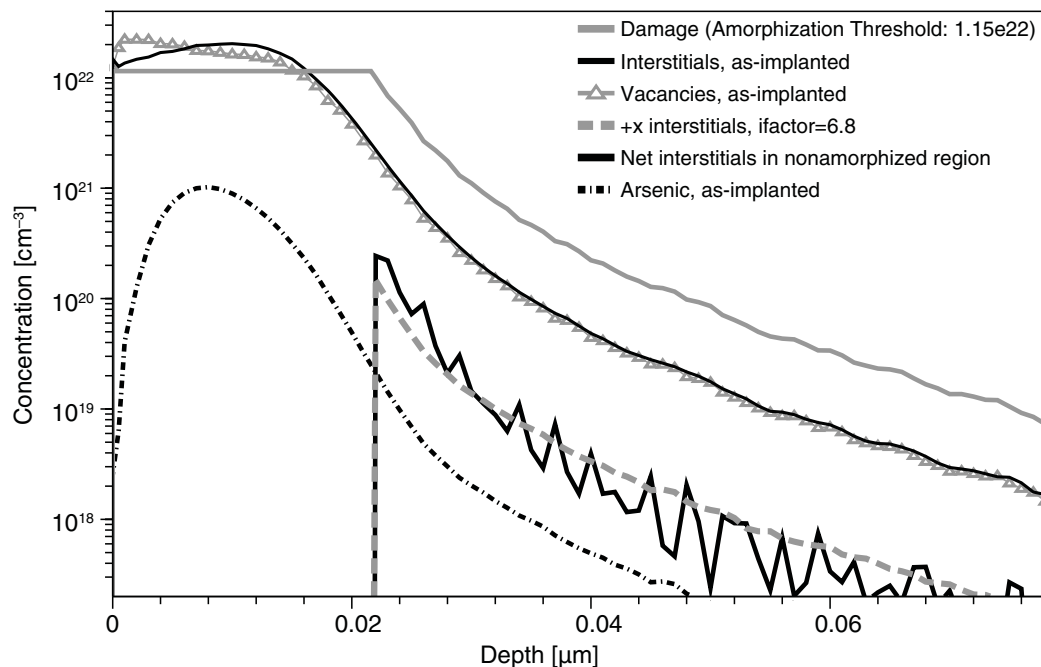
Giles [128] observed that using an `ifactor` of 1.0 gives good results for many situations. An `ifactor` of 1.0 means that, after the fast recombination of excess interstitials and vacancies generated by ion implantation, one interstitial atom survives per implanted ion. In `AdvCal_2022.03.fps`, an `ifactor` of 1.0 is used for the implantation of most species.

For high dose ($> 1 \times 10^{14} \text{ cm}^{-2}$) arsenic implantation (into silicon), a higher value of `ifactor` is used. In this case, `ifactor` is set in the procedure `ifactor_Arsenic` as a steady function of implantation energy and dose, and can have a value up to 9.0 for high-energy and high-dose implantation.

The higher value of `ifactor` will reflect a consequence of amorphization of the silicon surface layer by high-dose arsenic implantation. During solid phase epitaxial regrowth (SPER) of the amorphized surface region, all point defects in that region are eliminated.

Since the interstitials generated by collisions during ion implantation are (on average) located slightly deeper than the vacancies, a larger fraction of interstitials will be located in the deeper region inside silicon, which is not amorphized, and will survive the damage annealing by SPER. After recombination of all of the vacancies and interstitials that survived SPER, there remains an average number of interstitials per implanted ion higher than 1.0 in the nonamorphized region. This consideration can be investigated quantitatively by using the full cascade mode of Monte Carlo ion implantation simulation, as illustrated in [Figure 6](#).

Figure 6 Derivation of ifactor for As implantation (dose $1 \times 10^{15} \text{ cm}^{-2}$, energy 8 keV) by full-cascade MC simulation. The upper black solid line and the line with triangles show the interstitial and vacancy concentration, respectively, as calculated by full-cascade MC simulation. Near the surface (depth $< 0.008 \mu\text{m}$), the concentration of vacancies is higher; in other regions, the concentration of interstitials is higher than the concentration of vacancies. After SPER, only point defects in the nonamorphized region (depth $> 0.022 \mu\text{m}$) survive. The net interstitial concentration ($\text{Int} - \text{Vac}$; thick black line), calculated from the full-cascade MC results, is similar to the As concentration multiplied by ifactor close to 10. The dashed line shows the As concentration in the crystalline region, multiplied by 6.8, which is close to the ifactor for this process condition calculated by AdvCal_2020.09.fps.



ifactor is set to the value 0.5 for BF₂ implantation into silicon. This is meant to anticipate the capability of F to eliminate interstitials, which is not taken into account in the diffusion models used by Advanced Calibration by default.

If the Boolean parameter `AdvCal_IFactorsVFactorsZero` is set to 1, then the creation of excess interstitials and vacancies is suppressed. This parameter allows you to suppress transient-enhanced diffusion (TED) after ion implantation. It can be used to speed up process simulation for process parts, where TED can be neglected.

vfactor

vfactor is set to 0.0 for all implanted ions.

Chapter 2: Advanced Calibration for Silicon, SiGe, and Germanium

Part 3: Ion Implantation and Initial Conditions

dfactor

The damage scaling factors for analytic and Sentaurus MC implantation into silicon and germanium have been calibrated based on a wide range of experimental data, mainly TEM and RBS data from the literature. They differ from 1 to compensate for the default underestimation or overestimation of amorphization caused by implantation of these species.

For analytic implantation into silicon, the damage factor is decreased for B, but it is increased for Si. For As, BF₂, Ge, In, and P implantation, dfactor depends on the implantation energy and dose.

For MC implantation with Sentaurus MC, the damage is scaled by the parameter `MCDFactor`, which can be set individually for each implantation species. The values of `MCDFactor` have been calibrated for silicon and germanium with experimental data.

Finally, to improve the accuracy for the projected ranges of Ge implantations into silicon by Sentaurus MC, the empirical correction factor parameter for energy loss per collision (`nucl.cor`) has been set to a value less than 1. In addition, the parameters `Dacc` and `Dcrit`, which govern the damage accumulation and amorphization during Monte Carlo ion implantation with Crystal-TRIM, have been changed for silicon to improve the reproduction of the depth of amorphous layers after Si implantation into silicon.

Thermal Implantations

See sections 3.2, 3.6, and 3.7 of `AdvCal_2022.03.fps`.

Thermal implantations involve substrates kept at temperatures that differ from room temperature. Cold or cryogenic implantations are performed below room temperature. Under these conditions, there is less dynamic annealing and the implantation amorphizes more rapidly, leading to deeper amorphous layers and less implantation channeling [129][130][131]. Hot or heated implantations are performed above room temperature. Under these conditions, there is more dynamic annealing and the implantation amorphizes less rapidly, leading to shallower amorphous layers and more implantation channeling [132][133].

Dynamic annealing is lattice self-repair during the implantation. Implantation creates substantial damage, basically I and V, which can cluster into amorphous pockets. Like single I and V, the I and V in amorphous pockets can recombine and, therefore, reduce the damage. This recombination is hindered by an energy barrier, but it still occurs at relatively low temperatures during implantation.

Different implantation dose rates and temperatures lead to different balances of damage generation and lattice self-repair during implantation and, therefore, different amorphization and channeling. In addition, increased channeling due to the lower vibrational amplitude of

Chapter 2: Advanced Calibration for Silicon, SiGe, and Germanium

Part 3: Ion Implantation and Initial Conditions

the Si lattice at lower implantation temperatures is a much weaker effect than the reduction of channeling due to stronger amorphization.

These effects can all be simulated by default with Sentaurus Process Kinetic Monte Carlo [134] (see [Amorphization on page 273](#)). However, neither the implantation temperature nor the dose rate is taken into account by default in Advanced Calibration for Sentaurus Process. To account for the temperature dependency of implantation, section 3.2.4 contains the procedure `AdvancedThermalImplantModel`. On demand, this procedure switches on a consistent framework and calibration for thermal implantation.

To use this procedure, specify the command `AdvancedThermalImplantModel` after loading the Advanced Calibration file. An implantation temperature other than room temperature must be specified in the `implant` command:

```
implant Carbon dose=1.0e+15 energy=6.0 temperature=-100
```

At elevated temperatures, some dopants (for example, arsenic) diffuse during implantation. Since diffusion is not modeled in continuum during implantation, you must specify a corresponding `diffuse` command immediately after the `implant` command, with the diffusion temperature of the `implant` command and with the diffusion time depending on the dose (for example, $1\text{e}15 \text{ cm}^{-2}$) and the average dose rate (for example, $5\text{e}13 \text{ cm}^{-2} \text{ s}^{-1}$):

```
implant Arsenic dose=1.0e+15 energy=2.0 temperature=450
diffuse temp=450 time=[expr 1.0e+15/5.0e+13]<s>
```

Note:

When using Advanced Calibration Version R-2020.09 or earlier versions, to use the procedure `AdvancedThermalImplantModel` in combination with `SiGe_and_Stress_Effect`, place the commands in the following order (otherwise, some settings for initial conditions after thermal implantation are overwritten):

```
SiGe_and_Stress_Effect 1 x x x    ;# first
AdvancedThermalImplantModel      ;# afterwards
```

It is recommended to use the `ChargedReact` model for implant temperature diffusion. In addition, to allow diffusion at the implant temperature, the minimal diffusion temperature for which diffusion equations are solved must be set accordingly. In Advanced Calibration, it is 300°C . The minimal diffusion temperature is defined by:

```
pdbSetDouble Diffuse minT 300.0
```

The following sections describe the implementation and calibration of the procedure `AdvancedThermalImplantModel`.

Scope of Calibration

In `AdvancedThermalImplantModel`, a calibration is included only for Sentaurus MC implantation, which allows a calibration for amorphization and channeling at the same time. Since analytic implantation profiles are used for room temperature implantations in general, they might need adjustments for cold and hot implantations, which is beyond the scope of the `AdvancedThermalImplantModel` procedure.

The calibration covers thermal implantation from cold (-100°C) to hot (500°C) into silicon, based on data from AMAT-VSE [134] [135] for implanted ions included in the calibration, which are antimony, arsenic, boron, carbon, fluorine, germanium, indium, phosphorus, and silicon.

Thermal implantation into SiGe and Ge is currently not calibrated, meaning the parameters are independent of the implant temperature. However, the `AdvancedThermalImplantModel` procedure is compatible with the SiGe parameter interpolation and the calibration included in the `SiGe_and_Stress_Effect` procedure. This means that you can simulate thermal implantation into SiGe, but it is not necessarily accurate, since the SiGe parameters are linearly interpolated between the temperature-dependent Si parameters and the Ge parameters for room temperature.

Note:

Since calibration of thermal implantation is based on a specific smaller experimental dataset from AMAT-VSE, it is not necessarily identical at the default room temperature to the default calibration for damage and initial conditions.

Debye Temperature, Electronic Stopping, and Damage

The parameter `DebyeTemperature` is used in the Sentaurus Process model for lattice vibrations. In Sentaurus MC, these vibrations play a role in scattering ions out of the channeling directions of the silicon crystal. For modeling implantation of arsenic or boron at high energies, the most accurate calibration of ion channeling in silicon has been obtained by defining `DebyeTemperature` as a function of ion energy and wafer temperature. For phosphorus, the `Local.Debye.Model` is used. The parameters of this model are also defined as a function of ion energy and wafer temperature.

For arsenic and boron implantation, the parameter `LSS.pre`, which scales the energy loss due to nonlocal electronic stopping, is defined as a function of ion energy and wafer temperature as well.

For Sentaurus MC implantations, the implantation damage is adjusted in section 3.2.4.2 by changing the dynamic annealing factor, that is, the parameter for the survival rate of the Frenkel pairs for the noncascade damage model, by either increasing the value for cold implantations [134] or decreasing the value for hot implantations [135]:

```
pdbSet Si <species> surv.rat <value>
```

Chapter 2: Advanced Calibration for Silicon, SiGe, and Germanium

Part 3: Ion Implantation and Initial Conditions

This not only increases (or decreases) damage during implantation to influence channeling, but also leads to more (or less) amorphization at the end of the implantation.

Temperature dependencies of the MC implantation model parameters are defined in the implantation callback procedure `AdvancedThermalImpPreProcess`, so you can access the current implantation temperature. This callback procedure is defined exclusively in the `AdvancedThermalImplantModel` procedure and is called in the `_AdvCal::ImpPreProcess` procedure defined in section 3.6.

Initial Conditions

The temperature-independent damage scaling factors `mcdfactor` are adjusted for phosphorus, carbon, and silicon in section 3.2.4.3. The `mcdfactor` for other implanted species are aligned with standard Advanced Calibration values.

The interstitial scaling factors `ifactor` are defined to be temperature dependent for arsenic and phosphorus. While the initial activation for recrystallized regions (`aminit`) is assumed to be independent of the implantation temperature, the initial activation for crystalline regions (`acinit`) is defined to be temperature dependent for arsenic, phosphorus, and boron.

At room temperature, both `ifactor` and `acinit` values defined in the callback procedure `AdvancedThermalImpPreProcess` are aligned with standard Advanced Calibration values and with the values from SiGe parameter interpolation included in the procedure `SiGe_and_Stress_Effect`.

If you use the `ChargedReact` model, which is recommended for thermal implantations, the initial distribution of arsenic and boron in substitutional and interstitial configurations is defined in section 3.2.4.2 in the callback procedure `AdvancedThermalDiffPreProcess`. In pure silicon, 5% of implanted As atoms and 3% of implanted B atoms are directly put into As-I and B-I pairs, respectively. This procedure is defined exclusively in `AdvancedThermalImplantModel` and is called in the `_AdvCal::DiffPreProcess` procedure defined in section 3.7.

Implantation Preprocessing and Postprocessing

See section 3.6 of `AdvCal_2022.03.fps`.

Analytic Implantation

For implantations with dose $< 10^{12} \text{ cm}^{-2}$, `ChanDoseScaling=1`. The dose of 10^{12} cm^{-2} corresponds to the smallest entries in the double-Pearson Default implantation tables. With `ChanDoseScaling=1`, for doses smaller than the smallest entries in the table, the channeling dose scales linearly with the total dose.

Chapter 2: Advanced Calibration for Silicon, SiGe, and Germanium

Part 3: Ion Implantation and Initial Conditions

For dose $> 10^{12} \text{ cm}^{-2}$, `ChanDoseScaling` is irrelevant for single implantations. For several subsequent implantations, `ChanDoseScaling` is sometimes important because the `CoImplant` model is used in Advanced Calibration. In the `CoImplant` model, the damage from previous implantations is converted into an *equivalent dose*, as described in the *Sentaurus™ Process User Guide*. If this equivalent dose is smaller than the smallest dose in the table used, the calculation of the channeling dose depends on `ChanDoseScaling`.

For dose $> 10^{12} \text{ cm}^{-2}$, `ChanDoseScaling=1` for backward compatibility of results obtained with the `CoImplant` model.

Sentaurus Process offers an improved implantation table `boron_in_silicon_2012` for boron implantations with energy $> 200 \text{ keV}$. To automatically select this table for energy $> 200 \text{ keV}$, users of Advanced Calibration can set the parameter:

```
pdbSetBoolean ImplantData B UseHighEnergyBoronTable 1
```

With `UseHighEnergyBoronTable` set to 1, the alternative table is switched on for boron implantations with energy $> 200 \text{ keV}$ in the procedure `_AdvCal::ImpPreProcess`, which is called at the beginning of executing an `implant` command. In the procedure `_AdvCal::ImpPostProcess`, which is called at the end of executing an `implant` command, Sentaurus Process switches back to the Default table for boron implantations, which is usually preferred for low-energy boron implantations.

The table `boron_in_silicon_2012` uses the Taurus table format (and, additionally, for low energy (energy $< 85 \text{ keV}$), it is identical to the Taurus table for boron implantations). In the Taurus format tables, the `CoImplant` model is not applied. With the improved table, to take into account the reduction of high-energy boron ion channeling due to preceding implantations, you can use the PAI model. To do this, specify the keyword `pai` in the corresponding `implant` command.

Monte Carlo Implantation (General)

The procedures `_AdvCal::ImpPreProcess` and `_AdvCal::MCPostProcess` are used for the energy- and dose-dependent calibration of implantation profiles and amorphization by Sentaurus MC.

The parameters for As, B, BF₂, H, He, and P in silicon have been adjusted to improve the accuracy of as-implanted profiles. A more accurate peak position of As, B, H, He, and P implantation profiles is achieved by the calibration of the electronic stopping correction factor, `LSS.pre`.

Sentaurus MC uses two methods for the calculation of binary collisions. For most energies, scattering tables are used. For the highest energies, the collisions are calculated using a Coulombic form of the potential between the collision partners. In the Sentaurus MC defaults, the high-energy range starts when the so-called *dimensionless energy* exceeds the value of 1000. This corresponds to an energy of $\sim 9780 \text{ keV}$ for B–Si binary collisions and even higher energies for heavier particles. For H and He implantation, an older version

Chapter 2: Advanced Calibration for Silicon, SiGe, and Germanium

Part 3: Ion Implantation and Initial Conditions

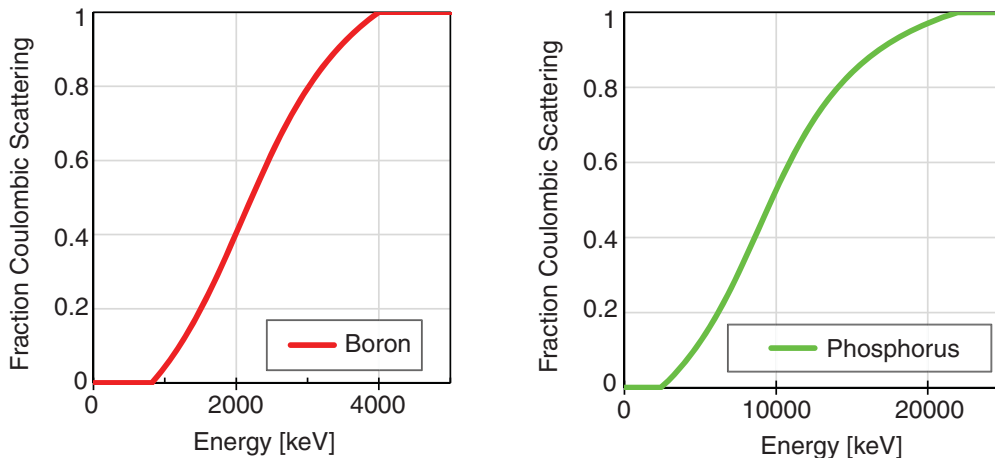
of the scattering tables is used. It has the same entries as the new version but is limited to an energy range up to a dimensionless energy of 100. This is achieved by setting the Boolean parameter `HighE.Scatter.Table` to 0, for H and He implantation.

You can define an energy range in which Sentaurus MC interpolates between the two methods. In `AdvCal_2022.03.fps`, such transition ranges are defined for B and P implantations. They are illustrated in [Figure 7](#). The following parameters are used, with values originating from optimization against SIMS data:

```
pdbSetDouble Si B Interp.Min.Energy      820
pdbSetDouble Si B Interp.Max.Energy       4000
pdbSetDouble Si B Interp.ATan.Min.Abscissa -1
pdbSetDouble Si B Interp.ATan.Max.Abscissa 1.5
pdbSetDouble Si P Interp.Min.Energy      2392.6
pdbSetDouble Si P Interp.Max.Energy       21968
pdbSetDouble Si P Interp.ATan.Min.Abscissa -1.212
pdbSetDouble Si P Interp.ATan.Max.Abscissa 2.44
```

The parameters `Interp.Min.Energy` and `Interp.Max.Energy` specify the energy range in which interpolation is performed. Instead of linear interpolation from 0% to 100% scattering in Coulombic form, Sentaurus Process uses a curved interpolation, as shown in the red and green curves in [Figure 7](#). The shape of these curves follows exactly the shape of the arctangent function in the interval [`Interp.Atan.Min.Abscissa`, `Interp.Atan.Max.Abscissa`].

Figure 7 Method for calculation of binary scattering for (left) B and (right) P implantation into Si, as defined in `AdvCal_2022.03.fps`. At low energies, scattering tables (0% Coulombic scattering) give the most accurate results. Then, a transition range is defined in which the scattering is interpolated between results from scattering tables and results from Coulombic scattering. At the highest energies, 100% Coulombic scattering is used.

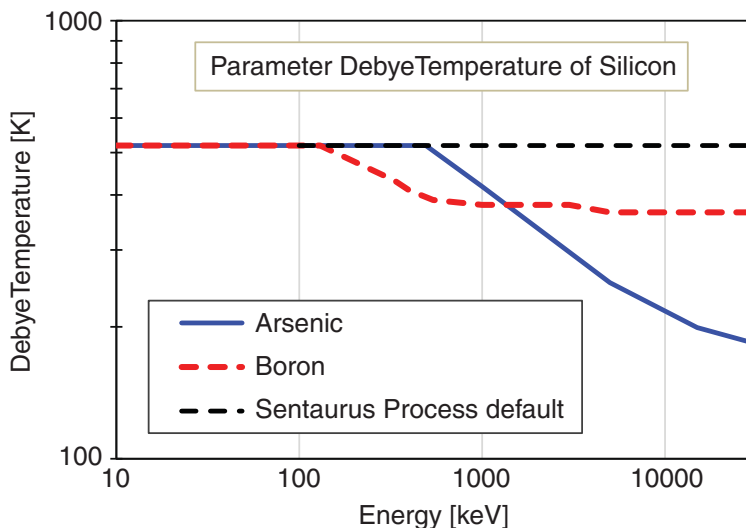


Chapter 2: Advanced Calibration for Silicon, SiGe, and Germanium

Part 3: Ion Implantation and Initial Conditions

The parameter `DebyeTemperature` is used in the Sentaurus Process model for lattice vibrations, which play a role in scattering ions out of the channeling directions of the silicon crystal. For As and B, `DebyeTemperature` has been calibrated as a function of implantation energy. The default value of 519 K is used for low and medium energies. At higher energies, the value is interpolated from a list of xy value pairs. This interpolation is performed with the function `XYLogInterpol`, which interpolates in log scale for both x- and y-values. The calibration for high implantation energies has been performed by matching the channeling tail of SIMS data provided by Applied Materials or extracted from [136] and [137]. Figure 8 shows the calibrated values for As and B implantation performed at room temperature.

Figure 8 Parameter `DebyeTemperature` calibrated as a function of initial ion energy to reproduce ion channeling for room temperature implantation of As or B into Si

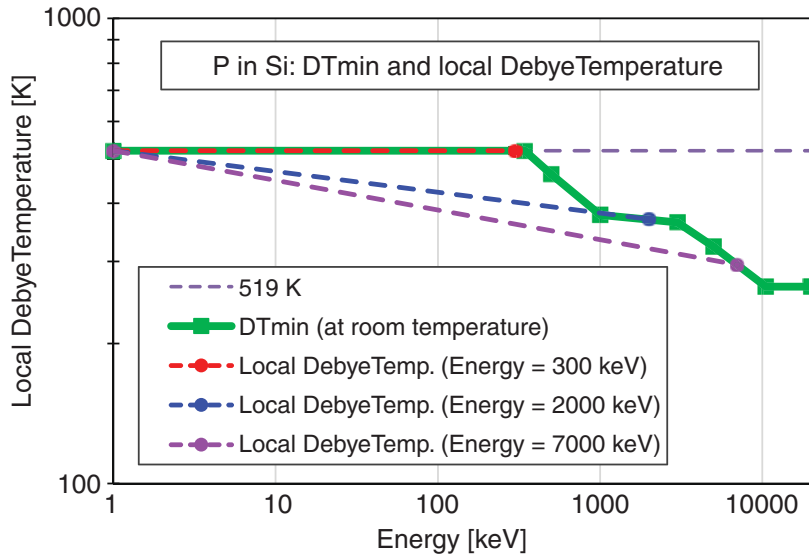


For phosphorus implantation with energies higher than 500 keV, the `Local.Debye.Model` is switched on. In that model, the Debye temperature used in the model for lattice vibration is not defined as a function of the initial ion energy, but as a function of the local ion energy, which decreases as the P ions lose energy along their paths. The parameters are defined in the following way:

```
pdbSet MCImplant Local.Debye.Model 1  
pdbSetDouble Si Local.Debye.Pre 1.0  
pdbSetDouble Si Local.Debye.Exp [expr log($DTmin/519.)/log($Energy)]
```

Here, `Energy` is the energy at which the P ion is implanted. `DTmin` is the value of the parameter `DebyeTemperature` to be used at this initial energy. `DTmin` itself depends on the initial ion energy as shown in Figure 9. With these parameters, the value of the local Debye temperature changes smoothly from `DTmin` at the initial energy to 519 K at 1 keV, as the P ion loses energy, as shown in Figure 9.

Figure 9 Definition of parameter $DTmin$ and local Debye temperature for P implantation into Si at room temperature. $DTmin$ depends on the initial energy as shown by the green line. The red, blue, and violet lines show the local value of Debye temperature to be used in the lattice vibration model as a function of the local ion energy, for different initial energies: 300 keV, 2000 keV, and 7000 keV, respectively.



For cold or hot implantation, the most accurate results for ion channeling have been achieved by defining the value of `DebyeTemperature` as a function of implantation energy and wafer temperature. For P implantation, the parameter `DTmin` is defined as a function of the implantation energy and wafer temperature. The corresponding calibration is selected when using the procedure `AdvancedThermalImplantModel`.

The parameters `nloc.pre` and `scr.par` are used by the MC model for local electronic stopping. They can be used for fine-tuning the depth of the channeling tail and the width of the peak of as-implanted profiles. For As and P high-energy implantations, the parameter `nloc.pre` is interpolated from a list of xy value pairs. The interpolation is performed with the function `XLogInterpol`, which performs logarithmic interpolation of the x-value (here, implantation energy) and linear interpolation of the y-value. The `scr.par` parameter is defined differently from the default for As, H, and He implantation.

The calibration for H covers the energy range 5–4000 keV. The calibration for He was tested against SIMS data from 1000 keV and 2000 keV He implantations. For high-energy implantation in the channeling direction (`tilt=0`), the channeling of H and He atoms is very sensitive to the tilt angle, and the calibration of `scr.par` is less reliable. The calibration of the parameters `d.sim` and `nloc.pre` helps to reproduce the channeling tail of low-energy B implantations. These parameters are reset to their default values in the procedure `_AdvCal::MCPostProcess`.

For As, BF_2 , and Ge implantation into silicon, the damage scaling defined in the callback procedure `mcdfactor_`\$Species depends on the implantation energy and dose. In

Chapter 2: Advanced Calibration for Silicon, SiGe, and Germanium

Part 3: Ion Implantation and Initial Conditions

particular, for accurate amorphization by high-dose As implantations, a high damage scaling factor is required. However, the dose dependency of the damage scaling factor has been introduced to reduce amorphization by low- and medium-dose As implantations, such as channel or pocket implantations in CMOS technology.

Carborane

It is recommended to use Sentaurus MC for molecular implantation (see [Molecular Implantation on page 169](#)).

In the case of Sentaurus MC implantation of carborane into silicon, the following settings defined in the procedures `_AdvCal::ImpPreProcess` and `_AdvCal::MCPostProcess` help to obtain accurate results for the amorphization and good initial conditions:

1. The procedure `_AdvCal::ImpPreProcess` is called before the implantation. It adjusts amorphization by carborane implantation. With `$Energy` as the energy of the carborane molecule, the following parameter values are set before the carborane implantation:

```
pdbSet      Si B surv.rat  [expr (25.0/$Energy+0.25)]  
pdbSet      Si C surv.rat  [expr (25.0/$Energy+0.25)]  
pdbSetDouble Si      d.sim   0.33  
pdbSetDouble Si B    nloc.pre 0.37
```

where `surv.rat` ('survival rate') scales the crystal damage, which is generated by nuclear collisions *during* the implantation. In particular for small energies, it must be set to very high values; otherwise, ion channeling during implantation is overestimated. In addition, the calibration of the parameters `d.sim` and `nloc.pre` helps to further improve the accuracy for the channeling tail.

2. The procedure `_AdvCal::MCPostProcess` is called after the MC implantation. In the case of carborane implantation, it resets `surv.rat` for B and C to the default values, as there might be other B or C ion implantations later in the process simulation:

```
pdbSet Si B surv.rat 0.225      ; # Sentaurus Process default  
pdbSet Si C surv.rat 0.45      ; # Sentaurus Process default
```

3. The procedure `_AdvCal::MCPostProcess` also switches off the hydrogen solution to save CPU time in subsequent anneals:

```
solution name=Hydrogen nosolve store
```

4. The procedure `_AdvCal::MCPostProcess` also sets the number of interstitials to be generated by carborane implantation. Otherwise, Sentaurus Process adds 'automatically' one interstitial for each C, B, and H atom. This is not reasonable for H, which probably comes to rest in an interstitial position and is unlikely to kick out Si atoms from the lattice site. In addition, one 'free' interstitial per C atom might be an overestimation, because 2/3 interstitials per C are already included in C_3I_2 clusters, which the C atoms are assumed to form immediately after implantation in the nonamorphized regions.

Chapter 2: Advanced Calibration for Silicon, SiGe, and Germanium

Part 4: Comprehensive and Slow Models

Therefore, a correction of the ‘automatic’ calculation of excess interstitials is implemented:

```
set ifactor [ifactor_C2B10H12 $Energy $Dose]
sel z = "Int_Implant - $ifactor * Hydrogen_LastImp - \
0.667*Carbon_LastImp" Silicon name=Int_Implant store
```

The amorphization of silicon by carborane implantation has been calibrated, with TEM data provided by AMAT-VSE, for implantation energies in the range from 2.6 keV to 20 keV.

Part 4: Comprehensive and Slow Models

The fourth part of `AdvCal_2022.03.fps` contains the procedure `AdvancedModels`. This procedure switches on a consistent calibration of some complex models for silicon, which are not used by default. To use this procedure, apply the command `AdvancedModels` immediately after loading the Advanced Calibration file. This switches on the following models:

- The `ChargedReact` model for the diffusion of B, As, P, In, and F. This is a good choice for any processes in which steep and shallow p-n junctions are formed.
- The `Full` model for interstitial clusters. In this model, the kinetics of formation and dissolution of small interstitial clusters, {311} defects, and dislocation loops is described by seven equations [22].
- The `ChargedCluster` model for boron–interstitial clusters (BICs) and indium clusters. Boron-clustering kinetics is described by the formation and dissolution of six types of BIC: B_2 , B_2I , B_2I_2 , B_3I , B_3I_2 , and B_3I_3 . Indium clustering is described by three clusters: In_2 , In_2I , and In_2V . In addition, initial conditions after indium implantation are redefined.
- `AdvancedFluorineModel` for fluorine uses the `ChargedCluster` model for fluorine clusters and allows you to simulate the fluorine effect on boron diffusion in a more accurate way compared to the model used by default.

In addition, other model parameters are adjusted for As, B, P, and In diffusion. These additional adjustments have been calibrated with SIMS data. They are needed because the simulation of transient-enhanced diffusion of these dopants is affected by switching on the `Full` model for interstitial clusters instead of the `1Moment` model, which is the default in Advanced Calibration.

The disadvantage of switching on the advanced models is that the total number of equations to be solved for dopant and defect clustering increases sharply, which leads to a typical increase of CPU time for annealing by a factor of three or more, in comparison to simulations with the Advanced Calibration standard models. Another disadvantage is that, due to the larger number of model parameters, additional calibration is typically more difficult than with the standard models.

Chapter 2: Advanced Calibration for Silicon, SiGe, and Germanium

Part 4: Comprehensive and Slow Models

In general, it is not recommended to use only part of the advanced models. In particular, for B USJ formation, you should not use the `ChargedCluster` model without switching on the `Full` model for interstitials, and vice versa. However, in devices where the maximum concentration of B or As is small, you might consider selecting a simple clustering model for this dopant to save CPU time.

The option `AdvancedModels` is interesting for fundamental research on process simulation models and for applications where the standard models are too simple to capture all trends correctly. These can include, for example, the modeling of dopant activation and defect annealing during low-temperature processes.

The next sections describe the contents of the procedure `AdvancedModels`.

Interstitial Clusters

See section 4.1 of `AdvCal_2022.03.fps`.

The advanced interstitial clustering model, first published in [22], is switched on by:

```
pdbSet Si Int ClusterModel      Full  
pdbSet Si Int MultiClusterModel Full { 2Moment Loop }
```

In this model, seven equations are solved to describe the kinetics of self-interstitial clusters:

- Three data fields (I_2 , I_3 , I_4) describe small interstitial clusters (SMICs).
- Two data fields (D_{311} , density of $\{311\}$ defects, and C_{311} , density of interstitials bound in $\{311\}$ defects) describe the presence of $\{311\}$ defects.
- Two data fields (D_{Loop} , density of dislocation loops, and C_{Loop} , density of interstitials bound in dislocation loops) describe dislocation loops.

For a complete description of the model and a comparison to experimental data, refer to the literature [22]. Figure 10 and Figure 11 illustrate the differences of this model to the default `1Moment` model.

The high supersaturation of interstitials in the initial phase of low-temperature annealing is important also for USJ formation with spike annealing, since all temperature ramps start at low temperature. Therefore, if the `Full` model is used for interstitial clusters, a suitable calibration of transient-enhanced diffusion of dopants that diffuse together with interstitials (B, P, In) requires either a dopant–interstitial clustering model or reduced diffusivities of dopant–interstitial pairs at low temperatures.

The following command defines the initial conditions:

```
pdbSet Si I2 InitPercent 1.0
```

Excess interstitials generated by ion implantation are placed in I_2 clusters.

Figure 10 Time evolution of interstitial supersaturation after low dose 40 keV silicon implantation, during annealing at 600°C; experimental data points are taken from [9]. For short-time anneals (< 1000 s), a high supersaturation is maintained by dissolution of SMICs (small interstitial clusters). This is reproduced correctly with the Full model, but not with the 1Moment model. For longer anneal times, the interstitial supersaturation is maintained by {311} defects. In this situation, the 1Moment model gives similar results to the Full model.

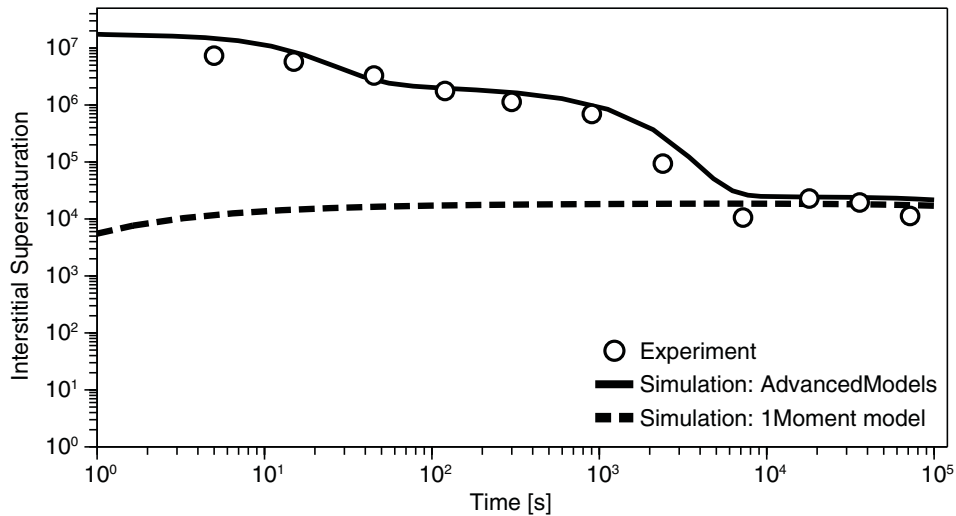
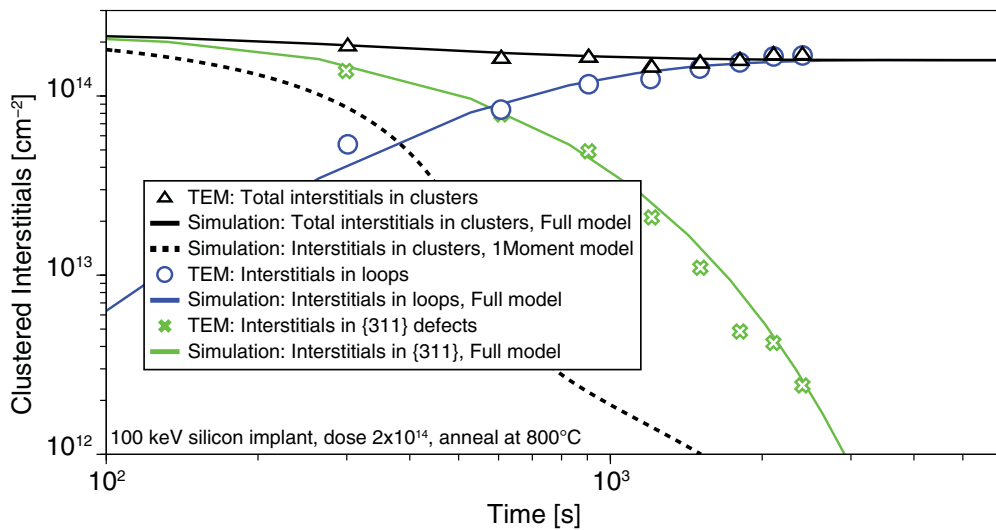


Figure 11 Time evolution of concentration of interstitials in {311} defects and dislocation loops after amorphizing silicon implantation, during annealing at 800°C. Experimental data points (TEM) are extracted from [138]. The Full model offers a good description of interstitials bound to {311} defects and dislocation loops. In contrast, the 1Moment model underestimates the stability of interstitial clusters in situations with dislocation loops.



Boron–Interstitial Clusters

See section 4.2 of `AdvCal_2022.03.fps`.

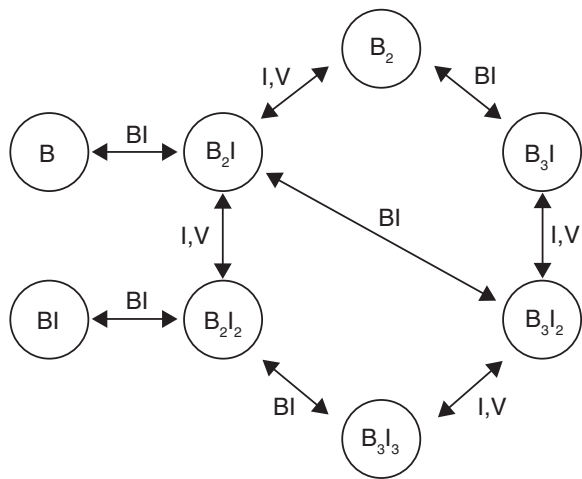
Boron–interstitial clusters (BICs) should be used in combination with the `Full` model for interstitial clusters. The BIC model is selected by:

```
pdbSet Si B ActiveModel ChargedCluster
```

All clusters are assumed to be electrically neutral. The most important model parameters are the formation energies of the various clusters. These have been optimized by comparison to a collection of SIMS data for various process conditions. The model reaction pathway is shown in [Figure 12](#). The five-stream (`ChargedReact`) diffusion model for B is switched on together with the BIC model.

Previously, the BIC model described the activation of B more accurately than the `Transient` cluster model, especially for thermal anneals with a low thermal budget, such as low-temperature rapid thermal annealing (RTA) or millisecond annealing [139]. However, this is no longer the case.

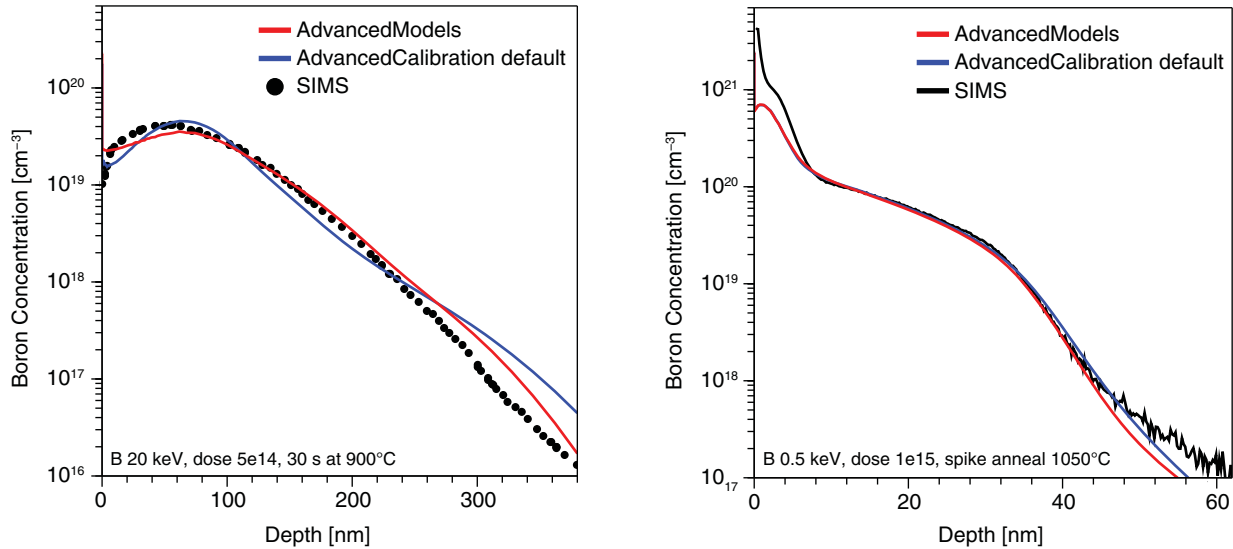
Figure 12 Reaction pathway for BIC model



In `AdvCal_2022.03.fps`, the `Transient` cluster model has been substantially improved, by better taking into account the role of interstitials in the formation of B clusters (see [Boron Clustering on page 41](#)). With this improvement, the `Transient` model describes the activation of B slightly better than the BIC model.

An example is shown in [Figure 13](#), where the `AdvancedModels` provides superior accuracy for RTA at 900°C (*left*). No substantial improvement is obtained for the spike anneal (*right*) for typical CMOS technology.

Figure 13 Comparison of simulated B profiles with AdvancedModels (red lines: Full model for interstitial clusters, ChargedCluster and ChargedReact models for B) and default Advanced Calibration model (blue lines: 1Moment model for interstitial clusters, Transient model for B clusters, ChargedReact model for B) to SIMS data. (Left) Boron profiles after RTA at 900°C (SIMS data from [140]). AdvancedModels is significantly more accurate. (Right) Boron profiles after a spike anneal at 1050°C (SIMS data from AMAT-VSE). All simulations are performed with AdvCal_2020.09.fps, either with or without the AdvancedModels option.



Arsenic Parameters in AdvancedModels

See section 4.3 of AdvCal_2022.03.fps.

The five-stream (ChargedReact) diffusion model for arsenic is switched on in AdvancedModels. Other parameters do not change.

Phosphorus Parameters in AdvancedModels

See section 4.4 of AdvCal_2022.03.fps.

The five-stream (ChargedReact) diffusion model for phosphorus is switched on in AdvancedModels. In addition, parameters are prepared for the trapping of P at EOR defects. However, by default, the EORTrap model is deactivated.

ChargedCluster Model for Indium

See section 4.5 of `AdvCal_2022.03.fps`.

Three types of indium cluster are taken into account: In_2 , In_2I , and In_2V . The following reactions for the formation and dissolution of clusters are considered:

- $\text{In}-\text{I} + \text{In} \rightleftharpoons \text{In}_2\text{I}$
- $\text{In}_2 + \text{I} \rightleftharpoons \text{In}_2\text{I}$
- $\text{In}_2\text{V} + \text{I} \rightleftharpoons \text{In}_2$

The most stable cluster type is In_2V . It is assumed that In_2I and In_2 clusters are formed at the very beginning of thermal annealing after implantation.

The five-stream (`ChargedReact`) diffusion model for In is switched on in `AdvancedModels`. The following lines help to improve the convergence of diffusion simulation with indium:

```
pdbSetDouble Si In Abs.Error 1e5  
pdbSetDouble Si In Rel.Error 1e-2
```

Fluorine Diffusion and Clustering

See section 4.6 of `AdvCal_2022.03.fps`.

The procedure `AdvancedFluorineModel` defines a physics-based model for fluorine diffusion and clustering in silicon. It can be used in combination with both models for interstitial clusters, that is, the default `1Moment` model and the full model of the `AdvancedModels` set.

Based on the literature [141][142][143], fluorine tends to stay in the interstitial position due to a strong interstitial fluorine binding. In the context of the five-stream diffusion model `ChargedReact`, this means that the neutral component of `ChargePair` is set to a relatively high value, leading to a higher interstitial fluorine (`FluorineInt`) concentration than the ‘substitutional’ fluorine (`Fluorine`) concentration in general. Moreover, the literature [141][142][143] indicates that interstitial fluorine prefers to decorate vacancies to form so-called fluorine–vacancy clusters. In the framework of the `ChargedCluster` model in which ‘substitutional’ impurities cluster with silicon point defects, these clusters of interstitial fluorines and vacancies (that is, F_3V) result in fluorine–interstitial clusters (that is, F_3I_2) through the following relation:



The allowed cluster types are F_2 , F_2I , and F_3I_2 with formation energies inherited *ab initio* [143]. The initial conditions of fluorine after ion implantation are mainly interstitial fluorine for crystalline silicon and partially clustered in F_2I , and F_3I_2 in recrystallized silicon.

Chapter 2: Advanced Calibration for Silicon, SiGe, and Germanium

Part 4: Comprehensive and Slow Models

The three-phase segregation model is selected as the Si–SiO₂ interface model for fluorine with parameter values allowing for strong dose loss. In addition, two F atoms located in the Si–SiO₂ interface are allowed to cluster with a B atom, resulting in a fluorine-dependent boron dose loss. In the presence of fluorine, some B atoms in the interface cluster with fluorine, thereby freeing interface traps for single B atoms. This leads to an increased total number of boron traps in the interface and, therefore, a stronger boron dose loss. The interface trap density, emission, and trapping rates, and the cluster formation and dissolution rates have been calibrated by Synopsys based on SIMS data. The Alagator implementation of the B–F cluster formation at Si–SiO₂ interfaces is part of the Advanced Calibration file.

See [Fluorine Diffusion and Clustering on page 171](#) for additional fine-tuning of the model.

Carbon Diffusion and Clustering

See section 4.7 of `AdvCal_2022.03.fps`.

Carbon segregation to the end-of-range defects can be modeled by the trapping of carbon by {311} defects and loops. The corresponding calibrated model can be optionally activated by setting:

```
pdbSetBoolean Si C EORTrap 1
```

following the `AdvancedModels` command.

Nitrogen Diffusion and Clustering

See section 4.9 of `AdvCal_2022.03.fps`.

The procedure `AdvancedNitrogenModel` defines a physics-based model for nitrogen diffusion and clustering in silicon. It can be used in combination with both models for interstitial clusters, that is, the default `1Moment` model and the full model of the `AdvancedModels` set.

According to the literature [144], nitrogen behaves differently from other group V impurities in bulk Si. While P, As, and Sb are shallow n-type dopants, substitutional nitrogen N_s is a deep-level impurity. Therefore, the neutral five-stream diffusion model `NeutralReact` is selected. Nitrogen has low solubility due to a strong interstitial nitrogen binding [144]. The stable nitrogen–interstitial N_i pair shows strong diffusion due to a low migration barrier [144][145]. In addition, substitutional nitrogen forms stable pairs with a vacancy [146].

The reaction N_i + V <=> N_s has been calibrated to allow for detailed balance with the reaction N_s + I <=> N_i, meaning that the reaction rates vanish in equilibrium.

Current understanding attributes nitrogen diffusion in silicon not only to the migration of interstitial nitrogen, but also to the migration of the nitrogen dimer N₂I₂ [145]. In this

Chapter 2: Advanced Calibration for Silicon, SiGe, and Germanium

Part 4: Comprehensive and Slow Models

calibration, the nitrogen dimer diffusion is activated by selecting the `Dimer` model for nitrogen:

```
pdbSet Si N Dimer NDimer
```

and defining a diffusivity for the nitrogen dimer. The nitrogen dimer can form immobile clusters with both interstitials and vacancies, which are stable to high temperatures [147]. These complexes then can suppress the formation of large vacancy or interstitial clusters. Again, all reactions have been calibrated to allow for detailed balance.

The `ThreePhaseSegregation` model describes nitrogen dose loss. At oxide–silicon interfaces, the parameter `Scale.PairSegregation_Silicon` is set to 1.0. This means that no silicon self-interstitials are left behind when N_i pairs cross the interface from silicon to oxide. When using `AdvancedNitrogenModel`, the nitrogen trapped at the oxide–silicon interface due to nitrogen dose loss has no impact on the oxidation rate in N_2O atmosphere.

See [Nitrogen Diffusion and Clustering on page 172](#) for additional fine-tuning of the N and N dimer clustering model.

Solid Phase Epitaxial Regrowth

See section 4.10 of `AdvCal_2022.03.fps`.

The solid phase epitaxial regrowth (SPER) model in continuum Sentaurus Process simulates the movement of amorphous–crystalline (a/c) interfaces due to the recrystallization of the amorphous silicon and the dopant dynamics during such a process. The procedure `AdvancedSPERModel` containing the calibration of the SPER phase field model is not activated by default. It can be switched on as an option and used in combination with all other models of Advanced Calibration.

The boundary movement during SPER is described with the specific solution fields, either the distance field by the level-set method or the phase field by the phase field method. The phase field method is selected by:

```
pdbSet Diffuse SPER.Model PhaseField
```

It uses a consistent mesh structure, so that the phase and the other solutions are coupled seamlessly into the Scharfetter–Gummel discretization scheme, which improves the convergence if there is high drift due to an abrupt phase change.

With the calibration parameters of `AdvancedSPERModel` and a decent fine mesh (1–2 nm spacing) in the amorphized region, the phase field method has proven to be robust in one and two dimensions, having no convergence or oscillation problems. The mesh spacing in amorphized regions should not exceed the phase transition width of 3 nm to allow for accurate and stable simulation results.

The use of the phase field method is straightforward. In the case of annealing after an amorphizing implantation, the phase field method assumes no diffusion in a crystalline

Chapter 2: Advanced Calibration for Silicon, SiGe, and Germanium

Part 4: Comprehensive and Slow Models

region during SPER, so that only recrystallization, diffusion in amorphous regions, and redistribution at a/c interfaces occur.

As soon as regrowth is completed, the phase field method is deactivated and the regular diffusion initialization is applied. The dopant activation in the regrowth region is performed with the `pdb` parameter `AmInit` or the term `${Sol}AmInit`. Finally, the standard equations for crystalline regions are solved for the remaining annealing time.

Recrystallization Speed

The calibration includes parameters for the recrystallization speed for undoped amorphous silicon (a-Si) in the (100) orientation as based on the literature [148].

The corresponding parameters are:

```
pdbSet Si SPER PhaseTransWidth 0.003
pdbSet Si SPER Lambda.Fac      1.61
pdbSet Si SPER Relax.Rate     { [Arr 3.08e8 2.68]/
                                [pdbGet Si SPER PhaseTransWidth]/[pdbGet Si SPER PhaseTransWidth] }
```

For the definitions of these parameters, see the *Sentaurus™ Process User Guide*. In general, you do not need to change these parameters. The phase transition width `PhaseTransWidth` has been chosen to be 3-nm to guarantee good convergence for regular meshes used in process simulation, with spacing less than 3-nm in regions of the a/c interface. Finally, the parameters `Relax.Rate` and `Lambda.Fac` have been chosen to give the correct recrystallization speed for the given `PhaseTransWidth`.

In addition, retardation of recrystallization by the presence of fluorine is taken into account, but to a smaller extent than reported in the literature [149]. The change in recrystallization speed is defined by the factor:

```
pdbSet Si SPER R.Fac "(0.8+0.2*3.e18/(3.e18+Fluorine))"
```

Enhancement of the recrystallization speed by both n-type and p-type doping is not included. According to Olson and Roth [148], the speed of SPER can be enhanced by a factor of approximately 10 in a-Si with a boron concentration $> 2\text{e}20 \text{ cm}^{-3}$. To adjust the recrystallization speed, change the expression of `R.Fac`.

In addition, the orientation-dependent parameters are set by:

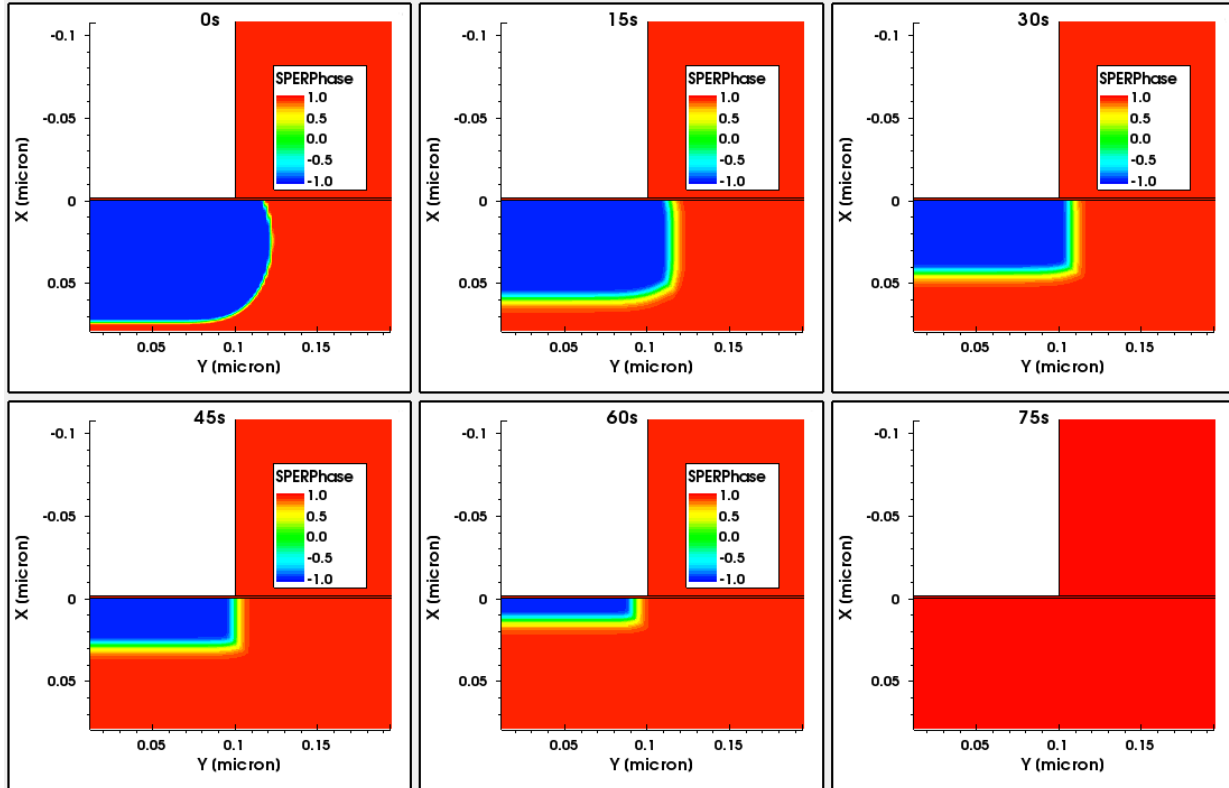
```
pdbSet Si SPER R.Fac.Aniso { 100 20.0 110 10.0 111 1.0 }
pdbSet Si SPER E.Aniso     { 100 0.0 110 0.0 111 0.0 }
```

This means that the recrystallization in the (100) orientation is twice as fast as in the (110) orientation, and 20 times as fast as in the (111) direction, following [150]. In the case of recrystallization of an amorphized pocket on a (100) wafer, recrystallization towards the surface is faster than in the lateral direction (see Figure 14).

Chapter 2: Advanced Calibration for Silicon, SiGe, and Germanium

Part 4: Comprehensive and Slow Models

Figure 14 Orientation-dependent SPER in 2D for an amorphized pocket on a (100) Si wafer: (upper left) SPER phase field shown in as-implanted Si, in partially recrystallized Si, and (lower right) deactivated in fully recrystallized Si. In this example, regrowth is faster in the vertical (100) direction than in the lateral (110) direction.



In the model, the reduced speed of SPER in the (110) and (111) directions leads to an increased snow plow effect. Whether dopants are really pushed more for SPER in the (110) direction than for SPER in the (100) direction has not been investigated yet in experiments. For the very slow regrowth in the (111) direction, the calibration of doping redistribution during SPER has not been tested yet.

The physical mechanism behind the anisotropy of SPER velocity is that recrystallization is slowest in (111) planes, and the recrystallization front propagates along (111) nanofacets in the (100) direction and along (111) nanoridges in the (110) direction, as explained in [151]. This mechanism and its consequences on SPER near material boundaries can be modeled accurately with lattice KMC simulations [150], but not yet with continuum process simulations.

In 2D and 3D continuum process simulations, after switching on `AdvancedSPERModel`, you can enforce equal SPER regrowth rate in all directions by inserting the line:

```
pdbSet Si SPER R.Fac.Aniso { 100 20.0 110 20.0 111 20.0 }
```

This might be considered the safest option when using `AdvancedSPERModel` because dopant redistribution during SPER in the (110) and (111) directions will not exceed the dopant redistribution in the (100) direction, which has been calibrated against SIMS data.

Doping Redistribution

A general calibration is provided for the doping or impurity redistribution of B, As, P, In, F, and C. For solutions to be redistributed during SPER, the diffusivity in a-Si (`DAmor`) and the segregation energy (`SPER.Energy`) must be defined. Nonzero diffusivities allow for diffusion in a-Si, while nonzero segregation energies allow for the snow plow effect by a semipermeable a/c interface.

Boron

According to Venezia *et al.* [152], no boron is swept by the recrystallization front. The diffusivity in a-Si, which was reported to be high at the very beginning of SPER and then to become smaller during SPER, as an effect of increasing order inside a-Si [153], was set to [`Arr 1.0 2.68`].

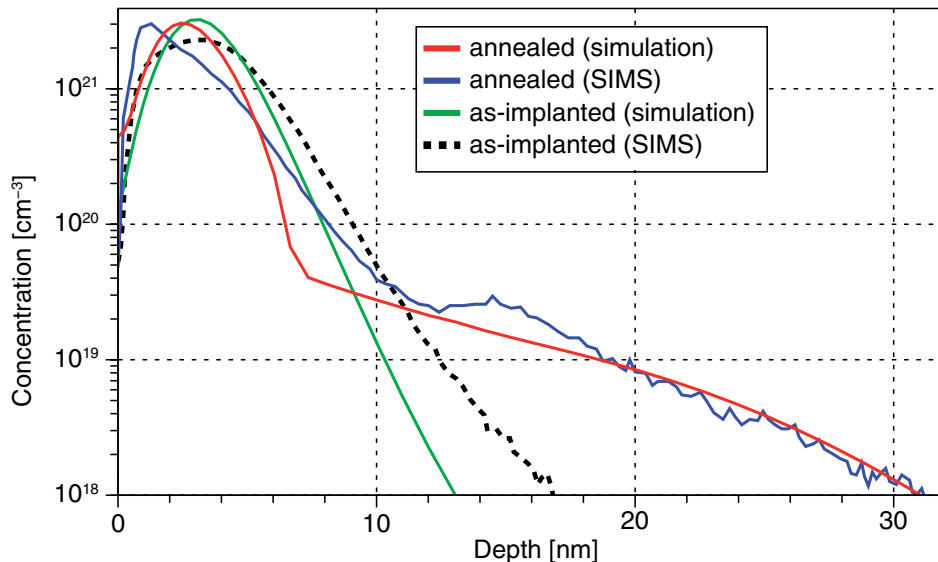
Clustering of B in a-Si is not taken into account in continuum Sentaurus Process. Note that the diffusivity of boron in a-Si has the same Arrhenius energy (2.68 eV) as the velocity of the a/c interface during SPER.

Arsenic

Following Venezia *et al.* [152] and Suzuki *et al.* [154], arsenic is swept by the recrystallization front (see [Figure 15](#)). Note that the diffusivity of As in a-Si has the same Arrhenius energy (2.68 eV) as the velocity of the a/c interface during SPER. With this choice, the snow plow effect for As is independent of the temperature at which SPER occurs.

A very small diffusivity in a-Si has been set for As, following Duffy *et al.* [155] reporting little significant As diffusion at 600°C.

Figure 15 Simulation of recrystallization with arsenic redistribution during SPER for Ge PAI + As 2 keV 10^{15} cm^{-2} implantation and anneal at 700°C for 2 hours [152]. The simulation results have been achieved with Advanced Calibration, with AdvancedModels and AdvancedSPERModel switched on, and with ifactor for Ge implantation set to 3.0.



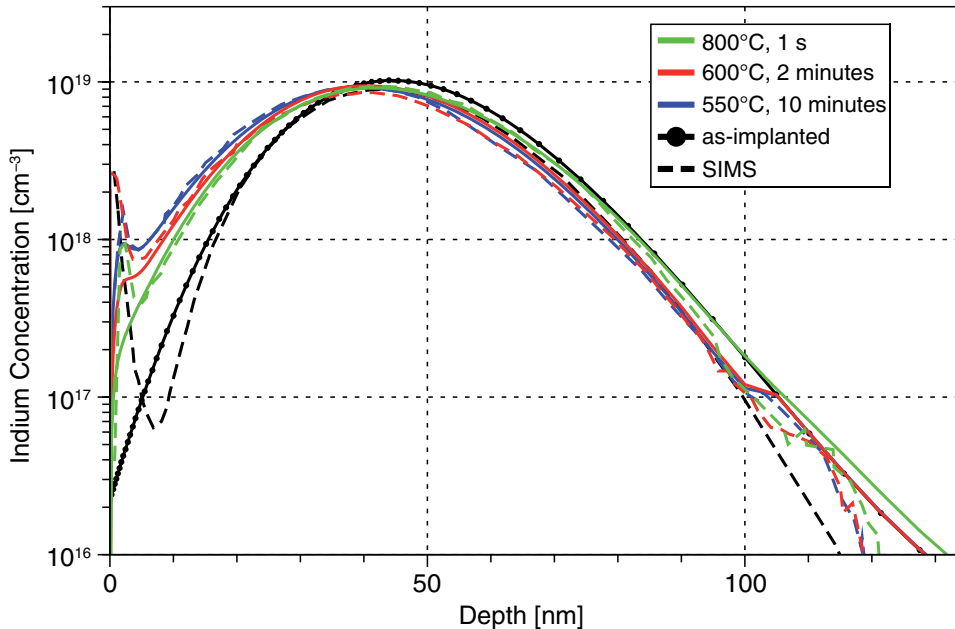
Phosphorus

Phosphorus is swept by the recrystallization front, and a small diffusivity in a-Si has been set for P, following Duffy *et al.* [155], reporting little significant P diffusion at 600°C.

Indium

Following Duffy *et al.* [156], indium is swept by the recrystallization front. The diffusivity in a-Si has been calibrated to [Arr 1.0 2.57]. The Arrhenius energy of the diffusivity (2.57 eV) is slightly smaller than the Arrhenius energy of the recrystallization velocity (2.68 eV). As a consequence, the snow plow effect for indium depends on temperature. The lower the temperature of SPER, the more indium is pushed towards the surface (see Figure 16).

Figure 16 Indium redistribution towards the surface during SPER at 550°C, 600°C, and 800°C; the snow plow effect is strongest if SPER is completed at the lowest temperature, and SIMS data is taken from [156]



Carbon

Carbon is swept by the recrystallization front, and the diffusivity has been calibrated to agree with SIMS.

Fluorine

Following the literature [149][157], fluorine is swept by the recrystallization front. For the diffusivity of F in a-Si, an Arrhenius energy of 2.6 eV has been selected, which is at the upper end of possible values reported by Nash et al. [158].

Germanium

Germanium is assumed to diffuse in amorphized regions. For deep amorphization of Si/SiGe layers, the diffusion of Ge during SPER can result in significant broadening of the Ge profile.

Melting Laser Anneal

See section 4.11 of `AdvCal_2022.03.fps`.

Melting laser anneal (MLA) uses an extremely short (submicrosecond) annealing time and achieves very high (almost 100%) levels of dopant activation and a low defect concentration in recrystallized molten regions. Therefore, MLA is ideal for backside processing without affecting the already existing front side of a thinned structure as in modern discrete power IGBTs [159][160] or backside imagers [161].

A phase field model for MLA has been implemented based on [162]. The phase field variable `HeatPhase` (φ) describes whether the material is liquid ($\varphi=0$) or solid ($\varphi=1$). Since the melting or solidification process occurs too quickly to observe the dopant diffusion in a solid region, it is assumed that the dopant atoms diffuse mostly in the liquid phase. The different chemical potentials of dopants at liquid, solid, and boundary regions induce segregation effects that are taken into account by the model. During MLA, the temperature varies greatly depending on location. Therefore, the dopant diffusion equation must be solved by coupling it to the heat equation and the phase equation. The heat generation rate G in the heat equation is calculated from the laser intensity profile. Dopant diffusion $\partial C / \partial t$ is coupled to the local temperature and depends on the diffusivity D , where D is a function of the phase field variable φ that follows from the phase equation.

In the beginning of a laser anneal, all dopants and point defects are initialized in the standard way using the `diffPreProcess` procedure according to the models selected. Then, during melting, all point defects and clusters are dissolved in the liquid phase. The point defect and cluster solutions are reset to zero in a molten region during diffusion, which implies that all dopants in a liquid (and subsequently recrystallized) region are fully activated. The instant recrystallization of an amorphous region, that is, the initialization of cluster solutions, is performed before diffusion, but information about the implanted damage is taken into account for calculating the degree of structural disorder α (degree of amorphization), which then affects the thermodynamic properties of solid material. In practically all cases, molten silicon solidifies as crystalline (single or poly, depending on the substrate), regardless of whether it was amorphous or crystalline before melting. This is taken into account by a special equation for α , which gradually reduces to zero upon melting.

Using AdvancedMLAModel for MLA Simulation

The procedure `AdvancedMLAModel` is part of the Advanced Calibration file to set parameters necessary for MLA simulations. In addition, the procedure contains some parameters that are already default but can be used as references for calibration. This procedure is not activated by default and must be called before the `diffuse` command corresponding to the MLA. Typically, MLA is applied at the end of a process simulation; however, when it is followed by other anneal steps, you need to restore some critical defaults that were changed in the `AdvancedMLAModel` procedure. In such cases, the procedure `AdvancedMLAModelReset` must be run after the MLA `diffuse` command.

Chapter 2: Advanced Calibration for Silicon, SiGe, and Germanium

Part 4: Comprehensive and Slow Models

Equipment-specific settings (such as light absorptivity, laser intensity model, and laser pulse intensity shape) and settings for the surface reflectivity are not included in `AdvancedMLAModel` and, therefore, must be specified in the input file explicitly.

The following commands provide an example of such settings as they might occur in 1D process simulations of MLA of SiGe, in which heat generation is calculated with the energy implantation method. In the example, the laser intensity as a function of pulse time is loaded from a file and scaled by the fluence and by $(1 - \text{reflectivity})$. The reflectivity is higher for melted Si than for solid Si. For simplicity, in this example, the same reflectivity is assumed for Si and Ge, and therefore for SiGe:

```
AdvancedMLAModel          ;# set params for MLA simulation

pdbSet Ge Absorptivity [expr 1.46e6] ;# 0.146/nm
pdbSet Si Absorptivity [expr 1.46e6] ;# 0.146/nm

pdbSet Heat Intensity.Model Table    ;# intensity from a table
source ./160ns.txt                  ;# file with normalized pulse shape
set    fluence 2.0                  ;# energy density in J/cm2

set Phase2nm "[ interpolate Si name= HeatPhase x=0.002\]"
;# phase at depth 2 nm
set TempK1nm "[ interpolate Si name= Temperature x=0.001\]"
;# T [K] at depth 1 nm
pdbSet Heat Intensity.Table.Factor "[expr $fluence * \
(1 - ($Phase2nm * (0.655 + 4e-5*$TempK1nm) + (1-$Phase2nm) * \
0.774)) \]"
;# heat generation factor

pdbSet Heat WaferThickness 400
```

Note:

A TCAD Sentaurus project facilitates the use of the MLA model. The project demonstrates the simulation of MLA backside processing integrated in a 2D IGBT process simulation [\[163\]](#).

In MLA simulations for devices on germanium substrates (instead of silicon substrates), add the following statement:

```
pdbSet Heat BulkMaterial Germanium
```

In 2D or 3D simulations of MLA with nonplanar geometry, accurate photon absorption can be calculated with Sentaurus Device Electromagnetic Wave Solver (EMW), as described in the *Sentaurus™ Process User Guide*. In EMW, melted silicon is best treated as a dispersive medium.

Seed Term

The phase field model describes the movement of the solid–liquid interface. In the absence of such an interface, to start the melting of a solid region, a *seed term* is used in the equation

Chapter 2: Advanced Calibration for Silicon, SiGe, and Germanium

Part 4: Comprehensive and Slow Models

for `HeatPhase`. The seed term is switched on when the value of `HeatPhase` is equal to or greater than the value of the parameter `SeedOnPhase` everywhere in the structure. The default value of `SeedOnPhase` is 1.0. Therefore, by default, the seed term is switched on only when the entire region is solid, typically at the beginning of MLA. The seed term remains switched on until `HeatPhase` is less than the value of the parameter `SeedOffPhase` (default: 0.001) somewhere in the structure.

The derivation of the phase field model does not include material interfaces explicitly. Therefore, this model does not describe the physics precisely when the solid–liquid interface reaches region boundaries during solidification. In its present formulation, the recrystallization rate is overestimated in the very last moment of recrystallization, when the solid–liquid interface reaches the interface to a different material, not subject to melting. This is accompanied by a very short (< 1 ps) nonphysical spike in temperature near the surface of the silicon at the end of recrystallization.

In Version P-2019.03 and earlier versions of `AdvancedMLAModel`, this temperature spike was suppressed (at least in 1D simulations) by switching on the seed term again at the end of recrystallization, by setting `SeedOffPhase < SeedOnPhase < 1.0`. However, this sometimes would lead to poor convergence and frequent switching between seed on and seed off at the end of recrystallization. Therefore, in the new calibration, this approach is no longer used, and `SeedOnPhase` is set to 1.0. The temperature spike is so short that it typically has no impact on the simulation of dopant diffusion and activation.

The seed term is scaled by `Seed.Factor`, which is 0.2 by default. You can use more sophisticated definitions of `Seed.Factor` to switch off the seed term slowly instead of abruptly, or to make the seed term largest near the surface. For example, in 1D simulations, you can use:

```
pdbSet Heat Seed.Factor {[expr (0.4*exp(-x/0.007)* \
    (\[interpolate Si name= HeatPhase x=0.001\] > 0.4 ? 1 : \
    \[interpolate Si name= HeatPhase x=0.001\] / 0.4 ))] }
```

Here, `x` is the x-coordinate, and `Seed.Factor` is reduced smoothly when `HeatPhase` near the surface takes values smaller than 0.4.

Settings in AdvancedMLAModel

`AdvancedMLAModel` switches off interstitial clusters together with interstitial and vacancy transport equations with the following commands. This reduces the simulation time for typical MLA simulations:

```
pdbSet Si Int ClusterModel None
pdbSetBoolean Defect ForcedTurnOff 1
```

You can solve equations for point defects and point-defect clusters during MLA, but no calibration has been performed for typical MLA time scales.

Chapter 2: Advanced Calibration for Silicon, SiGe, and Germanium

Part 4: Comprehensive and Slow Models

To solve equations for point defects and point-defect clusters, insert the following commands directly after calling `AdvancedMLAModel`:

```
pdbSet      Si Int ClusterModel [pdbGet Si Int SavedClusterModel]
pdbUnSetBoolean Defect ForcedTurnOff
pdbSetBoolean Defect ForcedTurnOn 1
```

The following settings ensure steady numeric convergence in the MLA model:

```
pdbSet Math NegErrCntrl 1
math fullNewton
```

The accurate simulation of MLA requires the use of very small time steps during critical parts of the annealing. The following commands in `AdvancedMLAModel` control the time steps:

```
pdbSet      Heat MaxTimeStep          1.0e-8
pdbSet      Si   HeatPhase    Abs.Error    1.0e-4
pdbSet      Si   HeatPhase    Rel.Error    1.0e-5
pdbSet      Si   HeatPhase    Transient.Rel.Error 1.0e-5
pdbSet      Si   Temperature Abs.Error    5.0e-3
pdbSet      Si   Temperature Rel.Error    5.0e-6
pdbSetDouble Si   Temperature Transient.Rel.Error 2.0e-5
pdbSetDouble Si   Dopant     Abs.Error    1.0e-3
pdbSetDouble Si   Dopant     Rel.Error    1.0e-8
pdbSetDouble Si   Dopant     Transient.Rel.Error 1.0e-5
```

These values are often a good compromise for CPU time and numeric accuracy. To increase the precision, you can reduce the allowed error in the temperature equation. For example:

```
pdbSet      Si   Temperature Abs.Error    1.0e-3
pdbSet      Si   Temperature Rel.Error    1.0e-6
pdbSetDouble Si   Temperature Transient.Rel.Error 3.0e-6
```

In contrast, to speed up MLA simulations, consider relaxing the allowed error for dopants. For example:

```
pdbSetDouble Si   Dopant Transient.Rel.Error 3.0e-5
```

You can also take a more sophisticated approach and change the value of `Transient.Rel.Error` during MLA. You can do this by using the argument `movie` of the `diffuse` command. For example:

```
pdbSetDouble Si   Dopant Transient.Rel.Error 5e-4

diffuse temperature=500 time=5.0e-7<s> laser \
  movie= { \
    if { [simGetDouble Diffuse time] > 6e-8 } { \
      pdbSetDouble Si   Dopant Transient.Rel.Error 2e-5 \
    } \
  }
```

Such an approach can be used to allow for a larger error in the dopant profiles during the melting, and then you can use a stricter error control during recrystallization.

Meshing

The thickness δ of the interface region between the solid phase and the liquid phase is governed by the parameter `Heat.Phase.Width`. It is important that the same value is used for Si and Ge:

```
pdbSet Si Heat.Phase.Width 2.0e-7  
pdbSet Ge Heat.Phase.Width 2.0e-7 ;# 2 nm
```

Mesh spacing in the molten region must always be smaller than `Heat.Phase.Width` to reach proper convergence. A larger mesh spacing results in a faster simulation and less noise. Larger values of `Heat.Phase.Width` can speed up convergence even for a fixed mesh spacing. The simulated dopant distribution depends on both mesh spacing and `Heat.Phase.Width`.

For an equidistant 1D mesh, the simulation results are almost the same for all mesh spacing less than `Heat.Phase.Width`. For an inhomogeneous 1D mesh, the simulated melting front speed changes when the solid–liquid interface reaches the region of mesh inhomogeneity, unless the maximum mesh spacing is smaller than `Heat.Phase.Width/8`. A mesh finer than `Heat.Phase.Width/8` might result in a larger CPU time. This basically means that changes to the 1D mesh spacing are allowed only if the background mesh is finer than `Heat.Phase.Width/8`. Therefore, an equidistant mesh should be used in the melting region whenever possible.

Similarly, in 2D and 3D simulations, the mesh spacing perpendicular to the solid–liquid interface should be smaller than `Heat.Phase.Width` in the region that is subject to melting.

In 3D simulations, it might be advantageous to increase the value of `Heat.Phase.Width` in Si and Ge from `2.0e-7` (default) to `2.5e-7` or `3.0e-7`. This lowers the requirements for a good mesh and has a positive impact on simulation robustness and CPU time. However, it also has a small impact on results and, therefore, you should do this before any fine-tuning of the calibration of the diffusion of dopants or Ge atoms during MLA.

Thermodynamics of Silicon, Germanium, and SiGe

The thermal conductivity of crystalline Si and crystalline Ge has been calibrated as a function of temperature from published experimental data [164][165][166].

For crystalline SiGe, thermal conductivity depends on the Ge mole fraction and is approximately an order of magnitude smaller than for pure Si or pure Ge, because of alloy scattering of phonons. The alloy scattering contribution to thermal resistivity has been calibrated as a compromise for experimental data from [165][167][168][169][170].

For a-Si and a-Ge, thermal conductivity is set to `0.018 W/(cm·K)`, which is in reasonable agreement with the values measured by Zink [171] and He [172] for Si, and the values reported for Ge by Szyszko [173].

Chapter 2: Advanced Calibration for Silicon, SiGe, and Germanium

Part 4: Comprehensive and Slow Models

For liquid silicon (l-Si) and liquid germanium (l-Ge), thermal conductivity has been calibrated against data published by Yamasue [166]. The MLA model does not explicitly take into account the density change from 2.33 g/cm^3 (solid) to 2.57 g/cm^3 (liquid), to avoid volume changes. Therefore, in the definition of `Liquid.ThermalConductivity` for silicon, you use a formula corresponding to experimental data [166] multiplied by the factor $2.57/2.33$.

The thermal conductivity of SiO_2 and SiN has been chosen to give a reasonable agreement to data from Ryningen [174] and Ftouni [175].

For specific heat capacity, the Sentaurus Process defaults are kept for pure Si. These are in agreement with the publications [171][176][177]. The temperature-dependent value of the specific heat of amorphous silicon is set to be the same as in crystalline silicon, because they are close (depending on the exact state of amorphous silicon) [177], and little experimental data is available. The values for c-Ge and a-Ge were chosen to match data from Okhotin [178]. Like for Si, it is assumed that a-Ge has the same heat capacity as c-Ge. For liquid Ge, a temperature-dependent specific heat capacity has been fitted to data measured by Rhim [179]. Heat capacities of SiO_2 and SiN have been extracted from JANAF tables [180].

For the latent heat and the melting temperature of Si, a-Si, Ge, and a-Ge, the Sentaurus Process defaults are used. For simplicity, the temperature dependence of the latent heat is ignored at the moment. For the melting temperature of c-SiGe, the parabolic interpolation is based on the solidus curve published by Stöhr [181]. For the melting point of amorphous SiGe, the same bending in the parabolic interpolation as for crystalline SiGe is assumed.

The Vogel–Fulcher model is recommended for solid–liquid interface velocity simulations. The values of its parameters were set to obtain the maximum solid–liquid interface velocity of 15 m/s and 25 m/s for crystalline and amorphous silicon, respectively, as reported in [182]. For germanium, the same interface velocities are used as for Si. Since the melting temperature of Ge is smaller than that of silicon, a smaller value for the reference temperature of the Vogel–Fulcher model is defined for Ge.

Interface mobility is set to $20 \text{ cm}/(\text{J}\cdot\text{s})$ for c-Si, a-Si, c-Ge, and a-Ge. It is important that identical values are used in these materials. In planar structures, interface mobility determines how fast the phase field establishes its values in the interface region between the solid phase and the liquid phase. For 1D simulations, results are not very sensitive to this parameter. However, in 2D and 3D simulations, interface mobility has a large impact on the time evolution of the phase field when the solid–liquid interface is curved and the area of the solid–liquid interface might change during melting and recrystallization, especially at the corners and edges of the structure. With the previous value of interface mobility, $600 \text{ cm}/(\text{J}\cdot\text{s})$ taken from [183], it was observed that recrystallization was stuck in 2D geometries, at corners where a narrow region of crystalline silicon is covered by a broader region of melted silicon.

Even with $20 \text{ cm}/(\text{J}\cdot\text{s})$, due to the energy associated with surface tension between solid and liquid Si, recrystallization might sometimes be stuck at regions where further recrystallization would require a sharp increase of the area of the solid–liquid interface. In

Chapter 2: Advanced Calibration for Silicon, SiGe, and Germanium

Part 4: Comprehensive and Slow Models

such a situation, you can still achieve recrystallization by lowering the surface tension or by lowering the parameters for `Melting.Interface.Mobility`. For example:

```
pdbSet Si Melting.Interface.Mobility      6      ;# default is 20
pdbSet Si Amorphous.Melting.Interface.Mobility 6
pdbSet Ge Melting.Interface.Mobility      6
pdbSet Ge Amorphous.Melting.Interface.Mobility 6
```

Silicon Absorptivity

The recommended value of the light absorptivity in silicon for a 308 nm laser can be set by:

```
pdbSet Si Absorptivity 1.46e6    ;# (cm-1)
```

An absorptivity of $1.46\text{e}6 \text{ cm}^{-1}$ corresponds to the liquid silicon and is close to the value for crystalline silicon at room temperature [184]. It increases for large temperatures, but since the value $1.46\text{e}6$ is already sufficiently large, increasing absorptivity further does not greatly influence the melting dynamics. Therefore, the above constant value is recommended for the simulation of a 308 nm laser. In principle, any temperature- and phase-dependent expression can be used for absorptivity, which then becomes time dependent. In that case, the following flag must be switched on to account for this:

```
pdbSet Heat UpdateHeatRate 1    ;#default 0
```

The optical properties of monocrystalline silicon at room temperature for wavelengths from 234 nm to 840 nm can be found in [185].

Note:

For photons with energy smaller than the direct band gap of Si (for example, for 532 nm wavelength), absorptivity increases strongly with temperature. You must ensure a proper definition of absorptivity. If you use EMW for optical calculations, then you can define an extinction coefficient that depends on the local temperature.

MLA Calibration

Synopsys calibrated the MLA model in the framework of the ATEMOK project [186] to experimental results of the Excico UV 308 nm laser with a pulse duration of 150–200 ns. The laser irradiation area was approximately 1 cm^2 (full chip) per shot. Only flat silicon wafers with native oxide were used; therefore, the use of 1D simulation is fully justified in these cases. No structures with surface amorphization were considered; therefore, the resulting parameters are reliable only for MLA of crystalline silicon.

Chapter 2: Advanced Calibration for Silicon, SiGe, and Germanium

Part 4: Comprehensive and Slow Models

The calibration consisted of two stages:

- Calibration of melting dynamics to fine-tune the melting depth and the melting duration using temperature- and phase-dependent reflectivity of the wafer surface. Since reflectivity for the main pulse wavelength (308 nm) was not measured directly, it was the main calibration parameter for the melting depth in this model. It was entered into the parameter `Heat Intensity.Table.Factor`, which scales the intensity of laser radiation depending on the temperature and the phase of the exposed silicon surface. For the silicon covered with only thin native oxide, it has the following form:

```
pdbSet Heat Intensity.Table.Factor "\[expr $fluence*(1- \
($SurfPhase*(0.575+4e-5*$SurfTempK)+(1-$SurfPhase)*0.78))\]"
```

where:

- `$fluence` is the laser energy density (in the case of `Intensity.Table` normalized to 1 J/cm²).
- `$SurfPhase` is the current phase of the silicon near the surface (it can vary between 0 for the liquid state and 1 for the solid state).
- `$SurfTempK` is the silicon surface temperature.

Emphasis was placed on keeping the surface reflectivity similar between different experiments and close to the values suggested in the calibration performed by other ATEMOX partners earlier.

- Calibration of dopant diffusion in the liquid phase and its segregation at the solid–liquid interface was performed for boron and phosphorus. First, values of `Melting.Seg.E` were set according to experimental equilibrium partition coefficients of dopants from [187]. Second, the dopant diffusivities and interface chemical potentials were set to obtain the best visual fit of simulated profiles to SIMS profiles. Interface diffusivities (`Dils.0`) were set to a small value (5×10^{-7} cm²/s for B and 10^{-9} cm²/s for P) to avoid the formation of an artificial notch at the maximum melting depth position. No temperature dependency was set for the diffusivities because available data could be fitted without it.

[Figure 17](#) shows the results of the calibration for boron, and [Figure 18](#) shows the results of the calibration for phosphorus.

The SIMS profiles were provided to Synopsys within the ATEMOX project (most profiles are also published). The results and parameters for boron are qualitatively similar to the ones obtained in [188]. Note that SIMS profiles are usually more smooth (and their peaks are shifted in depth by several nanometers) than simulated dopant profiles after MLA.

This is caused by inaccuracy of the SIMS data (see the comparison of raw and convolved simulated profiles in [188]). The calibration for phosphorus was based on data from [189].

Chapter 2: Advanced Calibration for Silicon, SiGe, and Germanium

Part 4: Comprehensive and Slow Models

Figure 17 Comparison of simulated B profiles with SIMS profiles [188] for different laser energies (Elas); the same "200 ns" laser pulse shape was used for all simulated Elas shown

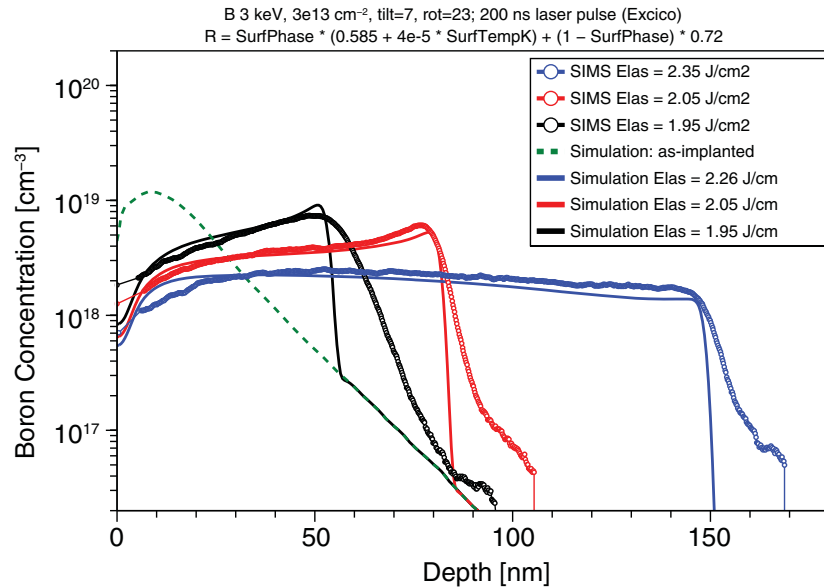
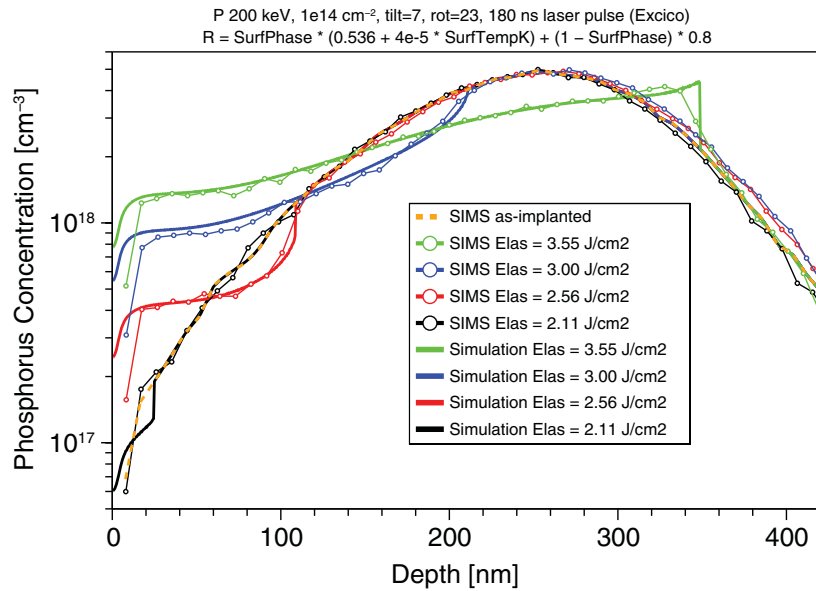


Figure 18 Comparison of simulated P profiles with SIMS profiles [189]; the same "180 ns" laser pulse shape was used for all simulated laser energies (Elas) shown



MLA Calibration for SiGe

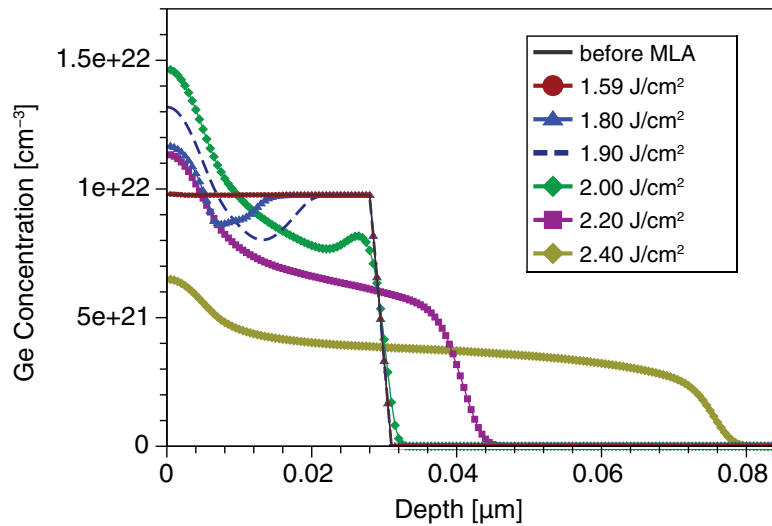
SiGe is typically modeled as silicon with a high Ge concentration. For melting laser anneals of SiGe, two aspects are important:

- Material parameters differ from pure Si. While many parameters can be well approximated by interpolation of values from corresponding values for Si and Ge, the thermal conductivity of SiGe is much smaller than the thermal conductivity of pure Si or pure Ge, because of alloy scattering. This leads to slower dissipation of heat and, thereby, to faster melting of SiGe. The reduced thermal conductivity of SiGe is captured by the calibrated parameters.
- Ge itself is redistributed during melting and subsequent recrystallization. This is illustrated in [Figure 19](#). The segregation of Ge at the interface between solid and liquid SiGe has been calibrated against data published by Dagault [\[190\]](#).

To switch on Ge redistribution during MLA, the following commands are included in the procedure `AdvancedMLAModel`:

```
solution      name= Germanium ifpresent= Germanium !negative Heat store
pdbSetString Si Ge InitHeatProc      InitLiquidDopant
pdbSetString Si Ge EquationHeatProc DopantLiquidBulk
```

Figure 19 Calculated Ge concentration in Si with a SiGe epitaxial layer on top, before and after MLA with different fluence. The simulation was performed with a 160 ns laser pulse and an absorptivity of $1.46 \times 10^6 \text{ cm}^{-1}$. Results are very close to SIMS data for similar process conditions, published by Dagault [\[190\]](#).



Limitations of MLA Model

The MLA model provides good simulation results for dopant redistribution during the melting process and dopant activation in the recrystallized region for typical quasi-1D cases. The following limitations remain in the model:

- MLA has not been calibrated for structures with amorphous regions. Amorphous Si has a lower melting temperature than solid Si. Immediately after melting, amorphous Si can be considered undercooled liquid Si, which can quickly recrystallize to poly-Si. In addition, the latent heat of amorphous Si is smaller than the latent heat of crystalline Si. Upon melting of a-Si and subsequent recrystallization as poly-Si, this difference in latent heat is released and might cause melting of additional a-Si in deeper regions. This might lead to an *explosive crystallization* as reported by Thompson [191]. It can, in principle, be described by the MLA model, but the dynamics of this process have not yet been calibrated. Only if the thermal budget of the MLA is sufficient to entirely melt an amorphous region and a few nanometers of crystalline Si below, you can expect recrystallization as a high-quality single crystalline layer and an accurate description by the MLA model.
- In 2D and 3D structures, the MLA model does not describe the possible change of the device geometry during melting and recrystallization. It is assumed that the shape of all regions is unchanged upon melting and recrystallization, which might not always be the case in actual processing.
- Only simple diffusion equations for dopants are coupled with the heat equation. For the remainder (such as complex clusters), only a constant temperature is supported. This impedes the simulation and calibration of dopant activation and defect annealing in the solid phase during MLA. Therefore, a dedicated calibration of the electrical activation of dopants immediately below the melted surface-near region has not yet been performed, that is, the simulated dopant activation and defect annealing in the solid phase during submicrosecond MLA might be inaccurate.

Part 5: Accelerating Simulations for Power Technologies

Part 5 of `AdvCal_2022.03.fps` is designed for the needs of process simulations for various power devices made of silicon such as LDMOS, VDMOS, IGBT, and superjunction MOSFET.

For many power devices, process simulation is time consuming because many mesh points are needed for a proper discretization of the simulation domain and because a high number of thermal anneals and oxidations is used in the fabrication process.

Chapter 2: Advanced Calibration for Silicon, SiGe, and Germanium

Part 5: Accelerating Simulations for Power Technologies

In addition, for many power devices, from the simulation perspective, the process simulation can be divided into two parts:

- In the first part of process simulation, the concentration of dopants is small (far below solid solubility), and the overall thermal budget for thermal annealing and oxidation is large.
- In the second part of process simulation, typically associated with the formation of electrical contacts, the dopant concentration can be very high (above solid solubility), and the thermal budget for thermal annealing after implantation is small or moderate.

In these devices, usually the first part of the process simulation consists of the majority of time-consuming process steps (in particular, oxidation steps). However, the CPU time spent for the corresponding process simulation can be reduced significantly by taking advantage of the low dopant concentration and high thermal budgets. To speed up the first part of the process simulation, you can use simpler models and simpler settings than those used by the default Advanced Calibration.

For the second part of the process simulation (typically, starting with the first high-dose dopant implantations into silicon), it is recommended to use the full set of standard Advanced Calibration models to obtain accurate results for dopant transient-enhanced diffusion and activation.

Part 5 of `AdvCal_2022.03.fps` contains the procedures `AdvancedPowerDeviceMode` and `AdvancedPowerDeviceModeReset`, which are designed to reduce CPU time for process simulation of power devices without sacrificing simulation accuracy. The procedure `AdvancedPowerDeviceMode` switches on settings for fast process simulation of the first part of power processes. The procedure `AdvancedPowerDeviceModeReset` reverts to the standard settings of Advanced Calibration for accurate simulation of dopant diffusion and activation in the second part of power processes.

Using `AdvancedPowerDeviceMode` in the first part of the process simulation and reverting to the standard models with `AdvancedPowerDeviceModeReset` for the second part of the process simulation typically result in a reduction of total process simulation CPU time by 20–40%, depending on the process flow.

In many applications, the simulation results do not change significantly when compared to simulations where Advanced Calibration standard models are used for the complete process flow. However, as a check, run a reference simulation without `AdvancedPowerDeviceMode` at least once. If results with and without `AdvancedPowerDeviceMode` are identical, then you can proceed. Otherwise, it is better not to use `AdvancedPowerDeviceMode` or to take measures to minimize the impact of the corresponding speedup on process simulation results. For example, use `AdvancedPowerDeviceMode` only for a reduced number of initial process steps, or set tighter controls for time-stepping and numeric accuracy.

Using AdvancedPowerDeviceMode

This section discusses how to use the `AdvancedPowerDeviceMode` procedure.

Variant 1: Explicitly Reverting to Standard Models

The procedure `AdvancedPowerDeviceMode` is called without arguments immediately after the `AdvancedCalibration` command line. The `AdvancedPowerDeviceModeReset` procedure is called when the first part of the process simulation (with low doping concentration in silicon) is completed and the second part of process simulation starts, for example, with high-dose (dose > 10^{14} cm $^{-2}$) implantations for contact regions.

To select the models and parameters, the process simulation input file contains the following flow of commands:

```
AdvancedCalibration 2022.03
AdvancedPowerDeviceMode
source ./mycalib.fps
...
      ;# first part of process
AdvancedPowerDeviceModeReset
...
      ;# second part of process
```

You can validate whether the acceleration or the process simulation with `AdvancedPowerDeviceMode` is justified by comparing the CPU time and simulation results to reference simulations, in which the lines `AdvancedPowerDeviceMode` and `AdvancedPowerDeviceModeReset` are commented out.

Variant 2: Automatically Reverting to Standard Models

The procedure `AdvancedPowerDeviceMode` is called with an argument `<value>`, which is interpreted as a dose. Sentaurus Process calls the `AdvancedPowerDeviceModeReset` procedure automatically at the first implantation with `dose > <value>` during the implantation preprocessing. A typical value of the argument is 10^{14} .

The process simulation input file contains the following flow of commands:

```
AdvancedCalibration 2022.03
AdvancedPowerDeviceMode 1e14
source ./mycalib.fps
...
      ;# first part of process
...
      ;# second part of process
```

This variant is convenient for TCAD beginners. Apart from ease of use, automatically reverting to the standard models has no advantage. In some use cases, it does not give the best results, and the first variant is preferred.

Use cases, where the first variant is preferred, include:

- Processes in which the first high-dose implantation is not intended to enter the silicon region of the device. For example, if the entire device is covered by polysilicon or photoresist, it might not be necessary to revert to the standard Advanced Calibration models at the first high-dose implantation.
- Processes in which the first high-dose implantation (`dose > <value>`) is part of a series of implantations. Here, the procedure `AdvancedPowerDeviceModeReset` must be called before the first implantation of that series, even if it is a low-dose implantation.

Contents of AdvancedPowerDeviceMode

Synopsys has investigated the simplifications contained in `AdvancedPowerDeviceMode` based on a large set of various power-device simulation projects. Besides simplified physics, the simplifications also include appropriate parameters for time-stepping and numeric solvers.

Increased Time Steps, Deposition Steps, and Temperature Steps

`AdvancedPowerDeviceMode` includes the lines:

```
# Numerics: Time steps
pdbSetDouble    Diffuse InitTimeStep      1.0e-3 ;# default 1.0e-4
pdbSet          Diffuse IncreaseRatio    4.0     ;# default 2.0
pdbSet          Diffuse ReduceRatio     0.20    ;# default 0.25
pdbSet          Math     Time.Step.Function Linear ;# default Damped

# Numerics: Deposition steps
pdbSet          Diffuse dThickness       0.001   ;# default 0.001;
                                         ;# 0.002 is faster
                                         ;# but less robust

pdbSet          Diffuse dThicknessEpi    0.50    ;# default 0.1

# Numerics: Temperature steps
pdbSet          Diffuse MaxGrowthStep   50.0    ;# default 4.0
pdbSet          Diffuse delT           50.0    ;# default 10
pdbSet          Diffuse delNT          50.0    ;# default 50
pdbSet          Diffuse delTox         50.0    ;# default 50
```

These lines increase the time steps, the deposition steps, the oxidation time steps (`MaxGrowthStep`), and the temperature steps compared to the default values of Advanced Calibration for Sentaurus Process.

The values are a good trade-off between simulation robustness (where small time steps help to eliminate noise from numeric errors and, in particular, to keep interfaces between oxide and silicon smooth during oxidation) and CPU time, where large time steps are

favorable. To further speed up power-device process simulation, it is useful to test at least once for each technology if the parameters `InitTimeStep` and `dThickness` can be increased without loss of simulation robustness. According to Synopsys' experience, in some power technologies, you can further reduce process simulation CPU time by an additional 20–40% by increasing `InitTimeStep` from `1.0e-3` to `2.0` and `dThickness` from `0.001` to `0.002`, without affecting simulation robustness or results.

In rare cases, the simulation robustness or numeric accuracy during a critical oxidation step might be insufficient with these settings. This might be evident when comparing simulation results with and without `AdvancedPowerDeviceMode`. In such situations, choose one of the following options:

- Set tighter numeric controls manually. For example, specify:

```
pdbSet Diffuse MaxGrowthStep 5
```

- Revert to the Advanced Calibration standard models before that oxidation step by specifying `AdvancedPowerDeviceModeReset`.

Simplified Physics

For low dopant concentrations (<< solid solubility), you can save CPU time by switching off the equations for dopant clusters. In `AdvancedPowerDeviceMode`, all dopants are made electrically active by setting `ActiveModel` to `None`.

For very high thermal budgets, typical for oxidation steps used in the first part of power-device process simulations, the TED of dopants caused by interstitials created during ion implantation can be neglected compared to regular diffusion of dopants. In `AdvancedPowerDeviceMode`, TED is suppressed by the line:

```
pdbSetBoolean AdvCal_IFactorsVFactorsZero 1
```

When `AdvCal_IFactorsVFactorsZero` is set to 1, the generation of interstitials or vacancies by ion implantation is suppressed (as implemented in section 3.3.1 of `AdvCal_2022.03.fps`). In the absence of TED, no equations need to be solved for interstitial clusters. In `AdvancedPowerDeviceMode`, the `ClusterModel` for interstitials is set to `None`. In addition, the parameters `Abs.Error`, `Rel.Error`, and `Transient.Rel.Error` for point defects are increased with respect to their default values, to allow for larger time steps in the diffusion solver.

Speedup Methods Not Included in `AdvancedPowerDeviceMode`

Synopsys tested other simplifications of physical models, but they were not found to be helpful in all application cases. None of them is included in `AdvancedPowerDeviceMode`.

Some comments about most of the simplifications are:

- Use the simpler `ChargedFermi` model for dopant diffusion instead of the `ChargedPair` model.

With this choice, the simulation of OED becomes very inaccurate. Using the `ChargedFermi` model saves CPU time (typically ~20%) and is suitable for selected technologies, but it is not recommended in general.

- Use the `ChargedFermi` model and – in addition – switch off the point-defect equations completely by setting the parameter `ForcedTurnOff` to 1.

With this choice, OED is completely suppressed. Diffusion of B and P during oxidation is severely underestimated. This choice is not recommended.

- Use local charge neutrality instead of the Poisson equation, by adding the line
`pdbSetBoolean Silicon Potential Poisson 0.`

This reduces the number of equations to be solved by one. However, it is often detrimental to convergence. Therefore, in most applications, it increases the CPU time.

- Switch off equations in polysilicon.

Usually, this has no impact on the CPU time.

- Use the `Segregation` model instead of the `ThreePhaseSegregation` model for dose loss of As, B, and P.

Usually, this has no impact on the CPU time.

The biggest potential to further accelerate accurate process simulation for power devices is to define a good meshing strategy and parameters for (adaptive) meshing. Since a good mesh depends on the details of the technology, meshing strategies and parameters for adaptive meshing are not included in `AdvancedPowerDeviceMode`. A method for creating good meshes for power-device process simulation is presented in [Meshing on page 190](#).

References

- [1] P. Pichler, *Intrinsic Point Defects, Impurities, and Their Diffusion in Silicon*, Computational Microelectronics, Vienna: Springer, 2004.
- [2] C. S. Rafferty *et al.*, “Simulation of cluster evaporation and transient enhanced diffusion in silicon,” *Applied Physics Letters*, vol. 68, no. 17, pp. 2395–2397, 1996.
- [3] IST Project 027152 ATOMICS, *Advanced Front-End Technology Modeling for Ultimate Integrated Circuits*, for more information, go to <https://www.iisb.fraunhofer.de/content/dam/iisb2014/en/Documents/Research-Areas/Simulation/final-report-atomics.pdf>.

- [4] A. Tsibizov, A. Terterian, and C. Zechner, "Influence of Poisson equation boundary conditions and quantum corrections to carrier concentrations at material interfaces in TCAD process simulation," *Physica Status Solidi C*, vol. 11, no. 1, pp. 101–104, 2014.
- [5] S. Strauss *et al.*, "Analytic model for ion channeling in successive implantations in crystalline silicon," *Materials Science and Engineering B*, vol. 124–125, pp. 376–378, December 2005.
- [6] H. Bracht, N. A. Stolwijk, and H. Mehrer, "Equilibrium Concentrations of Intrinsic Point Defects in Silicon Determined by Zinc Diffusion," in *Proceedings of the Seventh International Symposium on Silicon Materials Science and Technology (Semiconductor Silicon)*, vol. 94-10, San Francisco, CA, USA, pp. 593–602B, May 1994.
- [7] H. Bracht, E. E. Haller, and R. Clark-Phelps, "Silicon Self-Diffusion in Isotope Heterostructures," *Physical Review Letters*, vol. 81, no. 2, pp. 393–396, 1998.
- [8] A. Ural, P. B. Griffin, and J. D. Plummer, "Self-Diffusion in Silicon: Similarity between the Properties of Native Point Defects," *Physical Review Letters*, vol. 83, no. 17, pp. 3454–3457, 1999.
- [9] N. E. B. Cowern *et al.*, "Energetics of Self-Interstitial Clusters in Si," *Physical Review Letters*, vol. 82, no. 22, pp. 4460–4463, 1999.
- [10] B. Colombeau and N. E. B. Cowern, "Modelling of the chemical-pump effect and C clustering," *Semiconductor Science and Technology*, vol. 19, no. 12, pp. 1339–1342, 2004.
- [11] P. M. Fahey, P. B. Griffin, and J. D. Plummer, "Point defects and dopant diffusion in silicon," *Reviews of Modern Physics*, vol. 61, no. 2, pp. 289–388, 1989.
- [12] M. D. Giles, "Defect-Coupled Diffusion at High Concentrations," *IEEE Transactions on Computer-Aided Design*, vol. 8, no. 5, pp. 460–467, 1989.
- [13] I. Bork and H. Matsumoto, "On the Determination of Boron Diffusivities and Boron Interstitial Pair Binding Energies in Silicon," in *International Conference on Simulation of Semiconductor Processes and Devices (SISPAD)*, Tokyo, Japan, pp. 91–92, September 1996.
- [14] J. Vanhellemont, P. Spiewak, and K. Sueoka, "On the solubility and diffusivity of the intrinsic point defects in germanium," *Journal of Applied Physics*, vol. 101, no. 3, p. 036103, 2007.
- [15] J. Vanhellemont *et al.*, "Intrinsic point defect properties and engineering in silicon and germanium Czochralski crystal growth," in *5th International Symposium on Advanced Science and Technology of Silicon Materials*, Kona, HI, USA, November 2008.
- [16] J. Vanhellemont and E. Simoen, "Brother Silicon, Sister Germanium," *Journal of The Electrochemical Society*, vol. 154, no. 7, pp. H572–H583, 2007.
- [17] P. A. Packan and J. D. Plummer, "Temperature and time dependence of B and P diffusion in Si during surface oxidation," *Journal of Applied Physics*, vol. 68, no. 8, pp. 4327–4329, 1990.

- [18] P. B. Griffin and J. D. Plummer, "Process Physics Determining 2-D Impurity Profiles in VLSI Devices," in *IEDM Technical Digest*, Los Angeles, CA, USA, pp. 522–525, December 1986.
- [19] E. Napolitani *et al.*, "Silicon interstitial injection during dry oxidation of SiGe/Si layers," *Journal of Applied Physics*, vol. 97, no. 3, p. 036106, 2005.
- [20] P. A. Stolk *et al.*, "Physical mechanisms of transient enhanced dopant diffusion in ion-implanted silicon," *Journal of Applied Physics*, vol. 81, no. 9, pp. 6031–6050, 1997.
- [21] H. Saleh *et al.*, "Energy dependence of transient enhanced diffusion and defect kinetics," *Applied Physics Letters*, vol. 77, no. 1, pp. 112–114, 2000.
- [22] N. Zographos, C. Zechner, and I. Avci, "Efficient TCAD Model for the Evolution of Interstitial Clusters, {311} Defects, and Dislocation Loops in Silicon," in *MRS Symposium Proceedings, Semiconductor Defect Engineering—Materials, Synthetic Structures and Devices II*, vol. 994, San Francisco, CA, USA, p. 0994-F10-01, April 2007.
- [23] N. Zographos and A. Erlebach, "Process simulation of dopant diffusion and activation in germanium," *Physica Status Solidi A*, vol. 211, no. 1, pp. 143–146, 2014.
- [24] E. Napolitani *et al.*, "Transient enhanced diffusion of B mediated by self-interstitials in preamorphized Ge," *Applied Physics Letters*, vol. 96, no. 20, p. 201906, 2010.
- [25] L. F. Giles *et al.*, "Transient enhanced diffusion of B at low temperatures under extrinsic conditions," *Solid-State Electronics*, vol. 49, no. 4, pp. 618–627, 2005.
- [26] S. Uppal *et al.*, "Diffusion of boron in germanium at 800–900°C," *Journal of Applied Physics*, vol. 96, no. 3, pp. 1376–1380, 2004.
- [27] G. Impellizzeri *et al.*, "Role of fluorine in suppressing boron transient enhanced diffusion in preamorphized Si," *Applied Physics Letters*, vol. 84, no. 11, pp. 1862–1864, 2004.
- [28] B. J. Pawlak *et al.*, "Enhanced boron activation in silicon by high ramp-up rate solid phase epitaxial regrowth," *Applied Physics Letters*, vol. 86, p. 101913, 2005.
- [29] A. Satta *et al.*, "Diffusion, activation, and recrystallization of boron implanted in preamorphized and crystalline germanium," *Applied Physics Letters*, vol. 87, no. 17, p. 172109, 2005.
- [30] B. R. Yates *et al.*, "Anomalous activation of shallow B⁺ implants in Ge," *Materials Letters*, vol. 65, no. 23–24, pp. 3540–3543, 2011.
- [31] Y.-S. Oh and D. E. Ward, "A Calibrated Model for Trapping of Implanted Dopants at Material Interface During Thermal Annealing," in *IEDM Technical Digest*, San Francisco, CA, USA, pp. 509–512, December 1998.
- [32] A. N. Larsen *et al.*, "Heavy doping effects in the diffusion of group IV and V impurities in silicon," *Journal of Applied Physics*, vol. 73, no. 2, pp. 691–698, 1993.

- [33] S. T. Dunham and C. D. Wu, "Atomistic models of vacancy-mediated diffusion in silicon," *Journal of Applied Physics*, vol. 78, no. 4, pp. 2362–2366, 1995.
- [34] S. Brotzmann and H. Bracht, "Intrinsic and extrinsic diffusion of phosphorus, arsenic, and antimony in germanium," *Journal of Applied Physics*, vol. 103, no. 3, p. 033508, 2008.
- [35] M. Koike *et al.*, "Diffusion and activation of n-type dopants in germanium," *Journal of Applied Physics*, vol. 104, no. 2, p. 023523, 2008.
- [36] C. O. Chui *et al.*, "Germanium n-type shallow junction activation dependences," *Applied Physics Letters*, vol. 87, no. 9, p. 091909, 2005.
- [37] S. Koffel *et al.*, "Experiments and simulation of the diffusion and activation of the n-type dopants P, As, and Sb implanted into germanium," *Microelectronic Engineering*, vol. 88, no. 4, pp. 458–461, 2011.
- [38] P. Tsouroutas, D. Tsoukalas, and H. Bracht, "Experiments and simulation on diffusion and activation of codoped with arsenic and phosphorous germanium," *Journal of Applied Physics*, vol. 108, no. 2, p. 024903, 2010.
- [39] B. Sahli *et al.*, "Ab initio calculations of phosphorus and arsenic clustering parameters for the improvement of process simulation models," *Materials Science and Engineering B*, vol. 154-155, pp. 193–197, December 2008.
- [40] A. Chroneos *et al.*, "Vacancy-arsenic clusters in germanium," *Applied Physics Letters*, vol. 91, no. 19, p. 192106, 2007.
- [41] R. Kasnavi *et al.*, "Characterization of arsenic dose loss at the Si/SiO₂ interface," *Journal of Applied Physics*, vol. 87, no. 5, pp. 2255–2260, 2000.
- [42] A. Satta *et al.*, "Diffusion, activation, and regrowth behavior of high dose P implants in Ge," *Applied Physics Letters*, vol. 88, no. 16, p. 162118, 2006.
- [43] D. P. Bruno *et al.*, "Germanium: The Past and Possibly A Future Material for Microelectronics," *ECS Transactions*, vol. 11, no. 4, pp. 479-493, 2007.
- [44] V. Mazzocchi *et al.*, "Experimental Investigation of the Impact of Implanted Phosphorus Dose and Anneal on Dopant Diffusion and Activation in Germanium," in *MRS Symposium Proceedings, Doping Engineering for Front-End Processing*, vol. 1070, San Francisco, CA, USA, p. 1070-E01-08, March 2008.
- [45] V. Mazzocchi *et al.*, "Diffusion and activation of Boron and Phosphorus in preamorphized and crystalline Germanium using ultra fast spike anneal," in *17th IEEE International Conference on Advanced Thermal Processing of Semiconductors – RTP*, Albany, NY, USA, September 2009.
- [46] P. Tsouroutas *et al.*, "Modeling and experiments on diffusion and activation of phosphorus in germanium," *Journal of Applied Physics*, vol. 105, no. 9, p. 094910, 2009.

- [47] A. Chroneos *et al.*, "Engineering the free vacancy and active donor concentrations in phosphorus and arsenic double donor-doped germanium," *Journal of Applied Physics*, vol. 104, no. 11, p. 113724, 2008.
- [48] X. Li *et al.*, "Selective Epitaxial Si:P Film for nMOSFET Application: High Phosphorous Concentration and High Tensile Strain," *ECS Transactions*, vol. 64, no. 6, pp. 959–965, 2014.
- [49] J. Dabrowski *et al.*, "Mechanism of dopant segregation to SiO₂/Si(001) interfaces," *Physical Review B*, vol. 65, p. 245305, May 2002.
- [50] N. Ioannou *et al.*, "Germanium substrate loss during low temperature annealing and its influence on ion-implanted phosphorous dose loss," *Applied Physics Letters*, vol. 93, no. 10, p. 101910, 2008.
- [51] V. C. Venezia *et al.*, "Dopant redistribution effects in preamorphized silicon during low temperature annealing," in *IEDM Technical Digest*, Washington, DC, USA, pp. 489–492, December 2003.
- [52] C. Zechner, D. Matveev, and A. Erlebach, "Phase-field model for the dopant redistribution during solid phase epitaxial regrowth of amorphized silicon," *Materials Science and Engineering B*, vol. 114–115, pp. 162–165, 2004.
- [53] T. Aoyama, H. Tashiro, and K. Suzuki, "Diffusion of Boron, Phosphorus, Arsenic, and Antimony in Thermally Grown Silicon Dioxide," *Journal of the Electrochemical Society*, vol. 146, no. 5, pp. 1879–1883, 1999.
- [54] H. Rücker *et al.*, "Suppressed diffusion of boron and carbon in carbon-rich silicon," *Applied Physics Letters*, vol. 73, no. 12, pp. 1682–1684, 1998.
- [55] H. Rücker *et al.*, "Erratum: Suppressed diffusion of boron and carbon in carbon-rich silicon," *Applied Physics Letters*, vol. 75, no. 1, p. 147, 1999.
- [56] P. Lavéant *et al.*, "Engineering the diffusion behavior of dopants (B, Sb) in silicon by incorporation of carbon," *Nuclear Instruments and Methods in Physics Research B*, vol. 186, no. 1–4, pp. 292–297, 2002.
- [57] V. Moroz *et al.*, "Optimizing boron junctions through point defect and stress engineering using carbon and germanium co-implants," *Applied Physics Letters*, vol. 87, p. 051908, August 2005.
- [58] B. J. Pawlak *et al.*, "Suppression of phosphorus diffusion by carbon co-implantation," *Applied Physics Letters*, vol. 89, p. 062102, August 2006.
- [59] C. Zechner *et al.*, "Modeling Ultra Shallow Junctions Formed by Phosphorus-Carbon and Boron-Carbon Co-implantation," in *MRS Symposium Proceedings, Semiconductor Defect Engineering—Materials, Synthetic Structures and Devices II*, vol. 994, San Francisco, CA, USA, p. 0994-F11-17, April 2007.
- [60] S. Brotzmann *et al.*, "Diffusion and defect reactions between donors, C, and vacancies in Ge. I. Experimental results," *Physical Review B*, vol. 77, no. 23, p. 235207, 2008.

- [61] A. Chroneos, B. P. Uberuaga, and R. W. Grimes, "Carbon, dopant, and vacancy interactions in germanium," *Journal of Applied Physics*, vol. 102, no. 8, p. 083707, 2007.
- [62] A. Chroneos *et al.*, "Diffusion and defect reactions between donors, C, and vacancies in Ge. II. Atomistic calculations of related complexes," *Physical Review B*, vol. 77, no. 23, p. 235208, 2008.
- [63] F. J. Morin and J. P. Maita, "Electrical Properties of Silicon Containing Arsenic and Boron," *Physical Review*, vol. 96, no. 1, pp. 28–35, 1954.
- [64] B. E. Deal and A. S. Grove, "General Relationship for the Thermal Oxidation of Silicon," *Journal of Applied Physics*, vol. 36, no. 12, pp. 3770–3778, 1965.
- [65] A. Ohta *et al.*, "Dry Oxidation of Germanium (100) and (111) Surfaces - Impact of Oxidation Temperature on Ge Oxide Growth," in *International Conference on Solid State Devices and Materials (SSDM)*, Kyoto, Japan, pp. 743–744, September 2012.
- [66] W. Ting *et al.*, "Growth kinetics of ultrathin SiO_2 films fabricated by rapid thermal oxidation of Si substrates in N_2O ," *Journal of Applied Physics*, vol. 70, no. 2, pp. 1072–1074, 1991.
- [67] H. R. Soleimani, A. Philipossian, and B. Doyle, "A Study of the Growth Kinetics of SiO_2 in N_2O ," in *IEDM Technical Digest*, San Francisco, CA, USA, pp. 629–632, December 1992.
- [68] G. W. Yoon *et al.*, "Thickness uniformity and electrical properties of ultrathin gate oxides grown in N_2O ambient by rapid thermal processing," *Journal of Applied Physics*, vol. 72, no. 12, pp. 5706–5710, 1992.
- [69] H. B. Harrison *et al.*, "Substrate Doping and Orientation Effects on Dielectric Growth on Silicon in a Nitrous Oxide Environment," in *MRS Online Proceedings Library*, vol. 303, pp. 417–420, 1993 (<https://doi.org/10.1557/PROC-303-417>).
- [70] N. Bellafiore, F. Pio, and C. Riva, "Thin oxide nitridation in N_2O by RTP for non-volatile memories," *Microelectronics Journal*, vol. 24, no. 4, pp. 453–458, 1993 ([https://doi.org/10.1016/0026-2692\(93\)90052-G](https://doi.org/10.1016/0026-2692(93)90052-G)).
- [71] S. C. Sun and H. Y. Chang, "Oxidation Simulation and Growth Kinetics of Thin SiO_2 in Pure N_2O ," in *Simulation of Semiconductor Devices and Processes (SISDEP)*, vol. 5, Vienna, Austria, pp. 169–172, September 1993.
- [72] N. Zographos *et al.*, "Process Modeling of Chemical and Stress Effects in SiGe," in *19th International Conference on Ion Implantation Technology (IIT)*, Valladolid, Spain, pp. 212–216, June 2012.
- [73] M. Ogino, Y. Oana, and M. Watanabe, "The Diffusion Coefficient of Germanium in Silicon," *Physica Status Solidi A*, vol. 72, no. 2, pp. 535–541, 1982.
- [74] C. Ahn and S. T. Dunham, "Calculation of dopant segregation ratios at semiconductor interfaces," *Physical Review B*, vol. 78, no. 19, p. 195303, 2008.

- [75] N. E. Cowern, "Diffusion in a Single Crystal within a Stressed Environment," *Physical Review Letters*, vol. 99, p. 155903, October 2007.
- [76] N. E. B. Cowern *et al.*, "Overlayer stress effects on defect formation in Si and Ge," *Thin Solid Films*, vol. 518, no. 9, pp. 2442–2447, 2010.
- [77] Y. Zaitsu *et al.*, "Boron Diffusion in Compressively Stressed Float Zone-Silicon Induced by Si_3N_4 Films," *Journal of the Electrochemical Society*, vol. 145, no. 1, pp. 258–264, 1998.
- [78] R. Braunstein, A. R. Moore, and F. Herman, "Intrinsic Optical Absorption in Germanium-Silicon Alloys," *Physical Review*, vol. 109, no. 3, pp. 695–710, 1958.
- [79] Ioffe Physical Technical Institute, parameter database, for more information, go to <http://www.ioffe.ru/SVA/NSM/Semicond/SiGe/bandstr.html>.
- [80] G. M. Delpian *et al.*, "Ab initio calculations of vacancies in Si Ge_{1-x} ," *Applied Physics Letters*, vol. 81, no. 18, pp. 3383–3385, 2002.
- [81] P. Venezuela *et al.*, "Vacancy-mediated diffusion in disordered alloys: Ge self-diffusion in $\text{Si}_{1-x}\text{Ge}_x$," *Physical Review B*, vol. 65, no. 19, p. 193306, 2002.
- [82] P. Ramanarayanan, K. Cho, and B. M. Clemens, "Effect of composition on vacancy mediated diffusion in random binary alloys: First principles study of the SiGe_x system," *Journal of Applied Physics*, vol. 94, no. 1, pp. 174–185, 2003.
- [83] N. Zographos *et al.*, "Multiscale modeling of doping processes in advanced semiconductor devices," *Materials Science in Semiconductor Processing*, vol. 62, pp. 49–61, May 2017.
- [84] R. T. Crosby, *Evolution of Self-Interstitials Induced by Ion-Implantation in SiGe Alloys*, PhD thesis, University of Florida, USA, 2005.
- [85] V. Moroz *et al.*, "Dissolution of extended defects in strained silicon," *Journal of Vacuum Science & Technology B*, vol. 26, no. 1, pp. 439–442, 2008.
- [86] P. Castrillo *et al.*, "Physical modeling and implementation scheme of native defect diffusion and interdiffusion in SiGe heterostructures for atomistic process simulation," *Journal of Applied Physics*, vol. 109, p. 103502, May 2011.
- [87] C. Zechner and N. Zographos, "Silicon germanium interdiffusion in SiGe device fabrication: A calibrated TCAD model," *Materials Science in Semiconductor Processing*, vol. 42, pp. 230–234, February 2016.
- [88] R. Kube *et al.*, "Composition dependence of Si and Ge diffusion in relaxed $\text{Si}_{1-x}\text{Ge}_x$ alloys," *Journal of Applied Physics*, vol. 107, p. 073520, April 2010.
- [89] Y. Dong *et al.*, "A unified interdiffusivity model and model verification for tensile and relaxed SiGe interdiffusion over the full germanium content range," *Journal of Applied Physics*, vol. 111, p. 044909, February 2012.

- [90] G. Xia, J. L. Hoyt, and M. Canonico, "Si–Ge interdiffusion in strained Si/strained SiGe heterostructures and implications for enhanced mobility metal-oxide-semiconductor field-effect transistors," *Journal of Applied Physics*, vol. 101, p. 044901, February 2007.
- [91] N. E. B. Cowern *et al.*, "Diffusion in Strained Si(Ge)," *Physical Review Letters*, vol. 72, no. 16, pp. 2585–2588, 1994.
- [92] H. H. Silvestri *et al.*, "Diffusion of silicon in crystalline germanium," *Semiconductor Science and Technology*, vol. 21, no. 6, p. 758, 2006.
- [93] G. Xia and J. L. Hoyt, "Si–Ge interdiffusion under oxidizing conditions in epitaxial SiGe heterostructures with high compressive stress," *Applied Physics Letters*, vol. 96, p. 122107, March 2010.
- [94] A. N. Larsen and P. Kringhoj, "Diffusion of Sb in relaxed $\text{Si}_{1-x}\text{Ge}_x$," *Applied Physics Letters*, vol. 68, no. 19, pp. 2684–2686, 1996.
- [95] P. Laitinen, *Self- and Impurity Diffusion in Intrinsic Relaxed Silicon - Germanium*, PhD thesis, University of Jyväskylä, Finland, 2004.
- [96] N. Zangenberg, *Defect and Diffusion Studies in Si and SiGe*, PhD thesis, University of Aarhus, Denmark, 2003.
- [97] P. Kuo *et al.*, "Boron Diffusion in Si and $\text{Si}_{1-x}\text{Ge}_x$," in *MRS Symposium Proceedings, Strained Layer Epitaxy - Materials, Processing, and Device Applications*, vol. 379, pp. 373–378, 1995.
- [98] N. Moriya *et al.*, "Boron Diffusion in Strained $\text{Si}_{1-x}\text{Ge}_x$ Epitaxial Layers," *Physical Review Letters*, vol. 71, no. 6, pp. 883–886, 1993.
- [99] K. Rajendran and W. Schoenmaker, "Studies of boron diffusivity in strained $\text{Si}_{1-x}\text{Ge}_x$ epitaxial layers," *Journal of Applied Physics*, vol. 89, no. 2, pp. 980–987, 2001.
- [100] S. Uppal *et al.*, "Diffusion of Boron in Germanium and $\text{Si}_{1-x}\text{Ge}_x$ ($x > 50\%$) alloys," in *MRS Symposium Proceedings, CMOS Front-End Materials and Process Technology*, vol. 765, p. D6.16.1, January 2003.
- [101] C. Ahn, *Atomic scale modeling of stress and pairing effects on dopant behavior in silicon*, PhD thesis, University of Washington, USA, 2007.
- [102] S. Eguchi *et al.*, "Comparison of arsenic and phosphorus diffusion behavior in silicon–germanium alloys," *Applied Physics Letters*, vol. 80, no. 10, pp. 1743–1745, 2002.
- [103] S. Eguchi *et al.*, "Germanium-concentration dependence of arsenic diffusion in silicon germanium alloys," *Applied Physics Letters*, vol. 84, no. 3, pp. 368–370, 2004.
- [104] Y.-M. Sheu *et al.*, "Modeling Dopant Diffusion in Strained and Strain-Relaxed Epi-SiGe," in *International Conference on Simulation of Semiconductor Process and Devices (SISPAD)*, Tokyo, Japan, pp. 75–78, September 2005.
- [105] C. C. Wang *et al.*, "Boron diffusion in strained and strain-relaxed SiGe," *Materials Science and Engineering B*, vol. 124–125, pp. 39–44, December 2005.

- [106] P. E. Thompson, J. Bennett, and S. Felch, "The Use of SiGe Barriers During the Formation of p⁺ Shallow Junctions by Ion Implantation," in *MRS Symposium Proceedings, Silicon Front-End Junction Formation—Physics and Technology*, vol. 810, San Francisco, CA, USA, pp. C4.11.1–C4.11.6, April 2004.
- [107] F. K. LeGoues *et al.*, "Oxidation studies of SiGe," *Journal of Applied Physics*, vol. 65, no. 4, pp. 1724–1728, 1989.
- [108] T. Tezuka, N. Sugiyama, and S. Takagi, "Fabrication of strained Si on an ultrathin SiGe-on-insulator virtual substrate with a high-Ge fraction," *Applied Physics Letters*, vol. 79, no. 12, pp. 1798–1800, 2001.
- [109] Z. Y. Xue *et al.*, "Study of Ge loss during Ge condensation process," *Thin Solid Films*, vol. 557, pp. 120–124, April 2014.
- [110] M. Spadafora *et al.*, "Oxidation rate enhancement of SiGe epitaxial films oxidized in dry ambient," *Applied Physics Letters*, vol. 83, no. 18, pp. 3713–3715, 2003.
- [111] N. Sugiyama *et al.*, "Temperature effects on Ge condensation by thermal oxidation of SiGe-on-insulator structures," *Journal of Applied Physics*, vol. 95, no. 8, pp. 4007–4011, 2004.
- [112] B. Vincent *et al.*, "Fabrication of SiGe-on-insulator substrates by a condensation technique: an experimental and modelling study," *Semiconductor Science and Technology*, vol. 22, no. 3, pp. 237–244, 2007.
- [113] E. Long *et al.*, "Nano-structuring in SiGe by oxidation induced anisotropic Ge self-organization," *Journal of Applied Physics*, vol. 113, no. 10, p. 104310, 2013.
- [114] O. Gourhant *et al.*, "Ge Condensation using Rapid Thermal Oxidation for SGOI Substrate Preparation," *ECS Transactions*, vol. 64, no. 6, pp. 469–478, 2014.
- [115] V. Boureau *et al.*, "Strain/composition interplay in thin SiGe layers on insulator processed by Ge condensation," *Materials Science in Semiconductor Processing*, vol. 42, pp. 251–254, February 2016.
- [116] T. Shimura *et al.*, "Self-limiting oxidation of SiGe alloy on silicon-on-insulator wafers," *Applied Physics Letters*, vol. 89, no. 11, p. 111923, 2006.
- [117] Y. Zhang *et al.*, "Experimental evidence of oxidant-diffusion-limited oxidation of SiGe alloys," *Journal of Applied Physics*, vol. 106, no. 6, p. 063508, 2009.
- [118] W. S. Liu *et al.*, "Wet oxidation of GeSi at 700 °C," *Journal of Applied Physics*, vol. 71, no. 8, pp. 4015–4018, 1992.
- [119] M. Tanaka *et al.*, "Abnormal oxidation characteristics of SiGe/Si-on-insulator structures depending on piled-up Ge fraction at SiO₂/SiGe interface," *Journal of Applied Physics*, vol. 103, no. 5, p. 054909, 2008.
- [120] G. L. Bir and G. E. Pikus, *Symmetry and Strain-Induced Effects in Semiconductors*, New York: John Wiley & Sons, 1974.

- [121] C. G. Van de Walle, "Strain effects on the valence-band structure of SiGe," in *Properties of Silicon Germanium and SiGe:Carbon*, EMIS Datareviews Series, pp. 135–139, London: INSPEC, The Institute of Electrical Engineers, 2000.
- [122] M. Diebel, *Application of Ab-initio Calculations to Modeling of Nanoscale Diffusion and Activation in Silicon*, PhD thesis, University of Washington, Seattle, WA, USA, 2004.
- [123] Y. Kawamura *et al.*, "Self-diffusion in compressively strained Ge," *Journal of Applied Physics*, vol. 110, p. 034906, August 2011.
- [124] C. Ahn *et al.*, "Stress effects on impurity solubility in crystalline materials: A general model and density-functional calculations for dopants in silicon," *Physical Review B*, vol. 79, no. 7, p. 073201, 2009.
- [125] R. F. Lever, J. M. Bonar, and A. F. W. Willoughby, "Boron diffusion across silicon–silicon germanium boundaries," *Journal of Applied Physics*, vol. 83, no. 4, pp. 1988–1994, 1998.
- [126] J. S. Christensen, *Dopant diffusion in Si and SiGe*, PhD thesis, KTH, Royal Institute of Technology, Stockholm, Sweden, 2004.
- [127] G. Hobler and S. Selberherr, "Two-Dimensional Modeling of Ion Implantation Induced Point Defects," *IEEE Transactions on Computer-Aided Design*, vol. 7, no. 2, pp. 174–180, 1988.
- [128] M. D. Giles, "Transient Phosphorus Diffusion Below the Amorphization Threshold," *Journal of the Electrochemical Society*, vol. 138, no. 4, pp. 1160–1165, 1991.
- [129] A. Renau, "Device performance and yield - A new focus for ion implantation," in *Extended Abstracts of International Workshop on Junction Technology (IWJT)*, Shanghai, China, May 2010.
- [130] F. Khaja *et al.*, "Benefits of Damage Engineering for PMOS Junction Stability," in *18th International Conference on Ion Implantation Technology (IIT)*, Kyoto, Japan, June 2010.
- [131] F. A. Khaja *et al.*, "Physical understanding of cryogenic implant benefits for electrical junction stability," *Applied Physics Letters*, vol. 100, no. 11, p. 112102, 2012.
- [132] M. Posselt, L. Bischoff, and J. Teichert, "Influence of dose rate and temperature on ion-beam-induced defect evolution in Si investigated by channeling implantation at different doses," *Applied Physics Letters*, vol. 79, no. 10, pp. 1444–1446, 2001.
- [133] R. D. Goldberg, J. S. Williams, and R. G. Elliman, "Amorphization of silicon by elevated temperature ion irradiation," *Nuclear Instruments and Methods in Physics Research B*, vol. 106, no. 1–4, pp. 242–247, 1995.
- [134] H.-J. Gossmann *et al.*, "Predictive Process Simulation of Cryogenic Implants for Leading Edge Transistor Design," in *19th International Conference on Ion Implantation Technology (IIT)*, Valladolid, Spain, pp. 225–228, June 2012.

- [135] N. Zographos, A. Tsibizov, and C. Zechner, “Continuum Modeling of Implantation and Thermal Processes for Advanced Devices Formation,” in *20th International Conference on Ion Implantation Technology (IIT)*, Portland, OR, USA, pp. 189–194, June 2014.
- [136] S. I. Kondratenko, L. M. Rubin, and E. A. G. Webster, “Analysis of Very High Energy Implantation Profiles at Channeling and Non-Channeling Conditions,” in *22nd International Conference on Ion Implantation Technology (IIT)*, Würzburg, Germany, pp. 307–310, September 2018.
- [137] M. Current *et al.*, “Channeled MeV B, P and As Profiles in Si(100): Monte-Carlo Models and SIMS,” in *22nd International Conference on Ion Implantation Technology (IIT)*, Würzburg, Germany, pp. 251–254, September 2018.
- [138] J. Li and K. S. Jones, “{311} defects in silicon: The source of the loops,” *Applied Physics Letters*, vol. 73, no. 25, pp. 3748–3750, 1998.
- [139] C. Zechner *et al.*, “Simulation of dopant diffusion and activation during flash lamp annealing,” *Materials Science and Engineering B*, vol. 154-155, pp. 20–23, December 2008.
- [140] S. Solmi, F. Baruffaldi, and R. Canteri, “Diffusion of boron in silicon during post-implantation annealing,” *Journal of Applied Physics*, vol. 69, no. 4, pp. 2135–2142, 1991.
- [141] M. Diebel and S. T. Dunham, “*Ab Initio* Calculations to Model Anomalous Fluorine Behavior,” *Physical Review Letters*, vol. 93, no. 24, p. 245901, 2004.
- [142] M. Diebel and S. T. Dunham, “Reply to *Ab Initio* Calculations to Model Anomalous Fluorine Behavior,” *Physical Review Letters*, vol. 96, p. 039602, January 2006.
- [143] K. Vollenweider *et al.*, “Fluorine clustering and diffusion in silicon: *Ab initio* calculations and kinetic Monte Carlo model,” *Journal of Vacuum Science & Technology B*, vol. 28, no. 1, pp. C1G1–C1G6, 2010.
- [144] P. A. Schultz and J. S. Nelson, “Fast through-bond diffusion of nitrogen in silicon,” *Applied Physics Letters*, vol. 78, no. 6, pp. 736–738, 2001.
- [145] N. Stoddard *et al.*, “*Ab Initio* Identification of the Nitrogen Diffusion Mechanism in Silicon,” *Physical Review Letters*, vol. 95, no. 2, p. 025901, 2005.
- [146] J. S. Nelson, P. A. Schultz, and A. F. Wright, “Valence and atomic size dependent exchange barriers in vacancy-mediated dopant diffusion,” *Applied Physics Letters*, vol. 73, no. 2, pp. 247–249, 1998.
- [147] J. P. Goss *et al.*, “Vibrational modes and electronic properties of nitrogen defects in silicon,” *Physical Review B*, vol. 67, no. 4, p. 045206, 2003.
- [148] G. L. Olson and J. A. Roth, “Kinetics of Solid Phase Crystallization in Amorphous Silicon,” *Materials Science Reports*, vol. 3, no. 1, pp. 1–78, 1988.
- [149] S. Mirabella *et al.*, “Fluorine segregation and incorporation during solid-phase epitaxy of Si,” *Applied Physics Letters*, vol. 86, no. 12, p. 121905, 2005.

- [150] I. Martin-Bragado and V. Moroz, "Facet formation during solid phase epitaxy regrowth: A lattice kinetic Monte Carlo model," *Applied Physics Letters*, vol. 95, p. 123123, September 2009.
- [151] K. L. Saenger *et al.*, "A study of trench-edge defect formation in (001) and (011) silicon recrystallized by solid phase epitaxy," *Journal of Applied Physics*, vol. 101, no. 2, p. 024908, 2007.
- [152] V. C. Venezia *et al.*, "Dopant redistribution effects in preamorphized silicon during low temperature annealing," in *IEDM Technical Digest*, Washington, DC, USA, pp. 489–492, December 2003.
- [153] S. Mirabella *et al.*, "Mechanism of Boron Diffusion in Amorphous Silicon," *Physical Review Letters*, vol. 100, p. 155901, April 2008.
- [154] K. Suzuki *et al.*, "Analytical Model for Redistribution Profile of Ion-Implanted Impurities During Solid-Phase Epitaxy," *IEEE Transactions on Electron Devices*, vol. 54, no. 2, pp. 262–271, 2007.
- [155] R. Duffy *et al.*, "Dopant diffusion in amorphous silicon," in *MRS Symposium Proceedings, Silicon Front-End Junction Formation—Physics and Technology*, vol. 810, San Francisco, CA, USA, p. C10.2.1, April 2004.
- [156] R. Duffy *et al.*, "Influence of preamorphization and recrystallization on indium doping profiles in silicon," *Journal of Vacuum Science & Technology B*, vol. 22, no. 3, pp. 865–868, 2004.
- [157] G. Impellizzeri *et al.*, "Fluorine in preamorphized Si: Point defect engineering and control of dopant diffusion," *Journal of Applied Physics*, vol. 99, p. 103510, May 2006.
- [158] G. R. Nash *et al.*, "Activation energy for fluorine transport in amorphous silicon," *Applied Physics Letters*, vol. 75, no. 23, pp. 3671–3673, 1999.
- [159] M. Rahimo *et al.*, "Thin-Wafer Silicon IGBT With Advanced Laser Annealing and Sintering Process," *IEEE Electron Device Letters*, vol. 33, no. 11, pp. 1601–1603, 2012.
- [160] T. Gutt and H. Schulze, "Deep melt activation using laser thermal annealing for IGBT thin wafer technology," in *Proceedings of the 22nd International Symposium on Power Semiconductor Devices and ICs (ISPSD)*, Hiroshima, Japan, pp. 29–32, June 2010.
- [161] K. Huet *et al.*, "High Performance and High Yield Junction Formation with Full Device Exposure Laser Thermal Annealing," in *International Image Sensor Workshop (IISW)*, Hokkaido, Japan, p. R12, June 2011.
- [162] A. Karma and W.-J. Rappel, "Quantitative phase-field modeling of dendritic growth in two and three dimensions," *Physical Review E*, vol. 57, no. 4, pp. 4323–4349, 1998.
- [163] *IGBT Process Simulation With Backside Melt Laser Annealing and Its Device Simulations for DC, Switching, and Short-Circuit Characteristics*, available from TCAD Sentaurus Version T-2022.03 installation, go to Applications_Library/Power/IGBT_MeltLaserAnneal.

- [164] C. J. Glassbrenner and G. A. Slack, "Thermal Conductivity of Silicon and Germanium from 3°K to the Melting Point," *The Physical Review*, vol. 134, no. 4A, pp. A1058–A1069, 1964.
- [165] B. Abeles *et al.*, "Thermal Conductivity of Ge–Si Alloys at High Temperatures," *Physical Review*, vol. 125, no. 1, pp. 44–46, 1962.
- [166] E. Yamasue *et al.*, "Thermal conductivities of silicon and germanium in solid and liquid states measured by non-stationary hot wire method with silica coated probe," *Journal of Crystal Growth*, vol. 234, no. 1, pp. 121–131, 2002.
- [167] D. G. Cahill *et al.*, "Thermal conductivity of epitaxial layers of dilute SiGe alloys," *Physical Review B*, vol. 71, no. 23, p. 235202, 2005.
- [168] A. S. Lahwal, *Thermoelectric Properties of Silicon Germanium: An Investigation of the Reduction of Lattice Thermal Conductivity and Enhancement of Power Factor*, PhD thesis, Clemson University, Clemson, SC, USA, May 2015.
- [169] D. Li *et al.*, "Thermal conductivity of Si/SiGe superlattice nanowires," *Applied Physics Letters*, vol. 83, no. 15, pp. 3186–3188, 2003.
- [170] I. Yonenaga *et al.*, "Thermal and Electrical Properties of Czochralski Grown Germanium-Silicon Alloys," in *18th International Conference on Thermoelectrics*, Baltimore, MD, USA, pp. 436–439, August 1999.
- [171] B. L. Zink, R. Pietri, and F. Hellman, "Thermal Conductivity and Specific Heat of Thin-Film Amorphous Silicon," *Physical Review Letters*, vol. 96, no. 5, p. 055902, 2006.
- [172] Y. He, D. Donadio, and G. Galli, "Heat transport in amorphous silicon: Interplay between morphology and disorder," *Applied Physics Letters*, vol. 98, p. 144101, April 2011.
- [173] W. Szyszko, F. Vega, and C. N. Afonso, "Shifting of the thermal properties of amorphous germanium films upon relaxation and crystallization," *Applied Physics A: Materials Science and Processing*, vol. 61, no. 2, pp. 141–147, 1995.
- [174] B. Ryningen *et al.*, "The Effect of Crucible Coating and the Temperature Field on Minority Carrier Lifetime in Directionally Solidified Multicrystalline Silicon Ingots," in *27th European Photovoltaic Solar Energy Conference and Exhibition*, Frankfurt, Germany, pp. 926–932, September 2012.
- [175] H. Ftouni *et al.*, "Thermal conductivity of silicon nitride membranes is not sensitive to stress," *Physical Review B: Condensed Matter and Materials Physics*, vol. 92, no. 12, p. 125439, 2015.
- [176] R. K. Endo, Y. Fujihara, and M. Susa, "Calculation of density and heat capacity of silicon by molecular dynamics simulation," *High Temperatures-High Pressures*, vol. 35–36, no. 5, pp. 505–511, 2003.
- [177] P. Roura *et al.*, "Measurement of the specific heat and determination of the thermodynamic functions of relaxed amorphous silicon," *Journal of Applied Physics*, vol. 113, p. 173515, May 2013.

- [178] A. S. Okhotin, A. S. Pushkarskij, and V. V. Gorbachev, *Thermophysical Properties of Semiconductors*, Moscow: Atomizdat, 1972.
- [179] W.-K. Rhim, *Thermophysical Property Measurements of Molten Semiconductors in 1-g and Reduced-g Conditions*, Technical Report, Jet Propulsion Laboratory, California Institute of Technology, Pasadena, CA, USA, February 1999 (<https://ntrs.nasa.gov/archive/nasa/casi.ntrs.nasa.gov/19990040333.pdf>).
- [180] For information about the NIST-JANAF thermochemical tables, go to <https://janaf.nist.gov>.
- [181] H. Stöhr and, W. Klemm, “Über Zweistoffsysteme mit Germanium. I. Germanium/Aluminium, Germanium/Zinn und Germanium/Silicium,” *Zeitschrift für anorganische und allgemeine Chemie*, vol. 241, no. 4, pp. 305–323, 1939.
- [182] A. Mittiga, L. Fornarini, and R. Carluccio, “Numerical modeling of laser induced phase transitions in silicon,” *Applied Surface Science*, vol. 154–155, pp. 112–117, February 2000.
- [183] A. La Magna *et al.*, “A phase-field approach to the simulation of the excimer laser annealing process in Si,” *Journal of Applied Physics*, vol. 95, no. 9, pp. 4806–4814, 2004.
- [184] S. de Unamuno and E. Fogarassy, “A Thermal Description of the Melting of c- and a-Silicon Under Pulsed Excimer Lasers,” *Applied Surface Science*, vol. 36, no. 1–4, pp. 1–11, 1989.
- [185] G. E. Jellison Jr., “Optical functions of silicon determined by two-channel polarization modulation ellipsometry,” *Optical Materials*, vol. 1, no. 1, pp. 41–47, 1992.
- [186] ICT Project 258547 ATEMOK, *Advanced Technology Modeling for Extra-Functionality Devices*, for more information, go to <https://cordis.europa.eu/project/id/258547>.
- [187] J. P. Garandet, “New Determinations of Diffusion Coefficients for Various Dopants in Liquid Silicon,” *International Journal of Thermophysics*, vol. 28, no. 4, pp. 1285–1303, 2007.
- [188] M. Hackenberg *et al.*, “Modeling Boron Profiles in Silicon after Pulsed Excimer Laser Annealing,” in *19th International Conference on Ion Implantation Technology (IIT)*, Valladolid, Spain, pp. 241–244, June 2012.
- [189] K. Huet *et al.*, “Experimental and Theoretical analysis of Dopant Activation in Double Implanted Silicon by Pulsed Laser Thermal Annealing,” in *17th International Conference on Advanced Thermal Processing of Semiconductors (RTP)*, Albany, NY, USA, September 2009.
- [190] L. Dagault *et al.*, “Composition and Strain Evolution of Undoped $\text{Si}_{0.8}\text{Ge}_{0.2}$ Layers Submitted to UV-Nanosecond Laser Annealing,” *ECS Transactions*, vol. 86, no. 7, pp. 29–39, 2018.
- [191] M. O. Thompson *et al.*, “Melting Temperature and Explosive Crystallization of Amorphous Silicon during Pulsed Laser Irradiation,” *Physical Review Letters*, vol. 52, no. 26, pp. 2360–2363, 1984.

3

Guidelines for Additional Calibration

This chapter provides guidelines for additional calibration.

The Advanced Calibration file is the recommended starting point for accurate process simulation with Sentaurus Process. However, the Advanced Calibration cannot fully replace an additional calibration by the user for 2D or 3D applications. With a customized process calibration, the accuracy can always be further increased for any technology of interest. A customized calibration of process and device simulation models needs to be performed by the user or can be requested from Synopsys in the context of a customer service project.

To further improve the Advanced Calibration, Synopsys appreciates feedback from customers regarding the accuracy obtained with the parameter files for different process conditions, and suggestions for improved models or parameter values.

Accuracy and Limitations of Advanced Calibration of Sentaurus Process

The Advanced Calibration is based on scientific literature on process simulation models and on a continual calibration effort based on the Synopsys collection of SIMS profiles from state-of-the-art device manufacturing technology. A good agreement is obtained for a large portion of the SIMS data for silicon. However, in many cases, there is a significant mismatch between simulation results obtained with Advanced Calibration and the experimental data for several reasons:

- Many models are simplifications of real physics.
- Only a few parameters of diffusion and reaction physics in silicon can be determined by direct measurements. Therefore, the calibration is difficult.
- A very large range of possible experiment data needs to be reproduced with a single, consistent set of models. For example, in standard CMOS technology, dopant concentrations range from 10^{16} cm^{-3} to 10^{22} cm^{-3} ; temperatures range from 500°C to 1350°C.

Chapter 3: Guidelines for Additional Calibration

Accuracy and Limitations of Advanced Calibration of Sentaurus Process

- In extreme conditions, the models used are often overburdened. For example, the dopant clustering models, which work well at dopant concentrations up to 10^{21} cm^{-3} , are less reliable at higher dopant concentrations, which might occur after high-dose ion implantation at very low energies or after epitaxial growth of highly doped layers.
- The experimental data is not perfectly accurate. Errors arise from insufficient equipment calibration (implanter dose, furnace temperature), from SIMS measurements, and from missing details in the process description such as thickness of the oxide layer on top of silicon. As a result, occasionally, small discrepancies are observed between data obtained by different groups for the same nominal process conditions.
- For some physical phenomena, no adequate calibration is available, either due to the lack of a physical model in Sentaurus Process or to the lack of data for performing a reliable calibration.

In this section, the accuracy of the Advanced Calibration is discussed in detail. In particular, it will be explained for which process conditions the accuracy is limited and which parameters can be tuned by users to increase the accuracy in a process window of interest. Unless mentioned otherwise, the discussion focuses on the default model switches of Advanced Calibration. For the option `AdvancedModels` (part 4 of `AdvCal_2022.03.fps`), see [Part 4: Comprehensive and Slow Models on page 94](#).

Error Control

By default, the `Math` option `NegErrCntrl` (as well as `FTS.NegErrCntrl` and `AMS.NegErrCntrl`) is switched off. When switched on, `NegErrCntrl` enforces stricter error control at Newton iterations and, typically, leads to an increased CPU time for the simulation of thermal annealing.

With `NegErrCntrl` switched off, the simulation results can include the corresponding numeric errors. For many applications, these numeric errors are small. However, it is worthwhile checking the numeric errors at least once for a process simulation setup. If simulations with and without the option `NegErrCntrl` produce different results, it is recommended to switch on `NegErrCntrl` (or `FTS.NegErrCntrl` and `AMS.NegErrCntrl`) either globally or for selected diffusion steps and data fields, to avoid numeric errors.

Point Defects

This section discusses point defects.

Bulk Parameters

The parameter values for the equilibrium concentration, diffusivity, and charge-state distribution of point defects in silicon have been chosen by Synopsys, as a careful compromise between various suggestions in publications [1][2][3][4][5][6][7].

The bulk recombination is based on the assumption that there is no energy barrier for I–V recombination, and that interstitials and vacancies with the same charge state do not recombine.

Changing any of these parameters might affect the diffusion and activation behavior of several dopants. Therefore, for the purpose of improving the accuracy of diffusion of one dopant, it is not recommended to change point-defect parameters for both silicon and germanium, due to the possible unwanted effects on other dopants.

Surface Boundary Conditions

At the Si–SiO₂ interface, fast recombination is assumed for interstitials and vacancies. The parameter `Ksurf` is defined such that the recombination length is 1 nm. Sometimes, in technology-specific calibration, the parameter `Ksurf` for interstitial recombination at Si–SiO₂ interfaces is reduced to slow down the surface recombination of excess interstitials created by ion implantation.

For nitride–silicon interfaces, the point-defect surface boundary conditions have not yet been calibrated, due to a lack of suitable data. The parameter `Ksurf` is set to values that correspond to a recombination length of 10 nm. Therefore, point-defect recombination or injection at Si–SiN interfaces is assumed to be slower than at Si–SiO₂ interfaces. As it is unclear whether this is correct, in process simulations of structures that include Si–SiN interfaces, an adjustment of `Ksurf` should be considered for fine-tuning.

Gas–Si interfaces are rarely used in process simulation. Bare Si surfaces should usually be covered by a thin native oxide, which is necessary for modeling dopant dose loss at Si surfaces. However, during epitaxy, gas–Si interfaces occur. For gas–Si interfaces, fast recombination is used for interstitials and, since Advanced Calibration Version S-2021.06, also for vacancies.

From experiments, there is no direct evidence whether vacancy recombination at gas–Si surfaces should be fast or slow. In Advanced Calibration Version R-2020.09 and earlier, a 10⁵ times slower recombination of vacancies (recombination length 100 μm) was defined at gas–Si and gas–Ge boundaries, by the statements:

```
pdbSetDouble Gas_Si V Ksurf {[expr [pdbGet Si V Dv]*1e2]}\n pdbSetDouble Gas_Ge V Ksurf {[expr [pdbGet Ge V Dv]*1e2]}\n
```

Chapter 3: Guidelines for Additional Calibration

Accuracy and Limitations of Advanced Calibration of Sentaurus Process

Originally, this was found to be useful for modeling the measured phosphorus tail diffusion during epitaxy of P-doped Si, without a need to assume any grown-in defects. However, over time, for several process conditions, the slow vacancy recombination velocity at gas–Si interfaces was found to cause poor results for dopant diffusion, which included:

- Growth of epi layers immediately after a high-temperature anneal with a fast ramp-down (in this case, vacancies formed at high temperatures can still be present)
- Growth of epi layers after C implantation (in this case, vacancies are generated during the formation of C.I clusters)
- Thermal anneals for structures in which users forgot to place a native oxide on top of bare silicon surfaces

Therefore, in `AdvCal_2021.06.fps`, a fast vacancy recombination at gas–Si interfaces has been introduced. It is still used in `AdvCal_2022.03.fps`. This change affects P diffusion during epitaxial growth of P-doped Si. For this use case, results have changed between `AdvCal_2020.09.fps` and `AdvCal_2021.06.fps`. For recommendations, see [Phosphorus-Doped Epitaxial Silicon on page 154](#).

Oxidation-Enhanced Diffusion

Oxidation-enhanced diffusion (OED) is simulated by interstitial injection and a reduced concentration of vacancies at the moving Si–SiO₂ interface. The interstitial injection rate depends on the local oxide growth rate at the interface. The calibration for the intrinsic condition is based on literature data for the growth of thick oxide in O₂ atmosphere. For additional fine-tuning of OED in lowly doped regions, it is recommended to adjust the parameter `theta`. For a separate fine-tuning of OED in highly doped regions, it is recommended to adjust the parameters `m`, `mm` for n-type doping and the parameters `p`, `pp` for p-type doping.

In the process simulation of NMOS devices, increasing the value of `theta` during poly reoxidation typically increases the reverse short-channel effect by enhancing the B pileup towards the Si–SiO₂ interface under the gate, which is driven by the injection of interstitials at the oxidizing surfaces.

Clusters of Interstitials

The one-moment model suggested by Rafferty *et al.* [8] is used in the Advanced Calibration. It gives a reasonably accurate description of Si self-interstitial supersaturation during anneals, in which the transient-enhanced diffusion (TED) is dominated by the release and capture of interstitials by {311} defects. This is the case for annealing at medium or high temperatures ($T > 800^{\circ}\text{C}$) after nonamorphizing ion implantation.

The model is not suitable for investigating the initial stage of TED for low-temperature annealing ($< 800^{\circ}\text{C}$). For processes where the initial phase of TED is crucial, the Rafferty model is not the most accurate choice. Instead, consider using the procedure

Chapter 3: Guidelines for Additional Calibration

Accuracy and Limitations of Advanced Calibration of Sentaurus Process

AdvancedModels to benefit from complete modeling of small interstitial clusters, {311} defects, and dislocation loops.

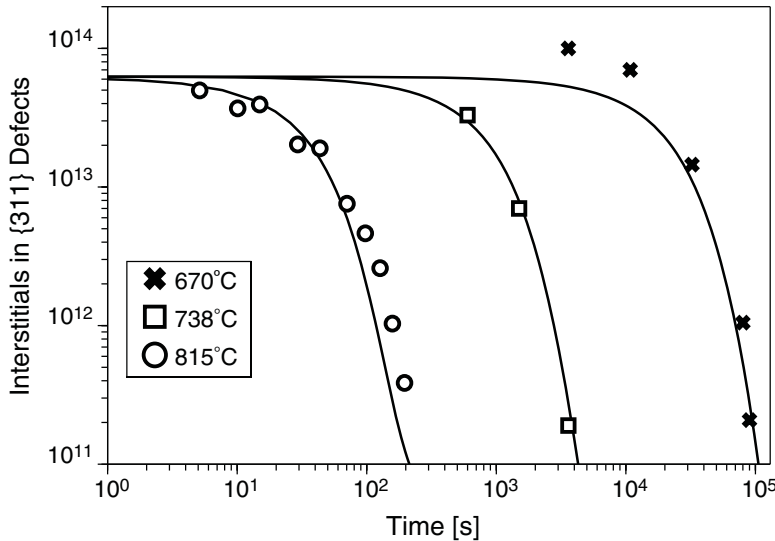
After amorphizing implantation, dislocation loops might form at the amorphous–crystalline interface. Loops are known to be much more stable interstitial clusters than {311} defects. As an effect, the rate of interstitial release is smaller. The formation and dissolution of dislocation loops is not included in the `Moment` model for TED. However, you can imitate the presence of dislocation loops by reducing the evaporation rate `Ikr` in the Rafferty model, after amorphizing implantations:

```
pdbSetDouble Silicon ICluster Ikr {[Arr value1 value2]}
```

With the default value of `Ikr` in `AdvCal_2022.03.fps`, the stability of the interstitial clusters is adjusted to the stability of {311} defects and is significantly lower than the expected stability of dislocation loops.

[Figure 20](#) shows the TEM data on the amount of interstitials in {311} clusters after a 40 keV, $5 \times 10^{13} \text{ cm}^{-2}$ silicon implantation and annealing at different temperatures. The experimental data (symbols) from the literature [9] is compared to the simulation results with `AdvCal_2022.03.fps` (solid lines).

Figure 20 TEM data points on the amount of interstitials in {311} clusters after 40 keV, $5 \times 10^{13} \text{ cm}^{-2}$ silicon implantation and annealing at different temperatures [9] compared to simulation results (lines)



If the `Full` cluster model is switched on for interstitial clusters by AdvancedModels, the initial conditions after implantation are specified by:

```
pdbSet Si I2 InitPercent 1.0
```

Chapter 3: Guidelines for Additional Calibration

Accuracy and Limitations of Advanced Calibration of Sentaurus Process

This means excess interstitials are placed into I₂ clusters at the beginning of post-implantation anneals. In most simulations, results are not sensitive to this particular choice of initial conditions. For very low (< 600°C) temperature anneals of B and P, or for thermal anneals that start with a very slow ramp from very low temperatures, the TED of B and P can be sensitive to these initial conditions. In such cases, you can adjust the diffusion tail from TED at very low temperatures, by initially placing interstitials into either more stable clusters or a combination of clusters. For example:

```
pdbSet Si I2 InitPercent 0.5  
pdbSet Si I3 InitPercent 0.5
```

Vacancy Clusters

In Advanced Calibration, vacancy clusters are not taken into account. This is justified for most processes, but not for the so-called defect-engineering [10], where vacancy-rich silicon regions are created near the surface by high-energy ion implantation, in order to form highly activated and steep boron profiles.

Boron Diffusion and Clustering

This section discusses boron diffusion and clustering

Diffusion and Pairing in Silicon

The diffusivity of boron has been measured by many groups, with similar but not fully identical results [1]. Omitting the most extreme published values, the spread between the lowest and highest diffusivities for B is approximately a factor of two for high temperatures (900°C–1100°C). You should not change the B diffusivity by more than 30% in your own calibrations. At temperatures less than 800°C, the B diffusivity is much less reliable. In AdvCal_2022.03.fps, boron diffuses only using B–I pairs, with the diffusion coefficient given by:

```
pdbSetDoubleArray Si B Int D { 0 {[Arr 0.123 3.566]}  
                                1 {[Arr 3.00 3.640]}  
                                2 {[Arr 1.01 3.98]} }
```

Here, the first component represents B–I pair diffusion using B–I⁰ pairs, the second line represents diffusion using B–I⁺ pairs, and the third line represents diffusion using B–I⁺⁺ pairs. The largest contribution comes from B–I⁺ pairs. A fine-tuning of B diffusivity can be performed as follows:

- To increase or decrease B diffusivity in general, all contributions to B diffusivity can be increased by the same factor. This factor should not be far from 1.0 in order not to contradict literature data.

Chapter 3: Guidelines for Additional Calibration

Accuracy and Limitations of Advanced Calibration of Sentaurus Process

- To increase B diffusivity at very low temperatures only, you can consider adding a term with a small Arrhenius energy to the diffusivity of B^-I^+ pairs. For example, replace `{[Arr 3.00 3.640]}` with `{[expr [Arr 3.00 3.640] + [Arr 1e-6 2.5]]}`. While it might be questionable, such an increase of B diffusivity at low temperatures can be useful in NMOS simulations to increase the B pileup towards the gate oxide during a low-temperature spacer deposition step and, thereby, to increase the reverse short-channel effect.
- To influence the shape of the B profile after thermal anneal, alter the relative contribution of the diffusivity using B^-I^0 , B^-I^+ , and B^-I^{++} pairs. For PMOS p-n junctions, increasing the contribution of B^-I^0 will decrease the steepness of the tail, while increasing the contribution of B^-I^{++} will lead to a more box-like shape, as shown in [Figure 21](#). For NMOS p-n junctions, where B is used as a pocket dopant, increasing the contribution of B^-I^0 will change the shape of the B profile near the p-n junction, as shown in [Figure 22](#). For B and P, these changes must be undertaken with care in order not to conflict with direct experimental data summarized in [\[1\]](#). At temperatures higher than 900°C, to preserve the agreement with literature investigation on B diffusivity, B^-I^+ should contribute at least 75% of the B diffusivity in intrinsic silicon. For other species such as In, you might consider more significant adjustments in the charge distribution of diffusing dopant–defect pairs.

Figure 21 Impact of B diffusivity on the shape of a boron USJ profile. Increasing the relative contribution of diffusion using B^-I^{++} pairs to the diffusivity of B, while reducing the relative contribution of B^-I^+ pairs, results in a more abrupt profile. Increasing the relative weight of diffusion using B^-I^0 pairs results in a less steep profile.

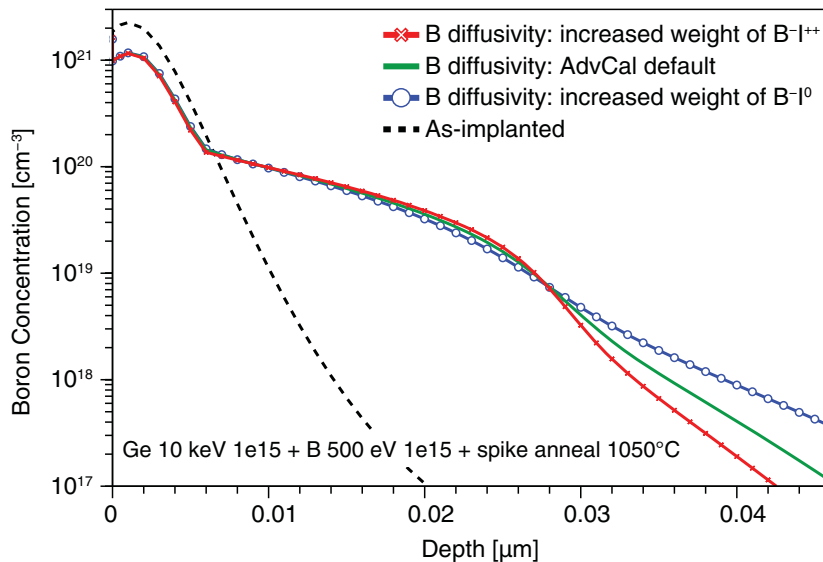
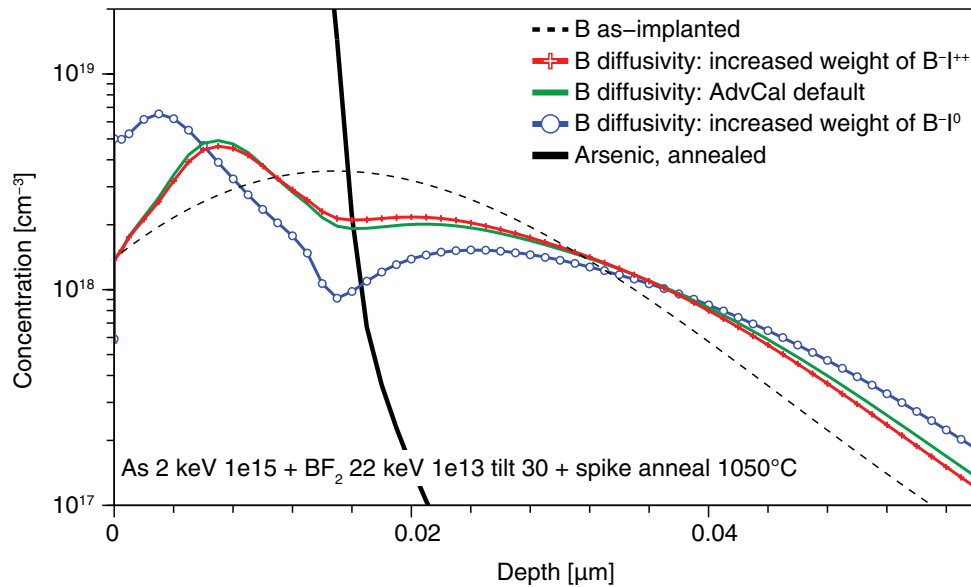


Figure 22 Impact of B diffusivity on the shape of a B pocket profile. Increasing the relative contribution of diffusion using B^-I^{++} pairs to the diffusivity of B, while reducing the relative contribution of B^-I^+ pairs, results in a flatter B profile at the B side of the p-n junction. Increasing the relative weight of diffusion using B^-I^0 pairs results in a pronounced minimum of the B concentration close to the p-n junction, due to the high electric field at the p-n junction.



A fine-tuning of the relative contributions of different dopant–defect charge states also can be considered as a means of calibration for all other dopants. The effect is similar to that illustrated in [Figure 21](#) and [Figure 22](#).

Boron diffusion during oxidation is enhanced because of interstitial injection at the oxidizing silicon surfaces. To fine-tune boron diffusion during oxidation, first consider adjusting the parameter `theta`, which scales the injection of interstitials at surfaces during oxidation.

Migration Distance (for ChargedReact Model)

The migration distance for B–I pairs has been extracted by Giles *et al.* [\[11\]](#). It is only relevant if the five-stream model is switched on by:

```
pdbSet Silicon Boron DiffModel ChargedReact
```

By default, the B diffusion model is `ChargedPair`. This is a simplified case of the `ChargedReact` model and allows significantly faster simulations due to better convergence of the equations and, therefore, larger time steps.

The migration distance `lambdaK` decreases with increasing temperature. For boron, at 600°C, it is 11 nm; at 1000°C, it is 1.4 nm. The `ChargedReact` model gives significantly different results from the `ChargedPair` model for the annealing of very steep B profiles at

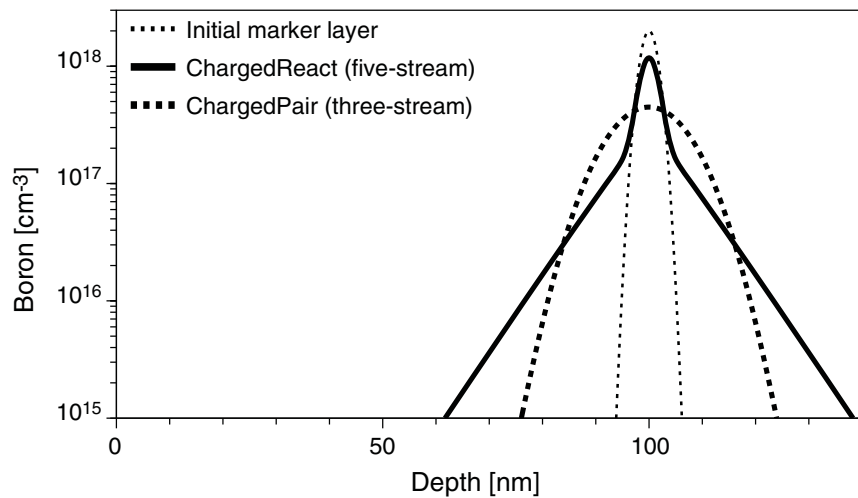
Chapter 3: Guidelines for Additional Calibration

Accuracy and Limitations of Advanced Calibration of Sentaurus Process

low temperatures. This is illustrated in [Figure 23](#) where a boron marker layer is annealed at 700°C.

[Figure 23](#) shows that the `ChargedPair` model gives a Gaussian shape to the profile and the `ChargedReact` model gives exponential-like tails, as observed in experiment. The slope of the exponential tail is a measure for the migration distance of B–I pairs at 700°C.

Figure 23 Boron marker layer at depth 100 nm, before and after Si implantation and anneal at 700°C



Furthermore, for spike annealing of shallow B implantations, there is sometimes a small difference in the diffusion tail, which is formed at the very beginning of the ramp-up, where the temperature is still low and the interstitial supersaturation is very high. For anneals and oxidations with a high thermal budget, it is well justified to use the faster `ChargedPair` model.

Effect of Fluorine

The presence of fluorine can affect the diffusion and activation of boron. It has been shown [\[12\]](#) that F does not form clusters with B at low concentrations and, therefore, does not reduce the diffusivity of B directly. Instead, fluorine–vacancy complexes, which are present in silicon after solid phase epitaxial regrowth (SPER), were found to be able to capture silicon self-interstitials. After capturing interstitials, F diffuses very fast towards the surface or deep into the silicon bulk. In addition, it was observed [\[12\]\[13\]](#) that F is redistributed towards the surface during SPER of amorphized regions, due to a strong segregation effect at the amorphous–crystalline interface. Furthermore, the speed of SPER is reduced by the presence of F, which might cause an increased dopant redistribution during the regrowth.

In Advanced Calibration, you have two options to simulate the influence of fluorine on boron diffusion. As the standard model of Advanced Calibration, the boron diffusivity is reduced in

Chapter 3: Guidelines for Additional Calibration

Accuracy and Limitations of Advanced Calibration of Sentaurus Process

regions with a high fluorine concentration. Fluorine is assumed to be immobile. The boron diffusivity is performed by the function:

```
term name=BoronDiffFactor add Si \
eqn="(5.4e20+0.01*Fluorine)/(5.4e20+Fluorine)"
```

For many cases, the above formula for an effective reduction of B diffusivity by F is useful. The formula has been calibrated by a comparison of SIMS data for boron diffusion after boron and BF₂ implantation. It often works well for the simulation of BF₂ annealing but, sometimes, the numbers used in the above formula need to be adjusted. The formula is not expected to be predictive for the simulation of ultrashallow junction formation after separate implantation of B and F atoms at different implantation energies.

To be more predictive in the case of fluorine coimplantation and also for BF₂ implantation, the physics-based but slower model can be used by calling the procedure:

```
AdvancedFluorineModel
```

This is called automatically if `AdvancedModels` is used, but it is also very useful in combination with the standard models of Advanced Calibration. For fine-tuning of the `AdvancedFluorineModel`, see [Fluorine Diffusion and Clustering on page 171](#).

The diffusivity of B in oxide is increased in the presence of F. This effect has also been calibrated for the simple model based on boron SIMS data measured after BF₂ implantation and annealing. As a result, the boron dose loss increases, as observed in the SIMS data.

Boron Clustering and Activation

As the default, the relatively simple `Transient` model is chosen for the clustering and electrical activation of boron. Four substitutional B atoms can form a B cluster. Only the substitutional B atoms will be assumed to be electrically active for the device simulation.

After ion implantation, only a limited concentration of B atoms is assumed to be substitutional. This concentration depends on the implantation dose in crystalline silicon and is 2.113×10^{20} in amorphized silicon. Values have been calibrated using annealed boron SIMS profiles and sheet resistance data. In amorphized Si, for fast ramp-up rates during solid phase epitaxial regrowth, slightly higher values are expected. Pawlak *et al.* [14] reported, for example, a value of 2.0×10^{20} for a ramp-up rate of 1 K/s and a value of 2.37×10^{20} for a ramp-up rate of 120 K/s.

For the solid solubility, a double Arrhenius function is used with a strong dependency of solubility on temperature at low temperatures and a smaller dependency at high temperatures. This temperature dependence has been calibrated against a large collection of SIMS and sheet resistance data, and it also reflects the data collected by Pichler [1].

Advanced Calibration defaults are:

```
pdbSet Si B Solubility {[ArrBreak 1.521e23 0.7102 1.50751e22
0.4566 1000]}
```

Chapter 3: Guidelines for Additional Calibration

Accuracy and Limitations of Advanced Calibration of Sentaurus Process

```
pdbSet Si B TotSolubility {[ArrBreak 4.563e23 0.7102 4.52253e22  
0.4566 1000]}
```

Here, you set the relation $\text{TotSolubility} = 3.0 \times \text{Solubility}$. It is recommended to keep this relation. When considering a change to `Solubility` and `TotSolubility`, you should change parameters carefully in such a way that boron solubility is steady at the `ArrBreak` break temperature.

In pure Si, the following parameters are recommended to be used to fine-tune B activation during thermal annealing, as explained in the following:

```
pdbSetDouble Si B TClusterForwardFac.Exp 3.088  
pdbSetDouble Si Int Int.In.B4.Cluster 1.152  
  
pdbSet Si B CluRate {[Arr 8.33e10 5.1635]}  
fproc mcdfactor_Boron { Energy Dose } { return 0.8 }  
pdbSet Si B AmInit 2.113e20
```

The rate of B_4 cluster formation is scaled by the term `BoronTClusterForwardFac`, which is defined as $(\text{Int}/\text{EqInt})^{\text{TClusterForwardFac.Exp}}$. This takes into account that B clusters form faster in regions of interstitial supersaturation ($\text{Int}/\text{EqInt} > 1$). If B deactivation is too fast in the presence of excess interstitials, then it is recommended to reduce `TClusterForwardFac.Exp` to a value smaller than 3.088. This might be necessary when modeling boron deactivation during low-temperature backend processes. In addition, as `EqInt` can become very small at low temperatures, you can consider replacing $(\text{Int}/\text{EqInt})$ with the expression $((\text{Int}+1e10)/(\text{EqInt}+1e10))$ or similar, and redefining the term `BoronTClusterForwardFac` by:

```
term Si name=BoronTClusterForwardFac store add \  
eqn= {((Int+1e10)/(EqInt+1e10))^[pdbGet Si B TClusterForwardFac.Exp]}
```

Adding $1e10$ to the nominator and denominator is a measure to avoid unrealistically high values of the ratio at very low temperatures.

Adding `ddt(B4*1.152)` to the equation solved for interstitials in silicon means that the formation of a B_4 cluster is accompanied by the consumption of 1.152 interstitials. Similarly, 1.152 interstitials are released when a B_4 cluster dissolves. Strictly speaking, it would be correct to talk about $B_4I_{1.152}$ clusters. The command `pdbUnsetString Si Int UserEquation` eliminates all previously defined changes to the interstitial equation. This command is included to ensure that the term `ddt(B4*1.152)` is not added twice when loading the Advanced Calibration file again. When changing this term after loading Advanced Calibration, you should also first erase the already defined term, before redefining it, for example with a value different from 1.152.

The factor `mcdfactor_Boron` scales the implantation damage created by Monte Carlo (MC) implantation of B. The implantation damage depends slightly on the wafer temperature during implantation and on the dose rate. Therefore, a small amount of fine-tuning might be justified. For B implantations in the dose range $2 \times 10^{15} \text{ cm}^{-2}$ to $5 \times 10^{15} \text{ cm}^{-2}$, that is, close to the amorphization threshold, the amorphization depth might be quite sensitive to

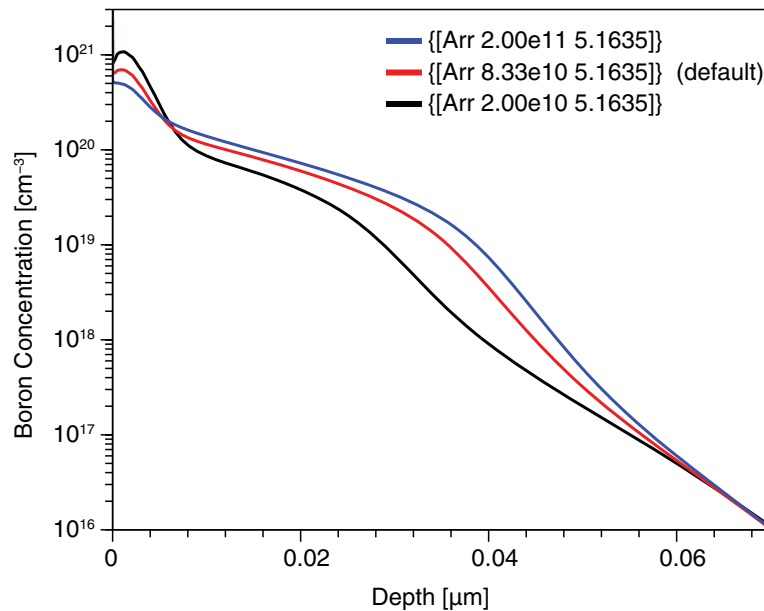
Chapter 3: Guidelines for Additional Calibration

Accuracy and Limitations of Advanced Calibration of Sentaurus Process

`mcdfactor`. For example, if transient-enhanced diffusion is overestimated after such a B implantation, consider increasing `mcdfactor`. This will increase the amorphization depth and, thereby, reduce the number of '+1'-interstitials created in the nonamorphized region.

Finally, the clustering rate `CluRate` has been calibrated to reproduce boron SIMS profiles and sheet resistance data for a wide range of conditions. Changing `CluRate` is a powerful way to fine-tune the junction depth and the sheet resistance. The effect of tuning the clustering rate is illustrated in [Figure 24](#).

Figure 24 Effect of boron clustering rate `CluRate` on final shape of a boron profile after 1 keV 10^{15} cm^{-2} boron implantation and spike annealing at 1050°C



In the following two scenarios, a reduction of `CluRate` was sometimes helpful:

- In PMOS device fabrication, when B or BF₂ implantation is followed by a temperature cycle of the following type: (1) spike anneal, (2) spacer deposition at low temperature (for example, 30 minutes at 600–800°C), and (3) spike anneal. Here, the release of B from boron clusters can be overestimated in the final spike anneal. Possibly, the low-temperature wafer processing leads to a stabilization of B clusters, which can be reflected by a strongly reduced value of `CluRate` in the TCAD model.
- If boron clusters are located in regions of high carbon concentration ($> 10^{20} \text{ cm}^{-3}$), then it might be necessary to reduce the clustering rate.

As shown in [Figure 24](#), `CluRate` mainly influences the high-concentration regions of the B profiles. The diffusion tail in the low-concentration regions can be adjusted by fine-tuning the amount of interstitials created by ion implantation.

Chapter 3: Guidelines for Additional Calibration

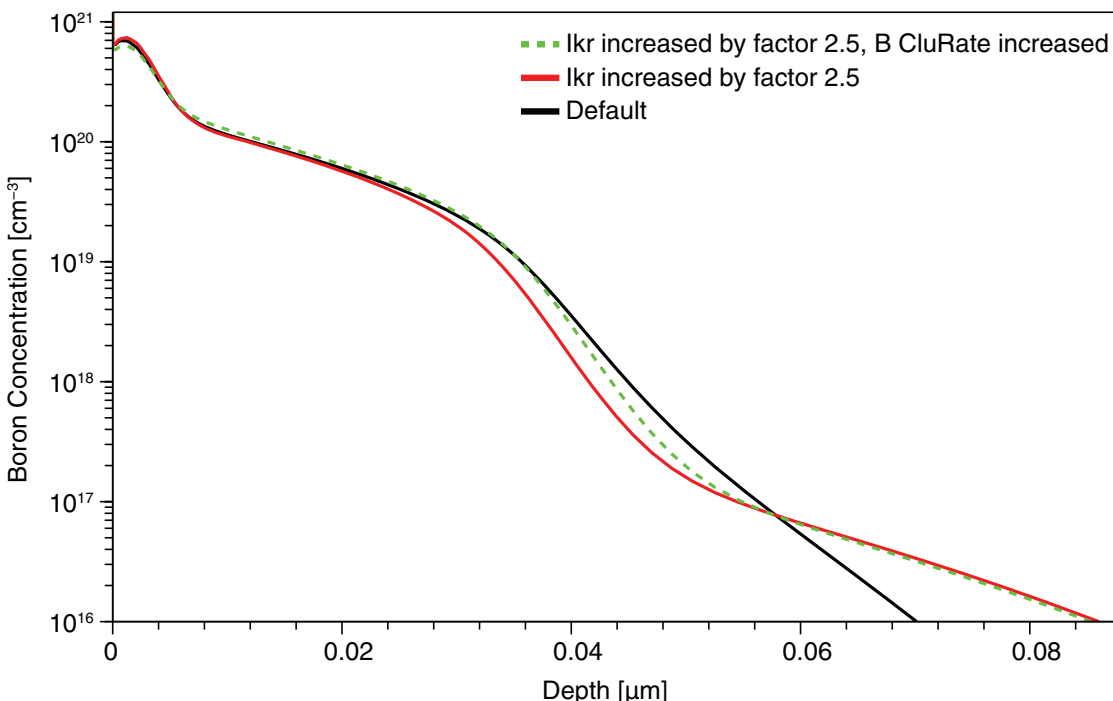
Accuracy and Limitations of Advanced Calibration of Sentaurus Process

The most convenient way to make such an adjustment is to redefine the procedure `ifactor_Boron` after sourcing the Advanced Calibration file. This is described in more detail in [Performing Additional Calibration on page 180](#).

The diffusion tail of a boron profile formed by a spike anneal can also be adjusted by varying the stability of interstitial clusters. The higher the dissolution rate I_{kr} for interstitial clusters, the earlier are the interstitials released during the ramp-up of the spike anneal. Consequently, interstitials from ion implantation are available for B diffusion at a lower temperature, where they are more effective for enhancement of B diffusion.

[Figure 25](#) illustrates the effect of increasing the interstitial dissolution rate. The diffusion in the tail region is widely driven by B atoms, which are substitutional at the beginning of the anneal. These diffuse more if I_{kr} is increased. Another effect of increasing I_{kr} is that most of the interstitials have already recombined before a substantial part of the B clusters that are near the surface are dissolved.

Figure 25 Effect of interstitial cluster dissolution rate I_{kr} on the final shape of a boron profile after 1 keV 10^{15} cm^{-2} B implantation and spike annealing at 1050°C



As a consequence, slightly less boron can diffuse out of the B clusters, as can be seen in the red line of [Figure 25](#). By changing the rate for interstitial cluster dissolution and B cluster dissolution (green line in [Figure 25](#)), you can modify the B tail almost independently from the highly doped region.

Chapter 3: Guidelines for Additional Calibration

Accuracy and Limitations of Advanced Calibration of Sentaurus Process

Preamorphization Implantation

If boron ultrashallow junctions are formed using a preamorphization implantation (Ge or Si), the accuracy can be reduced by an inaccurate calculation of the initial amount of interstitials in the structure. In this situation, you can consider adjusting the `ifactor` for Ge or Si implantation, for example, by defining a procedure `ifactor_Germanium`. Since Ge has a similar mass as arsenic, a high value for `ifactor` (2–10) can be justified, as illustrated for an amorphizing As implantation in [Figure 6 on page 84](#).

BIC Model

By executing the procedure `AdvancedModels` (see [Part 4: Comprehensive and Slow Models on page 94](#)), you can switch on the `ChargedCluster` BIC model for boron. Its disadvantage – six equations need to be solved instead of a single equation – is sometimes compensated by an increased accuracy of results.

With Advanced Calibration default parameters, all clustered boron in recrystallized regions is initially placed into B_2 clusters. Possibly, as BICs can be energetically more favorable than B clusters without interstitials bound inside, it can be beneficial to put some of the B into B_3I clusters after implantation. This will affect B activation kinetics and TED (by the release of interstitials during dissolution of BICs). For example:

```
pdbSetDouble Si B2 FractionAmor 0.8      ;# default 1.0  
pdbSetDouble Si B3I FractionAmor 0.2      ;# default 0.0
```

Boron Dose Loss

The parameters for the three-phase segregation model have been calibrated by Synopsys using SIMS data from B implantation and annealing experiments. In most situations, the dose loss of B into thermal oxide is accurately described. After BF_2 implantation, the dose loss of B is increased. This is taken into account by increasing the diffusivity of B in the oxide as a function of F concentration.

In device manufacturing, thermal oxide is not the only dielectric material used. In oxynitride, which is frequently used in gate dielectrics, the boron diffusivity is typically reduced, depending on nitrogen concentration. Deposited oxides can contain hydrogen atoms, which drastically increase the diffusivity of B in oxide. This might be important in devices with oxide spacers that are capped by a silicon-nitride layer, which can act as a barrier for hydrogen out-diffusion. Since B dose loss strongly depends on the type of oxide present, dose loss parameters such as `cMax` are often used for technology-specific fine-tuning. This also applies to other dopants.

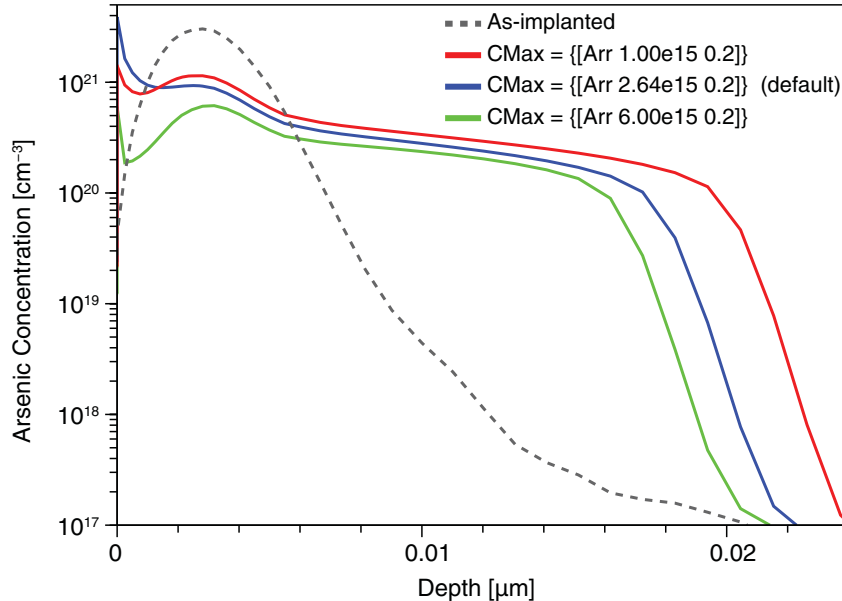
Arsenic Diffusion and Activation

The diffusion of arsenic in silicon is well calibrated for a wide range of process conditions, including the formation of ultrashallow junctions. Only a few accuracy problems are known to Synopsys:

- The model for arsenic diffusion and clustering is not very accurate for extremely high arsenic surface concentrations, which might occur after high-dose implantation with very low implantation energy (for example, $2 \times 10^{15} \text{ cm}^{-2}$ at an energy of 1 keV and less).
- In some situations, it is useful to perform additional fine-tuning of arsenic dose loss. In particular, the parameter C_{Max} , which specifies the concentration of arsenic atoms that can be built into the interface layer, can be considered for the fine-tuning of As ultrashallow junctions (see [Figure 26](#)).

For very shallow arsenic profiles, the steepness of the slope can be overestimated with the `ChargedPair` diffusion model. A flatter slope can be obtained with the `ChargedReact` model. Within the `ChargedReact` model, you can even adjust the steepness by tuning the arsenic–defect migration distance `lambda`.

Figure 26 Effect of C_{Max} on simulation result for arsenic USJ formation; graphs were calculated for 1.5 keV 10^{15} cm^{-2} As implantation, followed by a spike anneal at 1050°C (simulations performed with Advanced Calibration 2021.06)

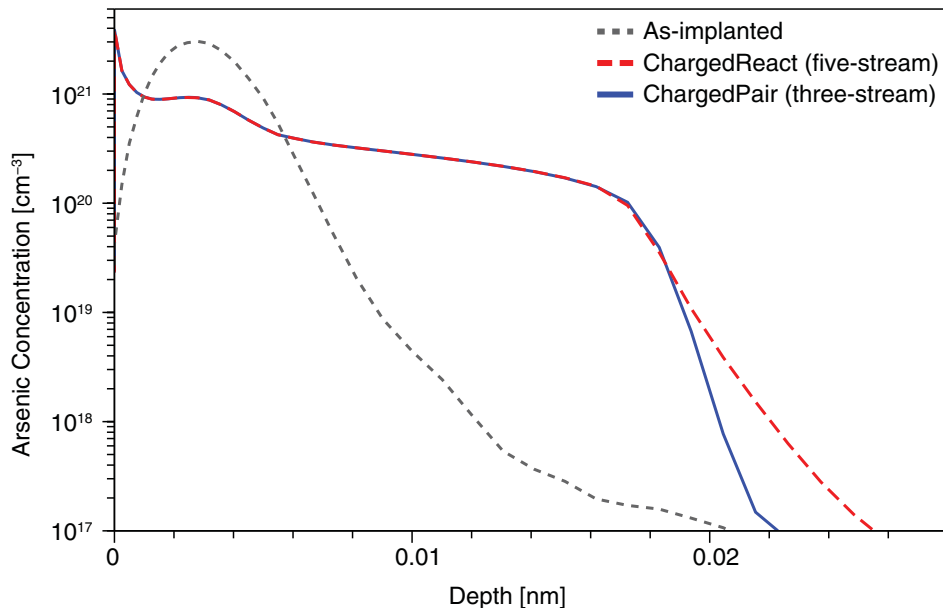


Chapter 3: Guidelines for Additional Calibration

Accuracy and Limitations of Advanced Calibration of Sentaurus Process

Figure 27 shows a comparison for an As ultrashallow junction, calculated with the ChargedPair model and the ChargedReact model with default parameters. Note that SIMS data tends to underestimate the slope of very steep profiles because, during the SIMS measurement itself, the profile is flattened due to the ‘knock-on’ effect.

Figure 27 Comparison of simulation results with ChargedPair and ChargedReact models for As USJ formation; graphs calculated for 1.5 keV 10^{15} cm^{-2} As implantation, followed by spike anneal at 1050°C (simulations performed with Advanced Calibration 2021.06)



Arsenic-Doped Epitaxy

In NMOS FinFETs, epitaxial growth of a thin source–drain extension layer with very high ($1.4 \times 10^{21} \text{ cm}^{-3}$) As doping has been proposed by Mochizuki *et al.* [15]. The calibration of As diffusion at such extremely high concentrations is not covered by AdvCal_2022.03.fps.

At such high concentrations, a large fraction of the As atoms is expected to be in electrically inactive clusters. For the process modeling of As-doped epi with very high As concentrations, two concepts might need to be considered.

First, similar to P clusters, it is possible that As clusters diffuse with a small diffusivity, leading to some broadening of the As distribution after epitaxy and subsequent anneals. The diffusion mechanism and the diffusivity for As clusters is unknown and needs to be adjusted to corresponding SIMS data. By default, As clusters are immobile.

Chapter 3: Guidelines for Additional Calibration

Accuracy and Limitations of Advanced Calibration of Sentaurus Process

The following statements demonstrate how you could add diffusion of As_3 clusters in Si to the models of Advanced Calibration. A term that describes diffusion of As_3 clusters is added to the equation, which is solved for As_3 clusters:

```
pdbSetDouble Si As As3_diff <value> ;# diffusivity
pdbSetString Si As3 EquationProc Mobile_As3
fproc Mobile_As3 { mat sol } {
    SubEqnTerm $mat $sol "[pdbGet $mat As As3_diff]*grad(As3)"
}
```

This simple example does not include Fermi-level or concentration dependence of As_3 diffusion. To include Fermi-level dependence, replace `grad(As3)` with "`Noni*grad(As3/Noni)`". Here, the term `Noni` is used and represents the ratio n/n_i , where n is the electron concentration and n_i is the intrinsic electron concentration. With this replacement in the example, As_3 would diffuse with a single negative charge and, therefore, As_3 diffusivity would effectively increase in regions of high electron concentration.

Second, to model P diffusion through a region of extremely high As concentration, a dedicated calibration of the impact of As on P might be needed (see [Co-diffusion of Arsenic and Phosphorus on page 158](#)). This can be done as follows:

1. Redefine the `PhosphorusIntDiffFactorDopant`, `PhosphorusVacDiffFactorDopant`, and `P3DiffFactor` factors. These factors are used in Advanced Calibration to modify the diffusion of P in regions of high As concentration. The calibration of these factors is based on data for As–P co-diffusion after implantation, where As concentration is typically smaller than $1.4 \times 10^{21} \text{ cm}^{-3}$.
2. Consider using mixed As_3P clusters. These are helpful if SIMS data indicates that the P concentration has a peak at the region of highest As concentration. The equations for the reaction $\text{As}_3 + \text{P} \rightleftharpoons \text{As}_3\text{P}$ are already defined in Advanced Calibration (see [As–P Clusters in Silicon on page 51](#)). A tuning of the parameters `As3P_k1` and `As3P_k2` might be needed.
3. Consider using As_6PI clusters, which form and dissolve by the reaction $2 \text{As}_3 + \text{PI} \rightleftharpoons \text{As}_6\text{PI}$. With such a reaction, mobile PI pairs can be trapped in As_6PI clusters in regions of very high As_3 cluster density. This can be useful for tuning the P tail diffusion through As-doped epilayers for different process conditions. As_6PI clusters are not predefined in Sentaurus Process or in `AdvCal_2022.03.fps`, so it requires some effort to use them. In section 2.6.2.3 of `AdvCal_2022.03.fps`, you can find the Alagator code for modeling P_7I clusters, which form and dissolve by a similar reaction $2 \text{P}_3 + \text{PI} \rightleftharpoons \text{P}_7\text{I}$. This code can be used as a reference for an Alagator implementation for As_6PI clusters.

In 2D or 3D simulations, epitaxy simulation can be time-consuming. It can be replaced by the simulation of a deposition and a thermal anneal, which has the same thermal budget as the epitaxy step. This is described in [Phosphorus-Doped Epitaxial Silicon on page 154](#).

Phosphorus Diffusion and Activation

The calibration of diffusion of phosphorus in silicon covers a wide range of process conditions, including USJ formation and phosphorus well anneals. Phosphorus has a higher solid solubility than arsenic.

For very high-dose and very low-energy ion implantation (for example, $5 \times 10^{15} \text{ cm}^{-2}$, 2 keV), where phosphorus concentrations close to 10^{22} cm^{-3} are reached, the Transient model with P₃ clusters underestimates the stability of P clusters. In simulations where the P peak concentration in Si exceeds 1e21, it is often helpful to include a second type of cluster in the model, by using the command `Use_P7I` (see [Phosphorus Clusters on page 49](#)).

Furthermore, if P implantation at low implantation energies is followed by low-temperature thermal annealing, then the so-called uphill diffusion of P toward the surface has been observed in experiments [16]. Uphill diffusion is not reproduced with the model for P in Advanced Calibration.

Phosphorus Diffusion in Silicon

In Advanced Calibration, at high donor concentrations, the diffusivities are modified by the `PhosphorusIntDiffFactor` and `PhosphorusVacDiffFactor` correction factors, as explained in [Arsenic–Phosphorus Co-Diffusion on page 52](#).

By default, the phosphorus diffusion model is `ChargedPair`. For FinFET or advanced CMOS technology (gate length < 65 nm), if phosphorus is used for source/drain, LDD, or pocket implantation, it is recommended to use the `ChargedReact` model. It can be switch on using:

```
pdbSet Si P DiffModel ChargedReact
```

In the `ChargedReact` model, to fine-tune the steepness of an almost perfectly exponential diffusion tail, typical for post-implantation TED at low temperatures, you can consider adjusting the parameters `lambdaK`, which govern the average distance between the formation and dissolution of P–I and P–V pairs. The default values are:

```
pdbSet Si P Int lambdaK {[Arr 1.1e-8 -0.40]}\n pdbSet Si P Vac lambdaK {[Arr 5.0e-9 -0.33]}
```

Phosphorus diffusion during oxidation is enhanced because of interstitial injection at the oxidizing silicon surfaces. To fine-tune phosphorus diffusion during oxidation, first consider adjusting the parameter `theta`, which scales the injection of interstitials at surfaces during oxidation.

Phosphorus Activation in Silicon

In Advanced Calibration, activation and deactivation of P are modeled by the Transient model, in which the only P clusters formed are P₃. By default, in the Transient model,

Chapter 3: Guidelines for Additional Calibration

Accuracy and Limitations of Advanced Calibration of Sentaurus Process

interstitial supersaturation has no affect on the formation and dissolution of P₃ clusters. In real silicon, a high supersaturation of Si self-interstitials can influence the rate of P cluster formation.

To fine-tune P clustering in post-implantation anneals with low thermal budget and high interstitial supersaturation, the Transient model for P can be tuned in a similar way as for B, by modifying forward (or backward) reaction rates with terms. For example, the P cluster formation rate will increase because of interstitial supersaturation, when defining:

```
term Si name=PhosphorusTClusterForwardFac store add \
eqn= "((Int+1e10)/(EqInt+1e10))^0.2"
```

Here, Int is the interstitial concentration, EqInt is the equilibrium concentration of interstitials, and 1e10 (or a similar number) is used to avoid too extreme values at very low temperatures, where EqInt is very small.

Phosphorus Dose Loss at Oxide–Silicon Interfaces

As in the case of arsenic, a useful parameter for the fine-tuning of P segregation is CMax.

Phosphorus-Doped Epitaxial Silicon

For advanced NMOS devices, contact area formation frequently includes epitaxial growth of silicon films, which are highly doped with phosphorus.

The epitaxy itself can be modeled by a diffuse command with the keyword Epi. By default, a moving-boundary algorithm is used. In three dimensions, this might not be fast and stable enough. You can replace it with a sequence of alternating doped deposition and inert annealing steps, by using either epi.model=1 or an explicit sequence of deposit and diffuse commands.

During epitaxy, you have a bare gas–Si interface. The vacancy surface recombination velocity at gas–Si interfaces affects the vacancy supply at the gas–Si interface and, therefore, the amount of P diffusion during epitaxy.

Since Version S-2021.06, fast vacancy recombination at such interfaces is used. In contrast, in previous versions of Advanced Calibration, a very slow vacancy recombination at gas–Si interfaces was assumed. Because of new vacancy surface boundary conditions, the amount of P diffusion during epitaxial growth of P-doped films is different between Advanced Calibration Version S-2021.06 and older versions. Other parameters that affect P diffusion during epitaxy, such as the diffusivity of P by using P–I pairs or P₃–V complexes, or clustering of P, were not changed from Advanced Calibration Version R-2020.09 to Advanced Calibration Version S-2021.06.

The impact of updated vacancy boundary conditions on P diffusion during epitaxy has been analyzed. In general, the increased vacancy recombination at gas–Si interfaces is an improvement (see [Surface Boundary Conditions on page 138](#)). For P-doped epi, however,

Chapter 3: Guidelines for Additional Calibration

Accuracy and Limitations of Advanced Calibration of Sentaurus Process

for some of the recipes investigated, including P data published by Li *et al.* [17], the tail diffusion of P during the growth of the epitaxial film is overestimated in simulations with Advanced Calibration Version T-2022.03, due to the update of vacancy boundary conditions at gas–Si interfaces.

Synopsys recommends an adjustment of the diffusivity of P_3 –V pairs for the fine-tuning of P diffusion during epitaxy. For example, consider changing the diffusivity of P through P_3 –V pairs from its Advanced Calibration default value of:

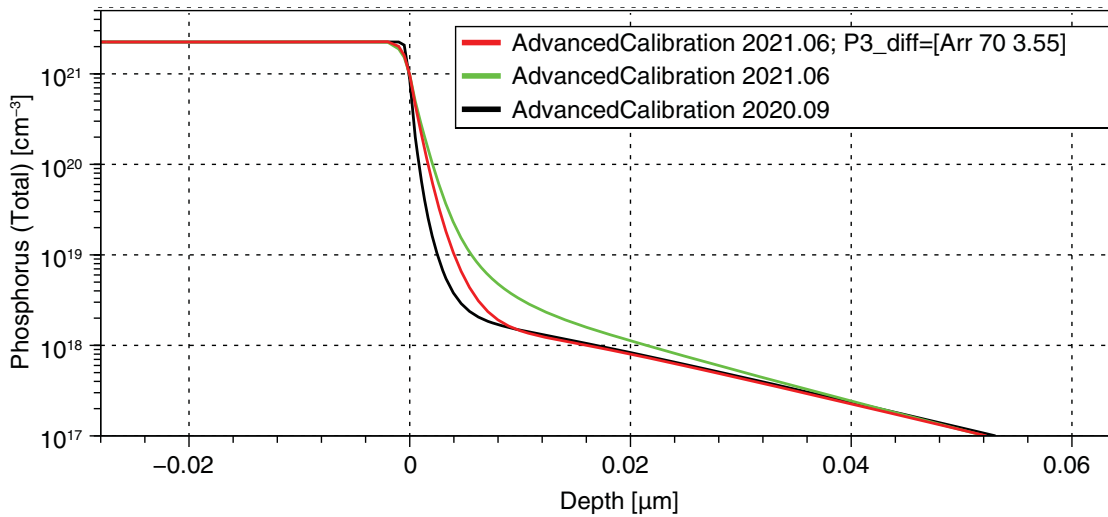
```
pdbSetDouble Si P P3_diff {[Arr 0.066 2.8]}
```

to:

```
pdbSetDouble Si P P3_diff {[Arr 70 3.55]}
```

This combined change of the Arrhenius prefactor and the Arrhenius energy would reduce the corresponding diffusivity at 700°C (typical temperature for Si epitaxy) to approximately 14% of the original value, while preserving the diffusivity at 976°C (a typical spike anneal temperature). [Figure 28](#) shows the impact of this change on P diffusion during epitaxy.

Figure 28 Simulated P profiles after growth of a P-doped epitaxial film, mimicked by deposition and subsequent anneal. Film thickness: 28 nm and total P concentration in the film: $2.25 \times 10^{21} \text{ cm}^{-3}$. Thermal budget of the epitaxy: 10 minutes at 700°C. The TCAD results with Advanced Calibration 2020.09 and 2021.06 differ because of the higher vacancy surface recombination rate at gas–Si interfaces in Version S-2021.06. The tail diffusion during epitaxy can be adjusted by fine-tuning the diffusivity of P_3 clusters by using P_3 –V pairs at low temperatures. In these simulations, the ChargedReact model was used for phosphorus diffusion, and stress effects were switched on by SiGe_and_Stress_Effect 0 1 1 0.



Chapter 3: Guidelines for Additional Calibration

Accuracy and Limitations of Advanced Calibration of Sentaurus Process

After epitaxy is completed and before subsequent thermal anneals, it is recommended to deposit a thin native oxide onto bare Si surfaces. This is needed to model dopant dose loss from Si into oxide–Si interface layers with the `ThreePhaseSegregation` model. At bare gas–Si interfaces, this model cannot be used.

Choice of Models

Often, the P concentration in epitaxially grown Si is very high ($> 10^{21} \text{ cm}^{-3}$). In this case, to model P diffusion and activation as well as strain relaxation, it is recommended to use the model for P_7I clusters (see [Phosphorus Clusters on page 49](#)). The following choices of Advanced Calibration are recommended for P-doped epitaxial silicon:

```
SiGe_and_Stress_Effect 0 1 1 0      ;# or 1 1 1 0 in presence of SiGe
pdbSet Si P DiffModel ChargedReact
Use_P7I
```

P and P_3 clusters cause tensile strain. The formation of P_7I clusters by the reaction $\text{P}_3 + \text{P}_3 + \text{PI} \rightarrow \text{P}_7\text{I}$ comes along with strain relaxation. PI pairs are trapped in this reaction. The trapping of PI pairs reduces the P tail diffusion. If the epitaxial film includes interstitial clusters (either by imperfect epitaxial growth or after an implantation), then some of the interstitials released from these clusters will be captured by this formation of P_7I clusters. For processes in which epitaxial films are grown with many defects and small tensile strain, you can consider performing the process simulation without the P_7I model and with reduced strain (reduced value of `Conc.Strain`) from P and P_3 clusters.

Phosphorus Dose Loss After Epitaxy

In processes that do not include implantation after epitaxial growth of a P-doped film, the dose loss of P into native oxide is typically less than in processes with implantation. Probably, a part of the usual P dose loss only occurs in the presence of some implantation damage at the oxide–Si interface. According to Synopsys' tests, this is especially true for the initial dose loss, governed by the parameter `CMax`. In contrast, the concentration of P that can be trapped in P_2 pairs formed at the interface does not show a strong sensitivity to implantation damage. In processes without implantation into P-doped epi, it is recommended to reduce `CMax` drastically. For example:

```
pdbSet Ox_Si P CMax {[Arr 2e+15 0.50]} ;# Default is {[4.6e+16 0.5]}
```

By redefining the term `PhosphorusCMaxFactor`, it is possible reduce phosphorus dose loss only in device regions that are free of implantation damage.

Initial Conditions and Phosphorus Tail Diffusion

The calibration of the P_7I model in Advanced Calibration is partially based on experimental data (SIMS, sheet resistance, and strain measurements) for highly strained phosphorus-doped epitaxial films from Applied Materials [17]. These have been measured on planar samples with very good quality (high tensile strain after epitaxy; no grown-in defects; epi-temperature close to 700°C).

Chapter 3: Guidelines for Additional Calibration

Accuracy and Limitations of Advanced Calibration of Sentaurus Process

The default initial conditions after epitaxy are:

- The epitaxially grown layer is free of defects.
- P is initially active up to a concentration of 2e20 (value of `Si P EpiInit`).
- All excess P is put into P_3 clusters.
- No P is initially put into P_7I clusters.

Apparently, this quality is not always obtained in epitaxy for highly doped P. Comparing data from various sources has revealed some variability in the P tail diffusion for very similar nominal process conditions. Data from some sources showed more P tail diffusion than the data reported in [17]. Possibly, this was driven by grown-in defects from which silicon self-interstitials were released during annealing. More imperfections should be expected when the P concentration and corresponding tensile strain are very high.

To model grown-in defects in epilayers, add interstitial clusters (`ICluster`). By default, such clusters have the properties of {311} defects, but in P-doped epi, they might differ in nature, and the dissolution rate of {311} defects might not be applicable. To adjust the fraction of defects that dissolves already during epitaxy, change the dissolution rate during epitaxy (`pdbSet Si ICluster Ikr <value>`).

It is also possible to put a fraction of P into P_7I clusters, as the initial condition. In the model, P_7I clusters cannot capture PI pairs. In addition, they compensate the tensile strain generated by P and P_3 . This option might be advisable if, otherwise, the tensile strain is too high compared to measurement at the end of the process simulation. (The final strain is passed on to the device simulation where it affects, for example, electron mobility. If necessary, the strain in P-doped epilayers can also be reduced directly by reducing the values of `Conc.Strain` for strain induced by P, P_3 , and P_7I .)

For special recommendations when P-doped epi is grown on regions with high As doping, see [Arsenic-Doped Epitaxy on page 151](#) and [Co-diffusion of Arsenic and Phosphorus on page 158](#).

Some recipes include a P implantation into a P-doped epitaxial film to achieve even higher surface concentrations of P. For very shallow P implantations, a large fraction of excess interstitials created by implantation will be captured by the reaction $P + I \Rightarrow PI$, followed by $PI + P_3 + P_3 \Rightarrow P_7I$. Only the remaining excess interstitials contribute to the diffusion tail of P. Currently, there is insufficient experimental data to test the model predictions for all possible recipes combining epitaxy, implantation, and post-epi anneals. In the few cases investigated, scaling the number of excess interstitials by increasing `ifactor` (for example, from 1.0 to 3.0) allowed a successful tuning of the P tail diffusion in thermal anneals after epitaxy and implantation.

Finally, to adjust the steepness of the P diffusion tail, consider adjusting the PI pair migration distance, specified by `pdbSet Si P Int lambdaK <value>`.

Co-diffusion of Arsenic and Phosphorus

The physics of the co-diffusion of As and P in high concentration in silicon is very complex for several reasons:

- The concentration of point defects is affected by the diffusion of As–I, As–V, P–I, and P–V pairs.
- The recombination of point defects in the presence of As and P is not precisely known.
- Arsenic and phosphorus can form mixed clusters.
- The Fermi-level dependence of P diffusivity has a large influence, but it is not known with high precision from the literature.
- Arsenic diffusivity sharply increases at concentrations of n-type dopants (As or P) higher than $2 \times 10^{20} \text{ cm}^{-3}$. Possible reasons for the increased As diffusion are:
 - (a) Diffusion is through small mobile clusters.
 - (b) Percolation-type diffusion of As–V pairs, where vacancies can hop from one donor atom to neighboring donor atoms.

The Synopsys calibration of the co-diffusion of As and P is considered a good starting point for technology calibration, but it is not predictive for all possible process conditions.

Depending on the process window of interest, different methods of parameter fine-tuning will result in a good overall agreement.

The following approaches have been identified by Synopsys to be suitable for such fine-tuning. They are listed in order of importance:

- Modify the number of As or P trapping sites at the Si–SiO₂ interface (`CMax`). This will increase or decrease the dose loss.
- Modify the impact of As on P trapping sites at the Si–SiO₂ interface (`PhosphorusCMaxFactor` and `P2trapMaxFactor`). This will change the dose loss of P in the presence of As.
- Modify the `PhosphorusVacDiffFactorDopant` and `PhosphorusIntDiffFactorDopant` terms.
- Modify the number of interstitials created by ion implantation (by changing `ifactor` or `dfactor` for P or As implantation).
- Switch on the `ChargedReact` model for phosphorus. When the `ChargedReact` model is switched on for P, the migration distance of P–I pairs (`pdbSet Si P Int lambdaK`) can be fine-tuned to adjust the steepness of the tail of the P profile outside the region with high As doping.

Chapter 3: Guidelines for Additional Calibration

Accuracy and Limitations of Advanced Calibration of Sentaurus Process

- Modify the ArsenicVacDiffFactorDopant and ArsenicTClusterBackwardFac terms.
- Create a term PhosphorusTClusterBackwardFac to enforce an influence of As on P cluster dissolution. For example:

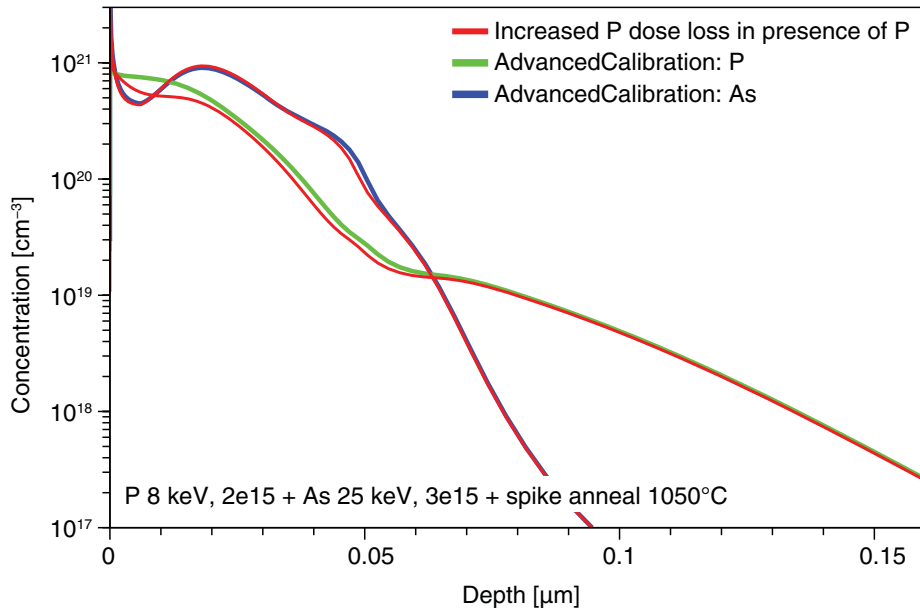
```
term Si name=PhosphorusTClusterBackwardFac store add \
eqn= "2.e19/(2e19+AsActive)"
```

The impact of these parameters is illustrated in [Figure 29](#) to [Figure 34 on page 162](#). All of these have been calculated for the following process recipe for As–P co-diffusion:

- P implantation: Dose $2 \times 10^{15} \text{ cm}^{-2}$, energy 8 keV
- As implantation: Dose $3 \times 10^{15} \text{ cm}^{-2}$, energy 25 keV
- Spike RTA with peak temperature 1050°C

In each figure, the straightforward simulation result, obtained with `AdvCal_2021.06.fps`, is compared to the result of a simulation in which one parameter for arsenic or phosphorus has been changed from the default.

Figure 29 As–P co-diffusion: Red lines show impact of increasing the dose loss of P in the presence of As. In this example, for the red curve, the `PhosphorusCMaxFactor` term changed to $(1.8e14/(1.8e14+Arsenic))$, and the `P2trapMaxFactor` term changed to $(2.5e14/(2.5e14+Arsenic))$. The dose loss of P at the Si–SiO₂ interface is reduced, but the impact on the profile tails is relatively small.



Chapter 3: Guidelines for Additional Calibration

Accuracy and Limitations of Advanced Calibration of Sentaurus Process

Figure 30 As–P co-diffusion: Red lines show impact of changing the term `PhosphorusIntDiffFactor` as a function of As concentration. For this plot, the factor `PhosphorusIntDiffFactorDopant` was reduced from “[Arr 2.2e25 1.5]+[Arr 4.2e31 3.0])/([Arr 2.2e25 1.5]+[Arr 4.2e31 3.0]+AsAs3)” (Advanced Calibration default) to “[Arr 2.2e25 1.5]+[Arr 4.2e31 3.0])/([Arr 2.2e25 1.5]+[Arr 4.2e31 3.0]+3.0*AsAs3)”. As a consequence, the diffusion tail for P shifts towards a lower concentration, while the As profile and the surface-near region of the P profile have hardly changed.

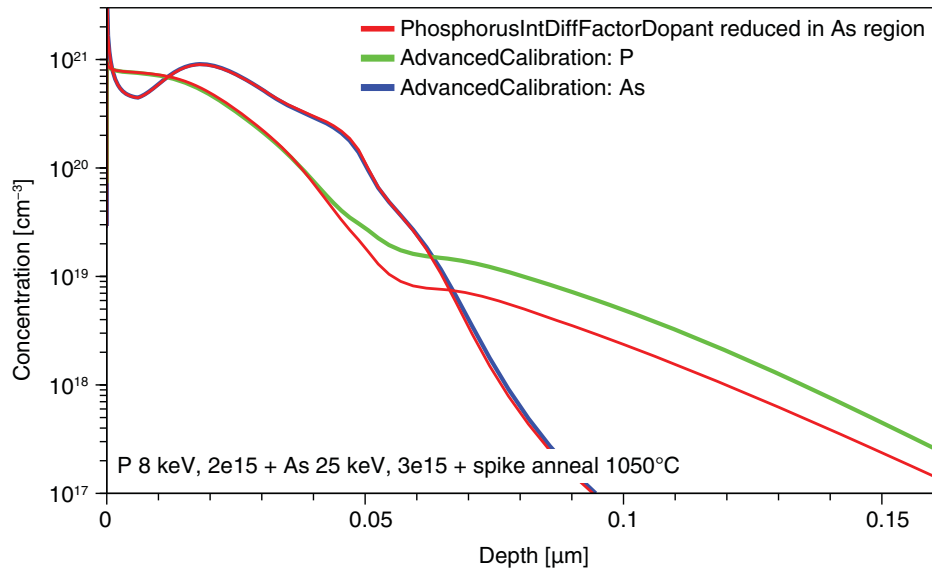
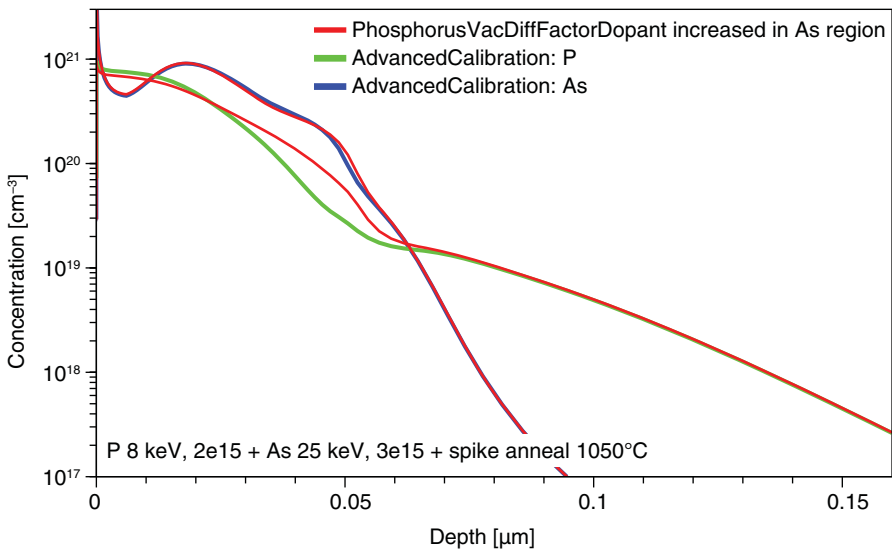


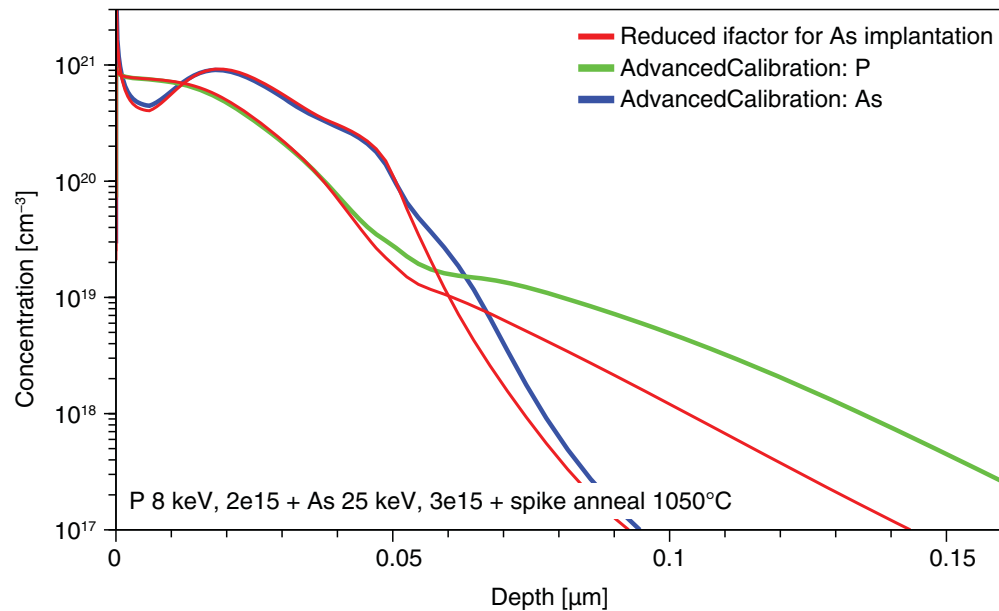
Figure 31 As–P co-diffusion: Red lines show impact of changing the term `PhosphorusVacDiffFactor` as a function of As concentration. For this plot, the factor `PhosphorusVacDiffFactorDopant` increased from “[Arr 2.7e22 0.5]/([Arr 2.7e22 0.5]+AsAs3)” to “1.0”. There is more P diffusion, but not in the P tail, which is dominated by P–I pair diffusion.



Chapter 3: Guidelines for Additional Calibration

Accuracy and Limitations of Advanced Calibration of Sentaurus Process

Figure 32 As–P co-diffusion: Red lines show impact of decreasing the number of interstitials created by As implantation. The ifactor for As implantation was reduced from 8.7 (Advanced Calibration default for this condition) to 3.0. Phosphorus diffusion is reduced (in particular in the tail region).



Chapter 3: Guidelines for Additional Calibration

Accuracy and Limitations of Advanced Calibration of Sentaurus Process

Figure 33 As–P co-diffusion: Magenta line shows impact of using the ChargedPair diffusion model for P instead of the ChargedReact model. With the ChargedReact model, the tail of the P profiles can be made flatter by increasing the migration distance of P–I pairs. In the red line, the corresponding parameter lambda has been increased by a factor of 2. (Using the ChargedReact model has a larger impact on thermal anneals at lower temperature.)

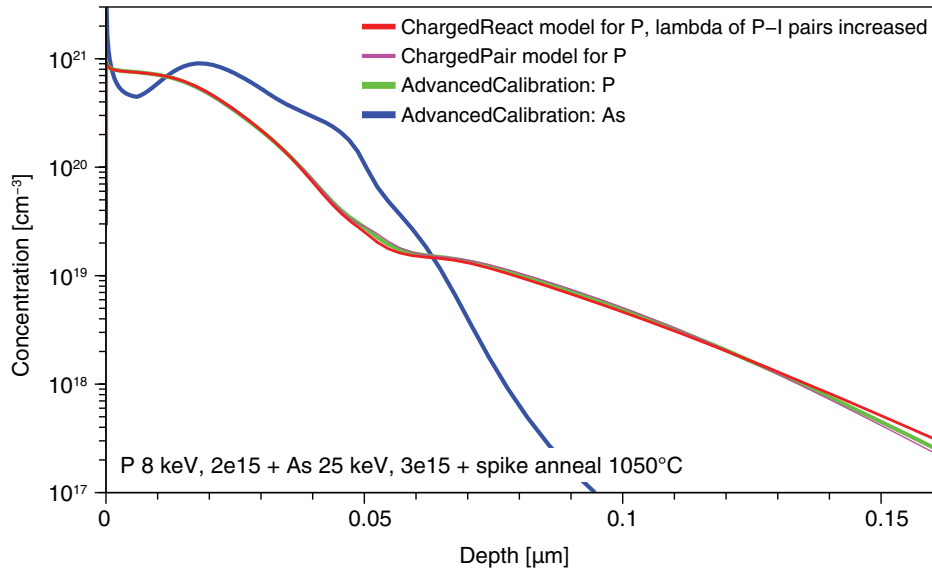
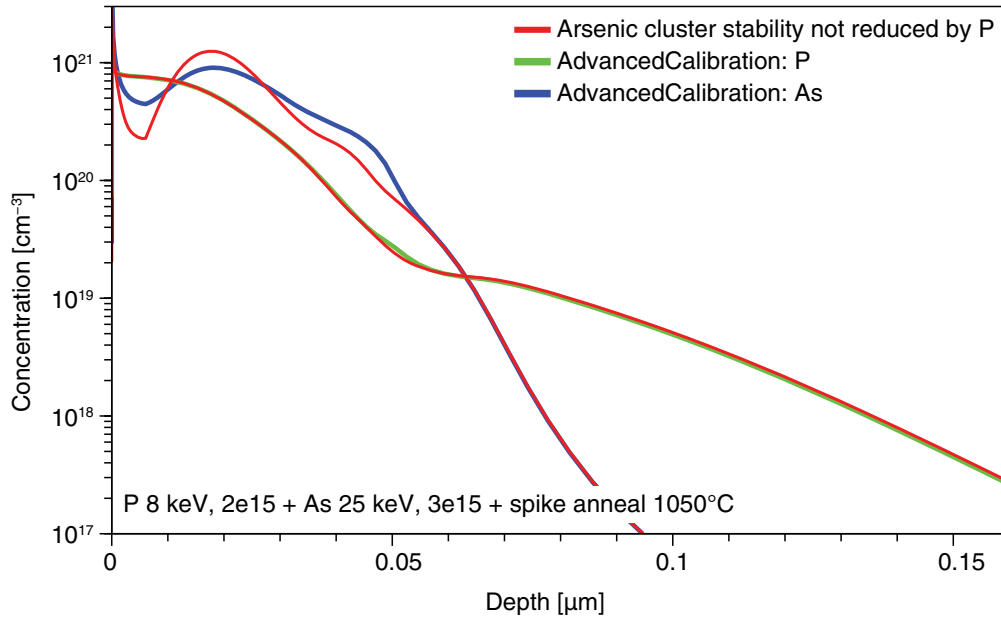


Figure 34 As–P co-diffusion: Red lines show impact of reducing the term ArsenicTClusterBackwardFac from “1.0+PActive/1e20” to “1.0”. Arsenic clusters become more stable in the region with high P co-doping.



Indium Diffusion and Activation

This section discusses indium diffusion and activation.

Nonamorphizing Condition

The calibration of indium diffusion in silicon and dose loss is very accurate for nonamorphizing conditions and usually does not require additional fine-tuning.

Amorphizing Ion Implantation

If amorphous layers are created by ion implantation, the behavior of indium is more complicated and cannot be modeled correctly with the chosen set of models in the Advanced Calibration. Several things might happen:

- Indium is swept out of silicon during solid phase epitaxial regrowth (SPER) of the amorphous layer [18].
- Indium might segregate to end-of-range defects [19].
- If a high concentration of indium is left in silicon after SPER, clusters might form due to the low solid solubility of indium.

The first effect is responsible for a pronounced increase of indium dose loss with increasing indium dose [20] for NMOS channel doping, when the indium dose is above the amorphization threshold. The procedure `AdvancedSPERModel` can be called to switch on a physics-based description of this effect (see [Solid Phase Epitaxial Regrowth on page 101](#)). An alternative, simple possibility for mimicking the sweep-out effect is to cut the indium concentration manually in amorphous regions, immediately after the ion implantation, using the `select` command of Sentaurus Process.

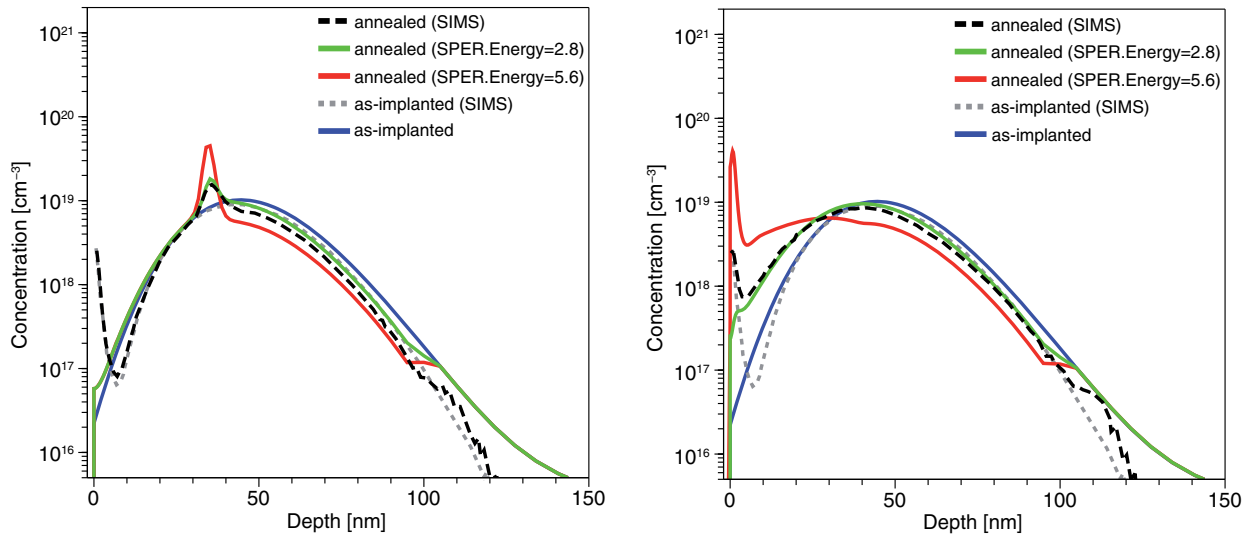
SPER Model Usage

The SPER phase field model can be used to simulate indium redistribution in the amorphized silicon region. In the procedure `AdvancedSPERModel`, a general calibration is provided for the doping or impurity redistribution, but additional calibration might be required in certain cases. For solutions to be redistributed during SPER, the diffusivity in a-Si (D_{Amor}) and the segregation energy ($\text{SPER}.\text{Energy}$) must be defined. Nonzero diffusivities allow for diffusion in a-Si, while nonzero segregation energies allow for the snow plow effect by a semipermeable a/c interface. [Figure 35](#) shows the sensitivities of these parameters.

Chapter 3: Guidelines for Additional Calibration

Accuracy and Limitations of Advanced Calibration of Sentaurus Process

Figure 35 Simulation of (left) incomplete and (right) complete recrystallization with indium redistribution during SPER for PAI + In 90 keV $4e^{13} \text{ cm}^{-2}$ implantation and anneal at 600°C. The influence of SPER.Energy on the indium redistribution is shown for the calibrated value (green) and the doubled value (red). A similar influence has DAmor giving almost the same simulation results for the calibrated and the doubled value (not shown here).



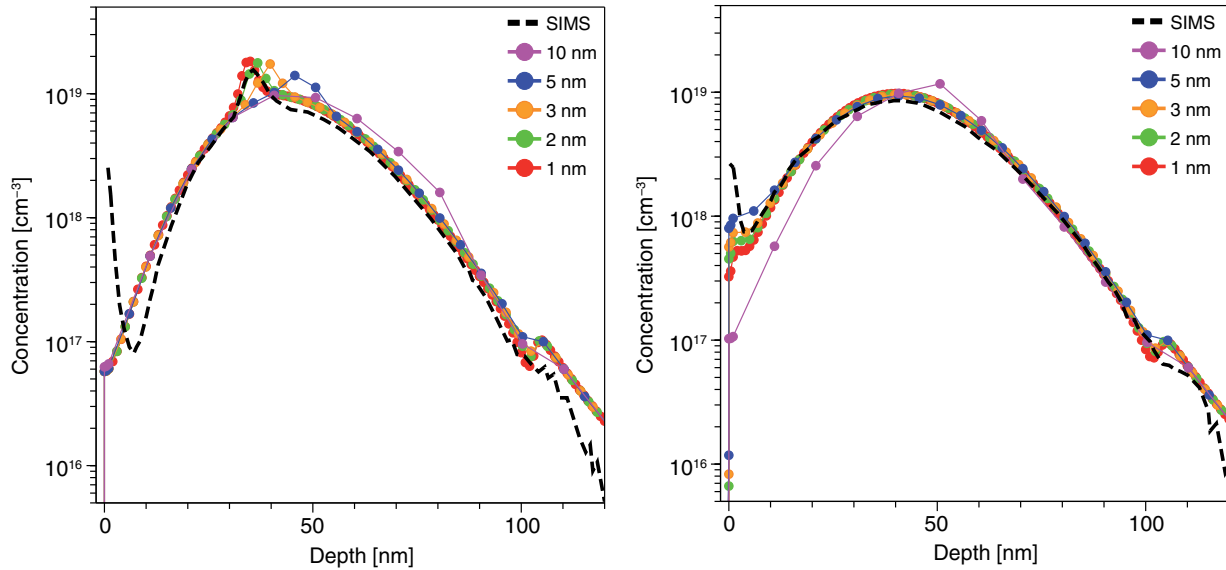
As stated in [Solid Phase Epitaxial Regrowth on page 101](#), a decent fine mesh (1–2 nm spacing) in the amorphized region is required by the phase field model to be robust and accurate in one and two dimensions.

The mesh spacing in amorphized regions should not exceed the phase transition width of 3 nm to allow for accurate and stable simulation results. [Figure 36](#) shows the mesh spacing sensitivity.

Chapter 3: Guidelines for Additional Calibration

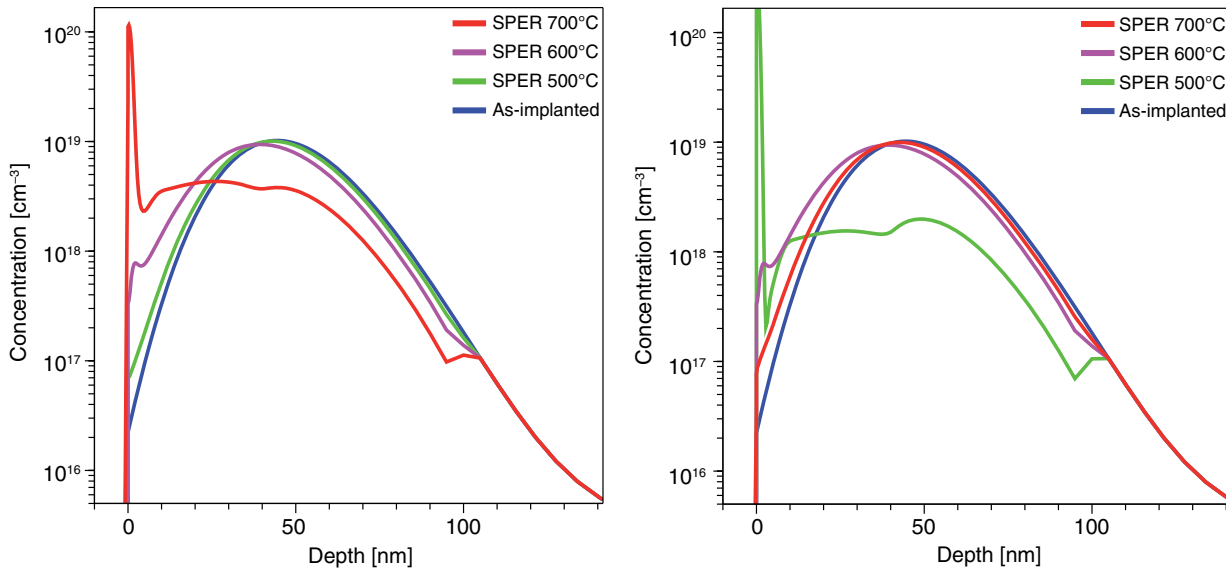
Accuracy and Limitations of Advanced Calibration of Sentaurus Process

Figure 36 The influence of the mesh spacing on the indium redistribution is shown for the simulation of (left) incomplete and (right) complete recrystallization with indium redistribution during SPER for PAI + In 90 keV $4e13 \text{ cm}^{-2}$ implantation and anneal at 600°C. For incomplete SPER after 60 s (left), the recrystallization speed is approximately the same for spacing < 3 nm, while it slows down significantly for coarser meshes. The total indium redistribution after complete SPER after 120 s (right) is comparable to spacing <= 3 nm. Note that the SPER for 10 nm is not completed after 120 s, while it is completed for spacing < 10 nm.



Depending on the activation energy of the diffusivity in a-Si, the doping redistribution during SPER has a specific temperature dependency. If the activation energy of the diffusivity in a-Si is similar to the SPER one (2.68 eV), the redistributed dopant shows little temperature dependency. However, if the activation energy of the diffusivity in a-Si is different from the SPER one, the dopant redistribution is temperature dependent (see [Figure 37](#) on page 166). Therefore, you must take care about the correct anneal temperature profile during ramp-up, even at low temperatures, to ensure accurate simulation.

Figure 37 The influence of the anneal temperature and a-Si diffusivity on the indium redistribution is shown for the simulation of complete recrystallization with indium redistribution during SPER for PAI + In 90 keV $4e^{13} \text{ cm}^{-2}$ implantation and anneal. If the activation energy of the diffusivity in a-Si is higher (for example, 3.3 eV) than the SPER one (2.68 eV), more In is redistributed for higher temperatures (left). If the activation energy of the diffusivity in a-Si is lower (for example, 2.2 eV) than the SPER one (2.68 eV), more In is redistributed for lower temperatures (right).



Antimony Diffusion and Activation

Antimony diffuses only with vacancies and, therefore, does not show transient enhanced diffusion with excess interstitials created by ion implantation. In addition, the diffusivity of Sb in silicon is low. The calibration of Sb diffusion and activation in silicon is based on the literature [1] and Sb data for ion implantation and subsequent annealing, with implantation energies of 50 keV and higher, and annealing temperatures ranging from 700°C to 1100°C. For these conditions, the calibration is very reliable.

Antimony ultrashallow junction (USJ) formation in silicon has not been taken into account yet in the Advanced Calibration.

If you are interested in Sb USJ formation, then an additional calibration of the Sb parameters is required. In particular, it will probably be necessary to define more sophisticated initial conditions for point defects and Sb activation after low-energy ion implantation, using the procedure `ifactor_Antimony`, and the parameters `AcInit` and `AmInit`.

Carbon

This section discusses various aspects of carbon.

Carbon–Interstitial Clusters

The NeutralCluster model has been used for C–I clusters in silicon to reproduce experimental data for USJ formation based on Ge+C+B or C+P *cocktail implantations* and subsequent spike anneals [21]. The model has not been calibrated yet for other process conditions where C implantation can be used, such as low-temperature annealing or As+C coimplantations.

The main effect of the C coimplantation in silicon is a reduction of interstitial supersaturation due to interstitial trapping by C–I clusters, leading to a reduction of dopant TED and deactivation. Carbon is mainly effective in combination with (pre)amorphization and recrystallization. In recrystallized regions, C is incorporated without an extra I and, therefore, is very efficient in trapping I. The simulation results are relatively sensitive to the amorphization layer thickness generated during implantation and, therefore, the *d*factor of preamorphizing implantations, or self-amorphizing C implantations, are recommended fitting factors.

For additional calibration of the C–I cluster model, you can consider modifying the initial conditions for C after implantation. By default, it is assumed that, in regions amorphized by ion implantation and recrystallized by solid phase epitaxy, carbon is in the substitutional state up to concentrations of $3.0 \times 10^{20} \text{ cm}^{-3}$ immediately after recrystallization. Higher concentrations are clustered as C_2 . In nonamorphized regions, carbon is assumed to be mostly in C_3I_2 clusters at the beginning of thermal annealing.

This assumption can be changed by the parameters `AcInit`, `AmInit`, `FractionCryst`, and `FractionAmor`. For example:

```
pdbSetDouble Si Carbon AcInit      1e18
pdbSetDouble Si C2I1   FractionCryst 0.5
pdbSetDouble Si C3I2   FractionCryst 0.5
pdbSetDouble Si Carbon AmInit      1e20
pdbSetDouble Si C2     FractionAmor  1.0
```

With these parameter values, C would be initialized as follows: In crystalline regions, only a maximum of $1 \times 10^{18} \text{ cm}^{-3}$ (`AcInit`) C atoms are substitutional initially. The additional C atoms are distributed to C_2I clusters (50%) and to C_3I_2 clusters (50%). In amorphized regions, the first $1 \times 10^{20} \text{ cm}^{-3}$ C atoms are put into substitutional sites. If the total concentration of C is higher, the rest is put into C_2 clusters initially. It should be mentioned that the interstitials that are contained in the C–I clusters represent an independent additional contribution to the total number of interstitials present after implantation.

Chapter 3: Guidelines for Additional Calibration

Accuracy and Limitations of Advanced Calibration of Sentaurus Process

For low C concentrations, the C–I model can be simplified by deactivating the C₂-cluster type, since it is only formed at high concentrations. The following command deactivates the C₂ cluster:

```
pdbSetString Si C Int ClusterSizes { {1 0} {1 1} {2 1} {3 2} {3 3} }
```

In addition, the initial conditions should not include C₂.

Carbon–Boron Clusters

According to [22], B and C can form relatively stable mixed clusters in silicon. The C–B clusters might not have a significant influence on B at high concentrations such as for USJ formation based on Ge+C+B coimplants, but B at low concentrations such as in B-doped NMOS channels can be deactivated by the presence of high C concentrations [23].

The following statements activate mixed C–B clusters in the form of the cluster type CBI, in addition to the C–I clusters and B₄ clusters of Advanced Calibration:

```
pdbSet Si B More.Active.Model.List ComplexCluster  
pdbSet Si C More.Active.Model.List ComplexCluster
```

Arbitrary calibrated reaction rates with diffusion-limited formation and a binding energy of 2.0 eV are defined by:

```
pdbSet Si BCI KF {[expr 1.0e8*[DiffLimit Si Int 0.0]}]  
pdbSet Si BCI KR {[Arr 1.0e5 2.0]}
```

To increase the agreement with SIMS and spreading resistance profiles of [23], cluster types with higher C content are beneficial.

To activate the cluster type C₂BI with arbitrary calibrated reaction rates, use the following statements:

```
pdbSet Si BCI Component.List { Boron 1 Carbon 2 Int 1 }  
pdbSet Si BCI KF {[expr 2.0e8*[DiffLimit Si Int 0.0]}  
pdbSet Si BCI KR {[Arr 1.0e3 2.0]}}
```

Impact of Carbon on Hole Mobility

Zschätzsch [24] reported that the presence of C in silicon reduces the mobility of holes in boron USJ causing an increase of the sheet resistance. To include this effect in device simulations, the following workaround can be used:

- At the end of the process simulation, 50% (or a lower percentage) of the C atoms is added to the concentration of arsenic substitutional atoms, and the same percentage of the C atoms is added to the B substitutional atoms, using the `select` command of Sentaurus Process. This changes the sum of donors and acceptors, but does not change the net active concentration of dopants.

Chapter 3: Guidelines for Additional Calibration

Accuracy and Limitations of Advanced Calibration of Sentaurus Process

If As and B are present in the device, and if the Transient model (default) is used for B and As activation, this can be performed by the lines:

```
select Si name=BActive z="BActive+CTotal/2.0" store
select Si name=Boron z="Boron+CTotal/2.0" store
select Si name=AsActive z="AsActive+CTotal/2.0" store
select Si name=Arsenic z="Arsenic+CTotal/2.0" store
diffuse temp=460 time=1e-30
```

- In device simulations with Sentaurus Device, use the DopingDep mobility model for the mobility in highly doped regions. In the DopingDep model, the total concentration of donors and acceptors is used to calculate the carrier mobility.

An alternative method to take into account the impact of C on carrier mobility is to use a physical model interface (PMI) for the calculation of mobility in high-concentration regions. The PMI can be implemented in such a way that the presence of carbon reduces the mobility of holes.

It is not known yet if carbon co-doping also impacts the mobility of electrons.

Molecular Implantation

Molecules such as borane ($B_{10}H_{14}$, $B_{18}H_{22}$) and carborane ($C_2B_{10}H_{12}$) can be used to implant C, B, and H at the same time [25][26]. In contrast to a subsequent implantation of C and B atoms, large molecules are implanted. For TCAD modeling, the main difference is that a molecule has a significantly higher capability to amorphize silicon. The many atoms of the molecule, which all enter the wafer at essentially the same position, are more likely to produce amorphous pockets in silicon than the implantation of individual atoms, which are not spatially correlated. This difference is most significant for low-energy implantations where the path length of the implanted atoms is relatively short. For high-energy implantations, the atoms of the molecule eventually separate so far that the damage that they produce no longer overlaps. Hydrogen is believed to out-diffuse rapidly without impact on B diffusion.

Carborane implantation is performed by implanting the species $C_2B_{10}H_{12}$, which is defined by default in Sentaurus Process:

```
implant C2B10H12 dose=1.0e14 energy=6.7
```

While the models for B diffusion and activation, and C–I cluster formation have been found to work well after carborane implantation, care needs to be taken for the implantation and for setting the initial conditions after implantation. The file `AdvCal_2022.03.fps` includes a calibration for implantation of BF_2 and carborane, but not for other molecules. This section summarizes the current recommendations of Synopsys for molecular implantation (other than BF_2).

Chapter 3: Guidelines for Additional Calibration

Accuracy and Limitations of Advanced Calibration of Sentaurus Process

Analytic Implantation

Sentaurus Process does not include implantation tables for molecules such as borane and carborane. Therefore, if analytic implantation is used for borane or carborane, Sentaurus Process converts the borane or carborane implantation into a B implantation with adjusted energy and dose. This underestimates the amorphization by borane or carborane implantation and ignores the implantation of C. Within analytic implantation, a better alternative is to replace the borane or carborane implantation directly by a combination of B and C implantation, with increased values of dfactor.

Sentaurus MC

It is recommended to use Sentaurus MC for molecular implantation. The file AdvCal_2022.03.fps includes a calibration for carborane implantation, with parameters integrated in callback procedures to obtain accurate results for the amorphization and good initial conditions (see [Implantation Preprocessing and Postprocessing on page 88](#)). However, for all other molecular implantations, the following settings must be defined by users in the case of a calibration:

1. Switch off the hydrogen solution to save CPU time in subsequent anneals:

```
solution name=Hydrogen nosolve store
```

2. Adjust amorphization by molecular implantation. If \$Energy is the energy of the molecule, the following parameters can be set as a function of \$Energy before the molecular implantation:

```
pdbSet Si B surv.rat <f($Energy)>
fproc mcdfactor_<molecule> { energy dose } { return f($energy) }
```

where surv.rat ('survival rate') scales the crystal damage, which is generated by nuclear collisions *during* the implantation. In particular for small energies, it must be set to very high values; otherwise, ion channeling during implantation is overestimated. mcdfactor_<molecule> will be called *after* the implantation for a final scaling of the crystal damage. With AdvCal_2022.03.fps, the value is applied once for each atom species of the molecule.

After the molecular implantation, you should reset surv.rat for B (and other species in the molecule) to the default values, as there might be other B ion implantations later in the process simulation:

```
pdbSet Si B surv.rat 0.225 ; # Sentaurus Process default
```

3. Set the number of interstitials to be generated by molecular implantation. When using AdvCal_2022.03.fps, Sentaurus Process adds *automatically* one interstitial for each atom of the molecule. However, this is not reasonable for H, which probably comes to rest in an interstitial position and is unlikely to kick out Si atoms from the lattice site.

Chapter 3: Guidelines for Additional Calibration

Accuracy and Limitations of Advanced Calibration of Sentaurus Process

A correction of the ‘automatic’ calculation of excess interstitials can be implemented with the callback procedure `UserMCPostProcess`:

```
proc ifactor_<molecule> { e d } { return 1.0 }
proc UserMCPostProcess { Species Name Energy Dose Tilt Rotation
                           Slice Mode MCIFac MCVFac } {
    if { $Species == "<molecule>" && $Name == "Hydrogen" } {
        set ifactor [ifactor_<molecule> $Energy $Dose]
        sel z = "Int_Implant - $ifactor * Hydrogen_LastImp"
        Silicon name=Int_Implant store
    }
}
```

The amorphization of silicon by molecular implantation other than carborane and BF_2 implantation has not been calibrated yet.

Fluorine Diffusion and Clustering

The procedure `AdvancedFluorineModel` defines a physics-based model for fluorine diffusion and clustering in silicon (see [Fluorine Diffusion and Clustering on page 99](#)). The model has been calibrated to reproduce experimental data for USJ formation based on F, BF_2 , and cocktail implantations ($\text{Ge}+\text{F}+\text{B}$, $\text{Ge}+\text{C}+\text{BF}_2$), and subsequent spike anneals [27].

The main effect of the F coimplantation is a reduction of interstitial supersaturation due to interstitial trapping by F–I clusters, leading to a reduction of dopant TED and deactivation. Fluorine is mainly effective in combination with (pre)amorphization and recrystallization. In recrystallized regions, F is incorporated as F_i or F–I clusters. The dissolution of F–I clusters leads to free F–I, by reactions that consume free I. The simulation results are relatively sensitive to the thickness of the amorphization layer generated during implantation. Therefore, the `dfactor` of preamorphizing implantations, or self-amorphizing F or BF_2 implantations, are recommended fitting factors.

For additional calibration of the F–I cluster model, you can consider modifying the initial conditions for F after implantation. By default, it is assumed that, in regions amorphized by ion implantation and recrystallized by solid phase epitaxy, fluorine is in the interstitial state up to concentrations of 10^{18} cm^{-3} immediately after recrystallization. Higher concentrations are clustered as F_2I and F_3I_2 . In nonamorphized regions, fluorine is assumed to be mostly in an interstitial position at the beginning of thermal annealing. This assumption can be changed by the parameters `AcInit`, `AmInit`, `FractionCryst`, and `FractionAmor`. For example:

```
pdbSetDouble Si F AmInit 1.0e20
pdbSetDouble Si F2I1 FractionAmor 0.0
pdbSetDouble Si F3I2 FractionAmor 1.0
pdbSetDouble Si F2I0 FractionAmor 0.0
```

With these parameter values, F would be initialized as follows: In amorphized regions, the first F atoms are put into interstitial sites. If the total concentration of F is higher than 10^{20} , the rest is put into only F_3I_2 clusters initially. Compared to the default initial conditions, more

Chapter 3: Guidelines for Additional Calibration

Accuracy and Limitations of Advanced Calibration of Sentaurus Process

interstitials would be present after solid phase epitaxy and, therefore, also more dopant TED.

The TED of dopants can be adjusted further by changing the stability of the F–I clusters, for example, by lowering the cluster binding energies:

```
pdbSetDoubleArray Si F Int ClusterFormE {Fluorine 0 F2 -2.3 F2I -3.3 \
F3I2 -6.2}
```

This will lead to an earlier decay of F–I clusters and, therefore, a stronger reduction of TED.

Finally, the fluorine-dependent boron dose loss can be deactivated by:

```
solution name=BF nosolve store
```

Nitrogen Diffusion and Clustering

The procedure `AdvancedNitrogenModel` defines a physics-based model for nitrogen diffusion and clustering in silicon (see [Nitrogen Diffusion and Clustering on page 100](#)). The model has been calibrated to reproduce experimental data for USJ formation based on N [28][29] and cocktail implantations (Ge+N+B, N+As), and subsequent RTA or spike anneals.

The main effect of the nitrogen coimplantation is a reduction of interstitial supersaturation due to interstitial trapping by N–I clusters, leading to a reduction of dopant TED and deactivation. Nitrogen is mainly effective in combination with (pre)amorphization and recrystallization. In recrystallized regions, N is assumed to be incorporated as $(N_i)_2V$ clusters that can capture free interstitials, thereby transforming into mobile $(N_i)_2$ or immobile $(N_i)_2I$ clusters.

The calibration included in `AdvancedNitrogenModel` provides a good starting point, but often does not provide satisfactory immediate accuracy. Fine-tuning is often needed. In the following, the most important parameters for the fine-tuning of `AdvancedNitrogenModel` are explained.

To increase the capability of nitrogen coimplantation to decrease dopant TED, the most important method is:

- Adjust the thickness of the amorphization layer generated during implantation. This can be modified by tuning the parameter `dfactor` (for analytic implantation) or the return value of `mcdfactor_Nitrogen` (for MC implantation). The thicker the amorphous layer, the more N is initially incorporated in $(N_i)_2V$ clusters, which contribute most to interstitial trapping.

Chapter 3: Guidelines for Additional Calibration

Accuracy and Limitations of Advanced Calibration of Sentaurus Process

To decrease the capability of nitrogen coimplantation to reduce TED, the most important methods are:

- Define `ifactor` greater than 0 for nitrogen implantation. (Typical values for nitrogen are in the range 0–1).
- Change the initialization of nitrogen in recrystallized regions. Instead of putting 100% of the nitrogen into $(N_i)_2V$ clusters, a significant percentage of nitrogen can be initialized as $(N_i)_2$ or $(N_i)_2I$ by changing the corresponding values of `FractionAmor`. Apart from increasing TED, this also will decrease the stability of nitrogen in recrystallized regions.

To fine-tune the nitrogen profile itself, the most important methods are:

- To achieve faster dissolution of nitrogen clusters, reduce the fraction of N that is initially put into $(N_i)_2V$ or $(N_i)_2I$ clusters, using the parameters `FractionCryst` (for nonamorphized regions) and `FractionAmor` (for amorphized regions).
- To change the stability of $(N_i)_2I$ clusters, reduce the binding energy for $(N_i)_2 + I \rightleftharpoons (N_i)_2I$. The default value (parameter `NDimer Int BindCluster`) is 2.65 eV. Good values are typically between 2.40 eV and 2.75 eV.

Diffusion in Strained Silicon and Silicon Germanium

Most of the calibration of the effects of Ge concentration and stress on dopant diffusivity have been performed by using published data based on marker layer experiments [30], as well as data from dedicated diffusion experiments executed by AMAT-VSE (Applied Materials - Varian Semiconductor Equipment) and provided to Synopsys. In this type of experiment, the diffusion of dopants is investigated by annealing experiments and subsequent SIMS measurements in wafers, which contain (biaxially) strained or relaxed Si and SiGe layers that are formed by molecular beam epitaxy (MBE). Often, the dopant atoms are built into the wafers during MBE.

The calibration for SiGe is not expected to be as accurate as the one for silicon, since it has not been tested to the same extent against data from device manufacturing processes, which combine ion implantation and rapid thermal annealing, and in which the concentration of point defects, defect clusters, and dopant–defect clusters are often far from thermal equilibrium. In particular, for elements other than B, and for high Ge mole fractions in general, little data has been published that allows for testing the accuracy of models for dopant diffusion and activation in strained Si and SiGe.

Advanced Calibration does not include any SiGe or stress effects for the implantation damage calibration. Since implantation into SiGe shows more amorphization than into pure Si [31], it is recommended to increase slightly the `dfactor`s in the case of SiGe implantation.

Chapter 3: Guidelines for Additional Calibration

Accuracy and Limitations of Advanced Calibration of Sentaurus Process

In the case of Monte Carlo implantation into SiGe, more accurate results are often achieved for as-implanted profiles if you assume implantation into pure Si instead of the compound material.

To treat SiGe as pure Si, the minimal concentration threshold can be increased to an arbitrary high value by the following command:

```
pdbSet Si SiliconGermanium.MCmin 1e30
```

As-Implanted Dopant Profiles

In general, the dopant distribution after ion implantation is calculated with high accuracy. For 1D structures, similar accuracy is obtained for Monte Carlo ion implantation and for analytic tables. This is because the tables have been generated by extraction of dual Pearson parameters from Crystal-TRIM simulations [21].

Note:

Sentaurus Process checks the implantation tables and sets the implantation mode to beam dose or wafer dose, both for analytic and MC implantation, depending on the implantation tables format. As a consequence, beam dose is selected for Ge, C, F, and N, while wafer dose is selected for the other species. You can use a global switch for the same dose control for all implantations:

```
pdbSet ImplantData DoseControl <WaferDose | BeamDose>
```

The entries of the `Default` implantation tables, which are used by default, depend on the species, energy, dose, tilt, and capping-layer thickness. For P, they also depend on the rotation; whereas, for all other species, the `Default` tables have been generated with the assumption `rotation=0`.

The amount of ion channeling must be fine-tuned frequently because it depends strongly on the dose rate and the wafer temperature during the implantation, as shown by experiments of [32]. Both parameters are usually not specified in the `implant` command. To fine-tune ion channeling in MC implantation, use the parameter `surv.rat` (Sentaurus MC) or `dacc` (Crystal-TRIM). To fine-tune ion channeling in analytic implantation, use the parameter `ratio`, which specifies the fraction of ions described by the first Pearson function.

For high-energy implantation into (100) wafers with zero tilt, the dopant profile is very sensitive to a small deviation of the tilt angle from `tilt=0`. For such conditions, a mismatch between SIMS and simulation might be due to insufficient experimental precision in the `tilt=0` ion implantation. In addition, for zero tilt, the dopant profile is also sensitive to the beam divergence, which can be specified in MC implantations with the parameter `BeamDivergence` (default is 0.5°).

If several implantations are performed subsequently without an intermediate diffusion step, the ion channeling is reduced due to the increasing implantation damage. In Monte Carlo ion implantation, this is taken into account automatically; in analytic ion implantation, the

Chapter 3: Guidelines for Additional Calibration

Accuracy and Limitations of Advanced Calibration of Sentaurus Process

`CoImplant` model is used for calculating the reduction of ion channeling. This model is described in the *Sentaurus™ Process User Guide*.

In 2D or 3D applications, the simulation results for Monte Carlo implantation and analytic implantation are often different, due to differences in the lateral distribution of dopants in structured geometries. Typically, the Monte Carlo simulation gives a more accurate lateral distribution of dopants. For CMOS technology, the difference in as-implanted profiles between Monte Carlo and analytic implantations is most important for the tilted halo implantations. The advantage of an analytic implantation is that it is much faster than a Monte Carlo implantation and that the result does not show any statistical noise. The latter is very important if you want to investigate the effect of small variations of implantation conditions on the device performance.

You can decide to use Monte Carlo implantation or analytic implantation outside of the calibration file by using one of the keywords `sentaurus.mc` and `crystaltrim`, or not.

Coimplantation Model

The coimplantation model is switched on by default. This model will automatically reduce the ion channeling in successive ion implantations.

However, the location of the crystal damage is not taken into account by the coimplantation model. Occasionally, in 2D and 3D process simulations, successive implantations are performed into different regions of the wafer, because implantation masks are removed and other masks are deposited between the implantation steps. In this case, the earlier implantation does not reduce the ion channeling of the latter implantation, and it is recommended to switch off the coimplantation model for these ion implantations.

Preamorphization Implantation Model

For analytic simulation of low-energy implantations that follow a preamorphization implantation (PAI), the PAI model is a superior alternative to the coimplantation model. For example, this might be the case for Ge+B source-drain implantations. The PAI model is also described in the *Sentaurus™ Process User Guide*.

To switch it on for a single boron implantation step, insert the keyword `pai` in the `implant` command.

Cold and Hot Implantation

Cold or cryogenic implantations are implantations with substrates kept below room temperature. Under these conditions, there is less dynamic annealing and the implantation amorphizes more rapidly, leading to deeper amorphous layers and less implantation channeling [33][34][35]. Hot or heated implantations are implantations with substrates kept above room temperature. Under these conditions, there is more dynamic annealing and the

Chapter 3: Guidelines for Additional Calibration

Accuracy and Limitations of Advanced Calibration of Sentaurus Process

implantation amorphizes less rapidly, leading to shallower amorphous layers and more implantation channeling [32][36].

You can simulate all these effects by calling the procedure `AdvancedThermalImplantModel` (see [Thermal Implantations on page 85](#)) or by using Sentaurus Process Kinetic Monte Carlo [37] (see [Amorphization on page 273](#)).

When using `AdvancedThermalImplantModel` in combination with Sentaurus MC implantation, as recommended, both simulated damage and doping profile are dependent on the implantation temperature. However for analytic implantation, only the damage is dependent on the implantation temperature, since analytic implantation profiles are only for room temperature implantations. For adjustments to the implantation tables for cold and hot implantations, you can change the ‘ratio’ of the two Pearsons to fit the channeling:

```
implant species=Phosphorus Silicon ratio=0.5
implant Phosphorus dose=1e+14 energy=30.0 tilt=0.0 rot=0.0
ResetImplantParams Silicon Phosphorus
```

Dose Loss at Silicon–Oxide Interfaces

For As, B, and P, the `ThreePhaseSegregation` model is used to describe dose loss at Si–SiO₂ interfaces. It takes into account that dopants can be trapped at the interface layer. In thermal equilibrium, the concentration of boron at both sides of the interface, which can be named as the segregation coefficient, can be expressed as:

$$\frac{B_{\text{Ox}}}{B_{\text{Si}}} = \frac{p/n_i}{\text{Segregation}} = \frac{\text{TrappingRate}_{\text{Si}}}{\text{TrappingRate}_{\text{Ox}}} * \frac{\text{EmissionRate}_{\text{Ox}}}{\text{EmissionRate}_{\text{Si}}} * \frac{5e22}{\text{Solubility}_{\text{Si}}}$$

Here, p/n_i is the normalized hole concentration at the silicon side of the interface. $\text{Solubility}_{\text{Si}}$ is the solid solubility of B in silicon, and the other parameters are specified in the sections on dose loss in `AdvCal_2022.03.fps`. In comparison, if the simple `Segregation` model is used, the same relation can be expressed as:

$$\frac{B_{\text{Ox}}}{B_{\text{Si}}} = \frac{p/n_i}{\text{Segregation}}$$

Here, `Segregation` is the parameter of the `Segregation` model. In some limiting cases in which the amount of dopants trapped at the interface can be neglected, you can achieve similar results with the `Segregation` model and the `ThreePhaseSegregation` model. For this, the parameter `Segregation` must be defined as:

$$\text{Segregation} = \frac{\text{TrappingRate}_{\text{Ox}}}{\text{TrappingRate}_{\text{Si}}} * \frac{\text{EmissionRate}_{\text{Si}}}{\text{EmissionRate}_{\text{Ox}}} * \frac{5e22}{\text{Solubility}_{\text{Si}}}$$

Chapter 3: Guidelines for Additional Calibration

Accuracy and Limitations of Advanced Calibration of Sentaurus Process

For As, B, and P, the Advanced Calibration parameters used in the ThreePhaseSegregation model correspond to the following values of Segregation in the Segregation model:

```
pdbSet Ox_Si As Segregation {[Arr 97777 0.6]}\n pdbSet Ox_Si B Segregation {[ArrBreak 1460.16 0.9502 144.721 \\ \n 0.6966 1000]}\n pdbSet Ox_Si P Segregation {[Arr 106666.7 0.5]}
```

When switching from the ThreePhaseSegregation model to the simpler Segregation model, consider defining the above values for Segregation, instead of the default values.

Note that, in both the ThreePhaseSegregation model and the Segregation model, segregation into oxide is enhanced for high dopant concentrations by the factor p/ni (P_{oni}) for acceptors and n/ni (N_{oni}) for donors, in agreement with experimental evidence.

Calibration of ThreePhaseSegregation Model

To increase dose loss, the easiest way is to increase the value of the parameter CMax or TrappingRate_Silicon.

During calibration, it might be necessary to change dose loss in a different way for high and low surface concentrations of a dopant. This can be achieved in two ways:

- Decreasing CMax and at the same time increasing TrappingRate_Silicon can have an opposite effect for high and low surface concentration. For high surface concentration, most interface traps can be filled. Reducing CMax will, therefore, reduce dose loss even for very high values of TrappingRate_Silicon. For low surface concentration, reducing CMax might be overcompensated by an increase of TrappingRate_Silicon.
- To increase dose loss especially for high concentrations of a dopant, you can consider to implement a pairing reaction for dopants in the interface layer, as it is done for P in AdvCal_2022.03.fps.

Sometimes, it might be necessary to adjust dose loss in a different way for inert and oxidizing atmospheres. During oxidation, the interface moves. The dopants do not have much time to cross the interface to establish segregation equilibrium between dopants in oxide and dopants in silicon. For this reason, for oxidation, the dose loss is more sensitive to the rate at which atoms change places. Changing all trapping rates and emission rates for a dopant by the same factor will have a much greater effect on dose loss for oxidizing atmospheres than for inert atmospheres.

A flexible instrument to modify dose loss is defining the terms CMaxFactor and Side.SS.Factor. CMax is multiplied by the first term, if defined, and the emission rate from the interface layer into silicon is multiplied by the second term, if defined.

Chapter 3: Guidelines for Additional Calibration

Accuracy and Limitations of Advanced Calibration of Sentaurus Process

In Advanced Calibration, `PhosphorusCMaxFactor` is used to reduce P dose loss in the presence of As at the oxide–silicon interface:

```
term name=PhosphorusCMaxFactor add Oxide /Silicon \
eqn = "1.8e13/(Arsenic+1.8e13)" store
```

You can adjust the value `1.8e13` during a technology-specific calibration. `Side.SS.Factor` is used in `SiGe_and_Stress_Effect` to take into account the modification of emission rates into strained silicon due to the impact of pressure on solid solubility. In CMOS process simulations, an important use case of `CMaxFactor` is to define a different dose loss into the gate oxide (which is typically oxynitride) and into the oxide spacer. For example:

```
term name=BoronCMaxFactor add Oxide /Silicon \
eqn = "(y<@<lgate/2.0>@) ? 0.2 : 1"
```

For phosphorus, it has been found that dose loss is smaller in processes without implantation, such as thermal annealing after epitaxial growth of P-doped layers covered by a thin native oxide. The Advanced Calibration default value of `CMax` has been calibrated for processes with P implantation. In processes without implantation, it is recommended to reduce the value of `CMax` for P at the Si– SiO_2 interface, for example, by a factor of 10. A similar reduction can be achieved by a corresponding definition of `PhosphorusCMaxFactor` in regions not affected by implantations.

The sensitivity of P dose loss to implantation damage mainly affects the dose loss described by the capture of single P atoms at the interface (governed by `CMax`). The concentration of P that can be trapped in P_2 pairs formed at the interface does not show such strong sensitivity. Therefore, the corresponding parameter `P2trapMax` is usually not adjusted for processes without implantation.

Oxidation

`AdvCal_2022.03.fps` includes parameters for the Massoud model for wet oxidation of silicon and oxidation parameters for germanium and SiGe. Some comments might be useful for additional fine-tuning of oxidation rates.

The growth of thick silicon oxides (thickness > 30 nm) is governed by the linear rate constant (B/A) in the Deal–Grove model. For very thick oxides (thickness > 100 nm), the parabolic rate constant (A) of the Deal–Grove model also becomes important. The default values of these parameters can be considered to be well calibrated in Sentaurus Process for dry, wet, and mixed atmospheres.

For thin oxides (thickness < 5 nm), the growth rate is dominated by the Massoud correction term of the Deal–Grove model. This correction term is taken from Sentaurus Process defaults for dry oxidation and has been calibrated for wet oxidation. Recommendations for the fine-tuning of the Massoud correction term for wet oxidation are presented in [Massoud Model Parameters for Wet Oxidation of Silicon on page 57](#).

Chapter 3: Guidelines for Additional Calibration

Accuracy and Limitations of Advanced Calibration of Sentaurus Process

For very thin oxides and oxynitrides (thickness < 2 nm), which are often grown at low temperatures, the models of Sentaurus Process are not sufficiently well calibrated to expect precise results. For CMOS gate oxides (oxynitrides), it is recommended to extract the oxide thickness from a comparison of simulated and measured C–V characteristics in accumulation, and to adjust the oxide thickness in process simulations by defining the thickness of the initial oxide layer.

Bird's Beak in CMOS Devices

CMOS devices sometimes exhibit a so-called bird's beak. During poly reoxidation, the gate oxide grows slightly thicker at the gate edge than in the middle of the transistor. For the calibration of the bird's beak, in principle, you can use high-resolution TEM pictures of the gate oxide, but often the bird's beak is too small to be visible in TEM. For thin gate oxides, the growth of the bird's beak is dominated by the Massoud correction term of the Deal–Grove model. This correction term has been calibrated for the growth of planar oxides, and it possibly needs to be modified for the oxide geometry at the gate edge.

The most radical modification is to completely suppress oxidant diffusion in the gate oxide during poly reoxidation. This will completely eliminate the formation of a bird's beak shape. An advantage of this approach is that the Si–SiO₂ interface remains perfectly parallel to the horizontal mesh lines, which is beneficial for the convergence of device simulation.

To completely suppress oxidant diffusion in the gate oxide, define the term O2DiffFactor (`H2ODiffFactor`):

```
term name=O2DiffFactor add Oxide store           \
eqn="((y<($lgate/2.0)) * (x>-0.01)) ? 0 : 1"
```

In this definition, it is assumed that the gate oxide is located in the region `y<($lgate/2.0)` and `x>-0.01`; whereas, other oxide is located outside this region.

Besides its impact on the final shape of the gate oxide, altering the bird's beak has an impact on the OED during poly reoxidation and, thereby, on the NMOS reverse short-channel effect.

Diffusion in Polysilicon and Out-Diffusion From Polysilicon

A calibration of dopant diffusion in polysilicon and the out-diffusion of dopants from polysilicon is not included in Advanced Calibration. In CMOS simulations, it is often sufficient to assume a constant doping profile in polysilicon, which can be adjusted manually with the help of C–V measurements.

For devices where diffusion and activation of dopants in polysilicon or the out-diffusion from polysilicon into silicon is important (such as in processes for the fabrication of bipolar devices or DRAM), you need to select the model and parameters for the dopants in polysilicon and for the dopant flux at the interface.

Dopant Penetration Through Gate Oxide

The dopant penetration through gate oxide has not been calibrated. This is a difficult task because, instead of pure oxide, oxynitride is commonly used as the gate dielectric material. Dopant diffusion from polysilicon through the gate oxide into the channel region can be completely suppressed by the user by setting the transfer coefficient at the polysilicon–oxide interface to 0.

Diffusion and Activation in Germanium

Sentaurus Process supports diffusion and activation in crystalline germanium with a Ge–GeO₂ interface. A basic calibration has been performed, and parameters for material properties, defect evolution, and dopant diffusion and activation have been introduced to the Sentaurus Process parameter database and Advanced Calibration.

In general, the calibration for germanium is less accurate than the one for silicon, since it is less mature and based on a smaller experimental dataset. Therefore, additional calibration might be required.

Defect recombination and dopant segregation are calibrated only for the GeO₂–Ge (GeOxide_Germanium) interface. GeO₂ is thermally unstable and water soluble, and uncapped GeO₂ surfaces lead to germanium substrate loss even in low-temperature processes [40]. Different capping layers (SiO₂, Si₃N₄) on the germanium surface can prevent substrate loss and lead to a different phosphorus dose loss [40]. However, the effect of different capping layers has not been calibrated, since surface conditions are not always specified in detail in the literature. Therefore, the dose loss might need additional calibration for specific cases. Since it is assumed that, even in the case of a SiO₂ capping on Ge, a small layer of GeO₂ is formed in between, specifying a Ge–GeO₂ boundary for Ge substrate simulations is reasonable. However, for usability and SiGe parameter interpolation, the parameters for the Ge–SiO₂ interface are defined in Advanced Calibration by inheriting the parameter values from Ge–GeO₂.

Note:

Sentaurus MC is recommended for implantation into germanium, since no implantation tables for germanium are available.

Performing Additional Calibration

For the process simulation of any new technology or technology node, it is recommended to use the Advanced Calibration as a starting point.

Calibration Procedure

In many cases, Advanced Calibration gives accurate results without requiring additional parameter fine-tuning. However, in most cases, especially for the development of innovative technology, additional fine-tuning is needed for a customized TCAD calibration.

The recommended way to perform the calibration of parameters for 2D (or 3D) process simulation is:

1. Compare SIMS data from your process flow with straightforward results obtained with Advanced Calibration. Check whether the agreement is good and whether additional parameter fine-tuning is needed to improve the agreement.
2. If additional models, or parameter fine-tuning, are needed, put the required additional calibration together in a single *user calibration file*, which will be sourced immediately after loading the default Advanced Calibration. For the remainder of this section, this user calibration file will be called `user_calib.fps`.
3. After a good agreement with SIMS data is obtained, make a setup for 2D process and device simulation. Before continuing with the calibration, ensure that the setup is good in terms of numerics (small CPU time, small numeric noise, and robustness).
4. Perform 2D (or 3D) process and device simulations, and compare the simulated and measured electrical device characteristics. Analyze whether there is insufficient accuracy, which is due to process simulation calibration.
5. Perform additional parameter fine-tuning if required. As in the case of 1D simulations, all fine-tuning in addition to the default Advanced Calibration should be put together in the `user_calib.fps` file, which is sourced immediately after the following command:

AdvancedCalibration 2022.03

6. As a result of the fine-tuning (calibration), the same file `user_calib.fps` should give accurate results in all 1D and 2D (or 3D) simulations.

It is reasonable to start with 1D simulations and SIMS data, because 1D simulations are much faster and the SIMS data provides direct information on the dopant distribution, whereas electrical device data does not always allow you to separate clearly the many effects that accumulate in a full 2D or 3D process flow.

Synopsys offers calibration service projects. In such projects, the optimized and calibrated input files for process and device simulation are created by expert application engineers at Synopsys, and the calibration steps are explained in detail to customers.

Fine-Tuning Parameters Defined in Callback Procedures

Several parameters specified in Advanced Calibration are defined in callback procedures. In particular, this applies to many parameters for ion implantation, which can depend on the implantation conditions, such as implantation species, energy, dose, and wafer temperature. These implantation conditions are handed over to the callback procedures as arguments.

An example is the procedure `ifactor_Carbon`, which defines the “interstitial +x factor” for a C implantation into Si, depending on the implantation energy. In `AdvCal_2022.03.fps`, there is:

```
fproc ifactor_Carbon { Energy Dose } {
    return [expr $Energy/($Energy+2.0)/3.0]
}
```

Here, only one parameter is defined as a return value. To fine-tune the formula defined in Advanced Calibration, you need to redefine the callback procedure.

Some callback procedures defined in Advanced Calibration are very long and define many parameters as a function of implantation conditions. In particular, this applies to the procedures `_AdvCal::ImpPreProcess` and `AdvancedThermalImpPreProcess`.

Sometimes, you might need to fine-tune some of the parameters defined in these procedures. For this purpose, specifying a new parameter value with an isolated `pdbSet` statement does not work, because that value is overwritten when Sentaurus Process calls the callback procedures when it executes an implantation statement.

Instead, to fine-tune a process model parameter that is defined in one of these two procedures, you have the following options, of which #2 is better because it keeps the user calibration file short:

1. Copy the complete definition of a callback procedure from the Advanced Calibration file into the user calibration file and make changes therein.
2. Define a procedure named `UserImpPreProcess`. If this procedure is defined, then Sentaurus Process calls it for every implantation statement, after calling `_AdvCal::ImpPreProcess` or `AdvancedThermalImpPreProcess`. Therefore, you can use commands inside `UserImpPreProcess` to overwrite some of the parameters defined in `_AdvCal::ImpPreProcess` or `AdvancedThermalImpPreProcess`. The syntax is:

```
fproc UserImpPreProcess {Species Energy Dose Tilt Rotation Slice Mode}
{
    ...
}
```

Loading a User Calibration File

An input file of a Sentaurus Process simulation with additional user calibration should have the following structure:

```
# Title
AdvancedCalibration 2022.03      ; # loads the Advanced Calibration
source ./user_calib.fps          ; # loads the additional calibration
line ...                         ; # rest of process simulation file
init ...                          ; # without any model parameters
implant ...
diffuse ...
deposit ...
save ...
exit
```

All project-specific calibration is contained in a separate file `user_calib.fps`, which is sourced after loading the Advanced Calibration defaults. This setup has several advantages:

- The simulation input file is easier to read if it is free of physical models and parameters. Changing the process conditions does not require a high level of TCAD expertise.
- All project-specific calibration is contained in a single file. Often, this file is short and contains only approximately ten changes with respect to the default Advanced Calibration. Ideally, it can be printed on a single page. Therefore, it is very easy to see what has been performed in the user calibration. The calibration work becomes clearer and easier. Furthermore, the user calibration from different technologies or technology nodes can be compared and exchanged conveniently.

See [Example of a User Calibration File on page 184](#).

Recommendations

This section provides information for additional calibration.

Miscellaneous

This section discusses how to avoid common errors in 2D simulations:

- In process recipes that contain tilted implantations, the implantation dose is defined either per wafer area or per beam area. To ensure that Sentaurus Process uses the required definition for all species, you should set the `DoseControl` parameter at the start of the command file:

```
pdbSet ImplantData DoseControl <WaferDose | BeamDose>
```

Chapter 3: Guidelines for Additional Calibration

Performing Additional Calibration

- A few nanometers of silicon are sometimes removed in cleaning steps. This might be important to take into account after low-energy ion implantation.
- Always assume that bare Si surfaces are covered by a natural oxide of 1–2 nm thickness. In practice, this can mean that it is necessary to add deposition steps of thin oxide layers in the process simulation. The dose loss model used in Advanced Calibration works only for Si–SiO₂ interfaces *not* Si–gas interfaces.
- In CMOS technology, the gate is not always rectangular. If possible, adjust the gate shape to a TEM picture, to obtain the correct as-implanted extension and halo dopant profiles.
- For spike annealing and, more importantly, for laser and flash lamp annealing, the heat cycle to be used in the `diffuse` statement ideally must be taken from a corresponding temperature profile measurement.

Lateral Diffusion Along Interface

The three-phase segregation model allows you to specify a dopant diffusivity in the interface layer. This model is used for B, As, and P in the Advanced Calibration. The interface diffusivities are set to 0 by using:

```
pdbSetDouble Ox_Si B D { 0 0 }
```

By setting positive values of the interface diffusivity, the lateral diffusion of dopants near the Si–SiO₂ interface can be increased without affecting the vertical diffusion far from the interface. This can be used, for example, to adjust the short-channel effect in deep submicron MOSFETs. More importantly, setting a positive value for the lateral diffusivity will also change the shape of the p-n junctions close to the interface [41].

Example of a User Calibration File

The following example is a typical user calibration file, which can be the result of a CMOS calibration project, for example. The file `user_calib.fps` is sourced after loading the default Advanced Calibration file:

```
# Calibration file for 90nm CMOS technology.
# Five changes after loading AdvCal_2022.03.fps.

# 1) Adjust ion channeling and rp for high energy P implant
proc UserImpPreProcess { Species Energy Dose Tilt Rotation \
Slice Mode } {
    ResetImplantParams Silicon Phosphorus ;      # reset to default
    if { $Species == "Phosphorus" && $Energy > 300 } {
        implant species=P Si ratio=0.9
        implant species=P Si rp=[expr 1.15e-3*exp(log($Energy)*0.99)]
    }
}
```

Chapter 3: Guidelines for Additional Calibration

Performing Additional Calibration

```
# 2) For nMOS extension (energy and dose dependence of TED)
proc ifactor_Arsenic { Energy Dose } {
    if { $Energy < 5.0 } {
        return [expr 2.0e14/($Dose+5e13) + (5-$Energy)/4.0]
    }
    return [expr 2.0e14/($Dose+5e13)]
}

# 3) For nMOS extension (dose loss)
pdbSetDouble Ox_Si Arsenic CMax {[Arr 5.0e17 0.8]}

# 4) For pMOS extension (energy and dose dependence of TED)
proc ifactor_Boron { Energy Dose } {
    if { $Energy < 2.5 } { return 0.5 } ; # pMOS extension implant
    return 1.0 ; # nMOS well implant
}

# 5) For pMOS extension (reduced diffusion after spacer deposition)
pdbSetDouble Si B CluRate {[Arr 5e11 5.42]}
```

This example calibration file, which is a hypothetical result of a CMOS calibration, can be embedded in a CMOS process simulation input file, as described in [Loading a User Calibration File on page 183](#). Its contents are discussed briefly.

This file changes five settings of the default calibration file. The first change improves the accuracy of as-implanted profiles. The next two changes target As extension profiles after annealing, and the last two changes relate to the B extension diffusion in the PMOS.

The implementation of `UserImpPreProcess` (first change) illustrates how to adjust the Pearson parameters. You must pay attention to the following aspects:

- If the modified values of the Pearson parameters should be applied only for some process conditions (for example, only for high-energy P implantation, but not for low-energy P implantation), you must ensure that the parameter changes are not permanent for all subsequent implantations. In this example, this is performed by including the command `ResetImplantParams`.
- When adjusting one of the Pearson parameters (`rp`, `stdev`, `rp2`, `stdev2`), you should avoid defining a fixed value. Instead, you can define them as functions of implantation parameters. In this example, `rp` is defined as a function of implantation energy in order not to destroy the energy dependency of `rp` by the calibration.

With a fixed value, the calibration is valid only for a single condition, but it is not predictive for a larger process window of interest. Only for the parameters `ratio`, `gamma`, `beta`, `gamma2`, and `beta2` can you use a fixed value in a larger window of interest.

A permanent change of diffusion parameters is performed with the `pdbSet`, `pdbSetDouble`, or `pbdSetDoubleArray` command. The initial conditions after ion implantation can also be calibrated in the user calibration file. For example, as demonstrated in the file above, the

Chapter 3: Guidelines for Additional Calibration

Recommended Numeric Settings for Monte Carlo Implantation

interstitial plus-factor (`ifactor`), which scales the amount of interstitials generated per implanted ion, can be adjusted as a function of implantation energy and dose. The default procedures of the Advanced Calibration for setting `ifactor` are implemented in section 3.2 of `AdvCal_2022.03.fps`.

By redefining the procedures `ifactor_Arsenic` and `ifactor_Boron`, you can overwrite the original dependency on implantation energy and dose. Using initial conditions that depend on implantation energy and dose is a very powerful method to calibrate dopant diffusion in the energy and dose window of interest for a given technology.

Recommended Numeric Settings for Monte Carlo Implantation

This section presents recommendations that allow for the reduction of numeric noise and CPU time for Monte Carlo implantations.

Monte Carlo Pocket Implantation

In process simulation of CMOS devices for 65 nm or smaller gate lengths, MC simulation is often preferred to analytic implantation models for the pocket implantation, because it allows for the calculation of the 2D (or 3D) dopant distribution under the gate corner with higher accuracy.

Recommendations are given to minimize the numeric noise and the CPU time needed for MC pocket implantations. These recommendations are given for 2D process simulation, but can be generalized for the 3D case:

- In 2D CMOS process simulation with a *single symmetric gate*, MC implantations can be performed on a half-structure, in which the half-gate is typically at the left side of the simulation domain. The following choices can be selected for the boundary conditions at the left-side and right-side simulation domain boundaries:

- `pdbSet MCImplant LeftBoundary Reflect`

This leads to the fastest simulations. Atoms that reach the left-side boundary are reflected. A small disadvantage is that ions, which travel in crystal channels before reflection, are scattered out of their crystal channeling, which might lead to a small maximum of concentration near the symmetry plane. This disadvantage can be avoided by using `TrueReflect` instead of `Reflect`. For details, see the *Sentaurus™ Process User Guide*.

- `pdbSet MCImplant RightBoundary Reflect`

This leads to the fastest simulations. It is not perfectly precise. In particular, at the right side of the device, for implantations with `rotation=90`, it will result in a decay of the profile.

Chapter 3: Guidelines for Additional Calibration

Recommended Numeric Settings for Monte Carlo Implantation

The alternative is:

```
pdbSet MCImplant RightBoundary Extend  
pdbSet MCImplant MinExtend 0.03 ;# example  
pdbSet MCImplant ExtensionLength 0.00
```

With this choice, the simulation domain is extended artificially by 30 nm (the best value depends on the implantation condition) at the right side to avoid the decay of the profile.

- In 2D CMOS process simulation with *multiple symmetric gates* in periodic arrangement, the best choice is to use `TrueReflect` boundary conditions on both sides of the half-structure:

```
pdbSet MCImplant LeftBoundary TrueReflect  
pdbSet MCImplant RightBoundary TrueReflect
```

With these settings, the simulation is fastest, and the shadowing of tilted implantations by the neighboring gate is taken into account correctly.

In comparison, using `Reflect` boundaries at both sides does *not* take into account the shadowing effect of the neighboring gate. (This is because, with `Reflect` boundaries, ions are not reflected as long as they travel in the gas phase.)

- The following switches should be used:

```
pdbSet MCImplant TrajectoryReplication 0  
pdbSet MCImplant TrajectorySplitting 0
```

They switch off trajectory replication and the trajectory-splitting algorithm. Trajectory replication reduces CPU time, but it carries the risk that a family of trajectories is not found in the initial search of possible particle pathways. For CMOS pocket implantations, it is better to switch it off, as the benefit in CPU time does not compensate for the numeric noise corresponding to that risk.

Trajectory splitting is an algorithm developed to improve the statistics of as-implanted profiles in regions that are reached only by a few pseudoparticles. However, in CMOS pocket implantation, the focus of interest is the region of maximum as-implanted dopant concentration, and not so much the profile tails. So improving the statistics in the profile tail (at the cost of using less CPU time for the profile maxima) is not beneficial for CMOS pocket implantations.

- Reduce the interval width from 50 nm to a smaller value, for example, 2 nm:

```
pdbSet MCImplant Intervals dy 0.002
```

This increases the CPU time because for each interval a number of pseudoparticles (particles) will be followed. However, it is better to use a larger number of small intervals with a small particle number each, than to use a small number of very large intervals with a large particle number, because as a matter of statistics, in the first case,

Chapter 3: Guidelines for Additional Calibration

Recommended Numeric Settings for Monte Carlo Implantation

the incident pseudoparticles are more evenly distributed over the whole simulation domain.

- Instead of using the same particle number for all rotation angles, use a higher particle number for implantations towards the gate corner (usually, `rotation=90`) and a reduced particle number for implantations away from the gate corner (usually, `rotation=270`).

For example, a good choice for a four-rotation pocket implantation, when simulating the right half-structure of a MOSFET, is:

- `rotation=0: particles=1000`
- `rotation=90: particles=4000`
- `rotation=180: particles=1000`
- `rotation=270: particles=300`

Note:

If the `TrueReflect` boundary condition is used at the left-side boundary, then you should use the same particle number for `rotation=90` and `rotation=270` to ensure good statistics in the middle of the device.

Monte Carlo Source/Drain Implantation

In CMOS technology, source/drain implantations are typically performed at tilt angles close to zero. By colliding with Si lattice atoms, a small percentage of implanted ions is deflected towards the middle of the channel, which can lead to a significant reduction of the threshold voltage. The accurate modeling of this requires good statistics of the ions deflected towards the middle of the channel. This can be achieved by the following recommended settings for MC source/drain implantation:

```
pdbSet      MCImplant TrajectorySplitting 1
pdbSetSwitch MCImplant SplitModel traj.density
```

With `SplitModel traj.density`, a particle is replaced by two child particles, with half the statistical weight each, when it reaches an element with a small trajectory density. This is much more suitable for obtaining good lateral statistics in the channel region under the gate than the default `SplitModel depth.sp`, where particle splitting depends on the depth (distance from the impact point) only.

Using `SplitModel traj.density` increases the CPU time, but this is more than compensated by the improved statistics of the ions implanted in the channel region. Compared to `SplitModel depth.sp`, often a much smaller number of implanted particles suffices to achieve an equally small statistical noise in device characteristics due to source/drain MC implantation.

Additional Calibration for Power Technologies

The process simulation of power technologies and smart-power technologies can require too much CPU time because of the large number of thermal anneals. [Part 5: Accelerating Simulations for Power Technologies on page 117](#) presents a recommended choice of model switches and numeric parameters to accelerate process simulations.

Calibration

Starting from the Advanced Calibration parameter set, a typical comprehensive calibration of process simulation for power and bipolar–CMOS–DMOS (BCD) technologies consists of several steps. This section describes frequently used parameters for technology-specific calibration.

Oxide Thickness and Oxide Shape

For LOCOS simulations, it is recommended to switch on the model for stress-dependent oxidation:

```
pdbSet Oxide O2 SDO 1  
pdbSet Oxide H2O SDO 1  
pdbSet Oxide Oxidant SDO 1
```

The shape of the LOCOS is usually fine-tuned against TEM reference data by calibrating the viscosity and stiffness (for example, `BulkModulus`) parameters for oxide and nitride, and calibrating the activation volume (parameters `vd` and `vk`) for stress-dependent oxidation rates.

Ion Implantation

You can use either MC or analytic implantation for ion implantation. MC implantation is more frequently used, because it is more physical and better describes lateral scattering in nonplanar structures. Often, MC implantation is accurate out of the box. If needed, the following parameters are sometimes considered for fine-tuning:

- `LSS.pre` adjusts the position of the profile peak.
- `surv.rat` increases or reduces the channeling tail, and scales the damage created during implantation. The more damage is created, the faster the crystal channels are blocked, and the fewer ions end up in the channeling tail for medium-dose or high-dose implantations.
- `DebyeTemperature` adjusts ion channeling for very high energies (MeV) and small doses. Often, for very high implantation energies, you need to decrease this parameter with respect to the default value (519 K in Si).

Chapter 3: Guidelines for Additional Calibration

Additional Calibration for Power Technologies

In analytic implantation, the parameter `ratio`, one of the double-Pearson parameters, scales the fraction of dopants in the first Pearson distribution.

Initial Conditions After Implantation

The excess interstitials created by implantation play an important role in TED. The number of interstitials is frequently fine-tuned with the scaling factor `ifactor`. You can either specify `ifactor` directly in an `implant` command or, better yet, overwrite the callback procedures `ifactor_Boron`, `ifactor_Arsenic`, or similar, with modified values.

After amorphizing implantations, only the nonamorphized regions contribute to excess interstitials. Therefore, the amorphization depth also impacts the number of excess interstitials created. For amorphizing implantations, the implantation damage, which determines the amorphization depth, can be scaled after implantation by adjusting the parameter `mcdfactor`. Again, the recommended way to do this is to overwrite the corresponding callback procedure, such as `mcdfactor_BF2`. In MC implantation, the implantation damage is also affected by the value of `surv.rat`.

Sometimes, you need to adjust the maximum concentration of dopants, which is initially active after implantation. This is best achieved by redefining the callback procedures `acinit_<species>` and `aminit_<species>` for nonamorphized and amorphized regions, respectively.

Thermal Annealing

Power-device fabrication processes frequently involve thermal oxidation. During oxidation, interstitials are injected at oxidizing surfaces, thereby enhancing the diffusion of B and P, which predominantly diffuse by way of interstitials. The diffusion of As, which partially diffuses by using a vacancy mechanism and partially through interstitials, is also enhanced, but to a lesser extent. The amount of interstitial injection that causes OED is scaled by the parameter `theta`. The value of `theta` for dry and wet oxidation is frequently adjusted to match dopant diffusion visible in SIMS data.

Dopant segregation at silicon–oxide interfaces is also frequently tuned. For B, P, and As, the `ThreePhaseSegregation` model is used to describe segregation from Si to Oxide, and segregation into the oxide–silicon interface layer. For information about adjusting the dose loss, see [Calibration of ThreePhaseSegregation Model on page 177](#).

Meshing

A well-designed mesh is important for 2D or 3D process simulations. The mesh should be fine enough in the critical regions to keep discretization errors small, but it should have a small total number of mesh points. Mesh refinement criteria are described in the *Sentaurus™ Process User Guide*.

Chapter 3: Guidelines for Additional Calibration

Additional Calibration for Power Technologies

For many applications, a good mesh can be obtained using adaptive meshing. Many adaptive refinement criteria are available to deal with different fields and situations. All functions involve some comparison between values on neighboring nodes and possible values between neighboring nodes.

Recommendations for Bulk Refinement With Adaptive Meshing

In this section, two frequently used refinement criteria for adaptive meshing are presented. These are the relative difference error and the local dose error that correspond to the `rel.error` and `max.dose.error` arguments of the `refinebox` command of Sentaurus Process (see *Sentaurus™ Process User Guide*, Adaptive Refinement Criteria). It is advisable to define one refinement box per diffusion species. By doing so, you can choose refinement box parameters for a certain species, independently from the other species based on the implantation conditions pertaining to that particular species.

It is possible to demonstrate that, in the case of a simple Gaussian doping distribution, a simple yet effective algorithm can be formulated to facilitate the choice of parameters for adaptive meshing of refinement boxes. To bypass complex technical issues, only the algorithm itself is discussed here, not the full theoretical foundation of the algorithm.

To apply the algorithm to a process flow, you review the process flow and copy all the implantation steps pertaining to a particular implantation species into a list. After the list has been obtained, you then find the implantation with the lowest dose (D_{min}) and compute the value of `max.dose.error` of the `refinebox` command as follows:

$$\text{max.dose.error} = \frac{D_{min}}{100.0} \quad (13)$$

As a next step, `rel.error` must be assigned a value that is typically between 0.5 and 1.0. The density of the mesh is sensitive to `rel.error` because it represents the target relative change of the field across an edge. For many typical situations, a value of 1.0 gives a coarse mesh, and a value of approximately 0.5 gives a fine mesh. The exact value of `rel.error` depends on the sensitivity of the simulated device characteristics to the process mesh variations and, therefore, the value must be found experimentally.

Then, the implantation with the smallest energy (E_{min}) is found, and the corresponding standard deviation (`stdev.min`) is obtained as:

```
set moments [implant material=Silicon $Species \
    energy= $Emin dose= $Dose get.moments]

set stdev.min [lindex $moments 5]
```

Chapter 3: Guidelines for Additional Calibration

Additional Calibration for Power Technologies

The smallest implantation standard deviation value determines the smallest allowed mesh spacing that can be set in the `refinebox` command. The value of `refine.min.edge` is calculated as follows:

$$\text{refine.min.edge} = \frac{\text{stdev.min} \cdot \text{rel.error}}{4.0} \quad (14)$$

Consider a process flow containing the following boron implantations:

```
implant boron dose= 1e13 energy= 400
implant boron dose= 5e12 energy= 800
implant boron dose= 1e14 energy= 40
implant boron dose= 2e15 energy= 10
```

Now, the parameters of an adaptive refinement box are obtained according to the proposed algorithm. The second implantation has the smallest dose, so `max.dose.error` can be set to `5e10`. The last implantation has the smallest energy and, therefore, the smallest standard deviation of 24 nm and, if `rel.error` equals 1.0, that gives the smallest allowed mesh spacing of 6 nm. Finally, the corresponding refinement box for boron would be:

```
refinebox name= Global_Boron adaptive Silicon \
refine.min.edge= "0.006 0.006 0.006" \
refine.max.edge= "10 10 10" \
max.dose.error= "Boron= 5e10" \
rel.error= "Boron= 1.0" \
abs.error= "Boron= 1e15"
```

where `abs.error` is a cut-off concentration level for the relative difference error refinement criterion.

When adaptive meshing is switched on, the default adaptive meshing parameters are applied. However, there are two issues with keeping the default refinement box. First, it applies one and the same parameter set for all species and this contradicts best practice. Second, it allows mesh refinement on implantation damage even when no damage sensitive model is used.

To deactivate the default adaptive refinement box, the following settings must be used along with user-defined refinement boxes:

```
pdbSet Grid AdaptiveField Refine.Abs.Error      1e30
pdbSet Grid AdaptiveField Refine.Rel.Error      1e30
pdbSet Grid AdaptiveField Refine.Target.Length  1e30
```

To accurately capture the amorphous–crystalline interface position, a damage refinement box must be placed. Note that this is not necessary in the first part of process simulations with `AdvancedPowerDeviceMode`, where models sensitive to implantation damage are switched off. A typical damage refinement box definition is:

```
set targetLength 2e-4
set minValue [pdbGet Silicon AmorpDensity]
set maxValue [expr 1.001 * $minValue]
```

Chapter 3: Guidelines for Additional Calibration

Calibration of Wet Etching Rate Modification by Ion Implantation

```
refinebox add name= PowerDeviceMesh_Damage adaptive Silicon \
    refine.fields= {Damage} refine.type= interval \
    target.length= "$targetLength" target.length.scaling= "1.0" \
    min.value= "Damage= $minValue" \
    max.value= "Damage= $maxValue"
```

In the above examples the refinement boxes are applied globally to the entire simulation domain. However, it might be necessary to place some additional refinement boxes in the critical device areas. If that is the case, you should follow the layout (mask)-driven refinement approach (see *Sentaurus™ Process User Guide*, Mask-Driven Meshing).

Refinement at Material Interfaces

For accurate modeling of boron dose loss at oxide–silicon interfaces, it is important to use a good mesh refinement perpendicular to the interface. Otherwise, the amount of boron dose loss (this is the dose of boron segregation from silicon into oxide) might strongly depend on the mesh.

A mesh with approximately 1 nm spacing, perpendicular to the interface, is often a good choice. When testing the use of coarser mesh refinements at some interface regions, you should ideally compare results with a reference simulation to a fine mesh, to check at least once whether the device simulation results are affected by numeric errors related to interface mesh refinement.

A good solution can combine a coarse global interface refinement, for example:

```
interface.materials=Silicon
min.normal.size=0.008 normal.growth.ratio=2.0
```

and a better refinement inside refinement boxes that cover the active device areas such as channel regions (for example, `min.normal.size=0.001`).

Calibration of Wet Etching Rate Modification by Ion Implantation

Sentaurus Process allows you to scale the etching rate with a user-defined field. You specify the field using the `etch.rate.modifier` argument of the `etch` command. This feature is available for etching simulations using the level set method.

In device fabrication, ion implantation can be used to modify the wet etching rate in surface regions affected by implantation. Modifying the wet etching rate for SiO₂ and SiN in diluted hydrogen fluoride (HF) has been studied using data provided by Applied Materials and published data [42][43].

This section summarizes key findings and recommendations from this calibration effort. The corresponding parameter settings are not yet included in the Advanced Calibration file.

Chapter 3: Guidelines for Additional Calibration

Calibration of Wet Etching Rate Modification by Ion Implantation

Calibration

The wet etching rate ratio (werr) is the ratio of the wet etching rate in implanted regions versus not implanted regions.

Ion implantations affect the werr of SiN and SiO₂ by the following mechanisms:

- The etching rate increases with implantation damage as follows:
 - For low doses, the etching rate increases linearly with the concentration of vacancies generated by implantation. Using Sentaurus Process, you can calculate this vacancy density with a full-cascade Monte Carlo implantation simulation. Alternatively, in good approximation, the etching rate also increases linearly with the implantation damage (Damage), which you can calculate with a regular Monte Carlo implantation simulation.
 - For medium and high doses, the impact of damage on the etching rate saturates towards a maximum damage-driven increase, which is a factor of approximately 2.5–6.0.
- For very high implantation doses, there is an additional chemical effect. The etching rate changes because implanted ions change the chemical composition of oxide or nitride. After thermal annealing, typically, there is no more damage effect on werr, but the chemical effect might be stable.

For the datasets studied, good agreement with measured werr has been achieved with the following formula. For the damage effect:

$$\text{werr}_{\text{Damage}} = 1.0 + (F - 1.0) \cdot \frac{\text{Damage}}{\text{Damage}_{\text{reference}}} \cdot \frac{1}{\left(1.0 + \left(\frac{\text{Damage}}{\text{Damage}_{\text{reference}}}\right)^{\alpha}\right)^{1/\alpha}} \quad (15)$$

where:

- F is the saturation value for very high implantation Damage .
- Damage is the implantation damage field as calculated with Sentaurus MC.
- α is a parameter that determines the sharpness of the transition between the low damage range at which werr increases linearly and the high damage range at which werr is close to its saturation value F .

A good fit to measured werr data for many implanted species, provided by Applied Materials has been obtained with the following calibrated coefficients:

- Oxide: $F = 2.70$, $\text{Damage}_{\text{reference}} = 5.2 \cdot 10^{21} \text{ cm}^{-3}$, $\alpha = 1.3$
- Nitride: $F = 2.45$, $\text{Damage}_{\text{reference}} = 8.0 \cdot 10^{21} \text{ cm}^{-3}$, $\alpha = 1.5$

Chapter 3: Guidelines for Additional Calibration

Calibration of Wet Etching Rate Modification by Ion Implantation

For data from other sources, different values might be needed to obtain an excellent match. In particular, [42] and [43] report about two times higher saturation values F compared to these values.

The reason for the difference between experimental findings from different sources is not known.

In addition to the damage effect, which dominates at low and medium implantation doses, the following formula has been applied to selected cases, to model the chemical effect on the wet etching rate:

$$\text{factor}_{\text{chemical}} = \frac{C_{\text{reference}} + \beta \cdot C_{\text{species}}}{C_{\text{reference}} + \gamma \cdot C_{\text{species}}} \quad (16)$$

Here, β and γ are coefficients. With [Equation 16](#), for small concentrations ($C_{\text{species}} \ll C_{\text{reference}}$), $\text{factor}_{\text{chemical}}$ equals 1.0. For huge concentrations ($C_{\text{species}} \gg C_{\text{reference}}$), $\text{factor}_{\text{chemical}}$ equals β/γ . Some implantation species (for example, F and P) increase the etching rate; whereas, other species (such as B, C, and Si) decrease it at high implantation doses ($\text{factor}_{\text{chemical}} < 1.0$). This chemical effect is specific for each species and has not been calibrated yet for all implantation species and concentrations. Therefore, it is the responsibility of users to find good parameters for [Equation 16](#) or a more suitable formula for modeling the chemical effect on werr for a particular use case.

Application

To calculate implantation damage in oxide and nitride, use the following statements:

```
pdbSetBoolean Oxide    Damage 1  
pdbSetBoolean Nitride  Damage 1
```

Ion implantation must be simulated with Sentaurus MC. In addition, you must use the latest version of Advanced Calibration, that is:

```
AdvancedCalibration 2022.03
```

Note:

Older versions of Advanced Calibration do not support the calculation of Damage in amorphous materials such as oxide and nitride.

It is recommended to set the parameter `MCDFactor` to 1.0 for all implantation species in oxide and nitride:

```
pdbSetDouble Oxide    Germanium MCDFactor 1.0  
pdbSetDouble Nitride  Germanium MCDFactor 1.0  
pdbSetDouble Oxide    Boron      MCDFactor 1.0  
pdbSetDouble Nitride  Boron      MCDFactor 1.0  
...  
...
```

Chapter 3: Guidelines for Additional Calibration

References

Without these statements, the Advanced Calibration functions `mcdfactor_<species>`, which are calibrated for implantation damage in silicon, are applied automatically to oxide and nitride, but it is better if you use 1.0.

Similarly, for analytic implantation, it is recommended to set the damage scaling factors in oxide and nitride to 1.0. For example:

```
fproc dfactor_Oxide_Boron { energy dose } { return 1.0 }
```

After setting `MCDFactor` or `dfactor` for oxide and nitride, the following example shows how to define the scaling of the etching rate for oxide as a function of implantation damage, using the calibration previously presented:

```
sel z="1.0+1.45*(Damage/8e21) / \
(exp((1.0/1.5)*log(1.0+exp(1.5*log(Damage/8e21)))))" \
Oxide name= EtchScale store
```

A subsequent `etch` command could be as follows:

```
etch time= 0.01 rate= 1 material= Oxide isotropic \
etch.rate.modifier = "EtchScale" steps=1 force.full.levelset
```

To ensure robust results for the etching, you might need to decrease the values of the `mgoals` arguments `dx`, `dy`, and `dz` with respect to their defaults. The best choice depends on the use case. For example:

```
mgoals dx=0.002 dy=0.002 dz=0.002
```

References

- [1] P. Pichler, *Intrinsic Point Defects, Impurities, and Their Diffusion in Silicon*, Computational Microelectronics, Vienna: Springer, 2004.
- [2] H. Bracht, N. A. Stolwijk, and H. Mehrer, “Equilibrium Concentrations of Intrinsic Point Defects in Silicon Determined by Zinc Diffusion,” in *Proceedings of the Seventh International Symposium on Silicon Materials Science and Technology (Semiconductor Silicon)*, vol. 94-10, San Francisco, CA, USA, pp. 593–602B, May 1994.
- [3] H. Bracht, E. E. Haller, and R. Clark-Phelps, “Silicon Self-Diffusion in Isotope Heterostructures,” *Physical Review Letters*, vol. 81, no. 2, pp. 393–396, 1998.
- [4] A. Ural, P. B. Griffin, and J. D. Plummer, “Self-Diffusion in Silicon: Similarity between the Properties of Native Point Defects,” *Physical Review Letters*, vol. 83, no. 17, pp. 3454–3457, 1999.
- [5] N. E. B. Cowern *et al.*, “Energetics of Self-Interstitial Clusters in Si,” *Physical Review Letters*, vol. 82, no. 22, pp. 4460–4463, 1999.

Chapter 3: Guidelines for Additional Calibration

References

- [6] P. M. Fahey, P. B. Griffin, and J. D. Plummer, "Point defects and dopant diffusion in silicon," *Reviews of Modern Physics*, vol. 61, no. 2, pp. 289–388, 1989.
- [7] I. Bork and H. Matsumoto, "On the Determination of Boron Diffusivities and Boron Interstitial Pair Binding Energies in Silicon," in *International Conference on Simulation of Semiconductor Processes and Devices (SISPAD)*, Tokyo, Japan, pp. 91–92, September 1996.
- [8] C. S. Rafferty *et al.*, "Simulation of cluster evaporation and transient enhanced diffusion in silicon," *Applied Physics Letters*, vol. 68, no. 17, pp. 2395–2397, 1996.
- [9] P. A. Stolk *et al.*, "Physical mechanisms of transient enhanced dopant diffusion in ion-implanted silicon," *Journal of Applied Physics*, vol. 81, no. 9, pp. 6031–6050, 1997.
- [10] L. Shao *et al.*, "Retardation of boron diffusion in silicon by defect engineering," *Applied Physics Letters*, vol. 78, no. 16, pp. 2321–2323, 2001.
- [11] L. F. Giles *et al.*, "Transient enhanced diffusion of B at low temperatures under extrinsic conditions," *Solid-State Electronics*, vol. 49, no. 4, pp. 618–627, 2005.
- [12] G. Impellizzeri *et al.*, "Role of fluorine in suppressing boron transient enhanced diffusion in preamorphized Si," *Applied Physics Letters*, vol. 84, no. 11, pp. 1862–1864, 2004.
- [13] J. M. Jacques *et al.*, "Fluorine-enhanced boron diffusion in amorphous silicon," *Applied Physics Letters*, vol. 82, no. 20, pp. 3469–3471, 2003.
- [14] B. J. Pawlak *et al.*, "Enhanced boron activation in silicon by high ramp-up rate solid phase epitaxial regrowth," *Applied Physics Letters*, vol. 86, p. 101913, 2005.
- [15] S. Mochizuki *et al.*, "Advanced Arsenic Doped Epitaxial Growth for Source Drain Extension Formation in Scaled FinFET Devices," in *IEDM Technical Digest*, San Francisco, CA, USA, pp. 811–814, December 2018.
- [16] R. Duffy *et al.*, "Low-temperature diffusion of high-concentration phosphorus in silicon, a preferential movement toward the surface," *Applied Physics Letters*, vol. 86, no. 8, p. 081917, 2005.
- [17] X. Li *et al.*, "Selective Epitaxial Si:P Film for nMOSFET Application: High Phosphorous Concentration and High Tensile Strain," *ECS Transactions*, vol. 64, no. 6, pp. 959–965, 2014.
- [18] V. C. Venezia *et al.*, "Dopant redistribution effects in preamorphized silicon during low temperature annealing," in *IEDM Technical Digest*, Washington, DC, USA, pp. 489–492, December 2003.
- [19] T. Noda, "Modeling of End-of-Range (EOR) Defects for Indium Channel Engineering," in *IEDM Technical Digest*, Washington, DC, USA, pp. 839–842, December 2001.
- [20] H. Graoui *et al.*, "TCAD Modeling and Experimental Investigation of Indium for Advanced CMOS Technology," in *14th International Conference on Ion Implantation Technology (IIT)*, Taos, NM, USA, pp. 126–130, September 2002.

Chapter 3: Guidelines for Additional Calibration

References

- [21] C. Zechner *et al.*, "Modeling Ultra Shallow Junctions Formed by Phosphorus-Carbon and Boron-Carbon Co-implantation," in *MRS Symposium Proceedings, Semiconductor Defect Engineering—Materials, Synthetic Structures and Devices II*, vol. 994, San Francisco, CA, USA, p. 0994–F11–17, April 2007.
- [22] C.-L. Liu *et al.*, "Ab initio modeling and experimental study of C–B interactions in Si," *Applied Physics Letters*, vol. 80, no. 1, pp. 52–54, 2002.
- [23] I. Ban, M. C. Öztürk, and E. K. Demirlioglu, "Suppression of Oxidation-Enhanced Boron Diffusion in Silicon by Carbon Implantation and Characterization of MOSFET's with Carbon-Implanted Channels," *IEEE Transactions on Electron Devices*, vol. 44, no. 9, pp. 1544–1551, 1997.
- [24] G. Zschätzsch *et al.*, "Fundamental Study on the Impact of C Co-Implantation on Ultra Shallow B Junctions," in *Extended Abstracts of the Ninth International Workshop on Junction Technology (IWJT)*, Kyoto, Japan, pp. 123–126, June 2009.
- [25] B. Colombeau *et al.*, "Ultra-Shallow Carborane Molecular Implant for 22-nm node p-MOSFET Performance Boost," in *Extended Abstracts of the Ninth International Workshop on Junction Technology (IWJT)*, Kyoto, Japan, pp. 27–30, June 2009.
- [26] C. I. Li *et al.*, "Enabling Solutions for 28nm CMOS Advanced Junction Formation," in *18th International Conference on Ion Implantation Technology (IIT)*, Kyoto, Japan, June 2010.
- [27] IST Project 027152 ATOMICS, *Advanced Front-End Technology Modeling for Ultimate Integrated Circuits*, for more information, go to <https://www.iisb.fraunhofer.de/content/dam/iisb2014/en/Documents/Research-Areas/Simulation/final-report-atomics.pdf>.
- [28] L. S. Adam *et al.*, "Diffusion of implanted nitrogen in silicon," *Journal of Applied Physics*, vol. 87, no. 5, pp. 2282–2284, 2000.
- [29] L. S. Adam *et al.*, "Diffusion of Implanted Nitrogen in Silicon at High Doses," in *MRS Symposium Proceedings, Si Front-End Processing—Physics and Technology of Dopant-Defect Interactions III*, vol. 669, p. J3.10, January 2001.
- [30] N. Zographos *et al.*, "Process Modeling of Chemical and Stress Effects in SiGe," in *19th International Conference on Ion Implantation Technology (IIT)*, Valladolid, Spain, pp. 212–216, June 2012.
- [31] R. Kögler *et al.*, "Excess vacancies in high energy ion implanted SiGe," *Journal of Applied Physics*, vol. 101, no. 3, p. 033508, 2007.
- [32] M. Posselt, L. Bischoff, and J. Teichert, "Influence of dose rate and temperature on ion-beam-induced defect evolution in Si investigated by channeling implantation at different doses," *Applied Physics Letters*, vol. 79, no. 10, pp. 1444–1446, 2001.
- [33] A. Renau, "Device performance and yield - A new focus for ion implantation," in *Extended Abstracts of International Workshop on Junction Technology (IWJT)*, Shanghai, China, 2010.

Chapter 3: Guidelines for Additional Calibration

References

- [34] F. Khaja *et al.*, "Benefits of Damage Engineering for PMOS Junction Stability," in *18th International Conference on Ion Implantation Technology (IIT)*, Kyoto, Japan, June 2010.
- [35] F. A. Khaja *et al.*, "Physical understanding of cryogenic implant benefits for electrical junction stability," *Applied Physics Letters*, vol. 100, no. 11, p. 112102, 2012.
- [36] R. D. Goldberg, J. S. Williams, and R. G. Elliman, "Amorphization of silicon by elevated temperature ion irradiation," *Nuclear Instruments and Methods in Physics Research B*, vol. 106, no. 1–4, pp. 242–247, 1995.
- [37] H.-J. Gossmann *et al.*, "Predictive Process Simulation of Cryogenic Implants for Leading Edge Transistor Design," in *19th International Conference on Ion Implantation Technology (IIT)*, Valladolid, Spain, pp. 225–228, June 2012.
- [38] A. Schmidt *et al.*, "Compact Process Model of Temperature Dependent Amorphization Induced by Ion Implantation," in *International Conference on Simulation of Semiconductor Processes and Devices (SISPAD)*, Bologna, Italy, pp. 197–200, September 2010.
- [39] N. Zographos, A. Tsibizov, and C. Zechner, "Continuum Modeling of Implantation and Thermal Processes for Advanced Devices Formation," in *20th International Conference on Ion Implantation Technology (IIT)*, Portland, OR, USA, pp. 189–194, June 2014.
- [40] N. Ioannou *et al.*, "Germanium substrate loss during low temperature annealing and its influence on ion-implanted phosphorous dose loss," *Applied Physics Letters*, vol. 93, no. 10, p. 101910, 2008.
- [41] Y.-S. Oh and D. E. Ward, "A Calibrated Model for Trapping of Implanted Dopants at Material Interface During Thermal Annealing," in *IEDM Technical Digest*, San Francisco, CA, USA, pp. 509–512, December 1998.
- [42] E. Bellandi and V. Soncini, "SiO₂ etch rate modification by ion implantation," *Thin Solid Films*, vol. 524, pp. 75–80, December 2012.
- [43] R. Charavel and J.-P. Raskin, "Etch Rate Modification of SiO₂ by Ion Damage," *Electrochemical and Solid-State Letters*, vol. 9, no. 7, pp. G245–G247, 2006.

4

Advanced Calibration for 4H-SiC Process Simulation

This chapter gives an introduction to the use of Advanced Calibration for silicon carbide (SiC).

Content of Advanced Calibration File for 4H-SiC Simulation

Sentaurus Process has one material corresponding to silicon carbide – SiliconCarbide – which also has an alias `SiC`. The default parameters for material `SiliconCarbide` correspond to the 4H-SiC polytype. The Advanced Calibration file for SiC contains the recommended settings for 4H-SiC simulations. Advanced Calibration mainly supports process simulation of the 4H-SiC polytype, because it is the most widely used SiC polytype in electronics production. Only some of its parameters are valid for other SiC polytypes, therefore, the parameter file must not be used for the simulation of other SiC polytypes as it is, but must be adapted appropriately by users. In general, this set of parameters is less mature than the one for silicon and SiGe, especially with respect to dopant activation and diffusion, and the treatment of point defects in SiC.

The Advanced Calibration file `AdvCal_SiC_2022.03.fps` for 4H-SiC is divided into the following parts, which contain numbered sections and are executed in sequence:

- Part 1: Basic model switches
- Part 2: Settings for Monte Carlo implantation
- Part 3: Ion implantation and initial conditions

Part 1: Basic Model Switches

Part 1 of the Advanced Calibration file offers a choice that is recommended by Synopsys for most SiC applications.

It is often useful to reduce the number of equations to be solved in order to save CPU time. On the other hand, it might be sometimes necessary to select models that are more

Chapter 4: Advanced Calibration for 4H-SiC Process Simulation

Part 1: Basic Model Switches

sophisticated than the default choice, even at the cost of increasing the CPU time. In this chapter, the possible changes with respect to the default model switches are explained.

The most elegant way to change a basic model switch is adding a corresponding line at the beginning of a project-specific or user-specific calibration file, which is sourced after loading the Advanced Calibration file. In this way, you can track the differences to the default suggestions of Synopsys.

First, `maxAnnealT` is increased to the melting point value in 4H-SiC (2730°C) from the default 1400°C to allow high-temperature annealings, which are typical for SiC process simulations:

```
pdbSet Diffuse maxAnnealT 2730.0
```

The `set4H-SiC` procedure sets the number of lattice parameters for the 4H-SiC polytype of Silicon Carbide. Although these parameters are the default ones, the procedure is placed into the Advanced Calibration file as a reference for users who want to create their own parameter files for other SiC polytypes, based on Silicon Carbide material.

Numeric solver parameters, which are necessary to ensure correct simulation results at low-temperature anneal (`NegErrCntrl`) and stable convergence with the transient activation model (`fullNewton`), are set by the following command:

```
math NegErrCntrl fullNewton
```

Poisson Equation

The Poisson equation is switched on in SiC by the following command:

```
pdbSet SiC Potential Poisson 1
```

Besides the formally more correct distribution of electrostatic potential and mobile carrier densities, simulations with the Poisson equation lead to better convergence with Fermi-dependent models, due to smoother potential and carrier profiles.

The value of permittivity for 4H-SiC is set to 10.03, that is, the one which applies to the $\{0001\}$ direction (parallel to the c-axis). The value of permittivity normal to the c-axis equals 9.66 [1]:

```
pdbSet SiC Potential Permittivity 10.03
```

The intrinsic carrier concentration (`ni`) of 4H-SiC is set by the density-of-states (DOS) model:

```
pdbSet SiC Potential Use.DOS 1
```

Dopant Cluster Models in 4H-SiC

In Sentaurus Process, the `Solid` model is the default for dopant activation in SiC. The default values of the `Solubility` parameters for Al and B are taken without calibration from [2]; whereas, the values of the `Solubility` parameters for N and P are based on theoretical work [3]. The phosphorus solubility value was increased by a factor of four to match experimental values of activation at 1700°C from [4].

A major disadvantage of the `Solid` model is that it does not reflect the nonequilibrium nature of dopant activation. For example, with the `Solid` model, the activation instantly follows the annealing temperature. In Advanced Calibration, the `Transient` activation model is switched on for Al, B, N, and P. Activation of dopants in SiC is a complex process, which includes dynamic interaction of dopants with different defects and defect agglomerations. It depends on the implantation conditions, the presence of co-implants, the anneal atmosphere, the ramp rates, and so on [5][6][7][8][9]. Although the `Transient` model itself cannot simulate such complex behavior in detail and cannot capture all the physical effects, it is still more physical than the `Solid` model and can emulate, to some extent, the nonequilibrium transient behavior of the activation process.

The current Advanced Calibration values of the `Transient` model parameters for Al, B, N, and P were obtained by qualitative calibration to sheet resistance, Hall measurements, and capacity measurements described in the literature. Most of the experimental structures had homogeneously implanted layers, obtained by multiple implantations, and were annealed at approximately 1500–1700°C [4][8][9][10][11][12][13][14][15], and at a higher temperature for aluminum [5][16]. In general, qualitative rather than quantitative agreement to published experiments was achieved. Some experimental trends (such as reduction of activation for Al with increasing annealing time at 1800°C in [5]) are not captured. Overall calibration quality is much worse than for the `Transient` activation model in silicon.

However, taking into account the strong dependency of the activation on particular process conditions, you should use the `Transient` activation parameters as a starting point for custom calibration of dopant activation. Since exact information about amorphization is not available in most publications (neither is it calibrated in Sentaurus MC for 4H-SiC), the `AcInit` and `AmInit` parameters for initial dopant activation are both set to the same value 10^{15} cm^{-3} , which is smaller than the typical background doping concentration in epitaxial layers. For fine-tuning dopant activation in SiC and, sometimes, also for improving the convergence of SiC process simulation, you can change the values of the parameter `CluRate` for selected dopants, as needed for a specific technology. `CluRate` scales the rate at which the equilibrium balance between active dopants and clustered dopants is established.

It is difficult to interpret the experimental results of dopant activation in SiC for various reasons:

- Uncertainties about the value of the Hall scattering factors (especially for holes) [17][18].
- Temperature dependency of the degeneracy factors of acceptors, which is not included in the `IncompleteIonization` model of Sentaurus Device [19][20][21].
- Uncertainties about the ionization levels of active dopants (especially for concentrations above 10^{19} cm^{-3}).
- The presence of high-concentration effects (for example, hopping transport) during the ionization of active dopants and carrier transport [22].

In addition, ion-implanted layers contain high concentrations of defects, which remain at relatively high concentrations even after high-temperature anneals. These defects serve as deep-doping compensation centers and carrier-scattering centers, thereby affecting the net active doping concentration, the concentrations of the mobile carriers, and the carrier mobility. An interesting approach for the consideration of such defects is suggested in [23].

Note:

Such defects have not been included in the simulations, which might explain the systematic underestimation of sheet resistance, which was observed in the calibrations.

Dopant Transport at the Oxide–SiC Interface

Dopant dose loss is not calibrated for the oxide–SiC (`Ox_SiC`) interface in TCAD Sentaurus tools. The existing Parameter Database default parameters of Sentaurus Process are copied literally from the `Oxide_Si` interface and, therefore, they do not guarantee the trustworthiness of simulation results.

Since there are no trustworthy parameters for the segregation of dopants, the simplest possible `HomNeumann` boundary condition is set explicitly at the `Ox_SiC` interface in the Advanced Calibration file. Of course, you can specify other types of boundary condition (for example, `Segregation` or `ThreePhaseSegregation`) at the `Ox_SiC` interface as well as the parameters for the boundary conditions.

Boron Evaporation From the SiC Surface

Significant boron dose loss has been observed experimentally after high-temperature ($> 1500^\circ\text{C}$) anneal of 4H-SiC [2][12][24]. Advanced Calibration simulates boron dose loss by boron evaporation at SiC–gas interfaces using natural boundary conditions:

```
pdbSetSwitch Gas_SiC Boundary BoundaryCondition Natural
```

Chapter 4: Advanced Calibration for 4H-SiC Process Simulation

Part 2: Settings for Monte Carlo Implantation

The boron evaporation rate is controlled by the `Ksurf` parameter. The value of `Ksurf` is set in Advanced Calibration by the following command:

```
pdbSetDouble Gas_SiC Boron Ksurf {[expr 1e4*[pdbGet SiC B Dstar]]}
```

This value is suitable for 1700°C anneals from [24], where low-temperature preannealing (2 hours at 900°C) was used to reduce boron dose loss: For high-temperature anneals without preannealing [12], an order of magnitude larger value of `Ksurf` is required. For the correct simulation of boron evaporation at high-temperature (> 1500°C) anneals, it is necessary to remove the covering oxide from the SiC surface. For all other dopants except for boron, zero values of `Ksurf` are set at SiC–gas interfaces by default, which is equivalent to the Neumann boundary conditions for these dopants.

Part 2: Settings for Monte Carlo Implantation

There has been additional calibration of Sentaurus MC to improve the accuracy of simulations for implantations of aluminum, boron, and nitrogen into 4H-SiC with a wafer surface orientation close to (0001).

The calibration is based on comparison of simulation results to SIMS measurements of as-implanted profiles, either taken from publications [25][26][27][28][29] or provided by companies who support the calibration efforts of Synopsys. The data includes implantations at room temperature as well as implantations into heated substrates. The calibration focused on the following range of implantation energies and doses:

- Aluminum and nitrogen:
 - Energy range between 10 keV and 5 MeV
 - Room temperature or hot (often 500°C) implantation
 - Focus on off-channel implantations and implantation in [0001] channeling direction; the calibration is less predictive for [1123] channeling
- Boron:
 - Energies between 10 keV and 5.8 MeV
 - Room temperature or hot (often 500°C) implantation
 - Focus on off-channel implantations; three data points for [0001] channeling direction
- Phosphorus:
 - Energies between 10 keV and 5 MeV
 - Room temperature only
 - Off-channel implantations and implantation in [0001] channeling direction

Chapter 4: Advanced Calibration for 4H-SiC Process Simulation

Part 2: Settings for Monte Carlo Implantation

In total, more than 200 SIMS profiles have been used for the calibration, typically, with a small wafer miscut angle and a small tilt angle. The largest number of SIMS profiles was used for the calibration of Al and N implantation. Only about 20 profiles were used for the calibration of P implantation.

When using tilted implantations into wafers with miscut, the results depend on the miscut angle, the direction of the miscut, the crystal orientation of the primary wafer flat, the tilt angle, and the ion beam rotation angle. In some published data used for the calibration, not all of the relevant angles and orientations were specified explicitly. Therefore, assumptions were made about correct angles, or data was omitted from the calibration.

The calibration is widely based on implantation data for off-channel directions and a smaller amount of data for [0001] channeling directions or close to the [0001] channeling direction. For MeV Al and P implantation, the shape of the channeling tails shows some mismatch with SIMS data used in the calibration. The calibration is less accurate for other channeling directions in SiC.

For hot implantations, the highest implantation energies of the experimental data that was referred are approximately 1000 keV, and the reproducibility of results for a higher energy than that might be less reliable. For P, the calibration is limited to implantations at room temperature and might need to be modified for implantations at different temperatures.

The displacement threshold and the temperature dependency of damage were adjusted taking into account experimental data from Kalinina [30] and the references therein. The displacement threshold in 4H-SiC is larger for Si atoms than for C atoms. It depends on the direction of the displacement, the nature of the impacting projectile, and the amount of already accumulated damage. The smallest displacement threshold value in a perfect crystal reported in the literature (for C atoms) is 18 eV [31]. In the binary collision simulators, typically some averaged values for the displacement threshold are used. Sentaurus MC allows only a single constant displacement threshold value in SiC. In Advanced Calibration for 4H-SiC, the `disp.thr` value has increased from the default 15 eV to 20 eV to achieve better correspondence to the real value.

Parameters Used in the Calibration

Part 2 of `AdvCal_SiC_2022.03.fps` contains calibrated model parameters for MC implantation of Al, B, N, and P into 4H-SiC and Oxide.

Some of the parameters depend on the implantation energy and on the wafer temperature during implantation. For a parameter definition as a function of energy, all parameters are defined within the callback procedure `_AdvCal::ImpPreProcess`, which is called by Sentaurus Process before executing the actual MC calculation, and to which the implantation conditions such as species, energy, and dose are handed over as arguments.

To overwrite the settings performed by the `_AdvCal::ImpPreProcess` procedure, you can define the `UserImpPreProcess` procedure in your own specific parameter file. The

Chapter 4: Advanced Calibration for 4H-SiC Process Simulation

Part 2: Settings for Monte Carlo Implantation

UserImpPreProcess procedure uses syntax similar to that of _AdvCal::ImpPreProcess (see [Example of a User Calibration File on page 184](#)).

The wafer temperature during implantation is accessed inside the procedure _AdvCal::ImpPreProcess by the simGetDouble Diffuse temp statement. You must specify the implantation temperature (in degree Celsius) in the implant command. For example:

```
implant Arsenic dose= 2.0e+13 energy= 160 tilt= 0 temperature= 450
```

If no temperature is specified, then the simGetDouble Diffuse temp statement gives the default implantation temperature (26.84°C), which is specified (in kelvin) by:

```
pdbSet MCImplant Temperature 300.0
```

The energy dependence and temperature dependence of parameters is usually expressed with the help of the Sentaurus Process function LinInterpol, which performs a piecewise linear interpolation based on a list of (x,y) pairs. For the energy dependence of the parameter DebyeTemperature at high energies, the function XYLogInterpol is used, which performs a piecewise linear interpolation between points in a plot, which is logarithmic in the x-axis and y-axis.

The following sections briefly discuss the parameters used in the calibration from a calibration perspective. For the definition of these parameters, see the *Sentaurus™ Process User Guide*.

LSS.pre, nucl.cor

The LSS.pre parameter scales the nonlocal electronic stopping. It is defined as a function of energy and, for B and N, also as a function of temperature. Small changes of LSS.pre can be used to adjust the depth of the profile, if needed.

For low energies (< 40 keV), the profile depth is not very sensitive to changes of LSS.pre. You can adjust the profile depth for low-energy implantations by fine-tuning the parameter nucl.cor, which scales the energy loss in nuclear scattering.

DebyeTemperature, d.sim

These parameters are relevant for scattering processes into channeling directions or out of channeling directions.

In theory, DebyeTemperature should be a material constant. It plays a role in the impact of thermal lattice vibrations on the scattering of ions and, thereby, influences the fraction of ions that travels along channeling directions and, for some implantation conditions, that form a second *channeling* peak. In practice, the best match to SIMS data over a wide range of implantation conditions is obtained when defining DebyeTemperature as a function of implantation energy and temperature. With increasing implantation energy, you must reduce

Chapter 4: Advanced Calibration for 4H-SiC Process Simulation

Part 2: Settings for Monte Carlo Implantation

`DebyeTemperature`, especially for room-temperature implantations. This is reflected in the formulas implemented.

The `d.sim` parameter also influences the rate of ion scattering from random directions into channeling directions, and vice versa. It is used when Sentaurus Process determines whether subsequent collisions should be considered to be multibody collisions. Like `DebyeTemperature`, you can use `d.sim` to adjust the fraction of ions in the channeling direction.

Fine-tuning `DebyeTemperature` is preferable to fine-tuning `d.sim`, because there are fewer side effects for implantations with different `tilt` or rotation angles. Therefore, in most practical cases (except perhaps implantations in [1123] channeling directions or close to them), it is recommended to use only `DebyeTemperature` for fine-tuning the fraction of ions in the “channeling peak” of a profile.

For medium and high doses, the value of `surv.rat` is also important (see [surv.rat](#), [sat.par](#)).

nloc.pre, nloc.exp, scr.par

The `nloc.pre` and `nloc.exp` parameters determine the fraction of *nonlocal* electronic stopping and, therefore, mainly affect the depth of channeling ions. The smaller `nloc.pre`, the less nonlocal electronic stopping, and the deeper the profile, especially in the channeling part. The `nloc.exp` parameter describes the dependence on implantation energy and is usually not touched for fine-tuning.

The `scr.par` parameter scales the energy loss by local electronic stopping. Often, a fine-tuning of `scr.par` has a similar affect on profiles as a fine-tuning of `nloc.pre`.

surv.rat, sat.par

The `surv.rat` parameter scales the amount of crystal damage created during implantation. With increasing crystal damage, the ion channels inside the SiC crystal eventually become blocked. Therefore, for medium and high doses, `surv.rat` governs the number of ions that end up in the channeling tail. Furthermore, the crystal damage is used to calculate the amorphization.

The `sat.par` parameter is important only for high doses and describes the saturation of crystal damage by recombination during implantation.

Interp.Min.Energy, Interp.Max.Energy

Sentaurus MC uses two methods for the calculation of binary collisions. For most energies, scattering tables are used. For the highest energies, the collisions are calculated using a Coulombic form of the potential between the collision partners. In the Sentaurus MC defaults, the high-energy range starts when the so-called *dimensionless energy* exceeds the table limit of 1000. This corresponds to an energy of ~5180 keV for B–C collisions and

Chapter 4: Advanced Calibration for 4H-SiC Process Simulation

Part 2: Settings for Monte Carlo Implantation

~9780 keV for B–Si binary collisions, and even higher energies for heavier particles. For N–C collisions, a dimensionless energy of 1000 corresponds to ~8600 keV.

You can define a transition energy range in which Sentaurus MC interpolates between the two methods. In `AdvCal_SiC_2022.03.fps`, such a transition range is defined for B implantations only. The following parameters are used:

```
pdbSetDouble SiC Boron Interp.Min.Energy 3800  
pdbSetDouble SiC Boron Interp.Max.Energy 5200
```

These mean that, up to 3800 keV, scattering tables are used. For collisions with B energies higher than 3800 keV, binary collisions are calculated using interpolation between the two methods. If energies exceed 5200 keV or if the dimensionless energy for collisions exceeds the value 1000, then binary collisions are calculated based on a Coulombic form of the interatomic potential.

Recommendations for Fine-Tuning of Amorphization

The calibration presented in this chapter is based entirely on comparison of simulated profiles to SIMS data. No calibration has been performed for a possible amorphization of SiC by high-dose ion implantations, due to lack of suitable experimental data.

If you want to study amorphization of SiC using Monte Carlo implantation, then you should test the accuracy of TCAD results against measured data on the existence and thickness of amorphized layers after implantation. The following parameters are recommended for fine-tuning of amorphization:

- `surv.rat`
- `sat.par`

A change of `surv.rat` has a stronger impact on the channeling tail of an as-implanted profile.

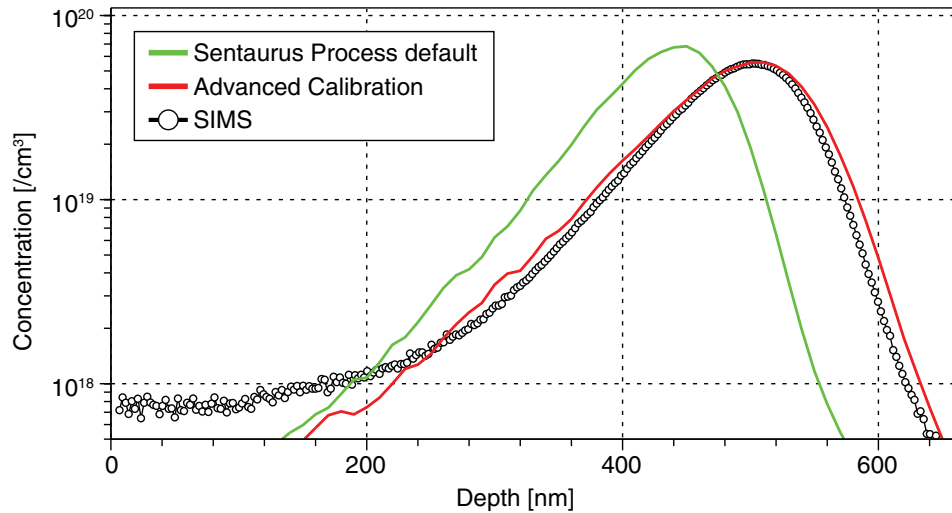
To completely suppress amorphization for hot implantations, set `sat.par` to a high value (for example, 10). This suppresses the increase of crystal damage beyond a level of $N_{\text{dens}} / \text{sat.par}$, where N_{dens} is the lattice density.

Illustration of Calibration Results

Typically, using the calibrated parameters will lead to a significantly better agreement between simulations results and SIMS data for high-energy implantations. This is illustrated in [Figure 38](#).

A detailed discussion of the simulation accuracy for all of the data studied is beyond the scope of this user guide.

Figure 38 Comparison of simulation results for default and calibrated parameters with nitrogen SIMS from [25]: implantation conditions are N 400 keV, dose $1.0e15 \text{ cm}^{-2}$, $\text{tilt}=7.2^\circ$, $\text{rotation}=0$, surface orientation (001), miscut= 3.5° towards (110). The direction of the primary wafer flat (110) is assumed, and simulations have been performed with Sentaurus Process Version T-2022.03.



Part 3: Ion Implantation and Initial Conditions

In most SiC simulations, very simple models such as the default Sentaurus Process Constant and Solid models for dopant diffusion and activation in SiC are used. Therefore, to reduce the simulation time, the point-defect transport equations are not solved in SiC by default. To compute the point-defect transport in SiC, use the following command:

```
pdbSet SiC Compute.Point.Defect 1
```

The following command provides correct initialization of the point defects in the beginning of a diffuse command:

```
pdbSet Diffuse Use.New.Init.Method 1
```

References

- [1] L. Patrick and W. J. Choyke, "Static Dielectric Constant of SiC," *Physical Review B*, vol. 2, no. 6, pp. 2255–2256, 1970.
- [2] M. K. Linnarsson *et al.*, "Aluminum and boron diffusion in 4H-SiC," in *MRS Symposium Proceedings, Silicon Carbide—Materials, Processing, and Devices*, vol. 742, pp. K6.1.1–K6.1.11, 2002.

Chapter 4: Advanced Calibration for 4H-SiC Process Simulation

References

- [3] M. Bockstedte, A. Mattausch, and O. Pankratov, "Solubility of nitrogen and phosphorus in 4H-SiC: A theoretical study," *Applied Physics Letters*, vol. 85, no. 1, pp. 58–60, 2004.
- [4] M. Laube *et al.*, "Electrical activation of high concentrations of N⁺ and P⁺ ions implanted into 4H–SiC," *Journal of Applied Physics*, vol. 92, no. 1, pp. 549–554, 2002.
- [5] Y. Negoro *et al.*, "Electrical activation of high-concentration aluminum implanted in 4H-SiC," *Journal of Applied Physics*, vol. 96, no. 9, pp. 4916–4922, 2004.
- [6] K. A. Jones *et al.*, "Effects of high-temperature anneals on 4H–SiC Implanted with Al or Al and Si," *Journal of Applied Physics*, vol. 96, no. 10, pp. 5613–5618, 2004.
- [7] A. Poggi *et al.*, "Effects of heating ramp rates on the characteristics of Al implanted 4H–SiC junctions," *Applied Physics Letters*, vol. 88, no. 16, p. 162106, 2006.
- [8] J. Senzaki, K. Fukuda, and K. Arai, "Influences of postimplantation annealing conditions on resistance lowering in high-phosphorus-implanted 4H–SiC," *Journal of Applied Physics*, vol. 94, no. 5, pp. 2942–2947, 2003.
- [9] Y. Negoro, T. Kimoto, and H. Matsunami, "Carrier compensation near tail region in aluminum- or boron-implanted 4H–SiC (0001)," *Journal of Applied Physics*, vol. 98, no. 4, p. 043709, 2005.
- [10] E. M. Handy *et al.*, "Variable-dose ($10^{17} – 10^{20}$ cm⁻³) phosphorus ion implantation into 4H–SiC," *Journal of Applied Physics*, vol. 88, no. 10, pp. 5630–5634, 2000.
- [11] C. P. Morath, *Electrical Characterization of Ion-Implanted 4H-Silicon Carbide*, Master's thesis, Air Force Institute of Technology, Air University, Ohio, USA, March 1999.
- [12] T. Troffer *et al.*, "Doping of SiC by Implantation of Boron and Aluminum," *Physica Status Solidi A*, vol. 162, no. 1, pp. 277–298, 1997.
- [13] M. V. Rao *et al.*, "Ion-implantation in bulk semi-insulating 4H–SiC," *Journal of Applied Physics*, vol. 86, no. 2, pp. 752–758, 1999.
- [14] N. S. Saks *et al.*, "Low-dose aluminum and boron implants in 4H and 6H silicon carbide," *Journal of Applied Physics*, vol. 90, no. 6, pp. 2796–2805, 2001.
- [15] N. S. Saks, S.-H. Ryu, and A. V. Suvorov, "Low-dose n-type nitrogen implants in 4H-SiC," *Applied Physics Letters*, vol. 81, no. 26, pp. 4958–4960, 2002.
- [16] R. Nipoti *et al.*, "Microwave Annealing of Very High Dose Aluminum-Implanted 4H-SiC," *Applied Physics Express*, vol. 4, no. 11, p. 111301, 2011.
- [17] F. Schmid *et al.*, "Hall Scattering Factor for Electrons and Holes in SiC," *Silicon Carbide, Advanced Texts in Physics*, W. J. Choyke, H. Matsunami, and G. Pensl (eds.), Berlin: Springer, 2004.
- [18] A. Koizumi, J. Suda, and T. Kimoto, "Temperature and doping dependencies of electrical properties in Al-doped 4H-SiC epitaxial layers," *Journal of Applied Physics*, vol. 106, no. 1, p. 013716, 2009.

Chapter 4: Advanced Calibration for 4H-SiC Process Simulation

References

- [19] H. Matsuura, "Investigation of a distribution function suitable for acceptors in SiC," *Journal of Applied Physics*, vol. 95, no. 8, pp. 4213–4218, 2004.
- [20] H. Matsuura, "Influence of excited states of a deep substitutional dopant on majority-carrier concentration in semiconductors," *Physical Review B*, vol. 74, no. 24, p. 245216, 2006.
- [21] H. Matsuura, "Determination Methods of Densities and Energy Levels of Impurities and Defects Affecting Majority-Carrier Concentration in Next-Generation Semiconductors," *Advances in Condensed Matter and Materials Research*, vol. 10, H. Geelvinck and S. Reynst (eds.), Hauppauge, New York: Nova Science Publishers, pp. 301–356, 2011.
- [22] A. Parisini *et al.*, "Remarks on the room temperature impurity band conduction in heavily Al⁺ implanted 4H-SiC," *Journal of Applied Physics*, vol. 118, no. 3, p. 035101, 2015.
- [23] F. Giannazzo, F. Roccaforte, and V. Raineri, "Acceptor, compensation, and mobility profiles in multiple Al implanted 4H-SiC," *Applied Physics Letters*, vol. 91, no. 20, p. 202104, 2007.
- [24] H. Bracht *et al.*, "Diffusion of boron in silicon carbide: Evidence for the kick-out mechanism," *Applied Physics Letters*, vol. 77, no. 20, pp. 3188–3190, 2000.
- [25] R. Stief, *Dotierung von 4H-SiC durch Ionenimplantation*, PhD thesis, University of Erlangen-Nuremberg, Germany, 1999.
- [26] J. Wong-Leung, M. S. Janson, and B. G. Svensson, "Effect of crystal orientation on the implant profile of 60 keV Al into 4H-SiC crystals," *Journal of Applied Physics*, vol. 93, no. 11, pp. 8914–8917, 2003.
- [27] K. Mochizuki *et al.*, "Detailed Analysis and Precise Modeling of Multiple-Energy Al Implantations Through SiO₂ Layers Into 4H-SiC," *IEEE Transactions on Electron Devices*, vol. 55, no. 8, pp. 1997–2003, 2008.
- [28] S. Morata, F. Torregrosa, and T. Bouchet, "Simulation of Ion Implantation in SiC: Dopant Profiling and Activation," *Materials Science Forum*, vol. 615–617, pp. 449–452, March 2009.
- [29] K. Mochizuki *et al.*, "Selection of ion species suited for channelled implantation to be used in multi-epitaxial growth for SiC superjunction devices," *Japanese Journal of Applied Physics*, vol. 58, no. 5, p. 050905, 2019.
- [30] E. V. Kalinina, "The Effect of Irradiation on the Properties of SiC and Devices Based on this Compound," *Semiconductors*, vol. 41, no. 7, pp. 745–783, 2007.
- [31] J. Lefèvre *et al.*, "Silicon threshold displacement energy determined by photoluminescence in electron-irradiated cubic silicon carbide," *Journal of Applied Physics*, vol. 105, no. 2, p. 023520, 2009.

Part II: Advanced Calibration in Sentaurus Process Kinetic Monte Carlo

This part of the *Advanced Calibration for Process Simulation User Guide* contains the following chapters:

- [Chapter 5, Using Advanced Calibration File of Sentaurus Process KMC](#)
- [Chapter 6, Contents of Advanced Calibration of Sentaurus Process KMC](#)
- [Chapter 7, Guidelines for Additional Calibration](#)

5

Using Advanced Calibration File of Sentaurus Process KMC

This chapter gives an introduction to the use of Advanced Calibration in a process simulation with Sentaurus Process Kinetic Monte Carlo (Sentaurus Process KMC).

Advanced Calibration is a selection of models and parameters, which is recommended by Synopsys to be used for accurate process simulation. In Sentaurus Process KMC, this selection of models and parameters is contained in a text file, which can be opened with any standard text editor.

By sourcing the Advanced Calibration file at the beginning of a process simulation, the standard calibration of Synopsys is selected. If needed, you can change or extend the Advanced Calibration. This can be performed by either sourcing an additional calibration file that contains the required parameter changes or editing the Advanced Calibration file with a text editor.

Location of Advanced Calibration File

The Advanced Calibration file is the ultimate product of Synopsys' calibration efforts. For each release of Sentaurus Process, there is a new Advanced Calibration file that includes the best and latest set of models and parameters. To ensure backward compatibility, previous Advanced Calibration files are still available.

The files for the Advanced Calibration of Sentaurus Process KMC in this release are located at:

```
$STROOT/tcad/$STRELEASE/lib/sprocess/TclLib/AdvCal
```

The default file is named `AdvCal_KMC_2022.03.fps`. It represents the first version of Advanced Calibration T-2022.03. Older versions of the Advanced Calibration file can be found in the same directory. For example, the file `AdvCal_KMC_2021.06.fps` contains the Advanced Calibration file for Version S-2021.06 and is available for backward compatibility.

Using Advanced Calibration

To use the Advanced Calibration of Sentaurus Process KMC, you must select the atomistic mode by using the command `SetAtomistic` followed by the command `AdvancedCalibration`, which is the same one as for the continuum Advanced Calibration. The command `AdvancedCalibration` checks whether the atomistic mode is set and loads the corresponding Advanced Calibration file. Therefore, at the beginning of the input file, insert the lines:

```
SetAtomistic  
AdvancedCalibration 2022.03
```

To load Advanced Calibration of Sentaurus Process KMC in continuum mode, you must use the `KMC` flag:

```
AdvancedCalibration KMC
```

Alternatively, a local copy of this file can be sourced by using:

```
source ./AdvCal_KMC_2022.03.fps
```

In addition, it is recommended to load Advanced Calibration for continuum Sentaurus Process before the one of Sentaurus Process KMC to select the calibration for continuum models that are also used in atomistic mode, such as those for mechanics and oxidation. Therefore, you should also select the command `AdvancedCalibration` for continuum Advanced Calibration before switching to the atomistic mode by using the `SetAtomistic` command.

Note:

The interoperability between Advanced Calibration for continuum Sentaurus Process and Advanced Calibration for Sentaurus Process KMC, meaning the mapping of solutions in continuum mode to particles in atomistic mode, is controlled by the commands `PDE2KMC` and `KMC2PDE` (see *Sentaurus™ Process User Guide, Translating Atomistic and Nonatomistic Information*).

For ultrashallow junction experiments, the recommended minimum simulation size is 500 nm × 40 nm × 40 nm. The depth (x-coordinate) of at least 500 nm is needed for accurate simulation of the point-defect evolution, and a surface (y-coordinate and z-coordinate) of 40 nm × 40 nm is needed for the accurate simulation of the damage accumulation during full cascade Monte Carlo implantation simulation.

Additional Calibration by Users

Advanced Calibration is based on the assumption that all parameters that are not changed in the parameter files are the default parameters of Sentaurus Process KMC. To use the Advanced Calibration file `AdvCal_KMC_2022.03.fps`, it must be sourced before the real process description.

After sourcing `AdvCal_KMC_2022.03.fps`, you can change the model switches or parameter values of the physical models. Ideally, this should be performed by experienced users with a good understanding of the models of Sentaurus Process KMC.

For the process simulation of silicon technology, Advanced Calibration is usually the best starting point. You can further increase the accuracy for a certain technology by additional fine-tuning of a few physical parameters.

The best way to perform this is to put all additional calibration in a user calibration file, for example, `my_calibration.fps`. This file includes all project-specific changes of physical parameters with respect to Advanced Calibration.

In the process simulation file, at the beginning of the process simulation, you insert the lines:

```
SetAtomistic  
AdvancedCalibration 2022.03  
source ./my_calibration.fps
```

This approach allows you to:

- Separate the calibration and the process descriptions completely.
- Use the Advanced Calibration file as a starting point.
- Summarize all project-specific calibration in a short and clear text file.

6

Contents of Advanced Calibration of Sentaurus Process KMC

This chapter explains the contents of the Advanced Calibration file of Sentaurus Process Kinetic Monte Carlo (Sentaurus Process KMC) and documents the origin of the parameter values.

Overview

The focus of Advanced Calibration is monocrystalline silicon, germanium, and SiGe for all Ge mole fractions. The calibration for silicon and SiGe with low Ge mole fraction (≤ 0.5) is the most mature and reliable. On the other hand, the calibration for pure germanium is less mature and reliable, and the calibration for SiGe with high Ge mole fraction (> 0.5) is the least mature and reliable. Most of the model equations and model parameters are taken from reliable publications. In addition, a rigorous calibration has been performed by Synopsys, based on a SIMS database.

The Advanced Calibration of Sentaurus Process in continuum mode (see [Chapter 2 on page 26](#)), which has proven good accuracy for a wide range of ultrashallow junction (USJ) experiments, serves as the starting point for the Advanced Calibration of Sentaurus Process KMC. Wherever possible, the parameters are inherited from the continuum approach to the kinetic Monte Carlo (KMC) approach.

However, the calibration of the continuum models is verified and optimized for a high temperature range (600°C–1100°C) only, whereas the kinetic Monte Carlo parameters should be valid below room temperature as well. Moreover, some parameters and models cannot be translated directly from the atomistic world to the continuum world. Taking into account these two restrictions, the strategy is to translate the continuum Advanced Calibration parameters if feasible, and to prefer or calibrate the default kinetic Monte Carlo parameters where it is favorable.

Chapter 6: Contents of Advanced Calibration of Sentaurus Process KMC

Overview

The Advanced Calibration file `AdvCal_KMC_2022.03.fps` is divided into the following sections, which contain numbered subsections and are executed in sequence:

- Section 1: Silicon material
- Section 2: Germanium material
- Section 3: SiGe material
- Section 4: Epitaxy

The first three sections cover the KMC particle parameters and the lattice KMC (LKMC) recrystallization parameters. These three sections are divided into two parts:

- Part 1: Model parameters for damage and point defects
- Part 2: Model parameters for impurities

The fourth section covers the LKMC epitaxy model parameters for silicon, germanium, and SiGe.

This chapter is organized slightly differently for simplicity:

- [Part 1: Model Parameters for Implantation Damage and Point Defects on page 218](#) for the materials silicon, germanium, and SiGe (of Sections 1–3)
- [Part 2: Model Parameters for Impurities on page 231](#) for the materials silicon, germanium, and SiGe (of Sections 1–3)
- [Section 4: Model Parameters for Epitaxial Growth on page 256](#)

Supported Materials

Advanced Calibration for Sentaurus Process KMC supports monocrystalline silicon, germanium, and SiGe.

Pure silicon is modeled by the Sentaurus Process material `Silicon` with a native oxide modeled by the Sentaurus Process material `Oxide`, while pure germanium is modeled by the Sentaurus Process material `Germanium` with the native oxide `GeOxide`.

SiGe is modeled by the Sentaurus Process material `Silicon` with a field `Germanium`, which Sentaurus Process KMC treats as a nonatomic impurity in silicon.

Note:

It is not recommended to use the Sentaurus Process material `SiliconGermanium`, mainly to prevent any artificial boundaries between the `Silicon` and `SiliconGermanium` materials.

Chapter 6: Contents of Advanced Calibration of Sentaurus Process KMC

Part 1: Model Parameters for Implantation Damage and Point Defects

The Ge mole fraction dependency of SiGe can be modeled in two ways:

- By default, Ge effects are modeled by linear correction factors. Furthermore, the calibration of Ge effects [1][2] is based on a relatively small set of measured data. It focuses on Ge concentration ranging between 0% and 50%, and it is not expected to be predictive for higher concentrations of Ge (> 50%).
- Optionally, you can activate Si and Ge parameter interpolation for SiGe by using the command:

```
KMC_SiGe_and_Stress_Effect 1 0
```

The procedure `KMC_SiGe_and_Stress_Effect` has two Boolean arguments: the first is `Ge_Chem_Eff` and the second is `Stress_Eff`. Setting `Ge_Chem_Eff` to 1 deactivates the default linear correction factors and uses the interpolation parameters defined for SiliconGermanium by the following parameter switches:

```
pdbSet Si Skip.Parameter.Interpolation 0  
pdbSet Ge Skip.Parameter.Interpolation 0
```

The calibration covers the full Ge mole fraction range (0–100%). However, due to the limited availability of experimental data for the high mole fraction range (> 50% and < 100%), the calibration is expected to be less mature in this range.

In addition, parameter interpolation for mechanical parameters in compound materials and the lattice mismatch model are activated by the following parameter switches:

```
pdbSet Mechanics Parameter.Interpolation 1  
pdbSet Mechanics Lattice.Constant.Mismatch 1
```

Part 1: Model Parameters for Implantation Damage and Point Defects

This part describes the model parameters for implantation damage and point defects for the materials silicon, germanium, and SiGe.

Amorphization and Recrystallization

The amorphization threshold, displacement thresholds, and interstitial–vacancy recombination in amorphous pockets have been calibrated by the comparison of literature data with simulated (temperature-dependent and dose rate-dependent) amorphous-crystalline transitions and amorphization-layer thicknesses generated by silicon, germanium, and carbon implantation into silicon [3] and into germanium [4][5][6]. The amorphization threshold is set to $1.0 \times 10^{22} \text{ cm}^{-3}$ for both silicon and germanium, which is slightly lower than the value used for continuum Advanced Calibration and is in the range of reported values for the critical point-defect concentration [7].

Chapter 6: Contents of Advanced Calibration of Sentaurus Process KMC

Part 1: Model Parameters for Implantation Damage and Point Defects

The binary collision displacement thresholds for most implanted species is 15 eV for both silicon and germanium substrate materials, which is consistent with reported values [8]. Higher displacement thresholds are used for light ions such as B, C, and F in combination with the MCImplant Cascades.Damage.Model Coupled model, which allows species-specific displacement thresholds so as not to overestimate the simulated damage compared to experimental data. This is a consequence of the limitations of the standard binary collision approximation (BCA) model, which assumes that the deposited energy that is lower than the displacement threshold is dissipated. Unfortunately, the improved BCA model (iBCA) is not a valid alternative due to its inefficiency in general applications and calibration.

The recrystallization velocity in Advanced Calibration for an undoped amorphous layer on top of (100)-oriented crystalline substrate is in agreement with the literature for silicon [9] and germanium [6], both for the standard isotropic and the anisotropic lattice kinetic Monte Carlo (LKMC) mode. The activation energy for solid phase epitaxial regrowth (SPER) is 2.68 eV in the case of silicon [9] and 2.17 eV in the case of germanium [10]. In addition for the LKMC mode, the recrystallization velocity depends on the substrate orientation with approximate ratios of 20:10:1 for the orientations (100), (110), and (111), respectively, for both silicon [11] and germanium [6].

The selected LKMC model for (100) SPER is the Planar one differentiating high and low coordination [12]. To activate the optional LKMC model, you must call the following command:

```
pdbSet KMC Si Damage SPER.Model LKMC
```

In the presence of n-type and p-type doping, the recrystallization velocity is enhanced, again following the literature [9][13][14]. The effect of specific impurities on the recrystallization is described in [Recrystallization on page 248](#).

During recrystallization, impurities and dopants can be redistributed by the recrystallization front. The selected redistribution model during recrystallization is the so-called Hops model. The amount of redistribution is impurity dependent or doping dependent, and is described in [Recrystallization on page 248](#).

Amorphous Silicon and Germanium

The defects in amorphous silicon, which are the dangling bonds of threefold-coordinated Si atoms and the floating bonds of fivefold-coordinated atoms, are simulated explicitly by enabling the amorphous.bonds model for silicon damage, which follows the literature [15][16].

The dangling bond and floating bond density after amorphization is set to 1.8%, and their diffusivities are assumed to be the same with a migration barrier of 2.6 eV, both as proposed by [15]. Moreover, the dangling bonds can be annihilated with floating bonds and bind to

Chapter 6: Contents of Advanced Calibration of Sentaurus Process KMC

Part 1: Model Parameters for Implantation Damage and Point Defects

impurity atoms. For details about the interaction of dangling bonds with B atoms, see [Boron on page 233](#).

For simplicity, the same parameters are assumed for amorphous germanium. However, the verification of this assumption has not been possible due to a lack of corresponding experimental data for amorphous germanium.

Diffusion, Generation, and Recombination

For silicon, the transport capacity for free interstitials:

$$D_i * C_{istar} = 1.59e25 \exp(-4.702eV/kT) \text{ cm}^{-1} \text{ s}^{-1}$$

is inherited from the Advanced Calibration of continuum Sentaurus Process (see [Bulk Parameters for Free Interstitials on page 37](#)).

The macroscopic diffusivity of continuum Sentaurus Process corresponds to the microscopical diffusivities of each charge state of Sentaurus Process KMC in the following way:

$$D_i = (D(I0)C(I0)+D(I+)C(I+)+D(I-)C(I-))/(C(I0)+C(I+)+C(I-))$$

For simplicity, the same diffusivities for charge states -1, 0, +1 and lower ones for charge states -2, +2 are assumed. Taking the diffusivity from the continuum Advanced Calibration (gained from the high-temperature experiments of Bracht *et al.* [17]), you have:

$$D_i = 51 * \exp(-1.77eV/kT) \text{ cm}^2 \text{ s}^{-1}$$

which is reasonable for high temperatures, but too small at room temperature. Therefore, a lower migration energy must be chosen [18], namely, 0.7 eV in the case of Advanced Calibration. The migration prefactor has been adjusted to obtain the same diffusivity as for the Advanced Calibration of continuum Sentaurus Process at 950°C. The resulting diffusivity is:

$$D_i = 0.002 * \exp(-0.7eV/kT) \text{ cm}^2 \text{ s}^{-1}$$

which is the better choice for the full temperature range.

Derived from the transport capacity and the diffusivity, the equilibrium concentration is:

$$\begin{aligned} C_{istar} &= 1.59e25 * \exp(-4.702eV/kT) / 0.002 / \exp(-0.7eV/kT) \text{ cm}^{-3} \\ &= 7.95e27 * \exp(-4.002eV/kT) \text{ cm}^{-3} \end{aligned}$$

The interstitial formation energy of 4.0 eV is in agreement with the literature [19].

In Sentaurus Process KMC, the interfaces set the equilibrium concentrations for point defects. According to the literature [20], the following relation is valid:

$$C_{istar} = 2/\alpha/\alpha^6/\lambda * D_{0FS} * \exp(-E_{Form}/kT)$$

Chapter 6: Contents of Advanced Calibration of Sentaurus Process KMC

Part 1: Model Parameters for Implantation Damage and Point Defects

where the silicon lattice constant is $\text{alpha}=5.43\text{e-}8\text{cm}$, the jump distance is $\text{lambda}=3.84\text{e-}8\text{cm}$, and the Sentaurus Process KMC point-defect interface model prefactor is D0FS and the formation energy is EForm . Therefore, the parameters are:

$$\text{Cistar} = 2/\text{alpha}/\text{alpha}^6/\text{lambda} * 75000 * \exp(-4.00\text{eV}/kT) \text{ cm-}3$$

For germanium, the transport capacity for free interstitials:

$$\text{Di} * \text{Cistar} = 1.59\text{e}25 \exp(-4.38\text{eV}/kT) \text{ cm-}1 \text{ s-}1$$

is inherited from the Advanced Calibration of continuum Sentaurus Process (see [Bulk Parameters for Free Interstitials on page 37](#)) as well.

For germanium, there is a lack of experimental data on self-interstitial properties. Therefore, only the interstitial diffusivity is estimated, based on the calculated migration energy (1.2 eV) of uncharged interstitials calculated by Vanhellemont *et al.* [21] and based on the assumption that the prefactor is the same as for silicon, for simplicity. The equilibrium concentration is estimated, based on the formation energy (3.18 eV) calculated by Vanhellemont *et al.* [22] and again based on the assumption that the prefactor is the same as for silicon, for simplicity.

For vacancies in silicon, the transport capacity is also inherited from the Advanced Calibration of continuum Sentaurus Process (see [Bulk Parameters for Free Vacancies on page 37](#)):

$$\text{DvCvstar} = 4.60\text{e}22 * \exp(-4.14\text{eV}/kT) \text{ cm-}1 \text{ s-}1$$

and the default diffusivity:

$$\text{Dv} = 5\text{e-}8 * \exp(-0.4\text{eV}/kT) \text{ cm2 s-}1$$

for neutral vacancies has been chosen with the migration barrier of 0.4 eV [18].

Therefore, the equilibrium concentration is:

$$\begin{aligned} \text{Cvstar} &= 9.20\text{e}29 * \exp(-3.74\text{eV}/kT) \text{ cm-}3 \\ &= 2/\text{alpha}/\text{alpha}^6/\text{lambda} * 8.68\text{e}6 * \exp(-3.74\text{eV}/kT) \text{ cm-}3 \end{aligned}$$

Again, the vacancy formation energy of 3.74 eV is in agreement with the literature [19].

For vacancies in germanium, the transport capacity is inherited from the Advanced Calibration of continuum Sentaurus Process (see [Bulk Parameters for Free Vacancies on page 37](#)) as well:

$$\text{DvCvstar} = 1.18\text{e}24 * \exp(-3.09\text{eV}/kT) \text{ cm-}1 \text{ s-}1$$

The formation energy of the dominating double negative-charged vacancy of 2.87 eV is based on [23]. Assuming the same prefactor as for silicon for simplicity, the equilibrium concentration is:

$$\text{Cvstar} = 9.20\text{e}29 * \exp(-2.87\text{eV}/kT) \text{ cm-}3$$

Chapter 6: Contents of Advanced Calibration of Sentaurus Process KMC

Part 1: Model Parameters for Implantation Damage and Point Defects

The formation energy for the neutral vacancy is derived from the following relation [24] depending on the local Fermi level e_F and the ionization energies e_0 :

$$\begin{aligned} E_F(V0) &= E_F(V--) + 2 * e_F - e_0(V-) - e_0(V--) = 2.87 + 0.74 - 0.3 - 0.1 \\ &= 3.21 \end{aligned}$$

The vacancy diffusivity of neutral charge and (single and double) negative charge is derived from the vacancy equilibrium concentration and the transport capacity that is based on the experimental vacancy-mediated self-diffusion coefficient of germanium ($13.6 \times \exp(-3.09 \text{eV}/kT) \text{ cm}^{-2}\text{s}^{-1}$) following [25]. The resulting migration barrier (0.22 eV) is also consistent with calculations by [23].

For the Si–SiO₂ and Ge–GeO₂ interfaces, the Allcharges model is selected to allow for the emission and capture of all the charge states of point defects. The recombination length of point defects at Si–SiO₂ and Ge–GeO₂ interfaces is assumed to be 1 nm for continuum and kinetic Monte Carlo. The one at Si–gas and Ge–gas interfaces is set to 1 nm as well. Parameters for Si–nitride and Ge–nitride interfaces are inherited from Si–SiO₂ and Ge–GeO₂ interfaces.

The bulk recombination of interstitials and vacancies in the Advanced Calibration of continuum Sentaurus Process is diffusion limited. In Sentaurus Process KMC, interstitials and vacancies form amorphous pockets when they are close (within capture radius) during their migration. The interstitial and vacancy recombine, and the amorphous pocket is dissolved if no more interstitials or vacancies are captured by the amorphous pocket beforehand. However, in contrast to the continuum Advanced Calibration, the I–V recombination is not instantaneous due to the energy barrier [26]. Therefore, the formation of I–V pairs is diffusion limited and the recombination of I–V pairs in silicon in the equation recombination rate is:

$$v = 5.0e-4 * \exp(-0.43\text{eV}/kT) \text{ cm}^2/\text{s}$$

The corresponding one for germanium is:

$$v = 5.0e-3 * \exp(-0.60\text{eV}/kT) \text{ cm}^2/\text{s}$$

The generation of I–V pairs has not been implemented in Sentaurus Process KMC due to its small contribution, whereas in continuum Advanced Calibration, the generation of I–V pairs is simulated.

Oxidation causes the injection of interstitials at the exposed surface. The calibration of Sentaurus Process KMC follows that for the continuum of interstitial injection for dry oxidation of silicon (see [Oxidation-Enhanced Diffusion on page 38](#)). No interstitial injection for oxidation of germanium is assumed.

Charge States

The charge levels for self-interstitials and vacancies have been studied [18]. Accordingly, the concentration for positively charged interstitials is:

$$C(I+) = C(I0) * \exp(-(E_f - e(I+))/kT)$$

where the Fermi level is E_f and the energy level is $e(I+)$, which is the energy needed to take an electron from the neutral interstitial measured from the valence band (Sentaurus Process KMC parameter $e_0(IP)$).

In continuum Sentaurus Process, the concentration for positively charged interstitials is:

$$C(I+) = C(I0) * k0(I+) \exp(-(E_f - E_i + kE(I+))/kT)$$

where the Fermi level is E_f , the intrinsic level is E_i , and the charge-state parameter is $k(I+) = k0(I+) * \exp(-kE(I+)/kT)$.

Therefore, the following relation is valid:

$$\exp(e(I+)/kT) = k0(I+) \exp((E_i - kE(I+))/kT) \quad (\text{Eq } x)$$

The intrinsic level depends on the band gap E_g , and the effective state density of the conduction (N_c) and valence (N_v) bands [27]:

$$E_i(T) = E_g(T)/2 + kT/2 * \ln(N_v/N_c)$$

In summary, the electronic levels in continuum Sentaurus Process refer to the intrinsic level, while the electronic levels in atomistic Sentaurus Process are measured from the valence band edge. This means that due to the temperature dependence of the energy difference of the intrinsic and valence band levels, an exact translation of the charge-state parameters from continuum Sentaurus Process to Sentaurus Process KMC is not possible.

Therefore, the electronic levels for interstitials and vacancies in silicon are taken as recommended in the literature [18]. In the temperature range from 700°C to 1100°C, the electronic level for I^+ of 0.4 eV corresponds to $k0(I+) = 12$ and $kE(I+) = 0.23\text{eV}$, and the one for I^- of 1.0 eV corresponds to $k0(I-) = 0.12$ and $kE(I-) = 0.4\text{eV}$.

The electronic levels for interstitials and vacancies in germanium are calibrated with guidance from the literature [22][23].

Extended Defects

In Sentaurus Process KMC, the evolution of extended defects of self-interstitials from small clusters to {311} defects and faulted dislocation loops is taken into account [28]. Small clusters have irregular shapes and are amorphous pockets in the terminology of kinetic Monte Carlo. Amorphous pockets capture any point defect (I and V) within their capture radius.

Chapter 6: Contents of Advanced Calibration of Sentaurus Process KMC

Part 1: Model Parameters for Implantation Damage and Point Defects

For silicon, the binding energies are taken from the parameter array `Eb.Cluster` and are based on the suggestions of [29] assuming a self-interstitial formation energy of 3.8 eV (see Table 7). The interstitial emission prefactor `D0.Cluster` is 135.

Table 7 Binding energies in keV for small interstitial clusters in silicon

N =	2	3	4	5	6	7	8	9	10	11	12	13	14
Cowern [29]	2.64	2.77	2.67	2.48	2.46	3.24	2.40	2.69	2.73	2.92	3.00	3.06	
Advanced Calibration	2.40	2.50	2.77	2.67	2.48	2.46	3.24	2.40	2.69	2.73	2.92	3.00	3.06

Above a threshold, the extended defects in silicon form rod-like {311} defects. The minimal size of a {311} `Min.AP.To.311.Size` has been chosen to be 15. {311} defects capture any neutral interstitial with which they are in contact. The binding energy of this size is 2.94 keV, the one of size 60 is 2.96 keV, and the ones for the intermediate sizes are linearly interpolated. Above the size of 60, the binding energies of size n are computed using the following equation:

$$Eb(n) = Eb_L - (Eb_L - Eb_S) * (n^a - (n-a)^a) / (2^{a-1})$$

where `Eb_L` (`Eb.LargeCluster`) is equal to 3.17 keV, `Eb_S` (`Eb.SmallestCluster`) is equal to 2.64 keV, and `a` (`Exponent.Cluster`) is equal to 3/4. The interstitial emission prefactor is the same as for amorphous pockets.

When {311} defects in silicon grow large enough, they transform into dislocation loops. The threshold size for this transformation `Min.311.To.111Loop.Size` is equal to 4500. In this calibration, dislocation loops cannot be formed directly from amorphous pockets, as the prefactor `D0.AP.To.111Loop` is set to 0.

Dislocation loops capture any incoming neutral interstitial. The binding energies are:

$$Eb(n) = Ef(I) + Ef(DL(n-1)) - Ef(DL(n))$$

with the dislocation loop formation energies:

$$Ef(DL(n)) = \pi\gamma R^2 + a^2\mu/6(1-\nu)R * \log(8R/b) - nEf(I)$$

taken from the literature [30], which are Sentaurus Process KMC defaults. The interstitial emission prefactor `D0.Loop` is 1e6 in silicon.

In germanium, small clusters and extended defects consisting of interstitials also have been observed [31][32][33][34][35]. As for silicon, Sentaurus Process KMC takes the binding energies from the parameter array `Eb.Cluster` and calculates the binding energies for defects above the size of 60. The binding energies and the interstitial emission prefactor `D0.Cluster` of 5 have been calibrated against literature data [33].

Chapter 6: Contents of Advanced Calibration of Sentaurus Process KMC

Part 1: Model Parameters for Implantation Damage and Point Defects

According to the literature [34][35], the observed extended defects in germanium are not {311} defects, but small dislocation loops. To account for this, the transformation of amorphous pockets to {311} defects is suppressed by setting `D0.AP.To.311` to 0, and the transformation to dislocation loops is allowed with `D0.AP.To.111Loop` equal to `1e12` and `E.AP.To.111Loop` equal to 1.3 eV in germanium.

The minimal size of a dislocation loop `Min.AP.To.111Loop.Size` has been chosen to be 33. Finally, the dislocation loop formation energies and the interstitial emission prefactor `D0.Loop` of `1e6` also have been calibrated against literature data [33].

The binding energies for small vacancy clusters up to size 10 in silicon are taken from the ATOMICS research project [36]. The vacancy emission prefactor `D0.Cluster` is 5. Voids are assumed to be vacancy clusters of size 20 and higher.

For germanium, the binding energies for small vacancy clusters up to size 4 are based on the literature [37]. While the binding energies of larger clusters are inherited from the silicon calibration. The vacancy emission prefactor `D0.Cluster` is `5e-2`. Again, voids are assumed to be vacancy clusters of size 20 and higher.

SiGe

This section discusses silicon germanium.

Linear Germanium Correction Factors

By default, the Ge effects are modeled by linear correction factors for silicon parameters. The calibration is valid for low Ge mole fractions ranging between 0% and 50%.

Amorphization and Recrystallization

It is assumed that there is a reduced interstitial–vacancy recombination rate during ion implantation and annealing in SiGe compared to pure silicon, according to [38]. This is performed by introducing a Ge effect for interstitial–vacancy recombination in amorphous pockets:

```
pdbSet KMC Si Damage Eb_AmorphousPocketGe [expr 1.50/5.e22]
```

Band Gap

Germanium reduces the band gap of silicon. The formula for Ge-induced bandgap narrowing for Ge mole fractions below 85%, which is identical to the one used for continuum Sentaurus Process (see [Effect of Germanium and Stress on page 60](#)), is:

$$dE(\text{BandGap}) = [\text{Ge}] / 5.e22 * (0.33 * ([\text{Ge}] / 5.e22) - 0.55) \text{ eV/cm}^3$$

Chapter 6: Contents of Advanced Calibration of Sentaurus Process KMC

Part 1: Model Parameters for Implantation Damage and Point Defects

and is implemented by defining:

```
pdbSet KMC Si BandGap GeNarrowing [expr -0.55/5.e22]
pdbSet KMC Si BandGap GeNarrowing2 [expr 0.33/5.e22/5.e22]
```

Diffusion, Generation, and Recombination

In the literature, there is no agreement on the impact of Ge (for low Ge mole fractions) on point-defect diffusion and generation except for the vacancy equilibrium concentration. Computational studies of vacancies in SiGe have found an ~1.0 eV vacancy formation energy decrease in Ge [39][40][41], in line with the Advanced Calibration parameters for silicon and germanium. For computational efficiency, to prevent the abundance of vacancies in SiGe, a value lower than the published ones is used in the Advanced Calibration of Sentaurus Process KMC, also lower than the one for continuum Advanced Calibration (see [Impact of Stress on Point-Defect Parameters on page 70](#)):

```
pdbSet KMC Si Vac EfGe V [expr -0.50/5.e22]
```

No Ge effect on the interstitial equilibrium concentration is assumed. Based on molecular dynamics calculations [42], the diffusivities of interstitials and vacancies are almost unchanged for low Ge mole fractions, but they change rapidly for higher ones. Therefore, no linear Ge effect is used for the interstitial and vacancy diffusivity.

Extended Defects

The {311} interstitial clusters are less stable in the presence of Ge, and the transformation of {311} defects into dislocation loops is faster [36][43][44]. The corresponding parameter adjustments have been calibrated by Synopsys based on experimental data generated within the ATOMICS research project [2].

The binding energies of small interstitial clusters, {311} defects, and dislocation loops are lowered in the presence of Ge:

```
pdbSet KMC Si Int Eb_ClusterGe [expr -0.20/5.e22]
pdbSet KMC Si Int Eb_311Ge [expr -0.20/5.e22]
pdbSet KMC Si Int Eb_LoopGe [expr -0.50/5.e22]
```

The transformation from {311} defects to dislocation loops occurs earlier in the presence of Ge:

```
pdbSet KMC Si Int E_311toLoopGe [expr -1.00/5.e22]
```

The binding energies of small vacancy clusters and voids are higher in the presence of Ge:

```
pdbSet KMC Si Vac Eb_ClusterGe [expr 0.20/5.e22]
pdbSet KMC Si Vac Eb_VoidGe [expr 0.20/5.e22]
```

Silicon and Germanium Parameter Interpolation

Optionally, you can activate Si and Ge parameter interpolation for SiGe using the command:

```
KMC_SiGe_and_Stress_Effect 1 0
```

This deactivates the default linear correction factors and uses the interpolation parameters defined for `SiliconGermanium`. The calibration covers the full Ge mole fraction range (0–100%).

In general, prefactor parameters are interpolated in logarithmic scale, and energy parameters are interpolated in linear scale.

Amorphization and Recrystallization

According to [38], the interstitial–vacancy recombination rate during ion implantation and annealing in SiGe is reduced, compared to the rate in pure silicon. This is in line with Advanced Calibration, where the interstitial–vacancy recombination rate at room temperature for small amorphous pockets is ~1000 times smaller in germanium compared to silicon. The SiGe interpolation for the interstitial–vacancy recombination rate prefactor is parabolic and is calibrated based on a limited experimental dataset for Ge implantation into Ge only [45][46]. Parabolic SiGe parameter interpolation is used for the displacement threshold in B implantation, which has been calibrated against experimental data from AMAT-VSE (Applied Materials - Varian Semiconductor Equipment).

The (100) recrystallization of germanium is much faster than the one of silicon. For SiGe, the recrystallization activation energy is interpolated parabolically with slightly higher or constant values for Ge mole fractions up to 40% and lower values for higher Ge mole fractions, following [47]. The KMC and all LKMC recrystallization prefactors for the different orientations are interpolated parabolically (in logarithmic scale) to match the regrowth rates of SiGe of different Ge mole fractions [46][48]. As a result, the recrystallization velocity is faster for SiGe of all Ge mole fractions compared to silicon.

Band Gap

Germanium reduces the band gap of silicon. The energy bandgap change along with the Ge mole fraction shows a very nonlinear curve due to the transition between the X-valley ($x < 0.8$) and the L-valley ($x > 0.8$) [49]. With SiGe parameter interpolation activated, the Ge-induced bandgap narrowing model is used, which is identical to the one used for continuum Sentaurus Process (see [Impact of Germanium on Electrostatic Potential on page 63](#)) and is implemented by defining:

```
pdbSet Si KMC BandGap Alloy.Narrowing.Model  
pdbSet Si KMC BandGap Eg0 1.170  
pdbSet Ge KMC BandGap Eg0 0.719
```

Diffusion, Generation, and Recombination

For vacancies, both equilibrium concentration and diffusivity are higher in germanium than in silicon. However, for interstitials, only the equilibrium concentration is higher, but the diffusivity is lower in germanium than in silicon.

Parabolic SiGe parameter interpolation in linear scale is used for both the formation energies and the migration barriers of point defects, while prefactors are interpolated linearly in logarithmic scale.

In addition, electronic levels at T=0 K are interpolated linearly between silicon and germanium.

The interpolation between silicon and germanium was calibrated based on SiGe interdiffusion experiments (see [SiGe Interdiffusion](#)). Following Castrillo et al. [50], vacancies with a double negative charge are the dominant contributor to the point-defect transport capacity starting at medium mole fractions (~ 0.3) up to mole fraction 1.

Note:

SiGe oxidation is not accurately modeled by KMC. Since Sentaurus Process KMC does not allow for point-defect injection correction (needed for vacancies) and for parameter interpolation (needed for OED), SiGe interdiffusion during oxidation is incorrect and, therefore, the Ge mole-fraction oxidation rate is incorrect as well (see the continuum model in [SiGe Oxidation on page 68](#)).

Extended Defects

The {311} interstitial clusters are less stable with higher Ge mole fractions, and the transformation of amorphous pockets and {311} defects into dislocation loops is faster [36][43][44]. Parabolic SiGe parameter interpolation is used for small and {311} defect binding energies, the minimum {311} cluster size, and the interstitial emission prefactor from dislocation loops. Other point-defect cluster parameters are interpolated linearly.

SiGe Interdiffusion

In undoped SiGe, the interdiffusion of Si and Ge atoms is a consequence of point-defect diffusion [50] (see [SiGe Interdiffusion on page 65](#)). Contributions from a direct exchange mechanism are neglected. SiGe interdiffusion is described as the sum of a contribution from vacancy diffusion and a contribution from interstitial diffusion. The KMC interdiffusion model accounts for different Si and Ge self-diffusivities by defining the relative probability of an I (or a V) moving a Ge or Si atom [50][51][52]. Therefore, changes to the interstitial and vacancy transport capacity due to excess point defects after implantation, or due to Fermi-level effects in the case of doping, directly lead to altered SiGe interdiffusion. In addition, when taking into account stress effects in KMC (see [Stress Effects on page 229](#)), interdiffusion is naturally stress dependent because the diffusivity and equilibrium concentration of point defects are modified in strained SiGe as a function of pressure.

Chapter 6: Contents of Advanced Calibration of Sentaurus Process KMC

Part 1: Model Parameters for Implantation Damage and Point Defects

The parameters for SiGe interdiffusion have been extracted and calibrated against data from the literature [53][54][55][56][57][58]. While the (dominant) interdiffusivity from vacancies can be extracted reliably, the parameter error might be larger for the smaller component of interdiffusivity from the diffusion of interstitials. The biggest uncertainties in calibration exist for highly n-doped SiGe, where interdiffusion is believed to have a dominant contribution from P–V or As–V pairs, which is not yet included in the calibration, due to a lack of experimental data suitable for calibration.

Stress Effects

The stress effects on damage, diffusion, and binding in Advanced Calibration for Sentaurus Process KMC are only taken into account if the KMC Stress switch is activated. This is accomplished by the command:

```
KMC_SiGe_and_Stress_Effect 0 1
```

The procedure KMC_SiGe_and_Stress_Effect has two Boolean arguments: the first is Ge_Chem_Eff and the second is Stress_Eff, which is dedicated for stress effects.

Alternatively, the KMC Stress switch can be activated directly:

```
pdbSet KMC Stress 1
```

The calibration of stress effects [1][2] is based on a relatively small set of measured data. The models have not yet been tested rigorously against SIMS data for all dopant species and nonequilibrium annealing conditions, and against electrical data from real-device fabrication processes.

Amorphization and Recrystallization

No stress effect on damage accumulation is implemented in this calibration. Stress effects on damage accumulation are not clearly experimentally evidenced and, at least, appear not to be the primary cause of enhanced damage production in the case of implantation into strained SiGe compared to relaxed Si [59].

The stress dependency of SPER is calibrated only for LKMC. The stress effect on in-plane uniaxial stresses is nonlinear and is simulated by a model assuming that {100} events occur through a dual-timescale atomistic mechanism [12][60]. In addition, compressive hydrostatic pressure results in an enhancement of the (100) regrowth velocity [60].

Band Gap

The bandgap narrowing for silicon due to stress is calculated according to the deformation potential theory as for continuum Sentaurus Process (see [Impact of Stress on Electrostatic Potential on page 69](#)). The deformation potential constants for Si and Ge proposed by Van

Chapter 6: Contents of Advanced Calibration of Sentaurus Process KMC

Part 1: Model Parameters for Implantation Damage and Point Defects

de Walle were chosen for Advanced Calibration. For strained SiGe, the model uses a simple linear interpolation between Si and Ge.

The model is activated by:

```
pdbSet KMC Si BandGap FullNarrowing 1
```

Diffusion, Generation, and Recombination

Compressive hydrostatic pressure decreases the equilibrium concentration of interstitials and increases the equilibrium concentration of vacancies. Similarly, the diffusivities of point defects are modified as a function of pressure. The activation volumes for the above prefactors were derived from the induced strain values calculated by Diebel [61][62], and the value for pure germanium has been adjusted to match experimental data reported by Kawamura *et al.* [63], in analogy to continuum Advanced Calibration (see [Impact of Stress on Point-Defect Parameters on page 70](#)).

In addition, interstitials show an anisotropy in the diffusivity as a function of biaxial strain according to [62]. Biaxial tension (as in strained silicon on SiGe) leads to significantly higher in-plane diffusion compared to the perpendicular direction.

The diffusivities and equilibrium concentrations of interstitials and vacancies in silicon, germanium, and SiGe are modified in the presence of stress in the following way:

```
pdbSetArray KMC Si Int VD { IMM -0.00014,-0.00007
                             IM  -0.00014,-0.00007
                             I   -0.00014,-0.00007
                             IP  -0.00014,-0.00007
                             IPP -0.00014,-0.00007 }
pdbSetArray KMC Ge Int VD { IMM -0.00014,-0.00007
                             IM  -0.00014,-0.00007
                             I   -0.00014,-0.00007
                             IP  -0.00014,-0.00007
                             IPP -0.00014,-0.00007 }
pdbSetArray KMC Si Vac VD { VMM 0.0012,0.0012
                            VM  0.0012,0.0012
                            V   0.0012,0.0012
                            VP  0.0012,0.0012
                            VPP 0.0012,0.0012 }
pdbSetArray KMC Ge Vac VD { VMM 0.0008,0.0008
                            VM  0.0008,0.0008
                            V   0.0008,0.0008
                            VP  0.0008,0.0008
                            VPP 0.0008,0.0008 }
pdbSetArray KMC SiGe Vac VD.X2 { VMM 0.0019,0.0019
                                 VM  0.0019,0.0019
                                 V   0.0019,0.0019
                                 VP  0.0019,0.0019
                                 VPP 0.0019,0.0019 }
```

Chapter 6: Contents of Advanced Calibration of Sentaurus Process KMC

Part 2: Model Parameters for Impurities

```
pdbSet KMC Si Int VF I -0.0012  
pdbSet KMC Ge Int VF I -0.0028  
pdbSet KMC Si Vac VF V 0.0013  
pdbSet KMC Ge Vac VF V 0.0013
```

Extended Defects

The {311} interstitial clusters are less stable in the presence of compressive hydrostatic pressure, and the transformation of {311} defects into dislocation loops is faster [36][43][64].

The binding energies of small interstitial clusters, {311} defects, and dislocation loops are lowered in the presence of compressive hydrostatic pressure:

```
pdbSet KMC Si Int VFCluster -0.01  
pdbSet KMC Si Int VF311      -0.01  
pdbSet KMC Si Int VFLoop    -0.02
```

The transformation from {311} defects to dislocation loops occurs earlier in the presence of compressive hydrostatic pressure:

```
pdbSet KMC Si Int VF311toLoop -0.04
```

The binding energies of small vacancy clusters and voids are not dependent on stress in this calibration.

Part 2: Model Parameters for Impurities

This part describes the model parameters for impurities for the materials silicon, germanium, and SiGe.

The calibrated impurities or dopants are boron, arsenic, phosphorus, indium, carbon, fluorine, and nitrogen. In addition, hydrogen and helium parameters have been included, but both species are assumed to be immobile for simplicity and computational efficiency. Finally, the parameters of antimony are also calibrated, but are included in the default set of Sentaurus Process and not in Advanced Calibration.

Implantation

For KMC, ion implantation is always performed by the binary collision approximation (BCA) of the Sentaurus MC implantation model in full cascade mode. The positions of the implanted and displaced particles are transferred to KMC for damage accumulation and annealing modeling. In return, the computed damage information is transferred back to the BCA model. For details about the damage calibration, see [Amorphization and Recrystallization on page 227](#).

Chapter 6: Contents of Advanced Calibration of Sentaurus Process KMC

Part 2: Model Parameters for Impurities

As in the case for continuum Sentaurus Process (see [Monte Carlo Implantation \(General\) on page 89](#)), the procedure `_AdvCal::ImpPreProcess` is used for the energy- and dose-dependent calibration of implantation profiles (but not amorphization) by Sentaurus MC.

The parameters for H, He, and P, as well as for As and B in the case of high-energy implantation, in silicon have been adjusted to improve the accuracy of as-implanted profiles in analogy to Advanced Calibration of continuum Sentaurus Process. A more accurate peak position of implantation profiles is achieved by the calibration of the electronic stopping correction factor, `LSS.pre`. The `scr.par` parameter has been calibrated to reproduce the width of the peak of as-implanted profiles and the channeling tail.

In addition, the calibration of `DebyeTemperature` is included, which plays a role in scattering ions out of the channeling directions of the silicon crystal. However, the parameter `d.sim` does not need to be calibrated in the case of KMC. For details about the Sentaurus MC calibration, see [Monte Carlo Implantation \(General\) on page 89](#).

Diffusion

The effective diffusivity of an interstitial-mediated and a vacancy-mediated dopant X in crystalline silicon or germanium is given by the sum of the contribution of all mobile species and can be reduced in continuum models using the Maxwell–Boltzmann approximation to:

$$D(X^-) = Si [D(X-I0) + D(X-I+)(p/ni) + D(X-I++)(p/ni)^2] + Sv [D(X-V0) + D(X-V+)(p/ni) + D(X-V++)(p/ni)^2]$$

for the negatively charged immobile substitutional dopant X⁻ and:

$$D(X^+) = Si [D(X+I0) + D(X+I-)(n/ni) + D(X+I--)(n/ni)^2] + Sv [D(X+V0) + D(X+V-)(n/ni) + D(X+V--)(n/ni)^2]$$

for the positively charged immobile substitutional dopant X⁺, where Si is the interstitial supersaturation, Sv is the vacancy supersaturation, and n, p, and ni are the electron, hole, and intrinsic concentration, respectively.

According to [\[18\]](#), the relation between the above diffusivity components and the microscopical parameters is:

$$\begin{aligned} D(X-I0) &= Uc * DiCi * 1/Vbk(Xi-) * Vm(Xi-) \\ D(X-I-) &= Uc * DiCi * 1/Vbk(Xi-) * Vm(Xi0) * \exp((e0(Xi-) - ei)/kT) \\ D(X-V0) &= Uc * DvCv * 1/Vbk(Xv-) * Vm(Xv-) \\ D(X-V-) &= Uc * DvCv * 1/Vbk(Xv-) * Vm(Xv0) * \exp((e0(Xv-) - ei)/kT) \end{aligned}$$

and:

$$\begin{aligned} D(X+I0) &= Uc * DiCi * 1/Vbk(Xi+) * Vm(Xi+) \\ D(X+I-) &= Uc * DiCi * 1/Vbk(Xi+) * Vm(Xi0) * \exp((ei - e0(Xi+))/kT) \\ D(X+V0) &= Uc * DvCv * 1/Vbk(Xv+) * Vm(Xv+) \\ D(X-V+) &= Uc * DvCv * 1/Vbk(Xv+) * Vm(Xv0) * \exp((ei - e0(Xv+))/kT) \end{aligned}$$

Chapter 6: Contents of Advanced Calibration of Sentaurus Process KMC

Part 2: Model Parameters for Impurities

where the effective capture volume is $U_C = 3 * \text{lambda}^3$ ($\text{lambda}=3.84\text{nm}$ is the distance in the silicon lattice from one atom to its second-nearest neighbor), the breakup frequencies are v_{bk} , the migration frequencies are v_m , the electronic levels are e_0 , and the intrinsic Fermi level is e_i (at a given temperature). The breakup frequencies are:

$$\begin{aligned}v_{bk}(X_{i-}) &= D_b(X_{i-}) * \exp(-(E_b(X_{i-}) + E_m(I0)) / kT) \\v_{bk}(X_{v-}) &= D_b(X_{v-}) * \exp(-(E_b(X_{v-}) + E_m(V0)) / kT) \\v_{bk}(X_{i+}) &= D_b(X_{i+}) * \exp(-(E_b(X_{i+}) + E_m(I0)) / kT) \\v_{bk}(X_{v+}) &= D_b(X_{v+}) * \exp(-(E_b(X_{v+}) + E_m(V0)) / kT)\end{aligned}$$

where the migration energies are E_m , the binding prefactor is D_b , and the energy is E_b .

This means that the diffusivities of Sentaurus Process Advanced Calibration can be translated to a fixed relation of migration and binding parameters for Sentaurus Process KMC: the bigger the binding energy, the bigger the migration energy to obtain the same diffusivity. For this calibration of Sentaurus Process KMC, the binding prefactor and energy as well as the electronic levels were first chosen reasonably, and the migration prefactors and energies were deduced. Then, the optimal combination of binding energy and electronic levels was searched, based on SIMS calibration, while the migration energies were shifted accordingly to keep the same diffusivity.

Since kinetic Monte Carlo can also simulate diffusion during implantation at room temperature, the consideration of as-implanted SIMS data is crucial for calibration of the binding energies. For the situation of full cascade implantation, many impurities pair with the abundant point defects because of their high implant energy and, therefore, they can diffuse even at room temperature if the migration energies are small. Higher binding energies, implying higher migration energies, can suppress migration at room temperature.

Boron

For silicon, the boron diffusivities of Pichler [65], on which also the continuum Advanced Calibration Version T-2022.03 is based (see [Boron Diffusion and Activation on page 40](#)):

$$\begin{aligned}D(B-I0) &= 0.123 * \exp(-3.566\text{eV}/kT) \\D(B-I+) &= 4.210 * \exp(-3.671\text{eV}/kT) \\D(B-I++) &= 39.8 * \exp(-4.373\text{eV}/kT)\end{aligned}$$

translate to microscopical diffusivities:

$$\begin{aligned}v_m(B_{i-}) &= 4.55e-5 * \exp(-0.364\text{eV}/kT) \\v_m(B_{i0}) &= 2.82e-3 * \exp(-0.707\text{eV}/kT) \\v_m(B_{i+}) &= 1.29e-1 * \exp(-1.912\text{eV}/kT)\end{aligned}$$

where the binding prefactors equal 1.0 and the energies equal 0.8 eV for B^- plus a neutral interstitial and 0.1 eV for B^- plus a vacancy and, for the following electronic levels for boron–interstitial pairs and boron–vacancy pairs:

```
pdbsSetDoubleArray KMC Si B e0 {BiM 0.8  
BiP 1.04}
```

Chapter 6: Contents of Advanced Calibration of Sentaurus Process KMC

Part 2: Model Parameters for Impurities

```
BVM 0.1  
BVP -5.0 }
```

The electronic levels at T=0 for the boron–interstitial pairs with a negative and a positive charge are taken from the literature [18], while the ones for boron–vacancy pairs are calibrated. The intrinsic Fermi level, $E_{fi}(T) = E_g(T)/2 - 0.5\ln(N_c/N_v) k_B T$, is used for the translation of the diffusivity from continuum to KMC simulation.

The binding energies for the negative-charged boron–interstitial and boron–vacancy pairs are derived from the following relation [18]:

$$\begin{aligned} Eb(Bi^-) &= Eb(Bi0) - e0(Bi-) + e0(I+) = 1.20 - 0.80 + 0.40 = 0.8 \\ Eb(BV^-) &= Eb(BV0) - e0(BV-) + e0(V+) = 0.17 - 0.10 + 0.03 = 0.1 \end{aligned}$$

with a binding energy of a neutral boron–interstitial pair of 1.2 eV that is close to the reported value of 1.1 eV [66], and with a binding energy of a neutral boron–vacancy pair of 0.17 eV in agreement with the literature [67].

The substitutional B⁻ as well as the B⁻ paired with any V are immobile.

In addition to diffusion in crystalline silicon, Advanced Calibration activates boron diffusion in amorphous silicon mediated by dangling bonds [15][16]. The microscopical diffusivity is set to:

$$Vm(Bi) = 72 * \exp(-2.8/kT)$$

where the binding prefactors equal 1.0, and the energies equal 0.2 eV [66] for B plus a dangling bond. The coefficient for dangling bond creation per B atom in amorphous silicon is set to 0.5 to obtain good accuracy with SIMS for boron implantation into amorphous silicon [16][68][69]. However, for amorphization of boron marker layers, a coefficient of 1.0 gives better accuracy, as reported in [15].

For germanium, the boron diffusivities of Uppal [70], on which also the continuum Advanced Calibration Version T-2022.03 is based (see [Boron Diffusion Coefficient on page 40](#)):

$$\begin{aligned} D(B-I0) &= 1.77e5 * \exp(-4.65eV/kT) \\ D(B-I+) &= 1.00e4 * \exp(-4.65eV/kT) \\ D(B-I++) &= 1.00e4 * \exp(-4.65eV/kT) \end{aligned}$$

translate to microscopical diffusivities:

$$\begin{aligned} Vm(Bi-) &= 65.5 * \exp(-2.87eV/kT) \\ Vm(Bi0) &= 3.70 * \exp(-2.70eV/kT) \\ Vm(Bi+) &= 3.70 * \exp(-2.73eV/kT) \end{aligned}$$

where the binding prefactors equal 1.0, and the energies equal 1.4 eV for B⁻ plus a neutral interstitial, 0.1 eV for B⁻ plus a vacancy, and for the following electronic levels for boron–interstitial pairs and boron–vacancy pairs:

```
pdbSetDoubleArray KMC Ge B e0 {BiM 0.2  
BiP 0.4}
```

Chapter 6: Contents of Advanced Calibration of Sentaurus Process KMC

Part 2: Model Parameters for Impurities

```
BVM 0.1  
BVP -5.0 }
```

The electronic levels and binding energies for the boron–interstitial and boron–vacancy pairs are calibrated. The substitutional B– as well as B– paired with any V are immobile in germanium, similar as in silicon.

Arsenic

For silicon, the arsenic diffusivities are close to the diffusivities reported by Martin-Bragado *et al.* [71], which are not the same but are similar to continuum Advanced Calibration Version T-2022.03 (see [Arsenic Diffusivity on page 46](#)):

```
D(As+I0) = 0.1350 * exp(-3.64eV/kT)  
D(As+I-) = 4200.0 * exp(-4.80eV/kT)  
D(As+V0) = 0.0780 * exp(-3.70eV/kT)  
D(As+V-) = 10.900 * exp(-4.24eV/kT)  
D(As+V--) = 7.500 * exp(-4.80eV/kT)
```

corresponding to microscopical diffusivities:

```
Vm(Asi+) = 5.0e-5 * exp(-0.40eV/kT)  
Vm(Asi0) = 1.6 * exp(-1.79eV/kT)  
Vm(AsV+) = 3.8e-4 * exp(-1.90eV/kT)  
Vm(AsV0) = 5.4e-2 * exp(-2.51eV/kT)  
Vm(AsV-) = 9.8 * exp(-1.04eV/kT)
```

where the binding prefactor equals 1.0 and the energy equals 0.76 eV for As⁺ plus a neutral interstitial, and the binding prefactor equals 0.4 eV and the energy equals 1.34 eV for As⁺ plus a neutral vacancy, for the following electronic levels:

```
pdbSetDoubleArray KMC Si As e0 {AsiP 0.2  
AsiM 5.0  
AsVP 0.6  
AsVM 1.1}
```

The electronic level at T=0 for arsenic–interstitial pairs and arsenic–vacancy pairs is calibrated. Compared to [71], the binding prefactors are doubled. In addition, the binding energy of the arsenic–interstitial pair is recalibrated based on low-temperature diffusion experiments. In agreement with [71], the binding energy for the arsenic–vacancy pair is based on [72] and is derived from the following relation [18]:

$$Eb(AsV+) = Eb(AsV0) + e0(AsV+) - e0(V-) = 1.34 + 0.6 - 0.6 = 1.34$$

leading to a binding energy of As⁺ plus a neutral vacancy that is close to another reported value [73].

The substitutional As⁺ as well as As⁺ paired with I⁻⁻ are immobile.

According to measurements by Larsen *et al.* [74], the diffusivity of As increases sharply for regions with high As concentration ($> 2.0 \times 10^{20} \text{ cm}^{-3}$).

Chapter 6: Contents of Advanced Calibration of Sentaurus Process KMC

Part 2: Model Parameters for Impurities

This effect has been attributed to As–V percolation, which is not simulated with Advanced Calibration for Sentaurus Process KMC. Another explanation is enhanced diffusion due to mobile clusters, in particular, As_2V [71], as discussed in [Arsenic on page 235](#).

For germanium, the arsenic diffusivities, dominated by As^+V^{--} pairs, are based on Zographos and Erlebach [75] and are identical to the diffusivities of the continuum Advanced Calibration Version T-2022.03 (see [Arsenic Diffusivity on page 46](#)):

$$\begin{aligned}\text{D(As+I0)} &= 0.1350 * \exp(-3.64\text{eV}/kT) \\ \text{D(As+I-)} &= 4200.0 * \exp(-4.80\text{eV}/kT) \\ \text{D(As+V0)} &= 0.0780 * \exp(-3.70\text{eV}/kT) \\ \text{D(As+V-)} &= 10.900 * \exp(-4.24\text{eV}/kT) \\ \text{D(As+V--)} &= 2.0\text{e}3 * \exp(-2.90\text{eV}/kT)\end{aligned}$$

corresponding to microscopical diffusivities:

$$\begin{aligned}\text{Vm(AsI+)} &= 5.0\text{e}-5 * \exp(-1.22\text{eV}/kT) \\ \text{Vm(AsI0)} &= 1.6 * \exp(-2.55\text{eV}/kT) \\ \text{Vm(AsV+)} &= 3.8\text{e}-4 * \exp(-2.17\text{eV}/kT) \\ \text{Vm(AsV0)} &= 5.4\text{e}-2 * \exp(-2.78\text{eV}/kT) \\ \text{Vm(AsV-)} &= 9.8 * \exp(-1.31\text{eV}/kT)\end{aligned}$$

where the binding prefactors equal 1.0, and the energy equals 0.76 eV for As^+ plus a neutral interstitial, 1.68 eV for As^+ plus a neutral vacancy, and for the following electronic levels:

```
pdbSetDoubleArray KMC Ge As e0 {AsiP 0.2  
AsiM 5.0  
AsVP 0.3  
AsVM 0.5}
```

The electronic levels for arsenic–vacancy pairs are based on [76]; those for arsenic–interstitial pairs are inherited from silicon. The binding energy for the arsenic–vacancy has been calibrated and is in the range of reported values [76][77]. The binding energy for arsenic–interstitial pairs are again inherited from silicon.

The substitutional As^+ as well as As^+ paired with I^{--} are immobile, as in silicon.

Phosphorus

For silicon, the phosphorus diffusivities, with their interstitial-mediated part taken from Pichler [65] and their vacancy-mediated part taken from continuum Advanced Calibration (see [Phosphorus Diffusivity on page 48](#)):

$$\begin{aligned}\text{D(P+I0)} &= 0.453 * \exp(-3.482\text{eV}/kT) \\ \text{D(P+I-)} &= 1.610 * \exp(-3.647\text{eV}/kT) \\ \text{D(P+V0)} &= 0.20 * \exp(-4.500\text{eV}/kT) \\ \text{D(P+V-)} &= 0.20 * \exp(-4.500\text{eV}/kT) \\ \text{D(P+V--)} &= 0.33 * \exp(-3.900\text{eV}/kT)\end{aligned}$$

Chapter 6: Contents of Advanced Calibration of Sentaurus Process KMC

Part 2: Model Parameters for Impurities

translate to microscopical diffusivities:

$$\begin{aligned} V_m(P_{i+}) &= 1.68e-4 * \exp(-1.310eV/kT) \\ V_m(P_{i0}) &= 5.96e-4 * \exp(-1.805eV/kT) \\ V_m(P_{V+}) &= 2.56e-2 * \exp(-2.100eV/kT) \\ V_m(P_{V0}) &= 2.56e-2 * \exp(-2.43eV/kT) \\ V_m(P_{V-}) &= 4.22e-2 * \exp(-1.97eV/kT) \end{aligned}$$

where the binding prefactors equal 1.0 and the energies equal 1.83 eV for P^+ plus a neutral interstitial and equal 1.34 eV for P^+ plus a neutral vacancy and, for the following electronic levels for the phosphorus interstitials and vacancy pairs:

```
pdbSetDoubleArray KMC Si P e0 {PiP 0.1  
PiM 5.0  
PVP 0.1  
PVM 0.29}
```

The electronic levels at T=0 for the phosphorus–interstitial or phosphorus–vacancy pairs are partly based on the literature [72].

The binding energies for the phosphorus–interstitial and phosphorus–vacancy pairs are based on [72], and are derived from the following relation [18]:

$$\begin{aligned} E_b(P_{i+}) &= E_b(P_{i0}) - e_0(P_{i+}) + e_0(I^-) = 0.83 - 0.10 + 1.0 = 1.73 \\ E_b(P_{V+}) &= E_b(P_{V0}) - e_0(P_{V+}) + e_0(V^-) = 1.04 - 0.10 + 0.6 = 1.54 \end{aligned}$$

However, a small adjustment of +0.1 eV to the phosphorus–interstitial binding energy and +0.2 eV to the phosphorus–vacancy binding energy were selected.

The substitutional P^+ is immobile as well as the P^+ is paired with I^{--} .

For germanium, the phosphorus diffusivities, dominated by P^+V^{--} pairs based on Zographos and Erlebach [75] and with phosphorus–interstitial contribution inherited from silicon:

$$\begin{aligned} D(P+I0) &= 0.453 * \exp(-3.482eV/kT) \\ D(P+I-) &= 1.610 * \exp(-3.647eV/kT) \\ D(P+V0) &= 1.0e-4 * \exp(-3.000eV/kT) \\ D(P+V-) &= 1.0e-4 * \exp(-3.000eV/kT) \\ D(P+V--) &= 2.0e-3 * \exp(-2.100eV/kT) \end{aligned}$$

translate to microscopical diffusivities:

$$\begin{aligned} V_m(P_{i+}) &= 1.68e-4 * \exp(-1.63eV/kT) \\ V_m(P_{i0}) &= 5.96e-4 * \exp(-2.07eV/kT) \\ V_m(P_{V+}) &= 4.90e-7 * \exp(-1.34eV/kT) \\ V_m(P_{V0}) &= 4.90e-7 * \exp(-1.61eV/kT) \\ V_m(P_{V-}) &= 9.80e-6 * \exp(-0.48eV/kT) \end{aligned}$$

Chapter 6: Contents of Advanced Calibration of Sentaurus Process KMC

Part 2: Model Parameters for Impurities

where the binding prefactors equal 1.0, and the energies equal 1.33 eV for P⁺ plus a neutral interstitial, equal 1.55 eV for P⁺ plus a neutral vacancy, and for the following electronic levels for the phosphorus interstitials and vacancy pairs:

```
pdbSetDoubleArray KMC Ge P e0 {PiP 0.10  
PiM 5.00  
PVP 0.10  
PVM 0.60}
```

The electronic levels for phosphorus–vacancy pairs are based on [76]; those for phosphorus–interstitial pairs are inherited from silicon. The binding energy for the phosphorus–vacancy has been calibrated and is in the range of reported values [76][77]. The binding energy for phosphorus–interstitial pairs has been calibrated.

The substitutional P⁺ as well as P⁺ paired with I[–] are immobile, as in silicon.

Indium

For silicon, the diffusivities of Pichler [65]:

$$\begin{aligned}D(\text{In-I0}) &= 3.13 * \exp(-3.668\text{eV}/kT) \\D(\text{In-I+}) &= 6.45 * \exp(-3.752\text{eV}/kT)\end{aligned}$$

translate to microscopical diffusivities:

$$\begin{aligned}V_m(\text{InI-}) &= 1.15e-3 * \exp(-0.426\text{eV}/kT) \\V_m(\text{InI0}) &= 2.39e-3 * \exp(-0.730\text{eV}/kT)\end{aligned}$$

where the binding prefactors equal 1.0, and the energies equal 0.76 eV for In plus a neutral interstitial and equal 1.25 eV for In plus a vacancy, for the following electronic levels:

```
pdbSetDoubleArray KMC Si In e0 {IniM 0.7  
IniP -5.0  
InVM 1.0  
InVP -5.0}
```

The electronic levels at T=0 for the indium–interstitial and indium–vacancy pairs are calibrated.

The substitutional In[–] as well as the In[–] paired with I⁺⁺ or any V are immobile.

Note:

Advanced Calibration for Sentaurus Process KMC does not include any parameters for indium in germanium.

Carbon

For silicon, the diffusivity of continuum Advanced Calibration Version T-2022.03 (see [Carbon Diffusion on page 55](#)):

$$D(C-\text{I0}) = 6.11 * \exp(-3.293\text{eV}/kT)$$

Chapter 6: Contents of Advanced Calibration of Sentaurus Process KMC

Part 2: Model Parameters for Impurities

translates to microscopical diffusivities:

$$Vm(Ci-) = 2.26e-3 * \exp(-0.791eV/kT)$$

where the binding prefactor equals 1.0 and the binding energy equals 1.5 eV for C plus a neutral interstitial [78]. In addition, C–V pairing is allowed with the binding prefactor equal to 1.0 and the binding energy equal to 0.25 eV for C plus a neutral vacancy. The substitutional C and the C–V pair are both immobile.

Note:

Advanced Calibration for Sentaurus Process KMC does not include any parameters for carbon in germanium.

Fluorine

Current understanding attributes fluorine diffusion in silicon primarily to the migration of interstitial fluorine from a bond-centered site or a tetrahedral site, both of which are also the ground-state configurations of fluorine [79][80]. To comply with this model for this calibration of Sentaurus Process KMC, a very stable and mobile Fi of neutral charge has been assumed [81], similar to the advanced fluorine model of continuum Advanced Calibration Version T-2022.03 (see [Fluorine Diffusion and Clustering on page 99](#)). In the context of Sentaurus Process KMC, interstitial fluorine (Fi) and fluorine–interstitial pairs (FI) are the same.

Note:

By default, Sentaurus Process KMC assigns the particle name F to the interstitial fluorine. To correctly rename the interstitial fluorine to Fi in Advanced Calibration, the Monte Carlo implantation name of fluorine is redefined by the command:

```
set MCnameOf(Fluorine) "FI"
```

The microscopical diffusivity for Fi is assumed to be:

$$Vm(Fi) = 1.00e-6 * \exp(-0.600eV/kT)$$

where the binding prefactors equal 1.0 and the energies equal 4.59 eV for F plus a neutral interstitial and 1.95 eV for F plus a neutral vacancy as reported in [81].

The substitutional F and the F paired with V are immobile.

In addition to diffusion in crystalline silicon, Advanced Calibration activates fluorine diffusion in amorphous silicon mediate by dangling bonds similar as for boron [15][16]. The microscopical diffusivity with activation energy taken from the literature [82] is set to:

$$Vm(Fi) = 0.15 * \exp(-2.2/kT)$$

where the binding prefactors equal 1.0, and the energies equal 0.2 eV for F plus a dangling bond. The coefficient for dangling bond creation per F atom in amorphous silicon is set to 0.5 to obtain good accuracy with SIMS for fluorine implantation into amorphous silicon [69].

Chapter 6: Contents of Advanced Calibration of Sentaurus Process KMC

Part 2: Model Parameters for Impurities

Note:

Advanced Calibration for Sentaurus Process KMC does not include any parameters for fluorine in germanium.

Nitrogen

Current understanding attributes nitrogen diffusion in silicon primarily to the migration of interstitial nitrogen from a bond-centered site or a split-interstitial site, both of which are also the ground-state configurations of nitrogen, and to the migration of nitrogen dimer [83][84]. Following the continuum model proposed by Adam *et al.* [85], a very stable and mobile Ni of neutral charge has been assumed for this calibration of Sentaurus Process KMC. The N_2l_2 nitrogen dimer diffusion, which is activated by default and modeled by the special dopant Nn, is switched off for simplicity by deactivating the following nonstandard interaction:

```
pdbSet KMC Si N SpecialReaction N,N,NnV false
```

Note:

By default, Sentaurus Process KMC assigns the particle name N to the interstitial nitrogen. To correctly rename the interstitial nitrogen to Ni in Advanced Calibration, the Monte Carlo implantation name of nitrogen is redefined by the command:

```
set MCnameOf(Nitrogen) "Ni"
```

Based on [84], the microscopical diffusivities for Ni and NV are defined to be:

$$\begin{aligned} V_m(\text{Ni}) &= 1.70e-3 * \exp(-0.560\text{eV}/kT) \\ V_m(\text{NV}) &= 1.00e-4 * \exp(-1.360\text{eV}/kT) \end{aligned}$$

where the binding prefactors equal 1.0, and the energies equal 3.5 eV [83] for N plus a neutral interstitial and 1.7 eV [67] for N plus a neutral vacancy.

The substitutional N is immobile.

Nitrogen is known to introduce deep levels into the electronic band gap and, therefore, does not serve as a dopant in silicon.

Note:

Advanced Calibration for Sentaurus Process KMC does not include any parameters for nitrogen in germanium.

Clusters

In Advanced Calibration for continuum Sentaurus Process, the transient dopant cluster model is, in general, used for dopant activation in crystalline silicon and germanium, which incorporates only impurities and no point defects in the dopant clusters (see [Defect Cluster Models in Silicon and Germanium on page 30](#)). For some impurities, the advanced models

offer dopant clustering with point defects (see [Part 4: Comprehensive and Slow Models on page 94](#)). In Sentaurus Process KMC, this phenomenon can be explained by a dopant–point defect clustering mechanism or dopant precipitation or both. Obviously, a straight translation from the continuum activation model to the kinetic Monte Carlo cluster reactions is only possible if a comprehensive dopant clustering model is available. Nevertheless, additional dopant cluster calibration for Advanced Calibration of Sentaurus Process KMC is performed to obtain a good agreement with SIMS and sheet resistance measurements.

For all impurity clusters, the corrections for the binding energies with bandgap narrowing are taken into account using the parameter flag:

```
pdbSet KMC Si BandGap Correct.Complex true
```

Boron

Based on [\[86\]\[87\]\[88\]](#), a comprehensive model for boron–interstitial clustering (BIC) in silicon is implemented. The allowed BIC configurations are B_nI_m with $0 < n < 9$ and $0 \leq m \leq 9$.

The potential energies and capture volumes of B_2 , B_2I , B_2I_2 , B_2I_3 , B_3 , B_3I , B_3I_2 , and B_3I_3 as well as the boron–interstitial pair and the interstitial emission factors were translated from the BIC model of [\[87\]](#), being part of the comprehensive models of continuum Advanced Calibration (see [Boron–Interstitial Clusters on page 97](#)). Since this continuum BIC model includes only the configurations B_2 , B_2I , B_2I_2 , B_3I , B_3I_2 , and B_3I_3 , the potential energies and capture volumes of the configurations BI_2 , B_2I_3 , and B_3 are calibrated in kinetic Monte Carlo only. The potential energies and capture volumes of all other BIC configurations are inherited from [\[88\]](#). To obtain a good agreement with a wide range of SIMS, the boron–interstitial pair emission factor is adjusted.

In addition to clustering in crystalline silicon, Sentaurus Process KMC allows dopant clusters in amorphous silicon. In the case of boron, B_2 and B_3 clusters including one or two dangling bonds are allowed to form with potential energies calibrated to SIMS [\[15\]\[68\]](#).

In the literature [\[89\]](#), segregation of boron to end-of-range defects is observed. To account for such an effect, the mobile boron–interstitial pairs can react with extended defects such as {311} defects and dislocation loops. The pair breaks up and the interstitial is incorporated into the extended defect, while the boron is regarded as substitutional.

For germanium, the same BIC model is implemented with identical cluster configurations and capture volumes. The potential energies of the BICs as well as the boron–interstitial pair and the interstitial emission factors were calibrated based on SIMS and sheet resistance data from the literature [\[90\]\[91\]](#).

Arsenic

Based on the density functional theory (DFT) calculations of Sahli *et al.* [72] and Harrison *et al.* [92], arsenic forms stable clusters with vacancies and with interstitials in silicon. The allowed As–V clusters are As_2V , As_3V , and As_4V . The allowed As–I clusters are:

- As_nI with $1 < n < 6$
- As_nI_2 with $0 < n < 7$
- As_nI_3 with $0 < n < 7$
- As_nI_4 with $1 < n < 5$

The allowed arsenic agglomerates are As_2 , As_3 , and As_4 . The corresponding potential energies are taken from [71], [72], or [92]. The capture volumes as well as the emission factors are calibrated.

The formation energies of As_3V , As_4 , and As_4V are even lower than the isolated substitutional As ($E_f(\text{As}_n\text{V}) = E_{\text{pot}}(\text{As}_n\text{V}) + E_f(\text{V}) < 0$) in silicon and, therefore, these are the most stable clusters. Including As_nI_m clusters in the arsenic-clustering model improves the accuracy for lower thermal budgets and higher interstitial supersaturations compared to the model where arsenic forms only stable clusters with vacancies, but not with interstitials [93].

Following [71] and [94], As_2V clusters are defined as mobile clusters:

```
pdbSet KMC Si As Dm_Complex As2V 4.0  
pdbSet KMC Si As Em_Complex As2V 2.0
```

With As_2V clusters being mobile, the high concentration effect of As diffusion in silicon [74] can be explained [71].

For germanium, the same As–V and As–I cluster model is implemented with identical cluster configurations and capture volumes. The potential energies of As_2V , As_3V , and As_4V are similar to the ones reported in [77], while the potential energies of the remaining arsenic clusters as well as the arsenic–point defect pair and the interstitial emission factors were calibrated. Unlike for silicon, As_2V clusters are defined as immobile clusters.

Phosphorus

For phosphorus, an approach was chosen following the suggestion of [72]. Phosphorus forms stable clusters with vacancies and with interstitials. The allowed P–V clusters are P_2V , P_3V , and P_4V . The allowed P–I clusters are:

- P_nI with $1 < n < 6$
- P_nI_2 with $0 < n < 7$

Chapter 6: Contents of Advanced Calibration of Sentaurus Process KMC

Part 2: Model Parameters for Impurities

- P_nI_3 with $0 < n < 7$
- P_nI_4 with $1 < n < 5$

The allowed phosphorus agglomerates are P_2 , P_3 , and P_4 . The corresponding potential energies are based on DFT calculations of [72], or follow the ones from As–I clusters (see [Arsenic on page 242](#)), while the capture volumes as well as the emission factors are calibrated by comparison with experimental data.

Unlike the neutral P–V and P–I clusters, the phosphorus agglomerates P_2 , P_3 , and P_4 are assumed to carry a single positive charge like substitutional phosphorus. This assumption is based on DFT calculations by Synopsys following [95].

To allow phosphorus deactivation at high concentrations and low thermal budgets, the percolation model for diffusion-less deactivation by immobile reactants is activated.

The allowed reactions are:

- $P + P \rightleftharpoons P_2$
- $P + P_2 \rightleftharpoons P_3$
- $P + P_3 \rightleftharpoons P_4$
- $P + P_2V \rightleftharpoons P_3V$
- $P + P_3V \rightleftharpoons P_4V$

In analogy to arsenic, P_2V clusters are defined as mobile clusters and, to a lesser extent, also P_3V and P_4V clusters. Since P–V clusters are mobile, the high concentration effect of phosphorus diffusion in silicon can be explained.

To account for segregation of phosphorus to end-of-range defects in silicon, the mobile phosphorus–interstitial pairs can react with {311} defects, resulting in the pair being trapped at the edge of the extended defect. The corresponding binding energy and emission prefactor have been calibrated.

For germanium, the same P–V and P–I cluster model is implemented with identical cluster configurations, charges, and capture volumes. The potential energies of P_2V , P_3V , and P_4V are similar to the ones reported in [77], while the potential energies of the remaining phosphorus clusters as well as the phosphorus–point defect pair and the interstitial emission factors were calibrated. In line with silicon, the percolation model for diffusion-less deactivation by immobile reactants is activated with identical parameter values.

Arsenic and Phosphorus

According to Sahli *et al.* [72], arsenic and phosphorus can form mixed clusters in silicon with binding energies similar to pure arsenic or phosphorus clusters. Therefore, mixed arsenic–phosphorus clusters with interstitials or vacancies are allowed in this calibration. The allowed P–As–V clusters are $PAsV$, PAs_2V , P_2AsV , PAs_3V , P_2As_2V , and P_3AsV . The allowed

Chapter 6: Contents of Advanced Calibration of Sentaurus Process KMC

Part 2: Model Parameters for Impurities

P–As–I clusters are PAsI, PAs₂I, and P₂AsI. The allowed P–As agglomerates are PAs, PAs₂, and P₂As. The corresponding potential energies are taken from [72], while the capture volumes are inherited from pure arsenic and phosphorus clusters, and the emission factors have been calibrated.

Following [71], PAsV clusters are defined as mobile clusters:

```
pdbSet KMC Si P Dm_Complex PAsV 0.6  
pdbSet KMC Si P Em_Complex PAsV 2.0
```

With PAsV clusters being mobile, the high concentration effect of As diffusion in silicon [74] can be explained [71].

For germanium, the same mixed arsenic–phosphorus cluster model is implemented with identical cluster configurations and capture volumes. The potential energies of PAsV, PAs₂V, P₂AsV, PAs₃V, P₂As₂V, and P₃AsV are similar to the ones reported in [77], while the potential energies of the remaining arsenic clusters as well as the arsenic–point defect pair and the interstitial emission factors were calibrated. Unlike for silicon, PAsV clusters are defined as immobile clusters.

Indium

In this calibration, indium is assumed to form indium–interstitial and indium–vacancy clusters in silicon. The allowed In–V clusters are In₂V, In₃V, and In₄V. The allowed In–I clusters are InI₂, In₂I, and In₃I. The allowed In agglomerates are In₂, In₃, and In₄. The corresponding potential energies and capture volumes as well as the emission factors are calibrated by comparison with experimental data.

In the literature [96], segregation of indium to end-of-range defects is observed. To account for such an effect, the mobile indium–interstitial pairs can react with extended defects such as {311} defects and dislocation loops, resulting in the pair being trapped at the edge of the extended defect. The corresponding binding energy and emission prefactor have been calibrated.

Carbon

The model for carbon clustering in silicon in this calibration mainly follows the comprehensive model for carbon–interstitial clustering as proposed in [78]. The allowed carbon–interstitial cluster configurations are Cl₂, C₂, C₂I, C₂I₂, C₂I₃, C₃, C₃I, C₃I₂, C₃I₃, C₃I₄, C₄I₁, C₄I₂, C₄I₃, C₄I₄, C₄I₅, C₅I₃, C₅I₄, C₅I₅, C₅I₆, C₆I₄, C₆I₅, C₆I₆, and C₆I₇. In addition, the carbon–vacancy clusters C₂V and C₃V are allowed. The corresponding potential energies and capture volumes as well as the emission factors are calibrated by comparison with experimental data.

To account for segregation of carbon to end-of range defects in silicon, the mobile carbon–interstitial pairs can react with {311} defects and dislocation loops [78]. The pair breaks up

and the interstitial is incorporated into the extended defect, while the carbon is regarded as substitutional.

Boron and Carbon

According to [97][98], boron and carbon can form relatively stable mixed clusters in silicon. Therefore, mixed boron–carbon clusters with interstitials are allowed in silicon in this calibration. The allowed B–C–I clusters are BC_I, B₂C_I, BC₂I, BC₂I₂, BC₃I₂, BC₃I₃, BC₃I₄, BC₄I₃, BC₅I₆, and BC₅I₇. The allowed B–C agglomerates are BC, BC₂, and B₂C. The corresponding potential energies as well as the emission factors are calibrated, while the capture volumes are inherited from pure boron and carbon clusters.

Fluorine

In the literature [79][80], strongly bound fluorine–vacancy complexes in silicon are proposed. The F–V structures considered there are interstitial fluorine atoms decorating one or two vacancies. In the context of Sentaurus Process KMC, these structures are considered to be actually fluorine–interstitial clusters [81]. This means, for example, that the cluster type F₃V of [79][80], consisting of three interstitial F and one V, corresponds to an F₃I₂ in Sentaurus Process KMC. The allowed F–I clusters in silicon are FI₂, F₂, F₂I, F₃, F₃I, F₃I₂, F₄, F₄I, F₄I₂, F₄I₃, F₅, F₅I, F₅I₂, F₅I₃, F₆, F₆I₁, F₆I₂, F₆I₃, F₆I₄, F₇I₃, F₇I₄, F₈I₄, F₈I₅, and F₉I₅. The allowed F–V clusters are FV₂, F₂V, F₂V₂, and F₃V. The allowed fluorine agglomerates are F₂, F₃, F₄, F₅, and F₆. The corresponding potential energies are taken from [81]. The capture volumes as well as the emission factors are calibrated.

Nitrogen

According to the literature [65], nitrogen can cluster with interstitials and vacancies in silicon. The nitrogen dimer N₂I₂ is supposed to be very stable and even mobile [84]. In this calibration, nitrogen dimer is allowed to diffuse in silicon by setting:

```
pdbSet KMC Si N Dm_Complex N2I2 6.70e-5  
pdbSet KMC Si N Em_Complex N2I2 2.38
```

All other nitrogen–interstitial clusters are assumed to be immobile. The allowed N–I clusters are NI₂, N₂I, N₂I₂, and N₂I₃. The only allowed N agglomerate is N₂. The corresponding potential energies and capture volumes as well as the emission factors are calibrated by comparison with experimental data.

To account for segregation of nitrogen to end-of-range defects in silicon, mobile nitrogen–interstitial pairs can react with {311} defects and dislocation loops, resulting in the pairs being trapped at the edge of the extended defect. The corresponding binding energy and emission prefactor have been calibrated.

Boron and Nitrogen

Similar to the mixed boron–carbon clusters, mixed boron–nitrogen clusters with interstitials are allowed in silicon in this calibration. The allowed B–N–I clusters are BNI , BNI_2 , B_2NI , B_2NI_2 , BN_2I , and BN_2I_2 . The allowed B–N agglomerates are BN , BN_2 , and B_2N . The corresponding potential energies and the emission factors are calibrated, while the capture volumes are inherited from pure boron and nitrogen clusters.

Carbon and Nitrogen

In analogy to the mixed boron–nitrogen clusters, mixed carbon–nitrogen clusters with interstitials are allowed in silicon in this calibration. The allowed C–N–I clusters are CNI , CNI_2 , C_2NI , C_2NI_2 , CN_2I , and CN_2I_2 . The allowed C–N agglomerates are CN , CN_2 , and C_2N . The corresponding potential energies and the emission factors are calibrated, while the capture volumes are inherited from pure carbon and nitrogen clusters.

Segregation

The Si– SiO_2 , Ge– SiO_2 , and Ge– GeO_2 interface model accounting for dopant segregation is the three-phase segregation model, similar to the one of continuum Sentaurus Process and [99]. The Sentaurus Process KMC parameters `EMax.Surf` and `C0Max.Surf` correspond to the continuum parameter `CMax`, which defines the number of trap sites at the interface. While the interface segregation of the continuum model is controlled by dopant trapping and the parameters of the emission rates for each side of the interface, the parameters of the kinetic Monte Carlo interface model are the barrier and binding energies of dopants on each side of the interface.

The next sections explain the calibration of Si– SiO_2 , Ge– SiO_2 , and Ge– GeO_2 segregation for different dopants and impurities. In general, parameters for Si–nitride and Ge–nitride interfaces are inherited from Si– SiO_2 and Ge– GeO_2 interfaces and are not explained explicitly.

Boron

At the Si– SiO_2 interface, the number of interface traps for boron is temperature independent and corresponds to the one for Advanced Calibration for continuum Sentaurus Process at 647°C (see [Boron Dose Loss on page 44](#)). Interface barrier and binding energies for boron were calibrated based on a collection of boron SIMS profiles, for both crystalline and amorphous silicon.

The parameters of the Ge– SiO_2 and Ge– GeO_2 interfaces are set to the same values as for the Si– SiO_2 interface.

Since the interface barrier for boron trapping at the silicon side is relatively low, the limiting factor for boron dose loss, in general, is the number of interface traps. In the presence of

Chapter 6: Contents of Advanced Calibration of Sentaurus Process KMC

Part 2: Model Parameters for Impurities

fluorine trapped in the interface (such as in the case of BF_2 implantation or fluorine coimplantation after annealing), the number of boron interface traps is increased by the `Factor.Max.Surf` and `Exp.Max.Surf` parameters. As a result, boron dose loss is enhanced, similar as for continuum Sentaurus Process (see [Fluorine Diffusion and Clustering on page 99](#)).

Arsenic

At the $\text{Si}-\text{SiO}_2$ interface, the number of interface traps for arsenic is temperature independent and corresponds to the one for Advanced Calibration for continuum Sentaurus Process at 436°C (see [Arsenic Dose Loss on page 48](#)). Interface barrier and binding energies for arsenic were calibrated based on a collection of arsenic SIMS profiles.

The parameters of the $\text{Ge}-\text{SiO}_2$ and $\text{Ge}-\text{GeO}_2$ interfaces are set to the same values as for the $\text{Si}-\text{SiO}_2$ interface.

Phosphorus

At the $\text{Si}-\text{SiO}_2$ interface, the number of interface traps for phosphorus is much higher than the value from Advanced Calibration for continuum Sentaurus Process (see [Phosphorus Dose Loss on page 51](#)), because of the lack of P_2 accumulation at the interface for KMC. The interface barrier and binding energies for phosphorus were calibrated based on a collection of phosphorus SIMS profiles. In particular, a negative barrier for $\text{P}-\text{I}$ pairs was chosen to allow for strong phosphorus dose loss.

The parameters for interface barriers, interface binding energies, interface traps, and emission to oxide for the $\text{Ge}-\text{SiO}_2$ and $\text{Ge}-\text{GeO}_2$ interfaces were calibrated based on a collection of phosphorus SIMS profiles.

Indium

The number of interface traps at the $\text{Si}-\text{SiO}_2$ interface for indium cannot be taken from Advanced Calibration for continuum Sentaurus Process, where no third phase is modeled (see [Indium Parameters on page 54](#)), and is set to a high value to allow for strong dose loss. The $\text{Si}-\text{SiO}_2$ interface barrier and binding energies for indium were calibrated based on a collection of indium SIMS profiles.

Carbon

The number of interface traps at the $\text{Si}-\text{SiO}_2$ interface for carbon cannot be taken from Advanced Calibration for continuum Sentaurus Process, where no third phase is modeled.

The number of interface traps, the interface barrier, and the binding energies for carbon have been calibrated based on a collection of carbon SIMS profiles.

Fluorine

The number of Si–SiO₂ interface traps, the Si–SiO₂ interface barrier, and the binding energies for fluorine have been calibrated to allow strong dose loss from silicon. In addition, fluorine diffusion in oxide is strongly reduced to save CPU time.

Nitrogen

The number of Si–SiO₂ interface traps, the Si–SiO₂ interface barrier, and the binding energies for nitrogen have been calibrated to allow strong dose loss from silicon. In addition, the nitrogen emitted from the interface to the oxide is evaporated, and the nitrogen diffusion in oxide is strongly reduced to save CPU time.

Recrystallization

Solid phase epitaxial regrowth (SPER) can affect the impurity distribution. The recrystallization front can move dopants away, changing the concentration profiles [100]. Sentaurus Process KMC can model this effect by sweeping the dopant concentration stored in amorphous defects when the amorphous defects recrystallize [3]. The parameters `Pref.RecrystDeposit` and `Ener.RecrystDeposit` define the probability of a dopant remaining in the same position after the recrystallization front passes and, therefore, the parameters control the number of swept dopants.

In Sentaurus Process, the initial level of active concentration in amorphized regions after recrystallization can be specified per dopant as `AmInit`. For Sentaurus Process KMC, this corresponds to the prefactor `c0.Recryst.Max.Active` and the activation energy `E.Recryst.Max.Active`. For this calibration, the deposited dopant-cluster types during SPER are specified by `Recryst.Deposit.Complex` because the `Recryst.Max.Size` parameter is unset. The improved algorithm activated by the `Fix.Recryst.Max.Active` parameter is used for better resolution of the activation level for lower concentrations.

Boron

According to [100], no boron is swept by the recrystallization front in silicon. Therefore, the `Pref.RecrystDeposit` value is set to 100% [3]. The maximum active boron concentration after silicon recrystallization is temperature dependent, with 2.4×10^{20} at 550°C and $5.4 \times 10^{20} \text{ cm}^{-2}$ at 1050°C close to reported values [101]. These values are higher than the one for continuum Advanced Calibration (see [Boron–Interstitial Clusters on page 97](#)). The exceeding boron concentration is deposited as B₂ clusters [102]. Finally, boron has no effect on the silicon recrystallization velocity other than the doping effect (see [Amorphization and Recrystallization on page 218](#)).

As for silicon, no boron is swept by the recrystallization front in germanium. Therefore, the `Pref.RecrystDeposit` value is set to 100%. The maximum active boron concentration after germanium recrystallization is $5.0 \times 10^{20} \text{ cm}^{-2}$ [91] for all temperatures. The exceeding

boron concentration is deposited as B_2 clusters, in analogy to silicon. Finally, boron has no effect on the germanium recrystallization velocity other than the doping effect (see [Amorphization and Recrystallization on page 218](#)).

Arsenic

Following [100], arsenic is swept by the recrystallization front in silicon. The `Pref.RecrystDeposit` value is set to 20%. The maximum active arsenic concentration after silicon recrystallization is temperature dependent, with $6.0 \times 10^{20} \text{ cm}^{-2}$ at 550°C and $1.3 \times 10^{21} \text{ cm}^{-2}$ at 1050°C . These values are higher than the one for continuum Advanced Calibration. The exceeding arsenic concentration is deposited as As_2 and As_3 clusters in the ratio 1:1. Finally, arsenic is assumed to have no effect on the recrystallization velocity other than the doping effect (see [Amorphization and Recrystallization on page 218](#)).

As for silicon, arsenic is assumed to be swept by the recrystallization front in germanium. The `Pref.RecrystDeposit` value is set to 50%. The maximum active arsenic concentration after germanium recrystallization is $1.0 \times 10^{20} \text{ cm}^{-2}$ for all temperatures. The exceeding arsenic concentration is deposited as As_2 clusters only. Finally, arsenic has no effect on the germanium recrystallization velocity other than the doping effect (see [Amorphization and Recrystallization on page 218](#)).

Phosphorus

For silicon, the `Pref.RecrystDeposit` value for phosphorus is set to 10%. The maximum active phosphorus concentration after silicon recrystallization is temperature dependent, with $1.1 \times 10^{21} \text{ cm}^{-2}$ at 550°C and $2.4 \times 10^{21} \text{ cm}^{-2}$ at 1050°C . These values are higher than the one for continuum Advanced Calibration. The exceeding phosphorus concentration is deposited as P_3 clusters. Finally, phosphorus has no effect on the recrystallization velocity other than the doping effect (see [Amorphization and Recrystallization on page 218](#)).

As for silicon, phosphorus is assumed to be swept by the recrystallization front in germanium. The `Pref.RecrystDeposit` value is set to 25%. The maximum active phosphorus concentration after germanium recrystallization is temperature dependent, with $1.5 \times 10^{20} \text{ cm}^{-2}$ at 400°C and $2.4 \times 10^{20} \text{ cm}^{-2}$ at 550°C . The exceeding phosphorus concentration is deposited as P_2 clusters only. Finally, phosphorus has no effect on the germanium recrystallization velocity other than the doping effect (see [Amorphization and Recrystallization on page 218](#)).

Indium

Following [100], [103], and [104], indium is swept by the recrystallization front in silicon, and its incorporation during SPER of silicon is temperature dependent [105]. The `Ener.RecrystDeposit` value is set to 0.3 eV. The maximum active indium concentration after silicon recrystallization is temperature dependent, with $1.1 \times 10^{20} \text{ cm}^{-2}$ at 550°C and $2.4 \times 10^{20} \text{ cm}^{-2}$ at 1050°C . These values are higher and more realistic than the one for

continuum Advanced Calibration. The exceeding indium concentration is deposited as In_2 clusters. Finally, indium has no effect on the recrystallization velocity other than the doping effect (see [Amorphization and Recrystallization on page 218](#)).

Carbon

For silicon, the `Pref.RecrystDeposit` value for carbon is set to 50%. The maximum substitutional carbon concentration after silicon recrystallization is temperature dependent, with $6.0 \times 10^{20} \text{ cm}^{-2}$ at 550°C and $1.3 \times 10^{21} \text{ cm}^{-2}$ at 1050°C . The exceeding carbon concentration is deposited as C_2 [78] and C_3 . Finally, carbon has an impurity effect on the recrystallization velocity with a recrystallization activation energy of 2.8 eV for 100% carbon.

Fluorine

Following [106], fluorine is swept by the recrystallization front in silicon, and its incorporation during SPER of silicon is temperature dependent. The `Ener.RecrystDeposit` value is set to 0.5 eV. Concentrations below $1 \times 10^{18} \text{ cm}^{-2}$ are deposited as interstitial fluorine, while the rest is deposited as F_4I_3 clusters.

Finally, fluorine has an impurity effect on the recrystallization velocity with a recrystallization activation energy of 3.1 eV for 100% fluorine [9].

Nitrogen

In this calibration, no nitrogen is swept by the recrystallization front in silicon. Concentrations below $1 \times 10^{19} \text{ cm}^{-2}$ are deposited as interstitial nitrogen, while the rest is deposited as N_2 clusters.

Epitaxy

In Sentaurus Process, selective epitaxial growth (SEG) of silicon, SiGe, and germanium with *in situ* doping can be simulated by specifying total chemical concentrations of dopants in the `epi.doping` argument of the `diffuse` command. The initial level of active concentration in epitaxially grown regions can be specified per dopant as `EpiInit`.

For Sentaurus Process KMC and using LKMC for SEG, this corresponds to the prefactor `C0.Epi.Max.Active` and the activation energy `E.Epi.Max.Active`. The deposited inactive dopant-cluster types during SEG are specified by `Epi.Deposit.Complex`.

Boron

For the initial activation in the case of *in situ* boron-doped epitaxial growth of silicon or germanium, an activation level of $4 \times 10^{20} \text{ cm}^{-3}$ or $5 \times 10^{20} \text{ cm}^{-3}$, respectively, is assumed. The exceeding boron concentration is deposited as B_2 clusters.

Arsenic

For the initial activation in the case of *in situ* arsenic-doped epitaxial growth of silicon or germanium, an activation level of $2.5 \times 10^{20} \text{ cm}^{-3}$ or $1.0 \times 10^{20} \text{ cm}^{-3}$, respectively, is assumed. The exceeding arsenic concentration is deposited as As₂ clusters.

Phosphorus

For the initial activation in the case of *in situ* phosphorus-doped epitaxial growth of silicon or germanium, an activation level of $1.27 \times 10^{20} \text{ cm}^{-3}$ is assumed. The exceeding phosphorus concentration is deposited as P₄V clusters.

This assumption follows the literature [107][108][109], which attributes the incomplete activation and tensile strain measured after high-concentration Si:P epitaxy to the presence of the pseudocubic Si₃P₄ compound, corresponding to a P₄V cluster in the KMC formalism. (The Si₃P₄ compound consists of four substitutional P, three Si lattice atoms, and one Si vacancy. The KMC formalism ignores the lattice Si; therefore, P₄V.)

Carbon

The maximum substitutional carbon concentration in epitaxially grown silicon is assumed to be $8 \times 10^{20} \text{ cm}^{-3}$, which corresponds to 1.6%. The exceeding carbon concentration is deposited as C₂ clusters.

SiGe

This section discusses silicon germanium.

Linear Germanium Correction Factors

By default, the Ge effects are modeled by linear correction factors for silicon parameters. The calibration is valid for low Ge mole fractions ranging between 0% and 50%.

For low Ge mole fractions, the chemical effect of Ge on dopants is indirect by point defects, which themselves encounter a Ge chemical effect, and is direct mainly for dopant–defect pair diffusion [1][2]. There is no experimental evidence for any chemical effect of Ge on dopant solubility.

Boron

Boron diffusion is retarded in relaxed SiGe in comparison to the one in Si (see [Germanium Effect on Dopant Diffusivity on page 66](#)). The linear expression for the diffusivity activation energy was derived by Ahn [110] and confirmed for low mole fractions by measurements performed within the ATOMICS research project [36].

Chapter 6: Contents of Advanced Calibration of Sentaurus Process KMC

Part 2: Model Parameters for Impurities

In this calibration, the migration barrier and the formation energy of B–I pairs are increased in the presence of Ge:

```
 pdbSet KMC Si B EmGe BiM [expr 0.23/5.e22]
 pdbSet KMC Si B EmGe Bi [expr 0.23/5.e22]
 pdbSet KMC Si B EmGe BiP [expr 0.23/5.e22]
 pdbSet KMC Si B EfGe BiM [expr 0.30/5.e22]
```

To allow for boron segregation into SiGe [111], the formation energy of substitutional B decreases in the presence of Ge [51]:

```
 pdbSet KMC Si B EfGe B [expr -0.50/5.e22]
```

In addition, boron diffusion in amorphous SiGe is retarded in comparison to amorphous silicon [112]. Again, the migration barrier and the formation energy of boron and dangling-bond pairs increase in the presence of Ge.

Arsenic

Arsenic diffusion is enhanced in relaxed SiGe in comparison to the one in Si [113][114][115] (see [Germanium Effect on Dopant Diffusivity on page 66](#)). In this calibration, the migration barrier of As–I pairs is increased in the presence of Ge, while the migration barrier of As–V pairs is lowered in the presence of Ge. The corresponding pair formation energies are independent of Ge content.

Phosphorus

Phosphorus diffusion is enhanced in relaxed SiGe in comparison to the one in Si [114][116]. In this calibration, the migration barrier of P–I pairs is decreased in the presence of Ge, while the migration barrier of P–V pairs is unchanged in the presence of Ge. The P–I pair formation energy is independent of Ge content, while the formation energy of P–V pairs is increased in the presence of Ge.

Silicon and Germanium Parameter Interpolation

Optionally, you can activate Si and Ge parameter interpolation for SiGe using the command:

```
KMC_SiGe_and_Stress_Effect 1 0
```

This deactivates the default linear correction factors and uses the interpolation parameters defined for `SiliconGermanium`. The calibration covers the full Ge mole fraction range (0–100%).

In general, prefactor parameters are interpolated in logarithmic scale, and energy parameters are interpolated in linear scale.

Boron

According to experimental work [36][117], interstitial-mediated B diffusion in relaxed SiGe is retarded with increasing Ge content up to ~50%. For higher Ge content, boron diffusion is again enhanced [118]. Therefore, a parabolic dependency on Ge mole fraction of the diffusivity is assumed for the full Ge mole fraction range instead (see [Germanium Effect on Dopant Diffusivity on page 66](#)). However, the calibration based on SIMS for Si, SiGe [118][119], and Ge [34][70] revealed no need for parabolic interpolation of the microscopic parameters for the boron–interstitials (migration energy, prefactor, and binding energy) but for the ionization energies only. The nonlinear effect of Ge on macroscopic boron diffusivity in SiGe is a consequence of the parabolic dependency of interstitials on the Ge mole fraction.

For BIC potential energies and the initial activation after SPER, linear interpolation is assumed. The boron–interstitial cluster emission prefactor is interpolated parabolically.

Arsenic

Arsenic diffusion is enhanced in relaxed SiGe in comparison to the one in silicon [113][114][115] (see [Germanium Effect on Dopant Diffusivity on page 66](#)). In Advanced Calibration, only the migration rate of As⁺V⁻⁻ is larger in germanium than in silicon. For all other As–V and As–I pairs, they are larger in silicon than in germanium. Based on SIMS data provided to Synopsys by AMAT-VSE, parabolic interpolation for the arsenic–interstitial and arsenic–vacancy migration energy has been calibrated.

For the arsenic-cluster potential energies, the cluster emission prefactors, and the initial activation after SPER, parabolic interpolation is assumed. Moreover, the prefactor for As₂V migration is interpolated parabolically to limit cluster diffusion in SiGe.

For the interface with SiO₂, parabolic interpolation is used for the number of interface traps and the As⁺V⁻⁻ energy barrier.

Phosphorus

As for arsenic, phosphorus diffusion is enhanced in relaxed SiGe in comparison to the one in silicon [114][116] (see [Germanium Effect on Dopant Diffusivity on page 66](#)). In Advanced Calibration, the migration rate of P⁺V⁻⁻ and P–I pairs is larger in germanium than silicon. For all other P–V pairs, they are larger in silicon than in germanium. Based on SIMS data provided to Synopsys by AMAT-VSE [46] and SIMS data from the literature [120], parabolic interpolation for the phosphorus–interstitial and phosphorus–vacancy migration energy has been calibrated.

For the phosphorus-cluster potential energies, the cluster emission prefactors, and the initial activation after SPER, parabolic interpolation is assumed.

For the interface with SiO₂, parabolic interpolation is used for the P⁺V⁻⁻ energy barrier.

Stress Effects

The stress effects on dopants in Advanced Calibration for Sentaurus Process KMC are taken into account only if the `KMC Stress` switch is activated. This is accomplished by the command:

```
KMC_SiGe_and_Stress_Effect 0 1
```

The procedure `KMC_SiGe_and_Stress_Effect` has two Boolean arguments: the first is `Ge_Chem_Eff` and the second is `Stress_Eff`, which is dedicated for stress effects.

Alternatively, the `KMC Stress` switch can be activated directly:

```
pdbSet KMC Stress 1
```

The calibration of stress effects [1][2] is based on a relatively small set of measured data. The models have not yet been tested rigorously against SIMS data for all dopant species and nonequilibrium annealing conditions, and against electrical data from real-device fabrication processes.

The stress effect on dopants is indirect by stress-dependent point defects and is direct mainly for dopant–defect pair diffusion [1][2]. Dopant diffusion in Si or SiGe can be anisotropic in the presence of biaxial strain and, therefore, anisotropic diffusion tensors are used [121]. Dopant solubilities are changed in the presence of stress according to [122]. However, in this calibration, the dopant–defect cluster stability is kept independent of stress due to the limited availability of experimental data for calibration.

Boron

According to first-principles density functional theory calculations [61][123][124], boron diffusion in silicon shows an anisotropy as a function of biaxial strain. Biaxial tension (as in strained Si on SiGe) leads to significantly higher in-plane diffusion compared to the perpendicular direction. The diffusion barrier along the strain plane is decreased (with a value similar to continuum Advanced Calibration (see [Impact of Pressure on Dopant Diffusivity on page 71](#))), while the barrier in the vertical direction remains unchanged:

```
pdbSetArray KMC Si B VD { BiM -0.0024,0.0  
                           Bi   -0.0024,0.0  
                           BiP -0.0024,0.0 }
```

The formation energy of B–I pairs is independent of strain. To allow for boron segregation into SiGe [51], the formation energy of substitutional B decreases in the presence of strain:

```
pdbSetDoubleArray KMC Si B VF { B    -0.03  
                                 BiM  0.0 }  
pdbSetDoubleArray KMC Ge B VF { B    -0.03  
                                 BiM  0.0 }
```

Arsenic

According to first-principles density functional theory calculations [110][124], arsenic in silicon undergoes a total diffusivity enhancement under compressive strain [115] and little change under tensile strain [125]. The migration barrier of As–I pairs is increased under compressive strain, while the migration barrier of As–V pairs is lowered under compressive strain, with values similar to continuum Advanced Calibration (see [Impact of Pressure on Dopant Diffusivity on page 71](#)).

The diffusivity enhancement or retardation is isotropic and larger for the vacancy mechanism than for the interstitial mechanism:

```
pdbSetArray KMC Si As VD { AsiP -0.0040,-0.0040
                            Asi -0.0040,-0.0040
                            AsVP 0.0018,0.0018
                            AsV 0.0018,0.0018
                            AsVM 0.0018,0.0018 }
pdbSetArray KMC Ge As VD { AsiP -0.0040,-0.0040
                            Asi -0.0040,-0.0040
                            AsVP 0.0018,0.0018
                            AsV 0.0018,0.0018
                            AsVM 0.0018,0.0018 }
```

In this calibration, the formation energies of As–I and As–V pairs are independent of strain. To allow for arsenic segregation out of SiGe, the formation energy of substitutional As increases slightly in the presence of strain:

```
pdbSetDoubleArray KMC Si As VF { Asi 0.008
                                    AsiP 0.0
                                    AsVP 0.0 }
pdbSetDoubleArray KMC Ge As VF { Asi 0.008
                                    AsiP 0.0
                                    AsVP 0.0 }
```

Phosphorus

According to first-principles density functional theory calculations [110], phosphorus undergoes a total diffusivity retardation under compressive strain and enhancement under tensile strain. The migration barrier of P–I pairs is increased under compressive strain, while the migration barrier of P–V pairs is lowered under compressive strain, with values similar to continuum Advanced Calibration (see [Impact of Pressure on Dopant Diffusivity on page 71](#)). While strain has negligible impact on in-plane diffusivity, out-of-plane diffusivity is a modest function of strain:

```
pdbSetArray KMC Si P VD { PiP -0.0022,-0.0022
                            Pi -0.0022,-0.0022
                            PVP 0.0040,0.0040
                            PV 0.0040,0.0040
                            PVM 0.0040,0.0040 }
```

Chapter 6: Contents of Advanced Calibration of Sentaurus Process KMC

Section 4: Model Parameters for Epitaxial Growth

```
pdbSetArray KMC Ge P VD { PiP -0.0011,-0.0011  
Pi -0.0011,-0.0011  
PVP 0.0020,0.0020  
PV 0.0020,0.0020  
PVM 0.0020,0.0020 }
```

In this calibration, the formation energies of P–I and P–V pairs are independent of strain. To allow for phosphorus segregation out of SiGe [120], the formation energy of substitutional P increases slightly in the presence of strain:

```
pdbSetDoubleArray KMC Si P VF { P 0.004  
PiP 0.0  
PVP 0.0 }  
pdbSetDoubleArray KMC Ge P VF { P 0.04  
PiP 0.0  
PVP 0.0 }
```

Indium

According to first-principles density functional theory calculations [110], indium undergoes a total diffusivity retardation under compressive strain and enhancement under tensile strain. The migration barrier of In–I pairs is increased under compressive strain, with values similar to continuum Advanced Calibration (see [Impact of Pressure on Dopant Diffusivity on page 71](#)). The diffusivity enhancement or retardation is isotropic:

```
pdbSetArray KMC Si In VD { IniM -0.0009,-0.0009  
Ini -0.0009,-0.0009  
IniP -0.0009,-0.0009 }
```

In this calibration, the formation energy of In–I pairs is independent of strain:

```
pdbSetDoubleArray KMC Si In VF { IniM 0.0 }
```

Section 4: Model Parameters for Epitaxial Growth

This section describes the model parameters for epitaxial growth.

Selective epitaxial growth is simulated by LKMC, which must be activated by:

```
pdbSet KMC Epitaxy true
```

The default LKMC model for epitaxial growth is the `Coordinations.Planes` model.

Coordinations.Planes Model

The default model for selective epitaxial growth simulation is the one reported by Martin-Bragado and Moroz [126].

Chapter 6: Contents of Advanced Calibration of Sentaurus Process KMC

Section 4: Model Parameters for Epitaxial Growth

The (default) model switch is:

```
pdbSet LKMC Epitaxy.Model Coordinations.Planes
```

This computationally efficient atomistic model can reproduce the growth rates and shapes of selectively grown Si and SiGe. The growth process, which in reality depends on many aspects such as adsorption, desorption, surface diffusion, simultaneous etching, and chemistry as well as gas composition and pressure, is modeled simply by surface orientation-dependent net growth rates. Therefore, the calibration being part of Advanced Calibration is only a baseline one, but it cannot predict the absolute growth of all epitaxial processes due to the limited set of parameters included in the model. To fit the absolute growth, the recommended scaling factors are either the `epi.thickness` argument of the `diffuse Epi` command or the parameter:

```
pdbSet KMC Si Epitaxy prefactor.thickness <value>
```

The parameters for epitaxial growth of undoped (100) silicon and (100) germanium are based on low-temperature chemical vapor deposition (CVD) experiments [127][128][129]. The growth rates show an exponential dependency on temperature in the hydrogen desorption-limited regime of silicon ($\leq 800^{\circ}\text{C}$) and germanium ($\leq 700^{\circ}\text{C}$). The activation energies associated with the growth processes are 1.9 eV for silicon (dichlorosilane [127] and disilane [129]) and 0.4 eV for germanium (germane [127]). The prefactors for the different orientations and the correction energy for {311} planes are defined to have average values and to be in line with [126].

Linear SiGe parameter interpolation is assumed for epitaxial growth. The growth prefactors are interpolated in logarithmic scale, and the activation energies are interpolated in linear scale. In general, SiGe growth is faster than silicon growth and is performed at lower temperatures.

Coordinations Model

An alternative model for selective epitaxial growth simulation is activated by:

```
pdbSet LKMC Epitaxy.Model Coordinations
```

In contrast to the `Coordinations.Planes` model, the growth rates of the `Coordinations` model are based on species-dependent bonds and atomistic gas molecule arrival rates. The `Coordinations` model requires the specification of epitaxial gas conditions by specifying `ambients` in the `diffuse`, `temp_ramp`, or `gas_flow` commands. In addition, it is assumed that the net growth process is anisotropic and depends on the total binding energy of the site, which is the summation of all neighbor binding energies up to the third nearest neighbors of the diamond lattice [130]. Again, growth rates and faceting of selectively grown Si and SiGe can be reproduced, but many aspects of the growth process such as desorption, surface diffusion, simultaneous etching, and chemistry are ignored.

Chapter 6: Contents of Advanced Calibration of Sentaurus Process KMC

Section 4: Model Parameters for Epitaxial Growth

The parameters for epitaxial growth of undoped (100) silicon and (100) germanium are again based on low-temperature CVD experiments and are defined for the ambients dichlorosilane [127], germane [127], silane [128], and disilane [129].

The growth rates show an exponential dependency on temperature in the hydrogen desorption-limited regime of silicon ($\leq 800^{\circ}\text{C}$) and germanium ($\leq 700^{\circ}\text{C}$).

The calibrated parameters are set as the defaults of Sentaurus Process and, therefore, they are not included in the Advanced Calibration file.

Coordinations.Reactions Model

A second alternative model for selective epitaxial growth simulation is activated by:

```
pdbSet LKMC Epitaxy.Model Coordinations.Reactions
```

In line with the Coordinations model, the growth rates of the Coordinations.Reactions model are based on species-dependent bonds and atomistic gas molecule arrival rates. The Coordinations.Reactions model requires the specification of epitaxial gas conditions by specifying ambients in the `diffuse`, `temp_ramp`, or `gas_flow` commands. Its anisotropic net growth process depends on the total binding energy of the site, which is the summation of all neighbor binding energies up to the third nearest neighbors of the diamond lattice [130].

In addition, surface chemistry such as molecule adsorption, desorption, dissociation, and etching is modeled explicitly to take into account the hydrogen passivation of the surface and desorption. This allows a calibration for the entire temperature range including the hydrogen desorption-limited regime at low temperatures and the precursor supply- and dissociation-limited regime at high temperatures [46]. However, surface diffusion ignored for efficiency, which will likely lead to rougher surfaces in the simulation compared to reality.

Epitaxial Growth

The parameters for epitaxial growth of undoped (100) silicon and (100) germanium are again based on CVD experiments for the ambients dichlorosilane, germane, silane, disilane, phosphine, arsine, and diborane.

Silicon Growth

Epitaxial growth of undoped silicon for dichlorosilane ambients with H_2 carrier gas is calibrated against data for different temperatures, partial pressures, and orientations from the literature [127][131][132][133]. In this calibration, dichlorosilane (SiH_2Cl_2) adsorption is modeled by decomposition into the surface passivating products silylene (SiH^*) and hydrogen (H^*), while chlorine (Cl^*) is supposed to desorb immediately. Silylene decomposes into Si and a passivating H^* by a surface reaction; however, for this specific reaction, H^* is supposed to desorb immediately.

Chapter 6: Contents of Advanced Calibration of Sentaurus Process KMC

Section 4: Model Parameters for Epitaxial Growth

Epitaxial growth of undoped silicon for silane and disilane ambients with H₂ carrier gas is calibrated against data for different temperatures and partial pressures from the literature [133][134][135]. Silane (SiH₄) and disilane (Si₂H₆) adsorption is modeled by decomposition into the surface passivating products silylene (SiH₂^{*} or SiH₃^{*}) and H^{*}. Silylenes decompose into Si and two to three passivating H^{*} by a surface reaction; however, for this specific reaction, H^{*} is supposed to desorb immediately.

In situ doped epitaxial growth of silicon for phosphine, arsine, and diborane ambients with H₂ carrier gas is calibrated against data from the literature [136][137][138]. In line with silane and disilane, the adsorption of phosphine (PH₃), arsine (AsH₃), and diborane (B₂H₆) is modeled by decomposition into the surface passivating products PH₂^{*}, or AsH₂^{*}, or BH₂^{*}, and H^{*}.

PH₂^{*}, AsH₂^{*}, and BH₂^{*} decompose into P, As, or B and two passivating H^{*} by surface reactions; however, for these specific reactions, H^{*} is supposed to desorb immediately. In addition, surface segregation for P and As is assumed as suggested in the literature [139][140]. The exchange of the subsurface P and As with the surface Si leads to a dopant-rich surface that influences the epitaxial growth and limits dopant incorporation in the bulk.

Germanium and SiGe

To simulate germanium or SiGe epitaxial growth using the Coordinations.Reactions model, it is recommended to switch on an optional parameter set by calling:

```
LKMC_SiGe_Epitaxy
```

This activates a ten times higher hydrogen adsorption and desorption rate compared to the standard rates, which are needed to realize simulated germanium growth rates that are not growth time dependent. The higher hydrogen adsorption and desorption rates allow for a quick saturation of hydrogen coverage of the germanium surface and, therefore, stabilize the growth velocity. As a consequence, other adsorption rates have been adjusted to compensate for the higher hydrogen reaction rates. However, silicon growth can also be accurately simulated with the parameter set of LKMC_SiGe_Epitaxy, but the simulation times are one order of magnitude slower compared to the standard parameter set due to many more hydrogen events.

Epitaxial growth of undoped germanium for germane ambients with H₂ carrier gas is calibrated against data for different temperatures and partial pressures from the literature [141][138]. Germane (GeH₄) adsorption is modeled by decomposition into the surface passivating products germylene (GeH₂^{*}) and H^{*}. Germylene decomposes into Ge and two passivating H^{*} by a surface reaction; however, for this specific reaction, H^{*} is supposed to desorb immediately.

Epitaxial growth of undoped SiGe for dichlorosilane and germane ambients with H₂ carrier gas is calibrated against data for different temperatures and partial pressures from the literature [132][134][138][142][143]. To have both the growth rate and the grown Ge mole fraction in the correct range, surface segregation for Ge must be assumed as suggested in

Chapter 6: Contents of Advanced Calibration of Sentaurus Process KMC

Section 4: Model Parameters for Epitaxial Growth

the literature [140]. The exchange of the subsurface Ge with the surface Si leads to a Ge-rich surface that influences the epitaxial growth and limits Ge incorporation in the bulk. *In situ* doped epitaxial growth of SiGe for diborane ambients with H₂ carrier gas is calibrated against data from the literature [144].

Moreover, `LKMC_SiGe_Epitaxy` accounts for a Ge mole fraction–dependent lattice density when transferring the LKMC particles to KMC by setting:

```
pdbSet LKMC Lattice.Density.Corrrection 1
```

Therefore, to activate both Ge parameter interpolation and Ge mole fraction–dependent lattice density for KMC, it is recommended to also call:

```
KMC_SiGe_and_Stress_Effect 1 *
```

Etching

Etching of undoped silicon for HCl ambients with H₂ carrier gas is calibrated against data from the literature [145][146][147]. In this calibration, HCl adsorption is modeled by decomposition into the surface passivating products hydrogen (H*) and chlorine (Cl*). The etching process itself is modeled by an etch reaction by a surface passivating species SiHCl* – Cl* and a silicon surface atom form SiHCl* – which desorbs. The inclusion of H* in this reaction is neglected.

The faster etching of (110) silicon compared to the (100) silicon is achieved by a strong bonding of SiHCl* to the nearest neighbor (2 in the case of (100) silicon and 1 in the case of (110) silicon).

For low temperatures, the process is SiHCl* formation/desorption limited as well as hydrogen passivation limited, as shown in experiments [145] where the orientation dependency is strong for low temperatures and low for high temperatures. For high temperatures, the process is HCl adsorption limited, as demonstrated in experiments [146] where the etch rates depend strongly on the HCl/H₂ gas flow ratio at high temperatures.

Etching of undoped germanium and SiGe for HCl ambients with H₂ carrier gas is calibrated against data from the literature [148] in analogy to the one for silicon. The accuracy of simulations with and without `LKMC_SiGe_Epitaxy` is comparable.

Note:

The calibration for epitaxial growth and etching is based on simplistic assumptions for the surface chemistry and does not utilize the full potential of the `Coordinations.Reactions` model. More complex and physical surface reactions could be used, but accurate calibration is currently trailing.

References

- [1] N. Zographos *et al.*, "Process Modeling of Chemical and Stress Effects in SiGe," in *19th International Conference on Ion Implantation Technology (IIT)*, Valladolid, Spain, pp. 212–216, June 2012.
- [2] N. Zographos and I. Martin-Bragado, "Process modeling of stress and chemical effects in SiGe alloys using kinetic Monte Carlo," *Journal of Computational Electronics*, vol. 13, no. 1, pp. 59–69, 2014.
- [3] N. Zographos and I. Martin-Bragado, "A Comprehensive Atomistic Kinetic Monte Carlo Model for Amorphization/Recrystallization and its Effects on Dopants," in *MRS Symposium Proceedings, Doping Engineering for Front-End Processing*, vol. 1070, p. 1070-E03-01, 2008.
- [4] T. E. Haynes and O. W. Holland, "Comparative study of implantation-induced damage in GaAs and Ge: Temperature and flux dependence," *Applied Physics Letters*, vol. 59, no. 4, pp. 452–454, 1991.
- [5] S. Koffel *et al.*, "Amorphization kinetics of germanium during ion implantation," *Journal of Applied Physics*, vol. 105, no. 1, p. 013528, 2009.
- [6] B. L. Darby *et al.*, "Self-implantation energy and dose effects on Ge solid-phase epitaxial growth," *Nuclear Instruments and Methods in Physics Research B*, vol. 269, no. 1, pp. 20–22, 2011.
- [7] L. Pelaz *et al.*, "Atomistic modeling of amorphization and recrystallization in silicon," *Applied Physics Letters*, vol. 82, no. 13, pp. 2038–2040, 2003.
- [8] J. J. Loferski and P. Rappaport, "Radiation Damage in Ge and Si Detected by Carrier Lifetime Changes: Damage Thresholds," *Physical Review*, vol. 111, no. 2, pp. 432–439, 1958.
- [9] G. L. Olson and J. A. Roth, "Kinetics of Solid Phase Crystallization in Amorphous Silicon," *Materials Science Reports*, vol. 3, pp. 1–78, 1988.
- [10] G.-Q. Lu, E. Nygren, and M. J. Aziz, "Pressure-enhanced crystallization kinetics of amorphous Si and Ge: Implications for point-defect mechanisms," *Journal of Applied Physics*, vol. 70, no. 10, pp. 5323–5345, 1991.
- [11] L. Csepregi *et al.*, "Substrate-orientation dependence of the epitaxial regrowth rate from Si-implanted amorphous Si," *Journal of Applied Physics*, vol. 49, no. 7, pp. 3906–3911, 1978.
- [12] B. Sklenard *et al.*, "An atomistic investigation of the impact of in-plane uniaxial stress during solid phase epitaxial regrowth," *Applied Physics Letters*, vol. 102, no. 15, p. 151907, 2013.
- [13] B. C. Johnson and J. C. McCallum, "Dopant-enhanced solid-phase epitaxy in buried amorphous silicon layers," *Physical Review B*, vol. 76, no. 4, p. 045216, 2007.

Chapter 6: Contents of Advanced Calibration of Sentaurus Process KMC

References

- [14] D. D'Angelo *et al.*, "Role of the strain in the epitaxial regrowth rate of heavily doped amorphous Si films," *Applied Physics Letters*, vol. 93, p. 231901, December 2008.
- [15] S. Mirabella *et al.*, "Mechanism of Boron Diffusion in Amorphous Silicon," *Physical Review Letters*, vol. 100, p. 155901, April 2008.
- [16] I. Martin-Bragado and N. Zographos, "Indirect boron diffusion in amorphous silicon modeled by kinetic Monte Carlo," *Solid-State Electronics*, vol. 55, no. 1, pp. 25–28, 2011.
- [17] H. Bracht, N. A. Stolwijk, and H. Mehrer, "Equilibrium Concentrations of Intrinsic Point Defects in Silicon Determined by Zinc Diffusion," in *Proceedings of the Seventh International Symposium on Silicon Materials Science and Technology (Semiconductor Silicon)*, vol. 94-10, San Francisco, CA, USA, pp. 593–602B, May 1994.
- [18] I. Martin-Bragado *et al.*, "Physical atomistic kinetic Monte Carlo modeling of Fermi-level effects on species diffusing in silicon," *Physical Review B*, vol. 72, p. 035202, July 2005.
- [19] L. Pelaz *et al.*, "Front-end process modeling in silicon," *The European Physical Journal B*, vol. 72, no. 3, pp. 323–359, 2009.
- [20] I. Martin-Bragado, *Simulación atomística de procesos para Microelectrónica*, PhD thesis, Universidad de Valladolid, Valladolid, Spain, 2004.
- [21] J. Vanhellemont, P. Spiewak, and K. Sueoka, "On the solubility and diffusivity of the intrinsic point defects in germanium," *Journal of Applied Physics*, vol. 101, no. 3, p. 036103, 2007.
- [22] J. Vanhellemont *et al.*, "Intrinsic point defect properties and engineering in silicon and germanium Czochralski crystal growth," in *5th International Symposium on Advanced Science and Technology of Silicon Materials*, Kona, HI, USA, November 2008.
- [23] P. Spiewak, J. Vanhellemont, and K. J. Kurzydlowski, "Improved calculation of vacancy properties in Ge using the Heyd-Scuseria-Ernzerhof range-separated hybrid functional," *Journal of Applied Physics*, vol. 110, no. 6, p. 063534, 2011.
- [24] I. Martin-Bragado *et al.*, "Fermi-level effects in semiconductor processing: A modeling scheme for atomistic kinetic Monte Carlo simulators," *Journal of Applied Physics*, vol. 98, no. 5, p. 053709, 2005.
- [25] J. Vanhellemont and E. Simoen, "Brother Silicon, Sister Germanium," *Journal of The Electrochemical Society*, vol. 154, no. 7, pp. H572–H583, 2007.
- [26] L. Pelaz, L. A. Marqués, and J. Barbolla, "Ion-beam-induced amorphization and recrystallization in silicon," *Journal of Applied Physics*, vol. 96, no. 11, pp. 5947–5976, 2004.
- [27] S. M. Sze, *Physics of Semiconductor Devices*, New York: John Wiley & Sons, 2nd ed., 1981.

- [28] I. Martin-Bragado *et al.*, "From point defects to dislocation loops: A comprehensive modelling framework for self-interstitial defects in silicon," *Solid-State Electronics*, vol. 52, no. 9, pp. 1430–1436, 2008.
- [29] N. E. B. Cowern *et al.*, "Cluster ripening and transient enhanced diffusion in silicon," *Materials Science in Semiconductor Processing*, vol. 2, no. 4, pp. 369–376, 1999.
- [30] F. Cristiano *et al.*, "Formation energies and relative stability of perfect and faulted dislocation loops in silicon," *Journal of Applied Physics*, vol. 87, no. 12, pp. 8420–8428, 2000.
- [31] D. P. Hickey *et al.*, "Regrowth-related defect formation and evolution in 1 MeV amorphized (001) Ge," *Applied Physics Letters*, vol. 90, no. 13, p. 132114, 2007.
- [32] S. Koffel *et al.*, "End of range defects in Ge," *Journal of Applied Physics*, vol. 105, no. 12, p. 126110, 2009.
- [33] E. Napolitani *et al.*, "Transient enhanced diffusion of B mediated by self-interstitials in preamorphized Ge," *Applied Physics Letters*, vol. 96, no. 20, p. 201906, 2010.
- [34] F. Panciera *et al.*, "End-of-range defects in germanium and their role in boron deactivation," *Applied Physics Letters*, vol. 97, no. 1, p. 012105, 2010.
- [35] S. Boninelli *et al.*, "Role of the Ge surface during the end of range dissolution," *Applied Physics Letters*, vol. 101, no. 16, p. 162103, 2012.
- [36] IST Project 027152 ATOMICS, *Advanced Front-End Technology Modeling for Ultimate Integrated Circuits*, for more information, go to <https://www.iisb.fraunhofer.de/content/dam/iisb2014/en/Documents/Research-Areas/Simulation/final-report-atomics.pdf>.
- [37] A. Chroneos, R. W. Grimes, and H. Bracht, "Fluorine codoping in germanium to suppress donor diffusion and deactivation," *Journal of Applied Physics*, vol. 106, no. 6, p. 063707, 2009.
- [38] R. Kögler *et al.*, "Excess vacancies in high energy ion implanted SiGe," *Journal of Applied Physics*, vol. 101, no. 3, p. 033508, 2007.
- [39] G. M. Dalpian *et al.*, "*Ab initio* calculations of vacancies in $\text{Si}_x\text{Ge}_{1-x}$," *Applied Physics Letters*, vol. 81, no. 18, pp. 3383–3385, 2002.
- [40] P. Venezuela *et al.*, "Vacancy-mediated diffusion in disordered alloys: Ge self-diffusion in $\text{Si}_{1-x}\text{Ge}_x$," *Physical Review B*, vol. 65, no. 19, p. 193306, 2002.
- [41] P. Ramanarayanan, K. Cho, and B. M. Clemens, "Effect of composition on vacancy mediated diffusion in random binary alloys: First principles study of the $\text{Si}_{1-x}\text{Ge}_x$ system," *Journal of Applied Physics*, vol. 94, no. 1, pp. 174–185, 2003.
- [42] M. Haran, J. A. Catherwood, and P. Clancy, "Effects of Ge content on the diffusion of group-V dopants in SiGe alloys," *Applied Physics Letters*, vol. 88, no. 17, p. 173502, 2006.

Chapter 6: Contents of Advanced Calibration of Sentaurus Process KMC

References

- [43] P. F. Fazzini *et al.*, "Effect of Germanium content and strain on the formation of extended defects in ion implanted Silicon/Germanium," *Thin Solid Films*, vol. 518, no. 9, pp. 2338–2341, 2010.
- [44] R. T. Crosby, *Evolution of Self-Interstitials Induced by Ion-Implantation in SiGe Alloys*, PhD thesis, University of Florida, Gainesville, FL, USA, 2005.
- [45] A. Belafhaili *et al.*, "Influence of the Germanium content on the amorphization of silicon–germanium alloys during ion implantation," *Materials Science in Semiconductor Processing*, vol. 16, no. 6, pp. 1655–1658, 2013.
- [46] N. Zographos *et al.*, "Multiscale modeling of doping processes in advanced semiconductor devices," *Materials Science in Semiconductor Processing*, vol. 62, pp. 49–61, May 2017.
- [47] K. Y. Suh and H. H. Lee, "Composition dependence of activation energy in solid phase epitaxial growth of $\text{Si}_{1-x}\text{Ge}_x$ alloys," *Journal of Applied Physics*, vol. 80, no. 12, pp. 6716–6719, 1996.
- [48] T. E. Haynes *et al.*, "Composition dependence of solid-phase epitaxy in silicon-germanium alloys: Experiment and theory," *Physical Review B*, vol. 51, no. 12, pp. 7762–7772, 1995.
- [49] R. Braunstein, A. R. Moore, and F. Herman, "Intrinsic Optical Absorption in Germanium-Silicon Alloys," *Physical Review*, vol. 109, no. 3, pp. 695–710, 1958.
- [50] P. Castrillo *et al.*, "Physical modeling and implementation scheme of native defect diffusion and interdiffusion in SiGe heterostructures for atomistic process simulation," *Journal of Applied Physics*, vol. 109, p. 103502, May 2011.
- [51] P. Castrillo *et al.*, "Atomistic Modeling of Defect Diffusion in SiGe," in *International Conference on Simulation of Semiconductor Processes and Devices (SISPAD)*, Vienna, Austria, pp. 9–12, September 2007.
- [52] P. Castrillo *et al.*, "Atomistic modeling of defect diffusion and interdiffusion in SiGe heterostructures," *Thin Solid Films*, vol. 518, no. 9, pp. 2448–2453, 2010.
- [53] R. Kube *et al.*, "Composition dependence of Si and Ge diffusion in relaxed $\text{Si}_{1-x}\text{Ge}_x$ alloys," *Journal of Applied Physics*, vol. 107, no. 7, p. 073520, 2010.
- [54] Y. Dong *et al.*, "A unified interdiffusivity model and model verification for tensile and relaxed SiGe interdiffusion over the full germanium content range," *Journal of Applied Physics*, vol. 111, no. 4, p. 044909, 2012.
- [55] G. Xia *et al.*, "Strain dependence of Si–Ge interdiffusion in epitaxial $\text{Si}/\text{Si}_{1-y}\text{Ge}_y/\text{Si}$ heterostructures on relaxed $\text{Si}_{1-x}\text{Ge}_x$ substrates," *Applied Physics Letters*, vol. 88, no. 1, p. 013507, 2006.
- [56] G. Xia, J. L. Hoyt, and M. Canonico, "Si-Ge interdiffusion in strained Si/strained SiGe heterostructures and implications for enhanced mobility metal-oxide-semiconductor field-effect transistors," *Journal of Applied Physics*, vol. 101, p. 044901, February 2007.

Chapter 6: Contents of Advanced Calibration of Sentaurus Process KMC

References

- [57] N. E. B. Cowern *et al.*, "Diffusion in Strained Si(Ge)," *Physical Review Letters*, vol. 72, no. 16, pp. 2585–2588, 1994.
- [58] H. H. Silvestri *et al.*, "Diffusion of silicon in crystalline germanium," *Semiconductor Science and Technology*, vol. 21, no. 6, p. 758, 2006.
- [59] M. Vos *et al.*, "Channeling studies of implantation damage in SiGe superlattices and SiGe alloys," *Nuclear Instruments and Methods in Physics Research B*, vol. 66, no. 3, pp. 361–368, 1992.
- [60] B. Sklenard *et al.*, "Atomistic investigation of the impact of stress during solid phase epitaxial regrowth," *Physica Status Solidi C*, vol. 11, no. 1, pp. 97–100, 2014.
- [61] M. Diebel and S. T. Dunham, "Ab-initio Calculations to Predict Stress Effects on Defects and Diffusion in Silicon," in *International Conference on Simulation of Semiconductor Processes and Devices (SISPAD)*, Boston, MA, USA, pp. 147–150, September 2003.
- [62] M. Diebel, *Application of Ab-initio Calculations to Modeling of Nanoscale Diffusion and Activation in Silicon*, PhD thesis, University of Washington, Seattle, WA, USA, 2004.
- [63] Y. Kawamura *et al.*, "Self-diffusion in compressively strained Ge," *Journal of Applied Physics*, vol. 110, p. 034906, August 2011.
- [64] V. Moroz *et al.*, "Dissolution of extended defects in strained silicon," *Journal of Vacuum Science & Technology B*, vol. 26, no. 1, pp. 439–442, 2008.
- [65] P. Pichler, *Intrinsic Point Defects, Impurities, and Their Diffusion in Silicon*, Computational Microelectronics, Vienna: Springer, 2004.
- [66] J. Zhu *et al.*, "Ab initio pseudopotential calculations of B diffusion and pairing in Si," *Physical Review B*, vol. 54, no. 7, p. 4741–4747, 1996.
- [67] J. S. Nelson, P. A. Schultz, and A. F. Wright, "Valence and atomic size dependent exchange barriers in vacancy-mediated dopant diffusion," *Applied Physics Letters*, vol. 73, no. 2, pp. 247–249, 1998.
- [68] V. C. Venezia *et al.*, "Boron diffusion in amorphous silicon," *Materials Science and Engineering B*, vol. 124–125, pp. 245–248, December 2005.
- [69] R. Duffy *et al.*, "Dopant diffusion in amorphous silicon," in *MRS Symposium Proceedings, Silicon Front-End Junction Formation—Physics and Technology*, San Francisco, CA, USA, vol. 810, pp. C10.2.1–C10.2.6, April 2004.
- [70] S. Uppal *et al.*, "Diffusion of boron in germanium at 800–900°C," *Journal of Applied Physics*, vol. 96, no. 3, pp. 1376–1380, 2004.
- [71] I. Martin-Bragado, N. Zographos, and P. Castrillo, "Atomistic modelling and simulation of arsenic diffusion including mobile arsenic clusters," *Physica Status Solidi A*, vol. 211, no. 1, pp. 147–151, 2014.

Chapter 6: Contents of Advanced Calibration of Sentaurus Process KMC

References

- [72] B. Sahli *et al.*, "Ab initio calculations of phosphorus and arsenic clustering parameters for the improvement of process simulation models," *Materials Science and Engineering B*, vol. 154-155, pp. 193–197, December 2008.
- [73] D. C. Mueller, E. Alonso, and W. Fichtner, "Arsenic deactivation in Si: Electronic structure and charge states in vacancy-impurity clusters," *Physical Review B*, vol. 68, no. 4, p. 045208, 2003.
- [74] A. N. Larsen *et al.*, "Heavy doping effects in the diffusion of group IV and V impurities in silicon," *Journal of Applied Physics*, vol. 73, no. 2, pp. 691–698, 1993.
- [75] N. Zographos and A. Erlebach, "Process simulation of dopant diffusion and activation in germanium," *Physica Status Solidi A*, vol. 211, no. 1, pp. 143–146, 2014.
- [76] A. Chroneos, "Dopant-defect interactions in Ge: Density functional theory calculations," *Materials Science in Semiconductor Processing*, vol. 15, no. 6, pp. 691–696, 2012.
- [77] A. Chroneos *et al.*, "Engineering the free vacancy and active donor concentrations in phosphorus and arsenic double donor-doped germanium," *Journal of Applied Physics*, vol. 104, no. 11, p. 113724, 2008.
- [78] N. Zographos and I. Martin-Bragado, "Atomistic Modeling of Carbon Co-Implants and Rapid Thermal Anneals in Silicon," in *15th IEEE International Conference on Advanced Thermal Processing of Semiconductors (RTP)*, Catania, Italy, pp. 119–122, October 2007.
- [79] M. Diebel and S. T. Dunham, "Ab Initio Calculations to Model Anomalous Fluorine Behavior," *Physical Review Letters*, vol. 93, no. 24, p. 245901, 2004.
- [80] M. Diebel and S. T. Dunham, "Reply to Ab Initio Calculations to Model Anomalous Fluorine Behavior," *Physical Review Letters*, vol. 96, p. 039602, January 2006.
- [81] K. Vollenweider *et al.*, "Fluorine clustering and diffusion in silicon: Ab initio calculations and kinetic Monte Carlo model," *Journal of Vacuum Science & Technology B*, vol. 28, no. 1, pp. C1G1–C1G6, 2010.
- [82] G. R. Nash *et al.*, "Activation energy for fluorine transport in amorphous silicon," *Applied Physics Letters*, vol. 75, no. 23, pp. 3671–3673, 1999.
- [83] P. A. Schultz and J. S. Nelson, "Fast through-bond diffusion of nitrogen in silicon," *Applied Physics Letters*, vol. 78, no. 6, pp. 736–738, 2001.
- [84] N. Stoddard *et al.*, "Ab Initio Identification of the Nitrogen Diffusion Mechanism in Silicon," *Physical Review Letters*, vol. 95, no. 2, p. 025901, 2005.
- [85] L. S. Adam *et al.*, "Physical integrated diffusion-oxidation model for implanted nitrogen in silicon," *Journal of Applied Physics*, vol. 91, no. 4, pp. 1894–1900, 2002.
- [86] L. Pelaz *et al.*, "B diffusion and clustering in ion implanted Si: The role of B cluster precursors," *Applied Physics Letters*, vol. 70, no. 17, pp. 2285–2287, 1997.

- [87] C. Zechner *et al.*, "Simulation of dopant diffusion and activation during flash lamp annealing," *Materials Science and Engineering B*, vol. 154-155, pp. 20–23, December 2008.
- [88] M. Aboy *et al.*, "Kinetics of large B clusters in crystalline and preamorphized silicon," *Journal of Applied Physics*, vol. 110, no. 7, p. 073524, 2011.
- [89] J. Xia *et al.*, "Boron segregation to extended defects induced by self-ion implantation into silicon," *Journal of Applied Physics*, vol. 85, no. 11, pp. 7597–7603, 1999.
- [90] A. Satta *et al.*, "Diffusion, activation, and recrystallization of boron implanted in preamorphized and crystalline germanium," *Applied Physics Letters*, vol. 87, no. 17, p. 172109, 2005.
- [91] B. R. Yates *et al.*, "Anomalous activation of shallow B⁺ implants in Ge," *Materials Letters*, vol. 65, no. 23–24, pp. 3540–3543, 2011.
- [92] S. A. Harrison, T. F. Edgar, and G. S. Hwang, "Interstitial-Mediated Arsenic Clustering in Ultrashallow Junction Formation," *Electrochemical and Solid-State Letters*, vol. 9, no. 12, pp. G354–G357, 2006.
- [93] R. Pinacho *et al.*, "Modeling arsenic deactivation through arsenic-vacancy clusters using an atomistic kinetic Monte Carlo approach," *Applied Physics Letters*, vol. 86, p. 252103, June 2005.
- [94] J. Xie and S. P. Chen, "Diffusion and Clustering in Heavily Arsenic-Doped Silicon: Discrepancies and Explanation," *Physical Review Letters*, vol. 83, no. 9, pp. 1795–1798, 1999.
- [95] Y. Park *et al.*, "Dopant diffusion in Si, SiGe and Ge: TCAD model parameters determined with density functional theory," in *IEDM Technical Digest*, San Francisco, CA, USA, pp. 784–787, December 2017.
- [96] T. Noda, S. Odanaka, and H. Umimoto, "Effects of end-of-range dislocation loops on transient enhanced diffusion of indium implanted in silicon," *Journal of Applied Physics*, vol. 88, no. 9, pp. 4980–4984, 2000.
- [97] C.-L. Liu *et al.*, "Ab initio modeling and experimental study of C–B interactions in Si," *Applied Physics Letters*, vol. 80, no. 1, pp. 52–54, 2002.
- [98] Y. Shimizu *et al.*, "Impact of carbon coimplantation on boron behavior in silicon: Carbon–boron coclustering and suppression of boron diffusion," *Applied Physics Letters*, vol. 98, no. 23, p. 232101, 2011.
- [99] Y.-S. Oh and D. E. Ward, "A Calibrated Model for Trapping of Implanted Dopants at Material Interface During Thermal Annealing," in *IEDM Technical Digest*, San Francisco, CA, USA, pp. 509–512, December 1998.
- [100] V. C. Venezia *et al.*, "Dopant redistribution effects in preamorphized silicon during low temperature annealing," in *IEDM Technical Digest*, Washington, DC, USA, pp. 489–492, December 2003.

- [101] S. H. Jain *et al.*, “Metastable boron active concentrations in Si using flash assisted solid phase epitaxy,” *Journal of Applied Physics*, vol. 96, no. 12, pp. 7357–7360, 2004.
- [102] D. De Salvador *et al.*, “Experimental evidence of B clustering in amorphous Si during ultrashallow junction formation,” *Applied Physics Letters*, vol. 89, p. 241901, December 2006.
- [103] C. Zechner, D. Matveev, and A. Erlebach, “Phase-field model for the dopant redistribution during solid phase epitaxial regrowth of amorphized silicon,” *Materials Science and Engineering B*, vol. 114–115, pp. 162–165, 2004.
- [104] O. Dokumaci *et al.*, “Transient Enhanced Diffusion and Dose Loss of Indium in Silicon,” in *MRS Symposium Proceedings, Si Front-End Processing—Physics and Technology of Dopant-Defect Interactions*, San Francisco, CA, USA, vol. 568, pp. 205–210, April 1999.
- [105] R. Duffy *et al.*, “Influence of preamorphization and recrystallization on indium doping profiles in silicon,” *Journal of Vacuum Science & Technology B*, vol. 22, no. 3, pp. 865–868, 2004.
- [106] G. Impellizzeri *et al.*, “Fluorine in preamorphized Si: Point defect engineering and control of dopant diffusion,” *Journal of Applied Physics*, vol. 99, p. 103510, May 2006.
- [107] Z. Ye *et al.*, “High Tensile Strained In-Situ Phosphorus Doped Silicon Epitaxial Film for nMOS Applications,” *ECS Transactions*, vol. 50, no. 9, pp. 1007–1011, 2013.
- [108] X. Li *et al.*, “Selective Epitaxial Si:P Film for nMOSFET Application: High Phosphorous Concentration and High Tensile Strain,” *ECS Transactions*, vol. 64, no. 6, pp. 959–965, 2014.
- [109] S. K. Dhayalan *et al.*, “On the Evolution of Strain and Electrical Properties in As-Grown and Annealed Si:P Epitaxial Films for Source-Drain Stressor Applications,” *ECS Journal of Solid State Science and Technology*, vol. 7, no. 5, pp. P228–P237, 2018.
- [110] C. Ahn, *Atomic scale modeling of stress and pairing effects on dopant behavior in silicon*, PhD thesis, University of Washington, Seattle, WA, USA, 2007.
- [111] R. F. Lever, J. M. Bonar, and A. F. W. Willoughby, “Boron diffusion across silicon–silicon germanium boundaries,” *Journal of Applied Physics*, vol. 83, no. 4, pp. 1988–1994, 1998.
- [112] L. A. Edelman *et al.*, “Boron diffusion in amorphous silicon-germanium alloys,” *Applied Physics Letters*, vol. 92, no. 17, p. 172108, 2008.
- [113] P. Laitinen, *Self- and Impurity Diffusion in Intrinsic Relaxed Silicon - Germanium*, PhD thesis, University of Jyväskylä, Finland, January 2004.
- [114] S. Eguchi *et al.*, “Comparison of arsenic and phosphorus diffusion behavior in silicon–germanium alloys,” *Applied Physics Letters*, vol. 80, no. 10, pp. 1743–1745, 2002.

Chapter 6: Contents of Advanced Calibration of Sentaurus Process KMC

References

- [115] Y.-M. Sheu *et al.*, "Modeling Dopant Diffusion in Strained and Strain-Relaxed Epi-SiGe," in *International Conference on Simulation of Semiconductor Process and Devices (SISPAD)*, Tokyo, Japan, pp. 75–78, September 2005.
- [116] N. Zangenberg, *Defect and Diffusion Studies in Si and SiGe*, PhD thesis, University of Aarhus, Denmark, January 2003.
- [117] P. Kuo *et al.*, "Boron Diffusion in Si and $\text{Si}_{1-x}\text{Ge}_x$," in *MRS Symposium Proceedings, Strained Layer Epitaxy - Materials, Processing, and Device Applications*, vol. 379, pp. 373–378, 1995.
- [118] S. Uppal *et al.*, "Diffusion of Boron in Germanium and $\text{Si}_{1-x}\text{Ge}_x$ ($x > 50\%$) alloys," in *MRS Symposium Proceedings, CMOS Front-End Materials and Process Technology*, vol. 765, p. D6.16.1, January 2003.
- [119] C. C. Wang *et al.*, "Boron diffusion in strained and strain-relaxed SiGe," *Materials Science and Engineering B*, vol. 124–125, pp. 39–44, December 2005.
- [120] J. S. Christensen *et al.*, "Diffusion of phosphorus in relaxed $\text{Si}_{1-x}\text{Ge}_x$ films and strained Si/ $\text{Si}_{1-x}\text{Ge}_x$ heterostructures," *Journal of Applied Physics*, vol. 94, no. 10, pp. 6533–6540, 2003.
- [121] I. Martin-Bragado *et al.*, "Anisotropic dopant diffusion in Si under stress using both continuum and atomistic methods," *Journal of Computational Electronics*, vol. 7, no. 3, pp. 103–106, 2008.
- [122] C. Ahn *et al.*, "Stress effects on impurity solubility in crystalline materials: A general model and density-functional calculations for dopants in silicon," *Physical Review B*, vol. 79, no. 7, p. 073201, 2009.
- [123] L. Lin *et al.*, "Boron diffusion in strained Si: A first-principles study," *Journal of Applied Physics*, vol. 96, no. 10, pp. 5543–5547, 2004.
- [124] S. T. Dunham *et al.*, "Calculations of effect of anisotropic stress/strain on dopant diffusion in silicon under equilibrium and nonequilibrium conditions," *Journal of Vacuum Science & Technology B*, vol. 24, no. 1, pp. 456–461, 2006.
- [125] N. Sugii *et al.*, "Recrystallization, redistribution, and electrical activation of strained-silicon/ $\text{Si}_{0.7}\text{Ge}_{0.3}$ heterostructures with implanted arsenic," *Journal of Applied Physics*, vol. 96, no. 1, pp. 261–268, 2004.
- [126] I. Martin-Bragado and V. Moroz, "Modeling of {311} facets using a lattice kinetic Monte Carlo three-dimensional model for selective epitaxial growth of silicon," *Applied Physics Letters*, vol. 98, no. 15, p. 153111, 2011.
- [127] P. M. Garone *et al.*, "Silicon vapor phase epitaxial growth catalysis by the presence of germane," *Applied Physics Letters*, vol. 56, no. 13, pp. 1275–1277, 1990.
- [128] M. Liehr *et al.*, "Kinetics of silicon epitaxy using SiH_4 in a rapid thermal chemical vapor deposition reactor," *Applied Physics Letters*, vol. 56, no. 7, pp. 629–631, 1990.
- [129] H.-C. Tseng *et al.*, "Effects of isolation materials on facet formation for silicon selective epitaxial growth," *Applied Physics Letters*, vol. 71, no. 16, pp. 2328–2330, 1997.

- [130] R. Chen *et al.*, “A New Kinetic Lattice Monte Carlo Modeling Framework for the Source-Drain Selective Epitaxial Growth Process,” in *International Conference on Simulation of Semiconductor Processes and Devices (SISPAD)*, Glasgow, Scotland, pp. 9–12, September 2013.
- [131] D. Dutartre, A. Talbot, and N. Loubet, “Facet Propagation in Si and SiGe Epitaxy or Etching,” *ECS Transactions*, vol. 3, no. 7, pp. 473–487, 2006.
- [132] J. M. Hartmann *et al.*, “Growth kinetics of Si and SiGe on Si(100), Si(110) and Si(111) surfaces,” *Journal of Crystal Growth*, vol. 294, no. 2, pp. 288–295, 2006.
- [133] J. M. Hartmann *et al.*, “SiGe growth kinetics and doping in reduced pressure-chemical vapor deposition,” *Journal of Crystal Growth*, vol. 236, no. 1–3, pp. 10–20, 2002.
- [134] J. M. Hartmann *et al.*, “A benchmarking of silane, disilane and dichlorosilane for the low temperature growth of group IV layers,” *Thin Solid Films*, vol. 520 no. 8, pp. 3185–3189, 2012.
- [135] J. M. Hartmann *et al.*, “Potentialities of disilane for the low temperature epitaxy of intrinsic and boron-doped SiGe,” *Thin Solid Films*, vol. 557, pp. 19–26, April 2014.
- [136] P. D. Agnello, T. O. Sedgwick, and J. Cotte, “Growth Rate Enhancement of Heavy n- and p-Type Doped Silicon Deposited by Atmospheric-Pressure Chemical Vapor Deposition at Low Temperatures,” *Journal of the Electrochemical Society*, vol. 140, no. 9, pp. 2703–2709, 1993.
- [137] M. Schindler *et al.*, “Selective epitaxial growth of Arsenic-doped SiGe-structures with LPCVD,” *ECS Transactions*, vol. 1, no. 30, pp. 33–40, 2006.
- [138] Y. Bogumilowicz *et al.*, “High-temperature growth of very high germanium content SiGe virtual substrates,” *Journal of Crystal Growth*, vol. 290, no. 2, pp. 523–531, 2006.
- [139] J. M. Hartmann *et al.*, “Disilane-based cyclic deposition/etch of Si, Si:P and $\text{Si}_{1-y}\text{C}_y:\text{P}$ layers: I. The elementary process steps,” *Semiconductor Science and Technology*, vol. 28, no. 2, p. 025017, 2013.
- [140] S. Fukatsu *et al.*, “Self-limitation in the surface segregation of Ge atoms during Si molecular beam epitaxial growth,” *Applied Physics Letters*, vol. 59, no. 17, pp. 2103–2105, 1991.
- [141] J. Aubin *et al.*, “Very low temperature epitaxy of Ge and Ge rich SiGe alloys with Ge_2H_6 in a Reduced Pressure – Chemical Vapour Deposition tool,” *Journal of Crystal Growth*, vol. 445, pp. 65–72, July 2016.
- [142] J. M. Hartmann, “Low temperature growth kinetics of high Ge content SiGe in reduced pressure-chemical vapor deposition,” *Journal of Crystal Growth*, vol. 305, no. 1, pp. 113–121, 2007.
- [143] J. M. Hartmann *et al.*, “Reduced Pressure–Chemical Vapour Deposition of Si/SiGe heterostructures for nanoelectronics,” *Materials Science and Engineering B*, vol. 154–155, pp. 76–84, December 2008.

Chapter 6: Contents of Advanced Calibration of Sentaurus Process KMC

References

- [144] J. M. Hartmann *et al.*, “Growth kinetics and boron doping of very high Ge content SiGe for source/drain engineering,” *Journal of Crystal Growth*, vol. 310, no. 1, pp. 62–70, 2008.
- [145] J. M. Hartmann *et al.*, “HCl selective etching of SiGe versus Si in stacks grown on (110),” *ECS Transactions*, vol. 33, no. 6, pp. 985–993, 2010.
- [146] N. Loubet, A. Talbot, and D. Dutartre, “Silicon Etching Study in a RT-CVD Reactor with the HCl/H₂ Gas Mixture,” in *MRS Symposium Proceedings*, vol. 910, January 2006.
- [147] V. Destefanis *et al.*, “Low-thermal surface preparation, HCl etch and Si/SiGe selective epitaxy on (110) silicon surfaces,” *Semiconductor Science and Technology*, vol. 23, no. 10, p. 105018, 2008.
- [148] Y. Bogumilowicz *et al.*, “Chemical vapour etching of Si, SiGe and Ge with HCl; applications to the formation of thin relaxed SiGe buffers and to the revelation of threading dislocations,” *Semiconductor Science and Technology*, vol. 20, no. 2, pp. 127–134, 2005.

7

Guidelines for Additional Calibration

This chapter provides guidelines for additional calibration.

The Advanced Calibration file is the recommended starting point for accurate process simulation with Sentaurus Process Kinetic Monte Carlo (Sentaurus Process KMC). However, Advanced Calibration cannot fully replace an additional calibration by the user. With a customized process calibration, the accuracy can always be further increased for any technology of interest. A customized calibration of process and device simulation models needs to be performed by the user or can be requested from Synopsys in the context of a customer service project.

To further improve the Advanced Calibration, Synopsys appreciates feedback from customers regarding the accuracy obtained with the parameter files for different process conditions, and suggestions for improved models or parameter values.

Accuracy and Limitations of Advanced Calibration of Sentaurus Process KMC

The Advanced Calibration is based on scientific literature of process simulation models and on a continual calibration effort based on the Synopsys collection of SIMS profiles from state-of-the-art device manufacturing technology. A good agreement is obtained for a wide range of SIMS data. However, in some cases, there is a significant mismatch between kinetic Monte Carlo simulation results obtained with Advanced Calibration and the experimental data, for similar reasons as for continuum simulations listed in [Accuracy and Limitations of Advanced Calibration of Sentaurus Process on page 136](#).

In this section, the accuracy of the Advanced Calibration for Sentaurus Process KMC is discussed. In particular, it will explain for which process conditions the accuracy is limited and which parameters can be fine-tuned by users to increase the accuracy in a process window of interest.

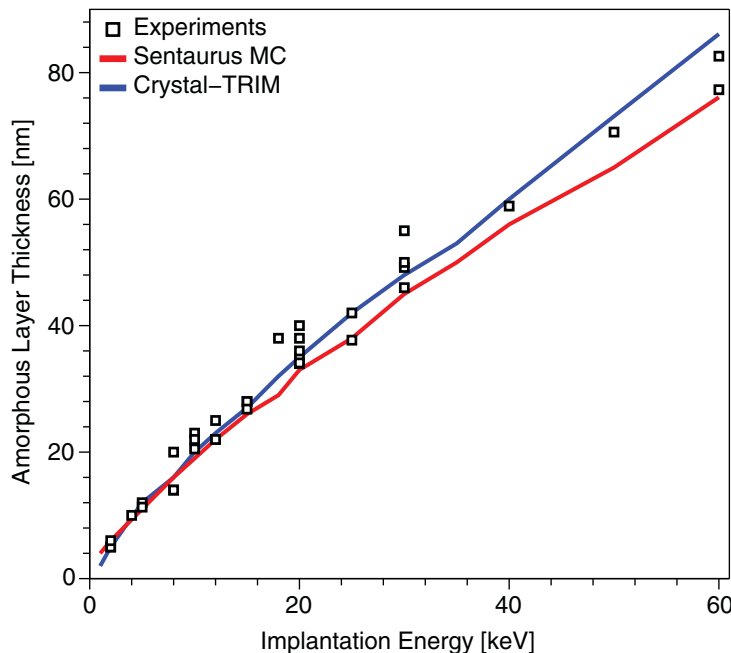
Damage and Point Defects

This section discusses damage and point defects.

Amorphization

The calibration of amorphization and recrystallization in silicon follows Zographos and Martin-Bragado [1]. In [Figure 39](#), the accuracy of the damage accumulation during implantation is shown by the comparison of literature data with simulated amorphization-layer thicknesses generated by germanium implantation.

Figure 39 Amorphous layer thickness versus Ge implantation energy, dose $1 \times 10^{15} \text{ cm}^{-2}$: comparison of experiments (squares) and simulations (solid lines) at dose rate of $5 \times 10^{12} \text{ cm}^{-2} \text{ s}^{-1}$



Obviously, the implantation dose rate as well as the implantation temperature strongly influence the amorphization and need to be considered by the user.

Note:

The default implantation dose rate is $1 \times 10^{12} \text{ cm}^{-2} \text{ s}^{-1}$ and is not changed within Advanced Calibration because it is considered to be a process parameter.

Chapter 7: Guidelines for Additional Calibration

Accuracy and Limitations of Advanced Calibration of Sentaurus Process KMC

To adjust the dose rate, define the `dose.rate` argument of the `implant` command or redefine the following procedure before the `implant` command:

```
proc DoseRate { dose } {
    set refDose 5e13           ; # dose rate of 5e13 cm-2 s-1
    expr $dose/$refDose
}
```

If the dose rate and temperature are not known exactly, they can be used as fitting parameters to adjust the damage and amorphization-layer thicknesses of implantations.

Germanium Preamorphization

In the case of germanium preamorphization implantation, the as-implanted germanium profiles for Sentaurus MC implantation are often slightly shallower than corresponding SIMS profiles and, therefore, the amorphization-layer thickness can also be slightly shallower.

The lower amorphization can be compensated partly by lowering the displacement threshold for the damage generation of Sentaurus MC implantation from 15 eV to 13 eV. However, the as-implanted germanium profiles for Crystal-TRIM implantation are, in general, slightly deeper and more accurate compared to SIMS and, therefore, could be used as an alternative. The difference between the amorphous-layer thicknesses for the two different Monte Carlo implant engines can be seen in [Figure 39 on page 273](#).

Cold and Hot Implantation

The damage accumulation has been calibrated on data of different implantation dose rates and temperature [1]. Therefore, the trends for implantation temperature dependency should be modeled accurately, for example, the increased amorphization during implantation at cold temperatures (lower than room temperature) [2], the decreased amorphization [3], and enhanced channeling during implantation at hot temperatures [4].

If the amorphization is underestimated, the displacement threshold for the damage generation of Sentaurus MC implantation can be decreased:

```
pdbSet Si B casc.dis 670
```

If the implant channeling is overestimated, the proportional factor for the switching probability from the crystalline to the amorphous model can be increased:

```
pdbSet Si B casc.amo 4.0
```

Recrystallization

While the recrystallization velocity for an undoped amorphous–silicon layer on top of (100)-oriented crystalline silicon is well known [5] and might not require any changes, its enhancement in the presence of n-type and p-type doping is less certain [6][7]. Therefore, the corresponding silicon damage parameters `v0.Recryst.ntype` and `v0.Recryst.ptype` can be used as fitting parameters. Since the diffusivities of dopants in crystallized and

Chapter 7: Guidelines for Additional Calibration

Accuracy and Limitations of Advanced Calibration of Sentaurus Process KMC

amorphous silicon are usually very different, the recrystallization velocity can influence the overall diffusion.

It is also known that the recrystallization depends on substrate orientation; however, by default, the recrystallization velocity in Advanced Calibration for Sentaurus Process KMC is independent of it. To activate the substrate orientation dependency, you should select:

```
pdbSet KMC Si Damage SPER.Model LKMC
```

Diffusion, Generation, and Recombination

The parameter values for the equilibrium concentration and diffusivity of point defects have been inherited from continuum Advanced Calibration and have been chosen by Synopsys as a careful compromise between various suggestions in recent publications (see [Point Defects on page 138](#)). The I–V pair recombination rate is part of the amorphization calibration (see [Amorphization on page 273](#)).

Changing any of these parameters might affect the diffusion and activation behavior of several dopants. Therefore, for the purpose of improving the accuracy of diffusion of one dopant, it is not recommended to change point-defect parameters, due to the possible unwanted effects on other dopants.

Extended Defects

Like the advanced TED model in the Advanced Calibration of continuum Sentaurus Process (see [Interstitial Clusters on page 95](#)), the comprehensive KMC model for extended defects of self-interstitials in silicon [8] describes accurately the initial phase of ultrahigh interstitial supersaturation after ion implantation, which was reported in [9] and is ascribed to the formation and dissolution of small interstitial clusters (see [Figure 40](#)).

The binding energies of larger cluster sizes have been calibrated from transmission electron microscope (TEM) data on the dissolution of {311} defects published by Stolk *et al.* [10] and Saleh *et al.* [11].

The calibration of the transformation rate from {311} defects to dislocation loops is based on data from the literature [12][13][14][15]. Due to low dislocation loop statistics in KMC, this calibration is difficult and not as accurate as for {311} dissolution. Therefore, the following parameters can be used as fitting parameters:

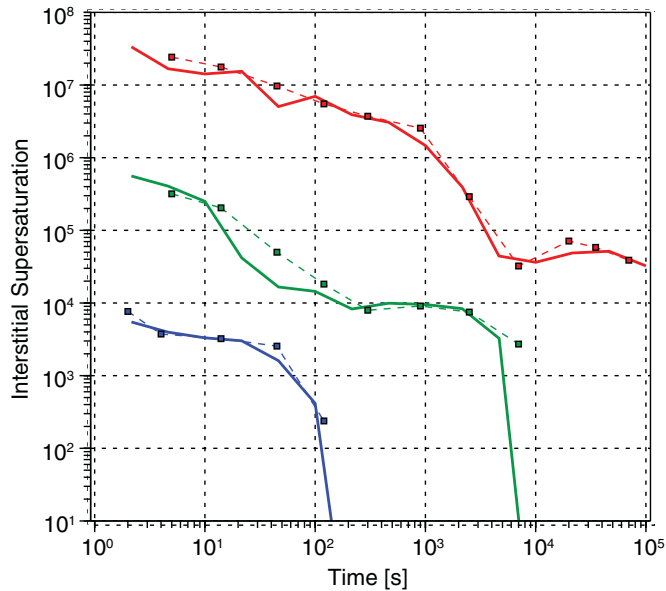
```
pdbSet KMC Si Int D0.311.To.Loop 4500  
pdbSet KMC Si Int E.311.To.Loop 0.0
```

The parameters for voids have been calibrated on a limited experimental dataset only [16] and, therefore, are subject to additional calibration in the case of vacancy engineering implantation.

Chapter 7: Guidelines for Additional Calibration

Accuracy and Limitations of Advanced Calibration of Sentaurus Process KMC

Figure 40 Self-interstitial supersaturation evolution: comparison of experiments (squares) and simulations (solid lines) for anneals at 600°C (red), 700°C (green), and 800°C (blue) (experimental data from [9])



Impurities

This section discusses impurities.

Diffusion

In general, the diffusivities are inherited from Advanced Calibration of continuum Sentaurus Process and are based on the literature and SIMS calibration. For details about the translation of the diffusivities to the migration and binding parameters for Sentaurus Process KMC, see [Diffusion on page 232](#).

For fine-tuning of the diffusivity, the binding, migration, and ionization energies of dopant–point defect pairs can be adjusted slightly. The influence of the binding, migration, and ionization energies is shown in [Figure 41](#).

The higher the binding energy, the more stable is the mobile pair and, therefore, the dopant encounters more diffusion. In contrast, the higher the migration barrier, the less the pair is mobile and, therefore, the dopant diffuses less.

A lower ionization level of a charge state allows that charge state to be more populated and, therefore, to have more influence on the overall diffusion. If the different charge states have different migration rates, changing the ionization levels results in a different overall migration rate.

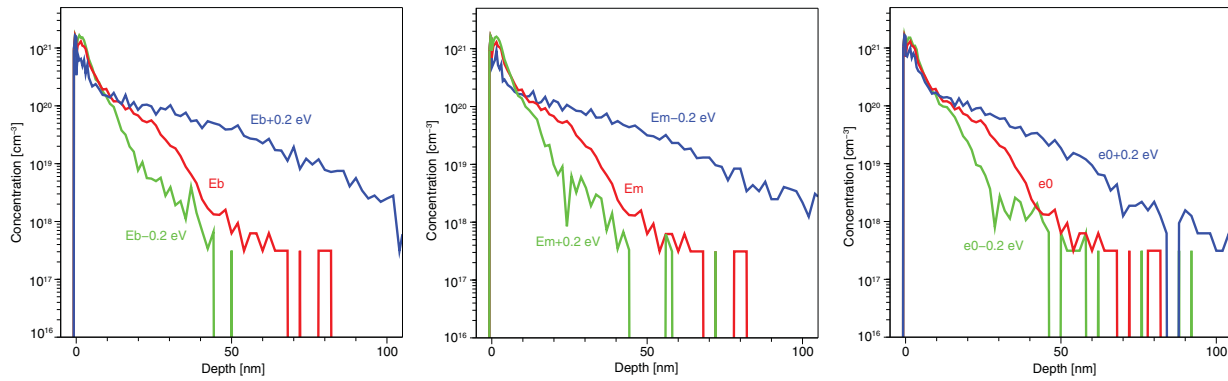
Chapter 7: Guidelines for Additional Calibration

Accuracy and Limitations of Advanced Calibration of Sentaurus Process KMC

Note:

Changing the binding energy and ionization levels of pairs also changes the impurity cluster formation, in particular, for reactions where the pair is involved. Since the binding energies of clusters are computed using the potential energies of the reactant, the potential energy of the pair (given by $-E_b(A_i^-) - e(-, 0)(A_i)$ for negative substitutional A) also influences the cluster stability. In addition, the migration barrier of the pair is involved in the emission of pairs from impurity clusters.

Figure 41 The influence of the binding (left), migration (middle), and ionization (right) energies on boron diffusion in silicon; the process conditions are $B\ 1e15$, 0.5 keV implantation followed by 1050°C spike anneal



Antimony

Advanced Calibration for Sentaurus Process KMC includes no parameters for antimony diffusion because the default parameters are based already on the translation of the continuum Advanced Calibration parameters and are verified against SIMS data.

Co-Diffusion of Arsenic and Phosphorus

As elaborated in [Co-diffusion of Arsenic and Phosphorus on page 158](#), the physics of the co-diffusion of arsenic and phosphorus in high concentration is very complex for several reasons. In general, Advanced Calibration for Sentaurus Process KMC underestimates the diffusion of arsenic in the presence of phosphorus at high concentrations. One reason for this might be the lack of an arsenic percolation-type diffusion model.

Diffusion in Amorphous Silicon

In Advanced Calibration for Sentaurus Process KMC, boron and fluorine are the only diffusing species in amorphous silicon. There is no evidence for significant diffusion of other species [\[17\]](#).

The boron diffusion, in combination with clustering, in amorphous silicon was calibrated [\[18\]](#) using literature data on completely amorphized SOI structures [\[19\]\[20\]](#) and deeply

Chapter 7: Guidelines for Additional Calibration

Accuracy and Limitations of Advanced Calibration of Sentaurus Process KMC

preamorphized bulk silicon structures [17]. The calibrated parameters for diffusion and clustering mediated by dangling bonds allow for good general agreement with experiments. The transient behavior of boron diffusion is well reproduced by the annihilation of dangling and floating bonds.

The coefficient for dangling bond creation per B atom in amorphous silicon is set to 0.5 in Advanced Calibration to obtain good accuracy with SIMS for boron implantation into amorphous silicon [19]. However, for amorphization of boron marker layers, a coefficient of 1.0 gives better accuracy, as reported in [18][20]. Therefore, the parameter:

```
 pdbSet KMC aSi B gamma 1.0
```

can be used as a fitting parameter, similar to the `ifactor` for ion implantation in continuum process simulation.

Activation

The responsible mechanism for deactivation/activation is the clustering/declustering of dopant–defect clusters. In Sentaurus Process KMC, the parameters for the dopant–defect cluster model are the potential energies, the emission prefactors, and the capture volumes. For recalibration, the most recommended fitting parameter is the emission prefactor `D0.Cluster` for dopant–defect pairs, while the one for point defects should not be changed for reasons of microscopic reversability.

Decreasing the emission prefactor results in decreasing the declustering rate, making the clusters more stable. Moreover, the solubility of impurities is governed by the potential energies of the clusters. Since most dopants can form several different cluster types, the potential energies of more than one cluster can influence the overall deactivation/activation.

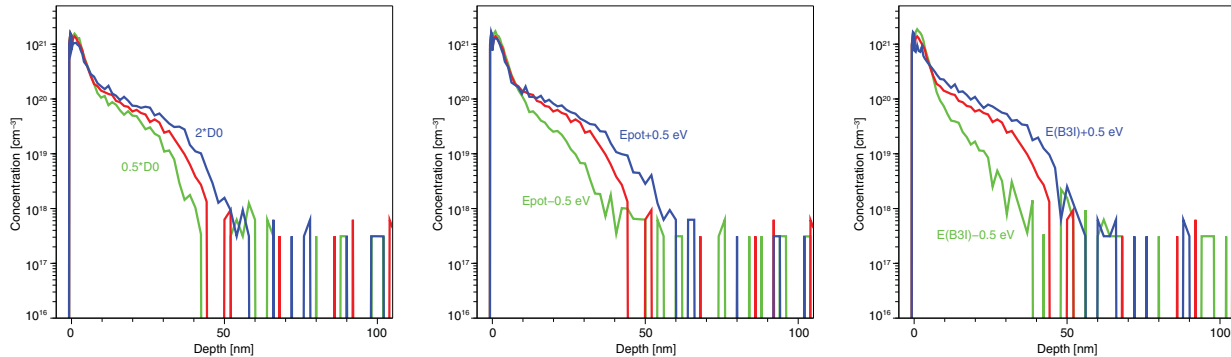
Therefore, the best way to tune the solid solubility of dopants is either to apply an overall shift for all cluster energies or to change the potential energy of the most stable clusters. The influence of the emission prefactor, the potential energies of all clusters, and the potential energy of the most stable cluster is illustrated in [Figure 42](#).

Finally, the capture volumes, which are specified relative to the substitutional dopant, are based on realistic guesses and can be changed only slightly.

Chapter 7: Guidelines for Additional Calibration

Accuracy and Limitations of Advanced Calibration of Sentaurus Process KMC

Figure 42 The influence of the BI emission prefactor (left), BIC potential energies (middle), and B_3I potential energy (right) on boron diffusion; the process conditions are B $1e15$, 0.5 keV implantation into silicon followed by 1050°C spike anneal



Segregation at End-of-Range Defects

Segregation of impurities to end-of-range defects is modeled by an interaction of the mobile impurity–interstitial pairs with extended defects such as {311} defects and dislocation loops. The pair breaks up and the interstitial is incorporated into the extended defect, while the impurity is regarded as substitutional. Obviously, the location of the impurity segregation depends on the end-of-range location, which depends on the amorphization-layer thickness generated by amorphizing implantation.

For carbon, this model works reasonably accurately [21]. However, in the case of indium, the segregation effect seems to be stronger [22] and can be modeled by selecting the following model:

```
pdbSet KMC Si In 311.Dopant.Model 1
pdbSet KMC Si In Loop.Dopant.Model 1
```

In this case, the neutral pair does not break up, but it is attached to the extended defect and stays attached until the dissolution of the extended defect.

Boron Interaction With Fluorine

It is known that the presence of fluorine can reduce diffusion and enhance the activation of boron. In Advanced Calibration, no direct interaction between boron and fluorine is assumed, as suggested by [23]. However, direct boron–fluorine interaction has been proposed by others [24]. Therefore, similar to boron–carbon clusters as proposed by [25] and described in [Boron and Carbon on page 245](#), you can study the direct interaction of boron with fluorine.

Chapter 7: Guidelines for Additional Calibration

Accuracy and Limitations of Advanced Calibration of Sentaurus Process KMC

To add fluorine–boron–interstitial clusters, for example BFI and BF, you must define the allowed reactions:

```
pdbSet KMC Si B ReactionsPointDefect Bi,F true  
pdbSet KMC Si F ReactionsPointDefect Fi,B true  
pdbSet KMC Si B ReactionsCluster BF,I true  
pdbSet KMC Si B ReactionsCluster BFI,V true
```

and specify the corresponding binding energy, capture volume, and emission prefactors:

```
pdbSet KMC Si B Etot.Complex BF -0.7  
pdbSet KMC Si B Etot.Complex BFI -5.6  
pdbSet KMC Si B CaptVol.Complex BF 1.3  
pdbSet KMC Si B CaptVol.Complex BFI 1.5  
pdbSet KMC Si B D0.Cluster BF,Bi 0.01  
pdbSet KMC Si B D0.Cluster BF,Fi 0.0001  
pdbSet KMC Si B D0.Cluster BF,I 0.5  
pdbSet KMC Si B D0.Cluster BF,V 0.5
```

Dose Loss

The dopant dose loss is controlled by the three-phase segregation model for the silicon–oxide interface model. Dopant trapping at the interface is diffusion limited; therefore, the dopant–point defect migration parameters also have an influence on the dose loss. The recommended fitting parameters for dose loss are the parameters for the maximum surface concentration of trapped particles `C0Max.Surf` and `EMax.Surf` as well as the parameter for the interface barrier `EBarrier_SurfSi`.

Recrystallization

For experiments with amorphizing conditions, the recrystallization parameters allow for a wide range of optimization, but the complex parameter interactions must be taken into account carefully. The maximum active doping concentration after recrystallization is an influential and sometimes critical parameter both for activation and diffusion, and the corresponding parameters `C0.Recryst.Max.Active` and `E.Recryst.Max.Active` serve as fitting parameters.

However, since the activation of doping during SPER usually is temperature dependent [26], the accurate anneal temperature at SPER is critical. Therefore, the specification of the accurate temperature profile during the anneal, especially the initial phase of the ramp-up with temperatures at 500°C and above, is important. In addition, the doping and impurity concentrations have an effect on the recrystallization velocity and can influence the activation during SPER. The corresponding parameters `V0.Recryst.ntype` and `V0.Recryst.ptype` are candidates for recalibration parameters. Finally, the portion of swept impurities by the recrystallization front can also be adjusted from case to case.

Chapter 7: Guidelines for Additional Calibration

Accuracy and Limitations of Advanced Calibration of Sentaurus Process KMC

Fluorine Effect

A special case is fluorine with its retarding effect on recrystallization [5]. By strongly slowing down SPER, the presence of (coimplanted) fluorine can not only result in incorporation of an higher active doping concentration during temperature ramp-up, but also allow more time for dopant diffusion in amorphous silicon.

In the case of boron, with its higher diffusivity in amorphous silicon than crystalline silicon [20], the influence of diffusion in amorphous silicon is enhanced. Therefore, for fine-tuning, you can tune not only the fluorine parameters for redistribution during SPER (`Pref.RecrysDepos` and `Ener.RecrysDepos`), but also the fluorine parameters for slowing down the recrystallization (`E.Recrys` and `E.Recrys.Exponent`).

BF_2 Implantation

While for boron implantation after preamorphization implantation, no boron is moved by the recrystallization front, this could be the case for BF_2 . Therefore, you can allow some portion of the boron swept by the recrystallization front by adjusting `Pref.RecrysDepos`.

In addition, the length of boron diffusion can be controlled by the incorporation of fluorine during SPER. Most fluorine is incorporated into silicon as fluorine interstitials and as so-called F–V clusters [27][28]. In the context of Sentaurus Process KMC, the F–V clusters are F–I clusters (see [Fluorine on page 239](#)) containing fewer interstitials than fluorine. Finally, the amount of interstitials incorporated into F–I clusters during SPER also influences the boron diffusion.

Stress and SiGe Effects

The calibration of the effects of Ge concentration and stress on defect and dopant diffusion, and clustering is part of Advanced Calibration for Sentaurus Process KMC. By default, the Ge effects are modeled by linear correction factors for silicon parameters and are valid only for low Ge mole fractions ranging between 0% and 50%. Optionally, you can activate Si and Ge parameter interpolation for SiGe using the following command with the first argument set to true:

```
KMC_SiGe_and_Stress_Effect 1 0
```

This deactivates the default linear correction factors and uses the interpolation parameters defined for `SiliconGermanium`. The calibration covers the full range of the Ge mole fraction (0–100%).

The stress effects on damage, diffusion, and binding in Advanced Calibration for Sentaurus Process KMC are taken into account only if the `KMC Stress` switch is activated. Stress effects are recommended to be activated by using the following command with the second argument set to true:

```
KMC_SiGe_and_Stress_Effect 0 1
```

Chapter 7: Guidelines for Additional Calibration

References

The calibration of Ge and stress effects [29][30] is based on a relatively small set of measured data. The models have not yet been tested rigorously against SIMS data for all dopant species and nonequilibrium annealing conditions, and against electrical data from real-device fabrication processes. Further calibration for specific applications might be required.

Stress Calculation

Sentaurus Process KMC uses the stress provided by Sentaurus Process, but Sentaurus Process KMC does not compute it. The stress fields are updated from Sentaurus Process for each diffuse step.

For calculating stress, it is recommended to use the mechanics parameters from Advanced Calibration for Sentaurus Process in continuum mode. Therefore, Advanced Calibration should also be called *before* enabling the KMC mode by `setAtomistic`.

For details about the mechanics parameters, see [Parameters for Mechanics on page 291](#).

Dopant Activation Under Stress

In Advanced Calibration for Sentaurus Process KMC, no stress effects are included for dopant–defect clusters. However, the solid solubility of dopants in silicon depends on the strain [31] and is modeled in continuum Advanced Calibration (see [Impact of Pressure on Dopant Activation on page 73](#)). In general, for compressive strain, the solubility of atoms smaller than Si increases; whereas, the solubility of larger atoms decreases. To change the cluster stability under strain, the stress correction volumes for potential energy can be defined for individual clusters:

```
pbSet KMC Si As VF.Complex As4V -0.01
```

References

- [1] N. Zographos and I. Martin-Bragado, “A Comprehensive Atomistic Kinetic Monte Carlo Model for Amorphization/Recrystallization and its Effects on Dopants,” in *MRS Symposium Proceedings, Doping Engineering for Front-End Processing*, vol. 1070, p. 1070-E03-01, 2008.
- [2] H.-J. Gossmann *et al.*, “Predictive Process Simulation of Cryogenic Implants for Leading Edge Transistor Design,” in *19th International Conference on Ion Implantation Technology (IIT)*, Valladolid, Spain, pp. 225–228, June 2012.
- [3] R. D. Goldberg, J. S. Williams, and R. G. Elliman, “Amorphization of silicon by elevated temperature ion irradiation,” *Nuclear Instruments and Methods in Physics Research B*, vol. 106, no. 1–4, pp. 242–247, 1995.

Chapter 7: Guidelines for Additional Calibration

References

- [4] M. Posselt, L. Bischoff, and J. Teichert, "Influence of dose rate and temperature on ion-beam-induced defect evolution in Si investigated by channeling implantation at different doses," *Applied Physics Letters*, vol. 79, no. 10, pp. 1444–1446, 2001.
- [5] G. L. Olson and J. A. Roth, "Kinetics of Solid Phase Crystallization in Amorphous Silicon," *Materials Science Reports*, vol. 3, pp. 1–78, 1988.
- [6] B. C. Johnson and J. C. McCallum, "Dopant-enhanced solid-phase epitaxy in buried amorphous silicon layers," *Physical Review B*, vol. 76, no. 4, p. 045216, 2007.
- [7] D. D'Angelo *et al.*, "Role of the strain in the epitaxial regrowth rate of heavily doped amorphous Si films," *Applied Physics Letters*, vol. 93, no. 23, p. 231901, 2008.
- [8] I. Martin-Bragado *et al.*, "From point defects to dislocation loops: A comprehensive TCAD model for self-interstitial defects in silicon," in *37th European Solid-State Device Research Conference (ESSDERC)*, Munich, Germany, pp. 334–337, September 2007.
- [9] N. E. B. Cowern *et al.*, "Energetics of Self-Interstitial Clusters in Si," *Physical Review Letters*, vol. 82, no. 22, pp. 4460–4463, 1999.
- [10] P. A. Stolk *et al.*, "Physical mechanisms of transient enhanced dopant diffusion in ion-implanted silicon," *Journal of Applied Physics*, vol. 81, no. 9, pp. 6031–6050, 1997.
- [11] H. Saleh *et al.*, "Energy dependence of transient enhanced diffusion and defect kinetics," *Applied Physics Letters*, vol. 77, no. 1, pp. 112–114, 2000.
- [12] J. Li and K. S. Jones, "{311} defects in silicon: The source of the loops," *Applied Physics Letters*, vol. 73, no. 25, pp. 3748–3750, 1998.
- [13] F. Cristiano *et al.*, "Ion beam induced defects in crystalline silicon," *Nuclear Instruments and Methods in Physics Research B*, vol. 216, pp. 46–56, February 2004.
- [14] Y. Lamrani *et al.*, "Direct evidence of the recombination of silicon interstitial atoms at the silicon surface," *Nuclear Instruments and Methods in Physics Research B*, vol. 216, pp. 281–285, February 2004.
- [15] P. Calvo *et al.*, "Thermal evolution of {113} defects in silicon: transformation against dissolution," *Nuclear Instruments and Methods in Physics Research B*, vol. 216, pp. 173–177, February 2004.
- [16] V. C. Venezia *et al.*, "Depth profiling of vacancy clusters in MeV-implanted Si using Au labeling," *Applied Physics Letters*, vol. 73, no. 20, pp. 2980–2982, 1998.
- [17] R. Duffy *et al.*, "Dopant diffusion in amorphous silicon," in *MRS Symposium Proceedings, Silicon Front-End Junction Formation—Physics and Technology*, vol. 810, San Francisco, CA, USA, p. C10.2.1, April 2004.
- [18] I. Martin-Bragado and N. Zographos, "Indirect boron diffusion in amorphous silicon modeled by kinetic Monte Carlo," *Solid-State Electronics*, vol. 55, no. 1, pp. 22–28, 2011.

Chapter 7: Guidelines for Additional Calibration

References

- [19] V. C. Venezia *et al.*, "Boron diffusion in amorphous silicon," *Materials Science and Engineering B*, vol. 124–125, pp. 245–248, December 2005.
- [20] S. Mirabella *et al.*, "Mechanism of Boron Diffusion in Amorphous Silicon," *Physical Review Letters*, vol. 100, p. 155901, April 2008.
- [21] N. Zographos and I. Martin-Bragado, "Atomistic Modeling of Carbon Co-Implants and Rapid Thermal Anneals in Silicon," in *15th IEEE International Conference on Advanced Thermal Processing of Semiconductors (RTP)*, Catania, Italy, pp. 119–122, October 2007.
- [22] T. Noda, S. Odanaka, and H. Umimoto, "Effects of end-of-range dislocation loops on transient enhanced diffusion of indium implanted in silicon," *Journal of Applied Physics*, vol. 88, no. 9, pp. 4980–4984, 2000.
- [23] G. Impellizzeri *et al.*, "Fluorine in preamorphized Si: Point defect engineering and control of dopant diffusion," *Journal of Applied Physics*, vol. 99, p. 103510, May 2006.
- [24] A. Halimaoui *et al.*, "Investigation of Fluorine Effect on the Boron Diffusion by Mean of Boron Redistribution in Shallow Delta-doped Layers," in *MRS Symposium Proceedings, Silicon Front-End Junction Formation—Physics and Technology*, vol. 810, San Francisco, CA, USA, p. C3.10, April 2004.
- [25] C.-L. Liu *et al.*, "Ab initio modeling and experimental study of C–B interactions in Si," *Applied Physics Letters*, vol. 80, no. 1, pp. 52–54, 2002.
- [26] S. H. Jain *et al.*, "Metastable boron active concentrations in Si using flash assisted solid phase epitaxy," *Journal of Applied Physics*, vol. 96, no. 12, pp. 7357–7360, 2004.
- [27] M. Diebel and S. T. Dunham, "Ab Initio Calculations to Model Anomalous Fluorine Behavior," *Physical Review Letters*, vol. 93, no. 24, p. 245901, 2004.
- [28] M. Diebel and S. T. Dunham, "Reply to Ab Initio Calculations to Model Anomalous Fluorine Behavior," *Physical Review Letters*, vol. 96, p. 039602, January 2006.
- [29] N. Zographos *et al.*, "Process Modeling of Chemical and Stress Effects in SiGe," in *19th International Conference on Ion Implantation Technology (IIT)*, Valladolid, Spain, pp. 212–216, June 2012.
- [30] N. Zographos and I. Martin-Bragado, "Process modeling of stress and chemical effects in SiGe alloys using kinetic Monte Carlo," *Journal of Computational Electronics*, July 2013.
- [31] C. Ahn *et al.*, "Stress effects on impurity solubility in crystalline materials: A general model and density-functional calculations for dopants in silicon," *Physical Review B*, vol. 79, no. 7, p. 073201, 2009.

Part III: Advanced Calibration for Mechanics Simulations

This part of the *Advanced Calibration for Process Simulation User Guide* contains the following chapters:

- [Chapter 8, Using Advanced Calibration File for Mechanics Simulations](#)
- [Chapter 9, Contents of Advanced Calibration for Mechanics Simulations](#)

8

Using Advanced Calibration File for Mechanics Simulations

This chapter describes the use of the Advanced Calibration file for mechanics simulations using Sentaurus Process and Sentaurus Interconnect.

Advanced Calibration is a selection of models and parameters that is recommended by Synopsys to be used for accurate process simulation, including mechanics simulation. In Sentaurus Process and Sentaurus Interconnect, this selection of models and parameters is contained in a text file, which can be opened with any standard text editor.

By sourcing the Advanced Calibration file at the beginning of a simulation, the standard calibration of Synopsys is selected. If needed, you can change or extend Advanced Calibration. This can be performed by either sourcing an additional calibration file, which contains the required parameter changes, or editing the Advanced Calibration file with a text editor.

Location of Advanced Calibration File

The Advanced Calibration file is the ultimate product of Synopsys' calibration efforts. For each release of Sentaurus Process and Sentaurus Interconnect, there is a new Advanced Calibration file that includes the best and latest set of models and parameters. To ensure backward compatibility, the previous Advanced Calibration files are still available.

The files for the Advanced Calibration of Sentaurus Process in this release are located at:

```
$STROOT/tcad/$STRELEASE/lib/sprocess/TclLib/AdvCal
```

The default file is named `AdvCal_2022.03.fps`. It represents the first version of Advanced Calibration Version T-2022.03. Older versions of the Advanced Calibration file can be found in the same directory. For example, the file `AdvCal_2021.06.fps` contains the Advanced Calibration file for Version S-2021.06 and is available for backward compatibility.

Mechanical parameters are located only in the Advanced Calibration file for silicon, SiGe, and germanium (the default one).

Chapter 8: Using Advanced Calibration File for Mechanics Simulations

Using Advanced Calibration

Note:

There are no settings related to mechanics in the Advanced Calibration file for 4H-SiC process simulation.

The files for the Advanced Calibration of Sentaurus Interconnect in this release are located at:

```
$STROOT/tcad/$STRELEASE/lib/sinterconnect/TclLib/AdvCal
```

The default file is named `AdvCal_2022.03.sis`. It represents the first version of Advanced Calibration Version T-2022.03. Older versions of the Advanced Calibration file can be found in the same directory. For example, the file `AdvCal_2021.06.sis` contains the Advanced Calibration file for Version S-2021.06 and is available for backward compatibility.

Using Advanced Calibration

To use Advanced Calibration for mechanics simulations in Sentaurus Process and Sentaurus Interconnect, at the beginning of the input file, insert the line:

```
AdvancedCalibration 2022.03
```

Alternatively, this file can be sourced by using:

```
source $AdvCalDir/AdvCal_2022.03.fps
```

or:

```
source $AdvCalDir/AdvCal_2022.03.sis
```

The recommended set of mechanical models and parameters is located in section 2.15 of the default Advanced Calibration file (in Sentaurus Process, it is the file for Si-, SiGe-, and Ge-based technology). In earlier versions of Advanced Calibration (E-2010.12 to K-2015.06), this set was activated manually by calling the `AdvancedCalibrationMechanics` procedure.

Note:

The set is applied by default, and the `AdvancedCalibrationMechanics` procedure is deprecated.

Earlier Versions of Advanced Calibration

You can source earlier versions of the Advanced Calibration file by inserting, for example, the line:

```
AdvancedCalibration 2021.06
```

Chapter 8: Using Advanced Calibration File for Mechanics Simulations

Earlier Versions of Advanced Calibration

This is converted internally to:

```
source $AdvCalDir/AdvCal_2021.06.fps
```

After sourcing the Advanced Calibration file, insert the line:

```
AdvancedCalibrationMechanics
```

This command calls the procedure including the parameters for mechanics simulation.

For earlier versions of the Advanced Calibration file of Sentaurus Process, see [Earlier Versions of Advanced Calibration on page 19](#).

Table 8 lists earlier versions of the Advanced Calibration file that can be loaded with Sentaurus Interconnect Version T-2022.03.

Table 8 Earlier versions of Advanced Calibration file and their corresponding commands

Advanced Calibration file	Corresponding command
AdvCal_2021.06.sis	AdvancedCalibration 2021.06
AdvCal_2020.09.sis	AdvancedCalibration 2020.09
AdvCal_2019.12.sis	AdvancedCalibration 2019.12
AdvCal_2019.03.sis	AdvancedCalibration 2019.03
AdvCal_2018.06.sis	AdvancedCalibration 2018.06
AdvCal_2017.09.sis	AdvancedCalibration 2017.09
AdvCal_2016.12.sis	AdvancedCalibration 2016.12
AdvCal_2016.03.sis	AdvancedCalibration 2016.03
AdvCal_2015.06.sis	AdvancedCalibration 2015.06
AdvCal_2014.09.sis	AdvancedCalibration 2014.09
AdvCal_2013.12.sis	AdvancedCalibration 2013.12
AdvCal_2013.03.sis	AdvancedCalibration 2013.03

This possibility is available to provide backward compatibility. You can run simulations with the latest version of Sentaurus Interconnect, but the simulations can still be based on an old calibration. For new TCAD projects, it is recommended to load the latest version of Advanced Calibration.

9

Contents of Advanced Calibration for Mechanics Simulations

This chapter describes the models and parameters used in Advanced Calibration for mechanics simulations.

Overview

Section 2.15 of the Advanced Calibration file includes a set of recommended mechanical parameters for the materials of the most common electronics as well as appropriate settings for mechanics simulations.

In previous releases (E-2010.12 to K-2015.06), this set was placed in the procedure `AdvancedCalibrationMechanics`. This procedure was switched off by default and had to be invoked explicitly to load the modified parameters described here. After sourcing the Advanced Calibration file of Version T-2022.03, the set is applied by default without calling the procedure `AdvancedCalibrationMechanics`.

Note:

The procedure `AdvancedCalibrationMechanics` is deprecated.

The set of mechanical parameters contains values from the literature (with corresponding references for the values that differ from the default ones) for silicon, germanium, polysilicon, SiO_2 (Oxide), Si_3N_4 (Nitride), TiN (TiNitride), HfO_2 , GeO_2 (GeOxide), and SiC (SiliconCarbide). The set is incomplete, that is, it does not include all parameters for all the materials and mechanical models available in Sentaurus Process and Sentaurus Interconnect, but it serves as an aggregated source of the most recent (and, sometimes, different from the default) parameters for mechanical simulations.

Switches for Interpolation in Mole Fraction–Dependent Mechanical Models

The set of recommended mechanical models and parameters includes the parameter interpolation syntax (see *Sentaurus™ Process User Guide*, Alloy Materials and Parameter

Chapter 9: Contents of Advanced Calibration for Mechanics Simulations

Overview

Interpolation) as well as the older syntax including deprecated syntax for Ge mole fraction dependency of mechanical parameters in Ge-doped silicon.

Using the new syntax is the best choice for devices with SiGe regions. However, the usage of the parameter interpolation can noticeably increase the simulation time for diffusion in the presence of Ge in silicon with the concentration `> Min.Conv.Conc` (or similarly, the presence of Si in germanium) even in cases where the influence of the Ge content on diffusion is not important. This might occur, for example, in a simulation of silicon devices with Ge preamorphization implantation (PAI) simulated with Monte Carlo implantation. Typically, within Advanced Calibration, these two cases are differentiated by the usage of the `SiGe_and_Stress_Effect` procedure:

- Where the Ge mole fraction is important for diffusion, use `SiGe_and_Stress_Effect` with the `Ge_Chem_Eff=1` argument.
- Where the Ge mole fraction is not important for diffusion, you can either:
 - Not call `SiGe_and_Stress_Effect` at all, which corresponds to:
`SiGe_and_Stress_Effect 0 0 0 0`
 - Call `SiGe_and_Stress_Effect 0 * * *` (where * is either 0 or 1).

Depending on the value of the argument `Ge_Chem_Eff`, either the modern syntax (for `Ge_Chem_Eff=1`) or the older syntax (for `Ge_Chem_Eff=0`) is used for mechanics simulations.

The following lines defining the default behavior of Advanced Calibration are included in section 2.14 of `AdvCal_2022.03.fps`:

```
pdbSet Si Skip.Parameter.Interpolation 1  
pdbSet Ge Skip.Parameter.Interpolation 1  
pdbSet Mechanics Lattice.Constant.Mismatch 0  
pdbSet Mechanics Parameter.Interpolation 0
```

These lines switch off parameter interpolation in SiGe (as well as interpolation of elastic constants and the coefficients of thermal expansion in all materials) and switch off the default lattice mismatch model for alloy materials. The same settings are applied in the procedure `SiGe_and_Stress_Effect` when `Ge_Chem_Eff=0`. If `Ge_Chem_Eff=1`, the opposite values are set for the above four parameters.

When the model of parameter interpolation for mechanical parameters in compound materials is deactivated using the following command, the deprecated syntax for interpolation of mechanical parameters in SiGe becomes active:

```
pdbSet Mechanics Parameter.Interpolation 0
```

In addition, the following command activates the old `Conc.Strain` model for Ge impurity in silicon:

```
pdbSet Mechanics Lattice.Constant.Mismatch 0
```

Chapter 9: Contents of Advanced Calibration for Mechanics Simulations

Parameters for Mechanics

Besides the usage of the modern or older syntax (and corresponding models), these switches determine which definition of the Ge mole fraction is used. That is, the models corresponding to the modern syntax use a more precise definition (see [Equation 2 on page 63](#)). Whereas, the old mechanical models use the old definition (see [Equation 3 on page 63](#)).

The value of the `Si Skip.Parameter.Interpolation` parameter controls which definition of the mole fraction is used for the `xMoleFraction` field saved into a TDR file after diffusion for material `SiliconGermanium` derived from material `Silicon`.

The following parameter setting leads to the new mole fraction definition being used for saving the `xMoleFraction` field:

```
pdbSet Si Skip.Parameter.Interpolation 0
```

Both the modern and older mechanics syntax allow similar functionality for SiGe simulations (and even very close results for low Ge mole fractions), but the modern syntax is superior in terms of functionality and precision for large mole fractions.

Note:

Versions T-2022.03 to K-2015.06 of the Advanced Calibration file for Sentaurus Interconnect do not include settings for mole fraction dependency of mechanical parameters and concentration-dependent stress models, which are present in the version for Sentaurus Process.

Parameters for Mechanics

The parameters for mechanics simulations are described here.

Suppression of Dilatational Viscosity

In Sentaurus Process and Sentaurus Interconnect, the viscoelastic response can be applied to both the deviatoric and volumetric parts. In fact, solid materials do not demonstrate dilatational viscosity. To restrict the viscoelastic response to the deviatoric part only, the following flag is set:

```
pdbSet Mechanics NoBulkRelax 1
```

Mole Fraction–Dependent Mechanics Parameters for SiGe

A simple linear interpolation between parameter values in silicon and germanium is used to calculate the elastic stiffness constants and the linear thermal expansion coefficient in SiGe.

Chapter 9: Contents of Advanced Calibration for Mechanics Simulations

Parameters for Mechanics

Note:

Due to some limitations in Sentaurus Process, you should use only temperature-independent coefficients of thermal expansion.

By default and in the case of `Ge_Chem_Eff=0`, the mole fraction-dependent model is invoked by the following older syntax:

```
pdbSetBoolean Si IsCompound 1  
pdbSetString Mechanics BCompoundList {Silicon Germanium}  
pdbSetDoubleArray SiliconGermanium CompoundInterp {0 0 1 1}
```

For epitaxially grown materials, the correct thermal stress model is set by the following string:

```
pdbSetBoolean Mechanics Compound.ThExpCoeff 1
```

The definition of lattice mismatch strain with respect to the relaxed local lattice constant is set by the following line:

```
pdbSet Mechanics Lattice.Mismatch.Strain LCC
```

Quadratic interpolation for the strain calculation using the lattice mismatch model in binary $\text{Si}_{1-x}\text{Ge}_x$ materials (lattice constant $a_{\text{SiGe}} = 5.431 + 0.201x + 0.026x^2 \text{ \AA}$) and $\text{Si}_{1-x}\text{C}_x$ materials (lattice constant $a_{\text{SiC}} = 5.431 - 2.4542x + 0.59x^2 \text{ \AA}$) is introduced [1]. In the parameter `Conc.Strain`, the strain is specified as a piecewise linear function of the mole fraction (the older mole fraction definition is used then; see [Equation 3 on page 63](#)). The modern syntax for the quadratic lattice constant interpolation for the lattice mismatch model in SiGe is given by:

```
pdbSet SiGe LatticeConstant.X2 -0.026
```

Cubic Crystal Anisotropy for Silicon and Germanium

For calculating stress, silicon and germanium are treated as anisotropic materials, defined by the following lines:

```
pdbSet Si Mechanics Anisotropic 1  
pdbSet Ge Mechanics Anisotropic 1
```

Temperature Dependency of Stiffness Coefficients for Silicon and Germanium

Temperature dependency of the stiffness coefficients for silicon and germanium have been introduced using the temperature derivatives at 300 K [2]. Both the modern syntax (using `T1`) and the older syntax (using `Rate`) are provided. The temperature dependency of the elastic coefficients of crystalline silicon and germanium leads to an approximately 10% reduction of their values at 1000°C in comparison to the room temperature ones.

Isotropic Elastic Moduli for Germanium

Germanium isotropic elastic moduli are calculated in the Voigt–Reuss–Hill [3] polycrystalline approximation from its single-crystal anisotropic elastic constants:

```
pdbSet Ge Mechanics BulkModulus 75.00e10  
pdbSet Ge Mechanics ShearModulus 54.44e10
```

Polysilicon

Polysilicon bulk modulus and shear modulus are calculated from the measured Young's modulus and the Poisson ratio [4]. Polysilicon is known to be a plastic material at high temperatures with a temperature-dependent plasticity threshold [5][6]. It is taken into account by the Arrhenius-type dependency of the yield stress as follows:

```
pdbSet PolySi Mechanics FirstYield 5.75e8  
pdbSet PolySi Mechanics FirstYieldW -0.23
```

The temperature-dependent yield stress can be used to increase accuracy of the stress memorization effect simulation [7]. The plasticity model is not switched on in Advanced Calibration. If needed, it can be switched on by the line:

```
pdbSetBoolean PolySilicon Mechanics IsPlastic 1
```

Temperature dependency has been introduced for the elastic moduli of polysilicon following the values for crystalline silicon [2]. The given rate values have been derived from the temperature dependency of the isotropic elastic moduli of polysilicon, which were calculated from the elastic constants of silicon in the Voigt–Reuss–Hill polycrystalline approximation. Both the modern syntax (using `T1`) and the older syntax (using `Rate`) are provided. The temperature dependency of the elastic moduli of polysilicon leads to an approximately 10% reduction of their values at 1000°C in comparison to the room temperature ones.

Viscosity of Oxide and Nitride

Temperature dependency also was included for the oxide and nitride stress-dependent viscosity activation volumes [8]:

```
pdbSet Ox Mechanics Vcrit0 1.25e-20  
pdbSet Ox Mechanics VcritW 0.35  
pdbSet Nit Mechanics Vcrit0 4.7e-21  
pdbSet Nit Mechanics VcritW 0.35
```

Isotropic Moduli for Titanium and Titanium Silicide

For Ti (Titanium) and TiSi₂ (Tisilicide), isotropic moduli based on the literature [9][10] are suggested:

```
pdbSet Ti    Mechanics BulkModulus 106.e10
pdbSet Ti    Mechanics ShearModulus 42.e10
pdbSet TiSi2 Mechanics BulkModulus 128.3e10
pdbSet TiSi2 Mechanics ShearModulus 59.2e10
```

The values for TiSi₂ are obtained from the measured value of the biaxial elastic modulus (220 GPa) [10] and the assumed Poisson ratio 0.30. No reliable measurement of the Poisson ratio for the stable (C54) phase of TiSi₂ was found in the literature. The value 0.22 ± 0.07 from [11] appears to be unreliable because it uses an improbably large value of the elastic modulus (259 GPa) obtained for bulk material from [12]. The spread of the elastic coefficient values is, in general, large for silicides: The values can vary by approximately 50% depending on the exact silicide stoichiometry and process conditions [13].

Amorphous Germanium Oxide

Isotropic elastic moduli and the linear coefficient of thermal expansion (LCTE) are introduced for vitreous (amorphous) GeO₂:

```
pdbSet GeOx Mechanics BulkModulus 23.87e10
pdbSet GeOx Mechanics ShearModulus 18.10e10
pdbSet GeOx Mechanics ThExpCoeff 9.06e-6
```

The values of the elastic moduli at 25°C are taken from [14]. These values correspond to the Young's modulus of 43.34 GPa, which is smaller than $53.5 \text{ GPa} \pm 10\%$ reported in [15]. LCTE = 9.06e-6 K^{-1} at 660°C is taken from [16]. In [15], LCTE = 1.0e-6 K^{-1} was measured at room temperature and, in addition, LCTE = 7.5e-6 K^{-1} and 7.7e-6 K^{-1} were referenced.

Titanium Nitride

Isotropic elastic moduli and the LCTE are introduced for TiN (TiNitride):

```
pdbSet TiNitride Mechanics BulkModulus 300e10
pdbSet TiNitride Mechanics ShearModulus 180e10
pdbSet TiNitride Mechanics ThExpCoeff 9.35e-6
```

The structure of TiN films is typically polycrystalline with cubic lattice and preferable [100] or [111] orientation [17], but for certain deposition conditions, it can be also amorphous [18]. The above TiN elastic moduli are obtained by averaging the measured values for coating films [19] and Voigt–Reuss–Hill isotropic ones calculated from single-crystal measurements [20]. They result in a Young's modulus equal to 450 GPa. Elastic moduli of TiN vary substantially depending on the deposition conditions and the film thickness, for example,

experimental Young's modulus values vary from 200 GPa to 488 GPa [19]–[26]. LCTE of TiN is taken from [22].

Hafnium Oxide

Isotropic elastic moduli and the LCTE are introduced for HfO₂:

```
pdbSet HfO2 Mechanics BulkModulus 234.615e10  
pdbSet HfO2 Mechanics ShearModulus 109.2e10  
pdbSet HfO2 Mechanics ThExpCoeff 8.5e-6
```

These elastic moduli are obtained for monoclinic HfO₂ in [27], and they correspond to a Young's modulus of 283.6 GPa. Depending on the manufacturing conditions, the structure of HfO₂ film can be amorphous or polycrystalline with a monoclinic or an orthorhombic lattice, or even a combination of the three [28][29]. Reported experimental Young's modulus values of HfO₂ vary from 152 GPa to 370 GPa [27][30][31][32][33]. The above isotropic LCTE of HfO₂ was calculated by averaging the anisotropic LCTE components of monoclinic HfO₂ from [34].

Silicon Carbide

Isotropic elastic moduli and the LCTE are introduced for SiC (SiliconCarbide):

```
pdbSet SiC Mechanics BulkModulus 220.552e10  
pdbSet SiC Mechanics ShearModulus 191.106e10  
pdbSetDouble SiC Mechanics ThExpCoeff 3.25622e-6
```

These SiC isotropic elastic moduli are calculated in the Voigt–Reuss–Hill approximation from experimental anisotropic elastic constants reported in [35]. The measurements of single-crystal samples showed that 4H and 6H-SiC have the same elastic constants within experimental uncertainties [35]. For 3C-SiC, isotropic elastic moduli based on a Young's modulus of 410 GPa and a Poisson ratio of 0.19 measured for single-crystal thin-film samples in [36] are BulkModulus=220e10 and ShearModulus=172e10 dyn/cm².

Measurements reported in [36] had substantial spread, depending on the structure of the samples. Additional references on experimental measurements of 3C-SiC elastic properties can be found in [37]. The above isotropic LCTE of SiC was calculated by averaging the anisotropic LCTE components of hexagonal 4H-SiC at 300 K from [38][39]. Both 6H and 3C polytypes have similar values of LCTE [40][41][42][43]. The results of LCTE measurements for 3C, 4H, and 6H-SiC were extended analytically for other SiC polytypes in [44].

References

- [1] D. De Salvador *et al.*, “Lattice parameter of $\text{Si}_{1-x-y}\text{Ge}_x\text{C}_y$ alloys,” *Physical Review B*, vol. 61, no. 19, pp. 13005–13013, 2000.
- [2] S. Adachi, *Handbook on Physical Properties of Semiconductors*, vol. 1, (p. 57, Table 2.3.5 and p. 142, Table 3.3.9), New York: Springer, 2004.
- [3] R. Hill, “The Elastic Behaviour of a Crystalline Aggregate,” *The Proceedings of the Physical Society*, vol. 65, no. 389A, pp. 349–354, 1952.
- [4] W. N. Sharpe, Jr. *et al.*, “Measurements of Young’s Modulus, Poisson’s Ratio, and Tensile Strength of Polysilicon,” in *Tenth Annual International Workshop on Micro Electro Mechanical Systems (MEMS)*, Nagoya, Japan, pp. 424–429, January 1997.
- [5] C.-S. Oh, G. Coles, and W. N. Sharpe, Jr., “High Temperature Behavior of Polysilicon,” in *MRS Symposium Proceedings, Nano- and Microelectromechanical Systems (NEMS and MEMS) and Molecular Machines*, vol. 741, Boston, MA, USA, pp. J3.6.1–J3.6.6, December 2002.
- [6] Yu. V. Milman, I. V. Gridneva, and A. A. Golubenko, “Construction of Stress-Strain Curves for Brittle Materials by Indentation in a Wide Temperature Range,” *Science of Sintering* vol. 39, no. 1, pp. 67–75, 2007.
- [7] C. Ortolland *et al.*, “Stress Memorization Technique—Fundamental Understanding and Low-Cost Integration for Advanced CMOS Technology Using a Nonselective Process,” *IEEE Transactions on Electron Devices*, vol. 56, no. 8, pp. 1690–1697, 2009.
- [8] V. Senez *et al.*, “Two-Dimensional Simulation of Local Oxidation of Silicon: Calibrated Viscoelastic Flow Analysis,” *IEEE Transactions on Electron Devices*, vol. 43, no. 5, pp. 720–731, 1996.
- [9] *Materials Properties Handbook: Titanium Alloys*, R. Boyer, G. Welsch, and E. W. Collings (eds.), Materials Park, Ohio: ASM International, 1994.
- [10] J. T. Pan and I. Blech, “*In situ* stress measurement of refractory metal silicides during sintering,” *Journal of Applied Physics*, vol. 55, no. 8, pp. 2874–2880, 1984.
- [11] P. J. J. Wessels *et al.*, “Stresses in sputtered Ti-Si multilayers and polycrystalline silicide films,” *Journal of Applied Physics*, vol. 63, no. 10, pp. 4979–4982, 1988.
- [12] G. V. Samsonov and I. M. Vinitskii, *Handbook of Refractory Compounds*, p. 287, New York: IFI/Plenum, 1980.
- [13] J. F. Jongste *et al.*, “Elastic constants and thermal expansion coefficient of metastable $\text{C}49 \text{TiSi}_2$,” *Journal of Applied Physics*, vol. 73, no. 6, pp. 2816–2820, 1993.
- [14] N. Soga, “Pressure Derivatives of the Elastic Constants of Vitreous Germania at 25°, –78.5°, and –195.8°C,” *Journal of Applied Physics*, vol. 40, no. 8, pp. 3382–3385, 1969.

Chapter 9: Contents of Advanced Calibration for Mechanics Simulations

References

- [15] S. Spinner and G. W. Cleek, "Temperature Dependence of Young's Modulus of Vitreous Germania and Silica," *Journal of Applied Physics*, vol. 31, no. 8, pp. 1407–1410, 1960.
- [16] D. B. Dingwell, R. Knoche, and S. L. Webb, "A Volume Temperature Relationship for Liquid GeO₂ and some Geophysically Relevant Derived Parameters for Network Liquids," *Physics and Chemistry of Minerals*, vol. 19, no. 7, pp. 445–453, 1993.
- [17] P. Patsalas, C. Gravalidis, and S. Logothetidis, "Surface kinetics and subplantation phenomena affecting the texture, morphology, stress, and growth evolution of titanium nitride films," *Journal of Applied Physics*, vol. 96, no. 11, pp. 6234–6246, 2004.
- [18] M. Leskelä and M. Ritala, "Atomic layer deposition (ALD): from precursors to thin film structures," *Thin Solid Films*, vol. 409, no. 1, pp. 138–146, 2002.
- [19] A. S. Maxwell, S. Owen-Jones, and N. M. Jennett, "Measurement of Young's modulus and Poisson's ratio of thin coatings using impact excitation and depth-sensing indentation," *Review of Scientific Instruments*, vol. 75, no. 4, pp. 970–975, 2004.
- [20] J. O. Kim *et al.*, "Elastic constants of single-crystal transition-metal nitride films measured by line-focus acoustic microscopy," *Journal of Applied Physics*, vol. 72, no. 5, pp. 1805–1811, 1992.
- [21] P. Jedrzejowski, J. E. Klemburg-Sapieha, L. Martinu, "Relationship between the mechanical properties and the microstructure of nanocomposite TiN/SiN_{1.3} coatings prepared by low temperature plasma enhanced chemical vapor deposition," *Thin Solid Films*, vol. 426, no. 1–2, pp. 150–159, 2003.
- [22] H. O. Pierson, *Handbook of Refractory Carbides and Nitrides: Properties, Characteristics, Processing and Applications*, Westwood, New Jersey: Noyes Publications, p. 193, 1996.
- [23] R. Berriche *et al.*, "Evaluation of Hard TiN Coatings by Depth Sensing Indentation and Scratch Testing Methods," *Advanced Performance Materials*, vol. 4, no. 4, pp. 357–370, 1997.
- [24] T. Namazu *et al.*, "Direct Measurement Technique of Strain in XRD Tensile Test for Evaluating Poisson's Ratio of Micro-Thick TiN Films," in *IEEE International Conference on Micro Electro Mechanical Systems (MEMS)*, Maastricht, The Netherlands, pp. 157–160, January 2004.
- [25] K. Holmberg *et al.*, "Residual stresses in TiN, DLC and MoS₂ coated surfaces with regard to their tribological fracture behaviour," *Wear*, vol. 267, no. 12, pp. 2142–2156, 2009.
- [26] H. Chen *et al.*, "Strength and elastic moduli of TiN from radial x-ray diffraction under nonhydrostatic compression up to 45 GPa," *Journal of Applied Physics*, vol. 107, no. 11, p.113503, 2010.

Chapter 9: Contents of Advanced Calibration for Mechanics Simulations

References

- [27] S. L. Dole, O. Hunter, Jr., and C. J. Wooge, "Elastic Properties of Monoclinic Hafnium Oxide at Room Temperature," *Journal of the American Ceramic Society*, vol. 60, no. 11–12, pp. 488–490, 1977.
- [28] M. C. Cheynet *et al.*, "Crystal structure and band gap determination of HfO_2 thin films," *Journal of Applied Physics*, vol. 101, no. 5, p. 054101, 2007.
- [29] M. Franta *et al.*, "Microstructure of HfO_2 and $\text{Hf}_x\text{Si}_{1-x}\text{O}_y$ Dielectric Films Prepared on Si for Advanced CMOS Application," in *Sixth International Conference on Advanced Semiconductor Devices and Microsystems (ASDAM)*, Smolenice Castle, Slovakia, pp. 47–50, October 2006.
- [30] D. K. Venkatachalam *et al.*, "Nanomechanical properties of sputter-deposited HfO_2 and $\text{Hf}_x\text{Si}_{1-x}\text{O}_2$ thin films," *Journal of Applied Physics*, vol. 110, no. 4, p. 043527, 2011.
- [31] K. Tapily *et al.*, "Nanoindentation Investigation of HfO_2 and Al_2O_3 Films Grown by Atomic Layer Deposition," *Journal of the Electrochemical Society*, vol. 155, no. 7, pp. H545–H551, 2008.
- [32] K. Tapily *et al.*, "Nanomechanical study of amorphous and polycrystalline ALD HfO_2 thin films," *International Journal of Surface Science and Engineering*, vol. 5, no 2-3, pp. 193–204, 2011.
- [33] R. G. Munro, "Elastic Moduli Data for Polycrystalline Ceramics," NISTIR 6853, National Institute of Standards and Technology, Gaithersburg, Maryland, <https://srdata.nist.gov/CeramicDataPortal/elasticity>, 2002.
- [34] R. N. Patil and E. C. Subbarao, "Axial Thermal Expansion of ZrO_2 and HfO_2 in the Range Room Temperature to 1400°C," *Journal of Applied Crystallography*, vol. 2, no. 6, pp. 281–288, 1969.
- [35] K. Kamitani *et al.*, "The elastic constants of silicon carbide: A Brillouin-scattering study of 4H and 6H SiC single crystals," *Journal of Applied Physics*, vol. 82, no. 6, pp. 3152–3154, 1997.
- [36] K. M. Jackson *et al.*, "Mechanical Properties of 3C Thin-Film Silicon Carbide," in *SEM Annual Conference on Experimental Mechanics*, Milwaukee, WI, USA, June 2002.
- [37] K. M. Jackson *et al.*, "Mechanical Properties of Epitaxial 3C Silicon Carbide Thin Films," *Journal of Microelectromechanical Systems*, vol. 14, no. 4, pp. 664–672, 2005.
- [38] Z. Li and R. C. Bradt, "Thermal expansion of the hexagonal (4H) polytype of SiC," *Journal of Applied Physics*, vol. 60, no. 2, pp. 612–614, 1986.
- [39] NIST Structural Ceramics Database (SCD), SCD Citation Number: Z00390 (go to <https://srdata.nist.gov/CeramicDataPortal/Scd/Z00390>).
- [40] Z. Li and R. C. Bradt, "Thermal Expansion of the Hexagonal (6H) Polytype of Silicon Carbide," *Journal of the American Ceramic Society*, vol. 69, no. 12, pp. 863–866, 1986.

Chapter 9: Contents of Advanced Calibration for Mechanics Simulations

References

- [41] NIST Structural Ceramics Database (SCD), SCD Citation Number: Z00077 (go to <https://srdata.nist.gov/CeramicDataPortal/Scd/Z00077>).
- [42] Z. Li and R. C. Bradt, "Thermal expansion of the cubic (3C) polytype of SiC," *Journal of Materials Science*, vol. 21, no. 12, pp. 4366–4368, 1986.
- [43] NIST Structural Ceramics Database (SCD), SCD Citation Number: Z00011 (go to <https://srdata.nist.gov/CeramicDataPortal/Scd/Z00011>).
- [44] Z. Li and R. C. Bradt, "Thermal Expansion and Thermal Expansion Anisotropy of SiC Polytypes," *Journal of the American Ceramic Society*, vol. 70, no. 7, pp. 445–448, 1987.